5-2018

Electrochemically Activated Persulfate for Ciprofloxacin Degradation

Laura Whitaker Matzek
University of Tennessee, lmatzek@vols.utk.edu

To the Graduate Council:

I am submitting herewith a dissertation written by Laura Whitaker Matzek entitled "Electrochemically Activated Persulfate for Ciprofloxacin Degradation." I have examined the final electronic copy of this dissertation for form and content and recommend that it be accepted in partial fulfillment of the requirements for the degree of Doctor of Philosophy, with a major in Civil Engineering.

Kimberly E. Carter, Major Professor

We have read this dissertation and recommend its acceptance:

Chris D. Cox, Qiang He, Thomas A. Zawodzinski

Accepted for the Council:
Dixie L. Thompson

Vice Provost and Dean of the Graduate School

(Original signatures are on file with official student records.)

Electrochemically Activated Persulfate for Ciprofloxacin Degradation

A Dissertation Presented for the
Doctor of Philosophy
Degree
The University of Tennessee, Knoxville

Laura Whitaker Matzek
May 2018

DEDICATION

I would like to dedicate this dissertation to my mother, Jane Whitaker, the first in our family to receive a doctorate and to my two girls, Claire and Amanda, who have the potential to achieve anything they dream.

ACKNOWLEDGEMENTS

I would like to sincerely thank my advisor, Dr. Kimberly Carter, for her knowledge, advise and support over the last four years. I would like to thank my department head, Dr. Chris Cox, for serving on my committee and for his encouragement during my time in graduate school. I would like to thank my graduate committee members Dr. Qiang He and Dr. Thomas Zawodzinski for knowledge gained in their classrooms and for serving on my committee.

I could not have completed my dissertation research without the help of several graduate and undergraduate students in my department. Much thanks to undergraduate students Seydou Diallo, Colin Szklarski and Logan Terheggen for sample analysis in the lab. Much thanks to graduate student colleagues Katherine Manx and Adrian Gonzalez for support with instrumentation. Much thanks to Matthew Tipton for partnering to complete papers from this research.

My family has offered immeasurable support. I want to thank my husband Mike Matzek for his never-ending encouragement during this process. Thank you to my children, Claire and Amanda, for their patience and enthusiasm. Thank you to my parents, Bill and Jane Whitaker, for your practical help almost every day.

ABSTRACT

Electrochemically activated persulfate (EAP) is a potential point source treatment for wastewater effluents containing high pharmaceutical content. This dissertation explores the fundamental mechanisms of EAP to better understand this technology for practical application. Ciprofloxacin, a fluoroquinolone antibiotic, was chosen as the model compound to assess parameters of EAP. Ciprofloxacin was selected for its high environmental risk factor and prevalence in hospital wastewater, a potential application for EAP. During the evaluation of EAP as a point source treatment, degradation kinetics and pathways of ciprofloxacin were elucidated.

In the first stage of this study, persulfate activation by solid iron with and without applied current was characterized and applied to the degradation of ciprofloxacin. It was found that persulfate activation increased with iron surface area and increased to a plateau with increasing current. Ciprofloxacin degraded via first-order kinetics; however, applied current did not affect ciprofloxacin removal.

In the second part of this study, electrochemical persulfate activation without iron, using boron-doped diamond (BDD) anodes and graphite or platinum cathodes, was examined. Sulfate radical formation at a BDD anode and persulfate activation at a graphite cathode were elucidated using different electrolytes and electrochemical set-ups. In this system, ciprofloxacin degraded via first order-kinetics, with persulfate electrolyte enhancing ciprofloxacin removal over sulfate or nitrate.

In the final phase of this study, parameters such as reactor configuration, electrode surface area, persulfate concentrations and the presence of a complex matrix were examined to determine their impact on contaminant removal. Due to mass transfer limitations and relative cathode sizes,

a flow-through reactor was least benefited by persulfate addition while a rotating-disk electrode reactor showed enhanced ciprofloxacin removal with persulfate electrolyte. Ciprofloxacin removal from synthetic hospital effluent using electrochemically activated persulfate was found to be less than that in pure electrolyte but still followed a first-order mechanism. Considerable total organic carbon removal of ciprofloxacin and other organic components of the effluent was achieved. Similar degradation was achieved with persulfate and sulfate electrolyte in the effluent. Chlorate, chlorite and perchlorate were formed in significant amounts during the electrochemical process, with formation independent of the presence of persulfate.

TABLE OF CONTENTS

LIST OF TABLES

LIST OF FIGURES

CHAPTER ONE: INTRODUCTION

Pharmaceuticals, including antibiotics, are classified as contaminants of emerging concern in ground and surface waters in the United States and worldwide[1, 2]. In many aquatic ecosystems, individual antibiotics are detected in the ng L^{-1} to low µg L^{-1} range[3-6]. As the antibiotic concentration increases, adverse ecological effects may include reproductive interferences in crustaceans[7-9], disruption of the nitrification process in nitrifying bacteria[10], toxicity to algae[11] and growth of antibiotic resistant bacteria[12]. Potential for ecological impacts arising from the cumulative or synergistic effect of multiple antibiotics in a single aqueous system may also exist, exacerbating the impacts of single contaminant behavior[6, 7, 13, 14].

Effluents from wastewater treatment plants (WWTPs) are a primary source of pharmaceutical introduction to surface water, and concern exists around localized "hotspots" where concentrations of antibiotics are relatively high[1, 2, 15-17]. Pharmaceuticals most often enter the waste stream from un-metabolized fractions found in human waste[18, 19]. Traditional wastewater treatment processes are ineffective in completely degrading pharmaceuticals, so a portion passes through the WWTP into surface water unchanged[20, 21]. Hospital wastewaters have been identified as a significant source of pharmaceuticals entering WWTPs[2, 22, 23]. Studies suggest a <10% to 50% hospital input to individual pharmaceuticals entering WWTPs, depending on the specific substance, and a hospital contribution from 10-94% to the amount of some pharmaceuticals found in the environment[24, 25]. Discharge from WWTPs servicing pharmaceutical manufacturers has also been shown to contain elevated pharmaceutical levels[26].

The fluoroquinolone antibiotic ciprofloxacin has been identified as an environmentally high-risk pharmaceutical in multiple studies, making it a prioritization for environmental

monitoring and remediation[1, 25, 27-32]. Hospital contribution to the environmental risk of ciprofloxacin was elucidated by Helwig et. al (2016), Ory et. al (2016), and Santos et. al (2013)[25, 28, 29]. Other sources of environmental ciprofloxacin include pharmaceutical manufacturer effluent and agricultural run-off, which are often untreated[31, 33].

The environmental hazards of ciprofloxacin include toxicity to algae and invertebrates, interference with plant growth /reproduction and contribution to antibiotic-resistance bacteria[1, 27, 28, 31]. Genotoxicity of hospital effluent has also been attributed to ciprofloxacin and other fluoroquinolone antibiotics[34]. Ciprofloxacin has the potential to create toxic synergistic impacts in the presence of other hazardous compounds[28]. Because of its high risk-factor and prevalence in hospital wastewater, ciprofloxacin has been selected as the compound of interest for the current series of studies.

Point source treatment of hospital effluent, where pharmaceutical concentrations are high, offers an effective solution to mitigate antibiotic entry to surface water[22, 28]. Membrane bioreactors, powdered activated carbon, ultraviolet light, and ozonation are the most commonly examined processes for the treatment of hospital wastewater[35]. Advanced oxidation processes (AOP) using ozone/hydrogen peroxide (O_3/H_2O_2), ozone/ultraviolet light (O_3/UV), Fenton's, sono-Fenton's, and UV/O_3/H_2O_2 have been studied for the destruction of ciprofloxacin, metronidazole, levofloxacin and trimethoprim in hospital effluent and other systems[36-39]. Many of these options have been investigated as pre-treatment steps, secondary stages or tertiary steps in lab-scale, pilot-scale and full-scale processes[24, 35, 40]. As noted by Verlicchi et. al (2015), the ideal treatment of hospital effluent takes into account a complex mixture of variables including hospital size, effluent composition, removal efficiencies for target compounds, receiving WWTP processes

and economic factors[35]. Less selective treatment methods are warranted as antibiotics and other pharmaceuticals exhibit varying properties. The availability of multiple treatment options enables better selection of the best process for a specific treatment challenge.

Electrochemical advanced oxidation processes (EAOPs) are a candidate for removal of fluoroquinolone antibiotics, pharmaceuticals and other targeted pollutants like x-ray contrast media[22, 41-45]. EAOPs are described in Chapter 4.1 and offer the advantage of eliminating total organic carbon (TOC), which may contain harmful transformation byproducts[46, 47].

Activated persulfate is another AOP recognized as a method to degrade an assortment of environmental contaminants, including many antibiotics that traditional wastewater treatment processes do not remove[48]. A comprehensive review of activated persulfate processes to treat over 70 organic compounds is offered in Chapter 2.

Electrochemically activated persulfate (EAP), explained in Chapter 2.4.1, may offer the advantages of both activated persulfate and EAOP for treatment of pharmaceuticals in hospital effluent. The research described in Chapters 3, 4 and 5 focuses on application of EAP to ciprofloxacin degradation. Throughout these studies, ciprofloxacin removal is analyzed in detail, while ciprofloxacin is also used as a model compound to understand the fundamentals of EAP. Chapter 3 explores EAP using an iron anode with and without applied current. Kinetics of persulfate activation and ciprofloxacin removal based on iron surface area and varying applied current are examined. Chapter 4 concentrates on EAP using a boron-doped diamond anode. Iron introduction to the system is avoided. Chapter 4 offers significant insight into anodic and cathodic processes involved in EAP. Kinetics of persulfate ciprofloxacin removal and persulfate activation are analyzed. Chapter 5 expands the focus of Chapter 4 by exploring the effects of reactor

configurations, cathode sizes and persulfate concentrates on ciprofloxacin removal using EAP without iron. Chapter 5 also evaluates ciprofloxacin removal from synthetic hospital effluent and inorganic disinfection by-products formed during the EAP process.

CHAPTER TWO: ACTIVATED PERSULFATE FOR ORGANIC DEGRADATION: A REVIEW

This chapter is revised based on a paper published by Laura W. Matzek and Kimberly E. Carter, as follows:

Matzek, L. W.; Carter, K. E., Activated persulfate for organic chemical degradation: A review. *Chemosphere* **2016,** *151*, 178-188.

Excerpts are also included from a paper published by Laura W. Matzek and Kimberly E. Carter, as follows:

Matzek, L. W.; Carter, K. E., Sustained persulfate activation using solid iron: Kinetics and application to ciprofloxacin degradation. *Chem Eng J* **2017,** *307*, 650-660.

2.1 Introduction

Peroxydisulfate, or persulfate, has been investigated for its ability to degrade recalcitrant organics[49-51]. Stable at room temperature, persulfate can be activated via heat, transition metals, ultraviolet (UV) light, or other means, forming the highly reactive sulfate radical (Equation 2.1) [49, 52, 53].

(2.1) $S_2O_8^{2-} + activator \rightarrow SO_4^{-\cdot} + (SO_4^{-\cdot} \text{ or } SO_4^{2-})$

Like the hydroxyl radical [54], the sulfate radical has a high oxidation potential (E^o=2.60V)[55], and is nonselective[56, 57]. Activated persulfate has widespread application for environmental remediation,[49, 58, 59] as formed radicals react with organic chemicals causing either partial or complete mineralization[60-62]. In situ remediation with activated persulfate oxidation may be preferred over peroxide-based hydroxyl-radical oxidation processes, as the persulfate anion is more stable and may be transported further in the subsurface before being activated for contaminant degradation[63, 64].

Tsitonaki et al. (2010) reviewed the use of persulfate for remediation of contaminated soil and groundwater, focusing on heat, iron and alkaline activations, effects of porous media, and in situ oxidation[65]. Enhancing the effectiveness of activated persulfate includes manipulation of traditional methods and development of novel techniques[56, 60, 66-68]. Recently, Zhang et al. (2015) reviewed sulfate radical technologies, covering radicals generated from peroxymonosulfate and peroxydisulfate[52], photochemical and heterogeneous activation systems, in-situ remediation, hydrothermal oxidation treatment, and air pollution control technologies[52].

The following review provides an extensive assessment of recently published parameters and results for the destruction of various organic compounds in aqueous systems via activated persulfate. Applicable variables and impacts on activated persulfate reactions are provided. Emerging methodologies for persulfate activation, such as electrochemical and activated carbon, are highlighted, along with potential for expanding knowledge areas and obstacles that must be overcome for future practical implementation.

2.2 Mechanisms of Persulfate Reactions

2.2.1 Sulfate, Hydroxyl, and Other Radical Formation

Heat, UV light, and ultrasound impart energy to the persulfate anion resulting in cleavage of the peroxide bond and forming two sulfate radicals (Equation 2.2)[63, 69]. Alternately, persulfate can undergo an oxidation-reduction reaction with an electron donor from a transition metal or the radiolysis of water, generating a single sulfate radical (Equation 2.3)[70, 71].

(2.2) $S_2O_8^{2-} + \text{energy input} \rightarrow 2SO_4^{-}\cdot$

(2.3) $S_2O_8^{2-} + e^- \rightarrow SO_4^{2-} + SO_4^{-}\cdot$

Enhancing the effect of activated persulfate degradation reactions are secondary radicals propagating from sulfate radical reactions[65, 72]. Sulfate radicals react with water at all pHs forming hydroxyl radicals (Equation 2.4)[71], which are the primary reactive species under basic conditions (Equation 2.5)[73]. At pH <7 sulfate radicals are the dominant reactive species; however, hydroxyl and sulfate radicals participate equally in reactions at neutral pHs[73].

(2.4) $SO_4^{-\cdot} + H_2O \rightarrow SO_4^{2-} + OH\cdot + H^+$ $(k\,[H_2O] < 2.7 \times 10^{-3}\ s^{-1})$

(2.5) $SO_4^{-\cdot} + OH^- \rightarrow SO_4^{2-} + OH\cdot$

While hydroxyl radicals degrade a wide range of organic contaminants [4], chain reactions (Equations 2.6 and 2.7) synthesize more reactive intermediates[63]. Likewise, peroxymonosulfate (HSO_5^-) may be activated generating sulfate radicals, as hydrogen peroxide may react with inorganic compounds producing additional free radicals. The formed radicals can subsequently participate in further reactions[74, 75].

(2.6) $SO_4^{-\cdot} + OH\cdot \rightarrow HSO_5^-$

(2.7) $2OH\cdot \rightarrow H_2O_2$

2.2.2 Degradation Mechanisms

Sulfate radicals react with organic molecules through hydrogen abstraction, addition on double bond, and electron transfer[76]. Because the sulfate radical is electrophilic, electron-donating groups will have faster reaction rates with the sulfate radical than electron-withdrawing groups[65]. Persulfate will react with some organics directly, forming sulfate radicals that propagate secondary reactions (Equation 2.8) or may create organic radicals (Equation 2.9)[57, 77], progressively decomposing the intended contaminant[53, 62, 78]. Overall contaminant degradation rates are

dependent on a complex combination of the sulfate radical chain propagation and terminating reactions.

(2.8) $S_2O_8^{2-} + R \rightarrow SO_4^{2-} + SO_4^{-\cdot} + R^*$ where R represents the organic and R* the oxidized organic

(2.9) $S_2O_8^{2-} + R \rightarrow 2SO_4^{-\cdot} + R\cdot$

2.3 Degradation Reactions by Activation Type

Without activation, the persulfate anion will react with some organic chemicals, but degree of removal is less than that obtained using activated persulfate because of the lower oxidation potential of the persulfate anion (E^o=2.01V)[79-83]. Persulfate activators and their properties are critical to the rate and extent of analyte mineralization[65, 84-86]; therefore, results using various activators are presented in the following sections.

2.3.1 Iron-Activated Persulfate for Analyte Degradation

Persulfate can be activated through one-electron transfer using metals such as silver, copper, iron, zinc, cobalt and manganese to form the sulfate radical (Equation 2.10)[61, 70, 87, 88].

(2.10) $S_2O_8^{2-} + M^{n+} \rightarrow M^{n+1} + SO_4^{2-} + SO_4^{-\cdot}$ where M represents the metal

Iron, the most widely studied metal, is an effective activator, relatively non-toxic, environmentally friendly, and more cost effective than other transition metals[89]. Ferrous iron (Fe^{2+}) reacts with persulfate to form the sulfate radical (Equation 2.11), with an activation energy of 50.23 kJ mol[1 90]. The second-order rate constant of sulfate radical formation from ferrous iron is reported as 2 x 10^1 L mol^{-1} sec^{-1} at 22 ^oC[91]. Indirect activation of persulfate by Fe^0 proceeds via the pathway of Equation 2.12[92]. The Fe^{2+} formed activates the persulfate per Equation 2.11[92].

(2.11) $S_2O_8^{2-} + Fe^{2+} \rightarrow Fe^{3+} + SO_4^{2-} + SO_4^{-\cdot}$ ($k = 2.7 \times 10^1\ M^{-1}\ s^{-1}$)

(2.12) $Fe^0 + S_2O_8^{2-} \rightarrow Fe^{2+} + 2SO_4^{2-}$

Insufficient iron concentration causes inefficient persulfate usage, while too much Fe^{2+} results in the iron scavenging the sulfate radical (Equation 2.13), reducing its effectiveness for degradation[93, 94]. The second-order rate constant for this reaction is reported as 4.6×10^9 L mol^{-1} sec^{-1} at pH 3-5 and the activation energy is -18 kJ mol^{-1} [88].

(2.13) $SO_4^{-\cdot} + Fe^{2+} \rightarrow Fe^{3+} + SO_4^{2-}$

Examples of iron-activated persulfate degradations and conditions contributing to optimal removal are presented in Appendix Table A1, and BTEX/phenols, pharmaceuticals, phenyls/dyes and various other organics are shown in Appendix Tables A2-A5.

For iron-activated persulfate, much work has gone into understanding ideal ratios of contaminant to persulfate to iron that enhance removal of contaminants, including antibiotics. Successful ratios vary greatly with contaminant and reaction conditions, but almost always involve excess input of persulfate from 10 to 200 times the molar amount of contaminant[95-97]. At least a 1:1 persulfate to iron ratio is typically needed to achieve maximum analyte removal[61, 98]; however, exact ratios vary with iron forms/states, addition methods and target analytes.

Sequential and continuous addition of iron to activate persulfate for analyte removal has been explored. Sequential and continuous addition of ferrous (Fe^{2+}) iron achieved success over batch additions for pharmaceuticals caffeine and phenacetin but not nicotine or ibuprofen[97]. Degradation of bisphenol A was enhanced from 49% to 97% using four sequential additions versus a single dose of Fe^{2+}, and continuous Fe^{2+} addition achieved 100% removal using the same amount of total iron and reaction time (Appendix Table A1)[99].

Results varied when using Fe^0 and nano-Fe^0 for activation as compared to Fe^{2+}[98, 100]. Fe^0 activates persulfate through a two-step process of ferrous iron generation as shown in equation 2.12 followed by the persulfate activation reaction shown in equation 2.11[92]. Fe^0 provides a measured release of Fe^{2+} through its reaction with persulfate, with higher surface areas of micro- and nano-Fe^0 amplifying persulfate activation[98, 99, 101]. In a side-by-side comparison, Fe^0 persulfate activation resulted in more complete removal of sulfamethoxazole than Fe^{2+} activation, with 100% removal achieved in the former case[95]. In the same study, bimetallic (cobalt/Fe^0 and silver/Fe^0) and trimetallic (cobalt/silver/Fe^0 and silver/cobalt/ Fe^0) plated activators also attained adequate sulfamethoxazole removal, with plating resulting in sustained persulfate activation in solution [95]. The size of Fe^0 has undergone further examination, with micrometric iron particles activating persulfate to remove 97% sulfamethoxazole in thirty minutes[102]. Recently, Naim et al. (2016) demonstrated 95% removal of the pharmaceutical ranitidine with microscale industrial iron scrap, opening the door for low cost, sustainable activation material that may have broad application for iron-activated persulfate degradation systems, including the solid iron activated system examined in Chapter 3[103]. Chapter 3 studies a sustained system for persulfate activation using solid iron, based on the need for in-depth development of persulfate to iron ratios and continuous persulfate activation identified in the preceding paragraphs. This system is applied to the degradation of ciprofloxacin.

Chelation is a potential method for continuous Fe^{2+} release and is commonly used for in situ persulfate activation[104, 105]. Results are mixed, with chelated Fe^{2+} producing similar degradation results to Fe^{2+} for ciprofloxacin but slightly better degradation for sulfamethoxazole[96]. EDTA is often used to chelate iron, forming strong Fe^{2+} complexes, while

citric acid is used for its biodegradability[104, 106]. Experiments comparing chelation with citric acid, oxalic acid and EDTA showed 60% aniline removal was achieved using citric acid chelated Fe^{2+} versus 45% using only Fe^{2+} to activate persulfate (Appendix Table A1)[106]. Sulfamethoxazole degradation removal was best achieved using EDTA rather than citric acid to chelate Fe^{2+}, while both were better than using only Fe^{2+} (Appendix Table A5)[96]. Use of the inorganic chelator, $Na_2S_2O_3$, for Fe^{2+} persulfate activation led to equivalent or better contaminant degradation compared to citric acid and EDTA, and eliminated the TOC introduced by organic chelators[107].

2.3.2 Mineral-based activators

Mineral-based activators including magnetite (Fe_3O_4), nano-magnetite (nano-Fe_3O_4), goethite (α-FeO(OH)) and birnessite (a manganese-based oxide) have been employed for persulfate activation (Appendix Table A5)[108, 109]. Unfortunately, minerals at naturally occurring levels have been proven to have limitations for practical application[110]. It was suggested that concentrations of naturally occurring minerals in the soils are not sufficient to effectively activate persulfate[110]. Further examination into the ability of thirteen naturally occurring minerals to activate persulfate, showed seven minerals slowed the persulfate activation while only four (cobaltite, siderite, pyrite, and ilmenite) significantly enhanced the degradation of the target analytes. It was concluded that most naturally occurring minerals do not effectively activate persulfate for organic degradation, possibly due to localized differences in pH or redox potentials at the surface, or functional groups on the surface that may scavenge radicals[111]. For specific minerals, including some Fe(III) and Mn(IV) oxides, mineral content greater than 2% of the aquifer solids increases the persulfate activation rates and higher percentages of these minerals could effectively aid contaminant degradation[112].

2.3.3 Heat-Activated Persulfate for Analyte Degradation

Persulfate forms two sulfate radicals through scission of the peroxide bond resulting from absorption of heat energy (Equation 2.14)[69]. The activation energy for the reaction is 119 to 129 kJ mol^{-1}, 134 to 139 kJ mol^{-1}, and 100 to 116 kJ mol^{-1} under neutral, basic and acidic conditions, respectively[87]. The rate constant of sulfate radical formation ranges from 1 x 10^{-7} sec^{-1} at 25 ^{o}C to 5.7 x 10^{-5} sec^{-1} at 70 ^{o}C, and pH 1.3[91].

(2.14) $S_2O_8^{2-} + \text{heat} \rightarrow 2SO_4^{-\cdot}$

Huang et al. (2005) studied heat-activated persulfate degradations of 59 volatile organic compounds[113]. Appendix Table A1 and Appendix Tables A6 – A8 list more recent results for heat-activated persulfate degradation studies. In all experiments, the reaction temperature was critical, resulting in increased degradation and solubility of the contaminants into the aqueous phase at elevated temperatures[114-117]. However, temperature optimization is used to minimize the energy input required for achieving desired results. For example, 100% removal of perfluorooctanoic-acid was accomplished at 60 ^{o}C and 90 ^{o}C, 60 ^{o}C was chosen for further experiments[81].

Comparing conventional to microwave heating for activated persulfate degradation (Appendix Tables A6-A7) concluded that microwave heating resulted in faster analyte degradation. It was suggested that microwave heating imparts the required energy more quickly to activate persulfate[115, 118]. Although both conventional and microwave heat-activated persulfate eliminate the need to remove dissolved solids and/or precipitants resulting from metal-catalyzed activation, heat activation is not typically used to remediate large groundwater zones due to the required energy input and associated costs[119]. Furthermore, as the temperature increases, so does

the rate of reaction for both sulfate radical formation and the potential scavengers, (e.g. chloride and bicarbonate ions) with the latter decreasing removal efficiency[120].

Simultaneous use of iron- and heat-activated persulfate has produced mixed results[49, 100, 121]. In the degradation of 1,4-dioxane at 60 ^{o}C, the addition of Fe^{2+} to the process decreased the pseudo-first order reaction rate from 0.0365 min^{-1} to 0.0250 min^{-1} (Appendix Table A1)[49]. It was hypothesized that elevated temperatures increased the rate of Fe^{3+} formation (Equation 2.11), resulting in ferric hydroxide precipitant and reaction inhibition[49]. Further, experiments using Fe^{0} with microwave heat-activated persulfate also exhibited no enhancement of cyclohexanoic acid or polyvinyl alcohol removal[92, 120]. In these cases, it was assumed that reactions of the sulfate radical and iron at elevated temperatures decreased the effectiveness for organic degradation (Equation 2.13)[94].

While the previously mentioned experiments exhibited decreased degradation rates, others achieved improved results with the addition of iron to heat-activated systems. During the removal of p-nitrophenol, Fe^{2+} had positive synergistic effects with heat-activated persulfate below 50 ^{o}C, but as temperatures increased, heat activation was the dominant mechanism (Appendix Table A6)[61]. The results suggested that the metal ions scavenged the sulfate radical at elevated temperatures, negating the synergistic effects observed at lower temperatures. Furthermore, precipitates formed at the higher temperatures limited the diffusion of persulfate and sulfate radicals in the solution[61].

2.3.4 UV Light Activated Persulfate for Analyte Degradation

Persulfate can be activated via UV light forming the sulfate radical (Equation 2.15)[122]:

(2.15) $S_2O_8^{2-} + h\nu \rightarrow 2SO_4^{-}\cdot$

The UV energy breaks the O-O bond, similar to heat-activated persulfate, and a quantum yield of unity has been proven for acidic, basic, and neutral conditions[123, 124]. The results from UV-activated persulfate degradation are presented in Appendix Table A1 and Appendix Tables A9-A10.

With UV activation, the wavelength and UV fluence rate plays an important role in persulfate activation and organic degradation. The most commonly utilized wavelength is 254 nm due to decreased reaction time requirements compared to other wavelengths[125]. A comparative study using 254 nm and 365nm UV-activated persulfate for polyvinyl alcohol destruction found that 100% removal was achieved in less than 5 minutes at 254 nm but only 93% removal in 30 minutes was observed using 365 nm, (Appendix Table A10)[125]. When higher fluence rates were used to activate persulfate, increased degradation and mineralization of beta-lactam antibiotics were observed (Appendix Table A9)[53]. For the removal of acid blue 113, 30 W of power resulted in a faster removal rate than 14 W (Appendix Table A1)[126]. Though UV activation is a cost-effective alternative to thermal activation, this method is limited as UV light has limited penetration into water and is unviable in the subsurface[112, 118, 127].

The synergistic effects of iron addition on UV-activated persulfate degradation of carbamazepine were tested and found enhanced removal was achieved by pairing the two methods (Appendix Table A9)[128]. Adding 50 mM of Fe^{2+} to UV-activated persulfate resulted in 95% removal of phenol in five hours (Appendix Table A10). Although the reaction took longer, a much lower concentration of persulfate was required to achieve 95% removal when Fe_3O_4 was added to the system[129].

2.3.5 Base-Activated Persulfate

Base-activated persulfate is one of the most commonly used techniques to for in situ remediation and is typically performed by adding sodium or potassium hydroxides to raise the pH between 11 to 12[105, 130]. The base catalyzes the hydrolysis of one persulfate molecule, forming the hydroperoxide (HO_2^-) intermediate, which in turn reacts with another persulfate molecule in a one-electron transfer generating a sulfate radical (Equation 2.16). The reaction is second order with respect to persulfate and sodium hydroxide[105]. Hydroxyl radicals are generated from sulfate radicals as previously illustrated (Equation 2.4).

(2.16) $$S_2O_8^{2-} + 2H_2O \xrightarrow{OH-} 2SO_4^- + SO_4^{-}\cdot + O_2^{-}\cdot + 4H^+$$

Hydroxyl radicals are the dominant reactive species at pH > 12, resulting in widespread organic degradation, and the superoxide radical may play a role in the extensive reactivity of base-activated persulfate[73, 105, 131].

Although higher base to persulfate ratios increases the reactive oxidizing species in a system, a 2:1 base to persulfate molar ratio is recommended to achieve neutral conditions at the end of the reaction for in situ use[131]. Maintaining base-activation may require additional base to neutralize the natural buffering capacity of the water and soil or the sulfuric acid generated from persulfate reactions[65, 118, 131]. Unfortunately, elevated base levels may cause changes in soil dispersion and metal concentrations, as well as increase the formation of scavenging species resulting in decreased analyte degradation[65, 118, 131].

Despite its prevalent use for in situ remediation of groundwater and soils, limited studies are available to determine ideal reaction parameters for specific recalcitrant organics using base-activated persulfate. This is in contrast to most activator types, which have been widely studied

and modified in the lab but not put into practice. Studies in which a wide range of organic analytes are degraded under variable conditions using base-activated persulfate would enable practitioners to quickly screen the efficacy of base-activated persulfate for specific remediation projects.

2.4 Unique Methods for Persulfate Activation

2.4.1 Electrochemically-Activated Persulfate for Analyte Degradation

Electrochemical techniques have proven to fully mineralize recalcitrant compounds not degraded via activated-persulfate alone[44, 132]. By combining electrochemistry and electrochemically-activated persulfate, superior removal results compared to either technique alone may be achieved, reducing persulfate and/or electricity usage. Few studies exist that describe the synergistic effects of combining electrochemistry and activated persulfate. Electrochemically activated persulfate (EAP) studies fall into two categories: those that use iron as a co-activator and those that use inert electrodes. These are presented in Appendix Table A11.

Studies investigating EAP without iron suggest persulfate activation, through direct electron transfer at the cathode, creates sulfate radicals (Equation 2.3)[59, 133]. Activated persulfate at the cathode is predicted to work in tandem with anodic electrochemical advanced oxidation processes (EAOP) to degrade organic constituents. The EAOP mechanism is attributed to hydroxyl radical formation (E^o = 2.74 V) that can occur at anode surfaces such as boron-doped diamond (BDD), tin dioxide, and lead dioxide (Equation 2.17)[44, 45, 47, 134, 135]. These hydroxyl radicals react to degrade organic contaminants and propagate other radicals, which can participate in degradation reactions[44, 45, 47, 134, 135]. Additionally, oxidation of the target contaminant by direct electron transfer at the anode can occur[135, 136].

(2.17) $H_2O \rightarrow OH\cdot + H^+ + e^-$

Increased TOC removal was observed for dinitrotoluene and aniline degradation using electrochemically-activated persulfate versus an electrochemical system without persulfate[50, 59]. Both studies found that the contaminant removal increased with the applied potential[50, 59].

Electrochemical persulfate activation accomplished with inert anodes and cathodes eliminates the need for iron addition. Because persulfate can be electrochemically generated from sulfate ions, it has been suggested that persulfate could be regenerated at the anode (Equation 2.18) after completion of an activated persulfate degradation reaction[78, 137-140]. In conjunction with cathodic activation (Equation 2.3), this would perpetuate a source of sulfate radicals.

(2.18) $SO_4^{2-} + SO_4^{-} \rightarrow S_2O_8^{2-} + e^-$ (anode)

Few if any publications are available that conclusively demonstrate persulfate regeneration during an organic chemical degradation reaction. Proof of this concept may lead to development of methods that reduce persulfate consumption while achieving desired contaminant removal. Chapter 4 focuses on understanding the fundamentals and mechanisms of EAP without iron as a co-activator. EAP is then applied to the degradation of ciprofloxacin.

Moving forward, studies are needed to determine electrode materials, including those commonly used for organic destruction (BDD, Ti/RuO2-IrO2, and Ti/SnO2-Sb), best suited for activating persulfate, the relationship between current density and activation, and the synergistic effects on degradation and mineralization of various classes of organics[140]. Chapter 4 covers some of these topics by comparing cathode materials for electrochemical persulfate activation and studying the relationship between current density and activation. Chapter 5 further explores variables influencing organic degradation by EAP, by examining anode:cathode size ratios, reactor configurations, and ciprofloxacin degradation in a complex matrix.

The effects of adding iron into a persulfate reaction vessel by applying an anodic current to iron electrodes have been investigated[141, 142]. Solid iron produces Fe^{2+} through chemical and anodic reactions (Equation 2.19), activates persulfate (Equation 2.11), and can be regenerated at the cathode (Equation 2.20) for additional persulfate activation[141]. Some studies found that the amount of iron added to solution is proportional to the applied current, thus controlling and enhancing the persulfate reaction through a slow release of iron, similar to other slow release methods that enhance degradation reactions[96, 97, 141].

(2.19) $Fe^0 \rightarrow Fe^{2+} + e^-$

(2.20) $Fe^{3+} + e^- \rightarrow Fe^{2+}$

Fe^{2+} generated from solubilized Fe^{3+} at the cathode can also activate persulfate (Equation 2.11)[141, 143]. The use of ferric iron to electrochemically generate ferrous iron resulted in significant achieved 76.5% bisphenol A removal. Optimized conditions of low pH, high persulfate concentration and high current density improved the removal to 100%[143].

Electrochemical generation of ferrous iron for persulfate activation, if controlled by current, may eliminate the need for further iron dosing. However, more work is needed to verify that Fe^{2+} recycling reduces iron requirements while achieving the same degradation results as traditional iron addition. Additionally. the synergistic effects of iron and electrochemically-activated persulfate on organic degradation, especially with regard to mineralization and the initial form of iron, are needed. Chapter 3 addresses these topics with an in-depth exploration of electrochemically-enhanced iron activated persulfate for the degradation of ciprofloxacin.

2.4.2 Ultra-sonication, Activated-Carbon, and Other Methods of Persulfate Activation for Analyte Degradation

Current publications covering lab-scale experiments of various novel activated-persulfate techniques are presented in Appendix Table A12. Degradation by ultrasonically-activated persulfate has shown promising results[56, 58, 144]. Localized high temperatures and pressures from ultrasonically produced cavitation result in homolysis of the O-O bond producing two sulfate radicals in the same energy-induced mechanism as heat and UV light radical generation[52]. The degradation of ammonia perfluorooctanoate significantly increased by combining persulfate and ultra-sonication (Appendix Table A12)[56]. Combining ultra-sonication with persulfate and Fe^0 achieved 99.1% removal of sulfadiazine versus only 50% using Fe^0 activated persulfate [144].

The addition of persulfate to gamma-irradiated for the destruction of ibuprofen achieved the same removal using less radiation, while combining persulfate/electron beam to degrade p-hydroxybenxoic acid did not enhance removal (Appendix Table A12)[60, 66]. Inducing a weak magnetic field on Fe^0 added to persulfate increased the removal rate of caffeine, 4-nitrophenol, benzotriazole and diuron and increased TOC removal of orange G from 7.6% to 36.4% in three hours[86].

Activated carbon (AC) was found to activate persulfate by a mechanism postulated by Liang et al. (2009) and shown in Equations 2.21 and 2.22[145].

(2.21) $\text{AC surface-OOH} + S_2O_8^{2-} \rightarrow SO_4^{-}\cdot + \text{AC surface-OO}\cdot + HSO_4^-$

(2.22) $\text{AC surface-OH} + S_2O_8^{2-} \rightarrow SO_4^{-}\cdot + \text{AC surface-O}\cdot + HSO_4^-$

Greater removal of perfluorooctanoic acid and trichloroethylene was achieved for an AC-persulfate system than could be accounted for through adsorption using AC alone[67, 145]. The

synergistic effects of persulfate and granular activated carbon (GAC) enabled the mineralization of azo dye acid orange 7[146] and the GAC was reused several times. Activated carbon fiber has also been shown to activate peroxymonosulfate[147], thus showing potential for peroxydisulfate activation.

Activated carbon is ubiquitous in water treatment, so widespread potential for adaption of an AC-persulfate process exists. The advantages over current AC systems include: decreased carbon usage rate (as the contaminant would be more fully mineralized by the persulfate rather than taking up sites on the carbon surface) and greater mineralization of the contaminant itself.

2.5 Additional Factors Influencing Activated Persulfate Degradation Reactions

2.5.1 Effects of Persulfate Concentration on Analyte Degradation

It has been widely recognized that analyte removal rate increases as the amount of persulfate increases[49, 106, 148]. Typical analyte to persulfate ratios range from 1:20 to 1:250, as shown in Appendix Tables A1-A12, but effective analyte removal has been achieved using a minimum molar ratio of 1:2[92, 149]. Alternatively, studies suggest there is an optimum amount of persulfate above which degradation is inhibited by the reaction of excess persulfate with sulfate radicals (Equation 2.23) reducing the effectiveness organic oxidation[82, 120, 150, 151].

(2.23) $SO_4^{-\cdot} + S_2O_8^{2-} \rightarrow SO_4^{2-} + S_2O_8^{2-\cdot}$

Customization of persulfate levels can optimize degradation of target analytes; however, this is not always feasible in the presence of multiple analytes with different degradation rates or the presence of scavenging species. While almost always reported as pseudo-first order based on the analyte concentrations[93, 115, 144, 152], reaction rates, in fact, follow second order kinetics with respect to the analyte and persulfate concentrations. Establishing second-order kinetics and rate

constants across categories of organic contaminant can help minimize the amount of persulfate needed to achieve desired results. Chapter 5 examines effects of persulfate concentration on ciprofloxacin degradation using three reactor configurations. It also evaluates second-order mechanisms between ciprofloxacin and persulfate on a rotating-disk electrode reactor.

2.5.2 Effects of pH on Analyte Degradation

The pH of the activated persulfate reaction has a significant effect on analyte removal, even in most cases where pH is below the range required for base activation. Although degradation reactions at acidic pH most frequently improve the degradation of the contaminants by forming hydroxyl radicals (Equation 2.4), improved removal was also observed at neutral pH (between 6 and 8) and slightly basic pH (between 9 and 10) depending on the analyte and activator type[79, 87, 100, 150, 153-155].

2.5.3 Interfering Effects of Ions on Activated Persulfate Reactions

Several ions naturally found in groundwater affect activated persulfate degradation of aqueous contaminants[128, 156]. The impacts of bicarbonate and chloride ions for the destruction of p-nitrosodimethylaniline using different persulfate activation types were studied and concluded that neither species affected iron-activated reactions at neutral pH. Heat-activated reactions were enhanced by chloride, while base-activated reactions were improved by the presence of both chloride and bicarbonate[157]. Enhanced UV-activated persulfate degradation of acetaminophen was followed by decreased removal reaction when the chloride concentration was greater than 20 mM[158]. Citric acid chelated Fe^{2+} activated persulfate degradation of trichloroethene experienced no hindrances with 1 mmol L^{-1} chloride, but removal decreased from 99% to 46% in the presence of 100 mmol L^{-1}chloride[159]. Similar results were seen for the microwave heat-activated persulfate

reaction of sulfamethoxaole[118]. Enhanced degradation may have occurred as low concentrations of chloride in solution can react with sulfate radicals forming chloride radicals that can degrade organic species while high levels may result in sulfate radical scavenging[151].

Bicarbonate was observed to have a negative effect on degradation reactions, across the range of activator types[57, 63, 94]. Natural organic matter (NOM) impedes activated persulfate reactions with reactions tylosin, geosmin, 2-methylisoborneol, atrazine and florfenicol[148, 150, 160, 161]. Subsequent studies for the degradation of 1,4-dichlorobenzene, benzene, and 1,4-dichloropropane in artificially contaminated water and real groundwater, determined the removal efficiency decreased in the groundwater due to the competing reaction of NOM with the sulfate radical[162].

2.6 Practical Applications for Activated Persulfate Use in Water Treatment

2.6.1 Wastewater Treatment

Specific wastewater applications, including industrial discharge and landfill leachate, have been investigated. Microwave heat activated persulfate at 85 ^{o}C was shown to remove 79.4% of the TOC from mature landfill leachate in 30 minutes (Appendix Table A8)[163], while an electrochemical Fe^{2+} persulfate activation system achieved 62% removal of chemical oxygen demand from landfill leachate (Appendix Table A11)[164]. Ibuprofen removal from aqueous solutions using heat-activated persulfate suggests that this process may be able to treat small volumes of concentrated effluents from hospitals or pharmaceutical manufacturers (Appendix Table A7)[165]. Additionally, heat activated persulfate at 65 ^{o}C resulted in 100% removal of the pharmaceutical bisoprolol in thirty minutes[165, 166]. In the degradation of the antibiotic florfenicol,

58.8% mineralization was achieved in two hours with UV/PS versus only 14% in the same time using UV/H_2O_2, and with less cost[167].

Activated persulfate may have broader applications for treating concentrated effluents containing a variety of contaminants and pharmaceuticals, including fluoroquinolones, penicillins, and piperacillins, as well as textile dyes[53, 96, 168, 169]. Unfortunately, limitations regarding persulfate reuse, as well as iron and sulfate removal, must be addressed. The recovery of nano-Fe_3O_4 using magnets after persulfate/nano-Fe_3O_4 reaction enabled the re-use of Fe_3O_4 up to four times with minimal leaching into water and was suggested as a cost-effective approach[109].

Chapter 5 applies EAP to synthetic hospital effluent to screen this technique for real-world application. In this final research chapter, the degradation of ciprofloxacin in synthetic hospital effluent using two reactor configurations is evaluated.

2.6.2 In Situ Groundwater Remediation

The most wide-spread use of activated persulfate includes in situ remediation of contaminated groundwater[130]. The subsurface properties affect reactivity and maintaining persulfate/activator levels in the subsurface are critical for successful implementation[162, 170, 171]. For instance, soil organic matter under basic conditions enhanced activated persulfate degradation of nitrobenzene and hexachloroethane, while a subsequent study proposed that activation by phenols contained in the soil was partially responsible[110, 171]. Superior removal of diclofenac was exhibited in real groundwater containing naturally occurring mineral ions as opposed to reactions in deionized water[172]. The exhibited enhancement contrasts with previous studies showing ions interfering with analyte degradation may be due to the differences in the ion species found in groundwater at various locations.

Properties of the organic species and the subsurface regions can affect the degradation of contaminants. For instance, though catalyzed hydrogen peroxide propagations can enhance removal of hydrophobic compounds sorbed to soil and subsurface solids, the same result was not accomplished using activated persulfate[119]. Preferential reactions between activated persulfate with soil organic matter may reduce adsorption of contaminants onto soils, enabling mobilization of the contaminants into uncontaminated regions[91]. A study into the effects of aquifer solids on persulfate activity determined that exhaustion of persulfate and activating agents inhibits long-term availability of persulfate[170].

Studies for overcoming the challenges and limitation of persulfate and activator maintenance have been undertaken. A proposed solution to maintain iron levels in situ is the use of hydroxylamine to quickly cycle Fe^{3+} back to Fe^{2+} has proven successful for completely degrading trichloroethylene (Appendix Table A1)[173]. Permeable reactive barriers can provide continuous persulfate release overcoming depletion issues while enabling the degradation of contaminants[174]. Slow release persulfate-paraffin-Fe^0 candles have been utilized to maintain activated persulfate concentrations for the removal of BTEX compounds[175].

2.7 Conclusions and Outlooks

Extensive review of recently published results confirms activated-persulfate is a viable method for the destruction of organic analytes for soil and groundwater remediation. Using optimized conditions, 100% removal can be accomplished for some recalcitrant organics. Unfortunately, challenges remain to optimize degradation reactions for efficient, cost-effective and timely contaminant removal in practical systems.

Development of methods to maintain persulfate and activator concentrations will improve utilization in situ. Broader understanding of environmentally friendly iron-chelator functionality under groundwater conditions will help identify cases where chelators can improve longevity of iron. At the same time, practitioners can move away from using traditional chelators that are now considered undesirable environmental additives. Determining second-order reaction kinetics between persulfate and analytes in the presence of chelated iron may help enhance optimization of reaction longevity. Relating subsurface parameters, including mineralogy and NOM, to activated persulfate degradation outcomes, will enable efficient assessment and prediction of activated persulfate treatment outcomes. Finally, physical techniques offering slow releases of persulfate into groundwater systems have been successful; however, supplementary experiments covering a broader range of chemicals and reaction conditions are needed.

Studies comparing or correlating organic degradation using persulfate activator type, particularly under groundwater or wastewater conditions, will offer a better understanding of the reaction mechanism and outcomes for activated persulfate degradation of various classes of organic species. Formulation of practical guidelines would increase the ability to theoretically predict and achieve desired degradation outcomes.

Studies regarding the cost-effectiveness of energy input versus degradation outcomes for energy-intensive activation methods, including heat, UV light, ultra-sonication and electrochemical, may have repercussion for implementation of activated persulfate. Persulfate is often successful for destroying relatively concentrated pollutants and removing recalcitrant organics at the site of contamination. Nonetheless, little work has been done to combine activated persulfate reactions with subsequent sulfate ion removal such as ion exchange or filtration. As

coupling different processes may be required for implementing activated persulfate in certain systems, assessment of the additional costs of sulfate ion removal against the potential to remove certain contaminants or by-product is necessary.

Although reaction outcomes typically improve with increased persulfate addition, the "more is better" approach can lead to wasted resources and depletion of reactants, limiting degradation of targeted contaminants. Improved understanding of second-order reaction rates with respect to both analyte and persulfate can allow for optimization of persulfate usage in specific systems. The novel technique of electrochemical persulfate activation may minimize persulfate or iron usage through regeneration, resulting in better mineralization than some other activation techniques. Other novel techniques may also be advantageous for complete contaminant removal or mineralization; for instance, activated-carbon can function as both a catalyst for persulfate activation and adsorbent for removal of some contaminants and by-products. Implementation of these novel methods requires follow-up studies verifying their usefulness for promoting effective activated persulfate degradation and refined parameters for practical application.

CHAPTER THREE: SUSTAINED PERSULFATE ACTIVATION USING SOLID IRON: KINETICS AND APPLICATION TO CIPROFLOXACIN DEGRADATION

This chapter is revised based on a paper published by Laura W. Matzek and Kimberly E. Carter, as follows:

Matzek, L. W.; Carter, K. E., Sustained persulfate activation using solid iron: Kinetics and application to ciprofloxacin degradation. *Chem Eng J* **2017,** *307,* 650-660.

3.1 Background

Limited studies have examined the use of Fe^0 in the form of solid iron bars/rods to sustain a controlled persulfate degradation reaction[141, 142]. With this method, current is applied to an iron electrode to electrochemically augment (Equation 2.19) the chemical corrosion of solid iron (Equations 2.12 and 3.1) into solution where it can react to activate persulfate (Equation 2.11)[92, 141, 153]. Additional ferrous ions are produced at the surface of the solid iron per equation 3.2[153]. Excess ferrous ions in solution may scavenge persulfate radicals via equation 2.13, decreasing the efficiency of persulfate to degrade the intended compound[98, 142].

(3.1) $Fe^0 + O_2 + 2H_2O \rightarrow Fe^{2+} + 4OH^-$

(3.2) $Fe^0 + 2Fe^{3+} \rightarrow 3Fe^{2+}$

Govindan et al. (2014) demonstrated degradation of pentachlorophenol (PCP) using an iron anode and cathode to activate persulfate[142]. Successively larger first-order PCP degradation rate constants were observed with increasing applied current[142]. Yuan et al. (2014) manipulated persulfate activation using current applied to an iron anode. It was established that the iron production increased with current and that a linear relationship (R^2=0.933) between iron production rate and persulfate decomposition existed when measured with analyte in solution. A

linear relationship between current and the trichloroethylene first-order reaction rate constant was also established[141].

It is postulated that solid iron activated persulfate offers an avenue for optimizing persulfate to iron ratios and minimizing the amount of iron needed to sustain the persulfate activation reaction. Solid iron may be advantageous over zero-valent nano- micro- and granular iron because unreacted amounts can more easily be removed from solution upon reaction completion. The addition of current or manipulation of surface area, which is simpler to accomplish with solid iron versus other forms, is expected to provide a way to control the solid iron dissolution rate. The current-regulated introduction of iron into the system should enable both controlled and sustained persulfate activation. The first stage of this study aimed to enhance current knowledge of solid iron activated persulfate systems by determining the fundamental relationships between iron surface area, applied current, iron production and persulfate activation. These experiments were completed without analyte in solution, a step often bypassed in current research which is critical to provide a foundation for the use of solid iron activated persulfate for environmental contaminant removal. The objective of the second stage of this study was to demonstrate the efficacy of solid iron activated persulfate in degrading environmental contaminants. The fluoroquinolone antibiotic ciprofloxacin was used as a model compound. Ciprofloxacin has been successfully degraded with granular ferrous iron activated persulfate and its use in this study is intended to provide an understanding of the solid iron activated persulfate process[96].

3.2 Materials and Methods

3.2.1 Chemicals

Acros Organics ciprofloxacin (98%) was purchased from Fisher Scientific (Pittsburg, PA). Sodium persulfate (98%) was purchased from Fisher Chemical. Iron rods were purchased from Sigma Aldrich (99.98%, 6.3 mm diameter). Electron Microscopy Science graphite rods (0.120-inch diameter) were purchased from Fisher. Other chemicals include 100 ppm fluoride standard (ThermoScientific Orion Ionplus Application solution), 1N sulfuric acid (J.T. Baker), Optima formic acid (Fisher Scientific), nitric acid (Fisher Scientific), hydrochloric acid, (Fisher Scientific) sodium hydroxide (Fisher), Optima Methanol (Fisher Chemical), potassium iodide (99+%, Acros Organic from Fisher), potassium sulfate (Fisher Scientific), sodium bicarbonate (Fisher Scientific), tert-butanol (Fisher) and Ferrover iron reagent powder pillows (Hach®, Loveland, CO). Deionized water (DI) (18.2 MΩ-cm) was generated by a Millipore Milli-Q system for all experiments.

3.2.2 Experimental Procedures

Physical Setup: All experiments were completed at 20 °C. Iron rods were rinsed with aqua Regia (3:1 hydrochloric acid to nitric acid) then DI water to ensure starting uniformity of the surface for each run[176]. 700 mL volumes were used for all experiments. All experiments were completed at least in duplicate. Stirring was maintained for the duration of each experiment using a magnetic stir bar. An iron rod was inserted to a depth corresponding with the desired surface area at time = 0 (immediately after first sampling). Surface areas were chosen based on the range of areas attainable within the physical limitations of iron rod and iron rod holder. For each series with applied current, a graphite rod was inserted 7 cm from the iron rod, to a depth of 4 cm. A constant current was applied to these systems with the positive terminal connected to the iron rod and the

negative terminal connected to the graphite rod. Current density was adjusted by adjusting current at a constant surface area. The physical set-up is illustrated in supplementary Figure 3.1.

Persulfate Activation Experiments: For each time series, 200 mL of a prepared 63 mmol L^{-1} sodium persulfate solution was mixed with 500 mL deionized water in an open 1 L beaker. The solution was stirred at 750 rpm for 5 minutes and sampled. 3 mL samples were taken at pre-designated time intervals and frozen to quench the persulfate activation reaction. The initial persulfate concentration was chosen to correspond with that used in ciprofloxacin degradation experiments as outlined in section 2.2.3. The pH was not controlled or buffered during the experiment to better examine natural reaction pathways of the system[104, 141, 177]. Initial pH values averaged 3.5, similar to initial reaction conditions of some other persulfate-based experiments[101, 104, 178]. Final pH values averaged 2.5, a drop in pH noted in several studies and attributed to generation of acid during persulfate decomposition[104, 177].

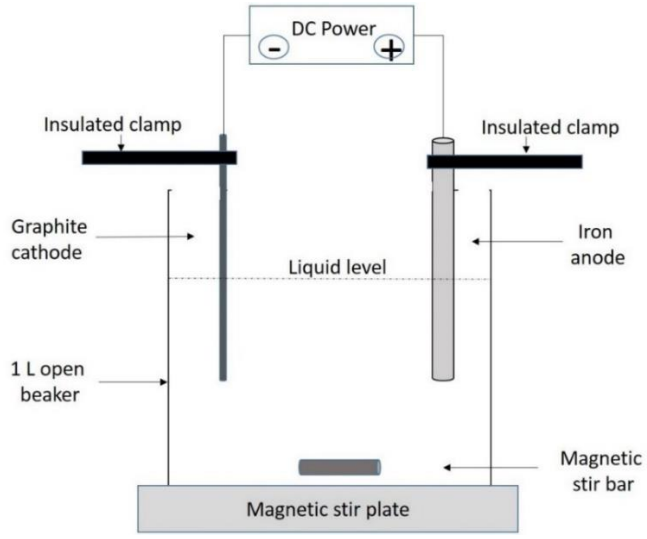

Figure 3.1. Schematic of iron-activated persulfate experimental setup

Ciprofloxacin degradation experiments: Batches of ciprofloxacin were prepared in 0.338 mmol L^{-1} concentration with 0.1% sulfuric acid (to aid dissolution) at least one day before experiment (also to ensure complete dissolution)[44]. For each time series, 200 mL of a prepared 63 mmol L^{-1} sodium persulfate solution was added to an open 1 L beaker. A predetermined amount of 0.338 mmol L^{-1} solution of ciprofloxacin was added to achieve the desired initial concentration (for example, 250 mL was added to reach 0.121 mmol L^{-1} in the final 700 mL mixture). An initial concentration of 0.121 mmol L^{-1} ciprofloxacin was used for all degradation experiments unless otherwise noted. This initial concentration falls within the range used in related pharmaceutical degradation experiments[44, 96, 97, 176]. It is above concentrations typically found in the environment in order to facilitate analysis of ciprofloxacin and avoid errors associated with dilution when working on the low microscale[97]. The persulfate concentration was chosen to achieve a 1:150 molar ratio of ciprofloxacin to persulfate. This ratio is within the range established by other successful contaminant degradation studies incorporating iron activated persulfate[96, 97, 179]. An appropriate amount of water was added to attain a total volume of 700 mL. The solution was stirred at 750 rpm for 5 minutes and sampled. The solution was then stirred an additional 25 minutes and sampled before insertion of iron rod, for a total of 30 minutes of stirring before iron rod inserted. All tests, with and without applied current, were completed using a constant iron surface area of 6.1 cm^{-2}. This surface area was high enough to minimize effects of surface area to reaction volume changes as samples were taken, while keeping the amount of iron introduced into the system to a minimum. 15 mL samples were taken at pre-designated time intervals and frozen to quench the persulfate activation reaction. As previously mentioned, pH was not controlled during the experiment to better investigate reaction pathways of the system[104, 141, 177]. Initial pH

values averaged 4.0 upon mixing of ciprofloxacin and persulfate and final pH values averaged 2.5 after 120 minutes of reaction. The ciprofloxacin was extracted after 24 hours as outlined in section 2.3.2. Radical scavenging experiments were completed using the same methodology but with the addition of 220 mmol L^{-1} methanol or tert-butanol.

3.2.3 Analytical Methods

Persulfate and Iron Analysis: Persulfate concentration was analyzed using a ThermoScientific Evolution 600 UV-Vis spectrometer (ThermoFisher, Pittsburg, PA) at a wavelength 352nm, based on a modification of the spectrophotometric technique[180, 181]. A 1 mol L^{-1} solution of potassium iodide (KI) containing 0.15 mmol L^{-1} sodium bicarbonate was prepared using high purity water (18.2 mΩ). For each analysis, 40 μL of persulfate sample was combined with 1 mL the potassium iodide-sodium bicarbonate solution to give an approximate molar ratio of 1:1000 persulfate to KI providing an overabundance to react with the persulfate. A 20-minute wait time followed, to allow a yellow color, created from the reaction of persulfate with potassium iodide to form iodine, to develop. The sample was diluted to an absorbance level within the calibration range by adding 9.5 mL of DI water and mixing. Each sample was measured against of background of potassium iodide-sodium bicarbonate solution. Calibration standards with known amounts of sodium persulfate were prepared and measured using the same technique. The linear dynamic range of the calibration curve is 4 to 120 μmol L^{-1} persulfate as diluted and measured, which corresponds to original sample concentrations of 0.8 mmol L^{-1} to 30.7 mmol L^{-1} persulfate. The method detection limit was 0.6 mmol L^{-1} persulfate in original, non-dilute samples. See additional statistical analysis in Table 3.1.

Table 3.1. Statistical Parameters for Persulfate Calibration Curve

	Slope (absorbance unit per μmol L^{-1})	Abs.
Value	0.0245	-0.0415
Standard error	0.00033	0.0315
R^2	0.9995	

Total iron concentration was analyzed using a ThermoScientific Evolution 600 UV-Vis spectrometer (ThermoFisher, Pittsburg, PA) at a wavelength of 510 nm, based on a modification of the spectrophotometric technique created by Hach® for use with their Ferrover iron reagent powder pillows for 5mL samples. These powder pillows make use of the 1,10 phenanthroline method. A small amount of sample solution (100-200 μL) was added to 5 mL of DI to dilute sample within analysis range of powder pillows. One Ferrover powder pillow was added to each diluted sample and allowed to react for 5 minutes before absorbance was measured. Standards were prepared and measured using the same procedure. The linear dynamic range of the calibration curve was 5.6 to 261 μmol L^{-1} total iron as diluted and measured. Sample dilution factors were adjusted from as needed so that samples ranging from 0.146 mmol L^{-1} to 13.3 mmol L^{-1} could be measured. The method detection limit was 0.08 mmol L^{-1} iron in original sample. See additional statistical analysis in Table 3.2.

Table 3.2. Statistical Parameters for Iron Calibration Curve

	Slope (absorbance unit per μmol L^{-1})	Abs.
Value	0.0113	-0.0279
Standard error	4.38E-05	0.00635
R^2	0.9999	

Ciprofloxacin analysis: Ciprofloxacin concentration was analyzed using a Thermo Scientific Evolution 600 UV-Vis spectrometer at a wavelength of 272nm (ThermoFisher,

Pittsburg, PA). To prepare for analysis, ciprofloxacin was extracted from the sample to avoid absorbance interference by iron. Prior to extraction, the pH of each sample was lowered to 1.5 using sulfuric acid. This adjustment to a low pH provided >98% extraction efficiency during development of the extraction method, versus 90% extraction efficiency at a pH of 3.0, and 80% efficiency at a neutral pH, so pH adjustment by sulfuric acid was established as part of the method. As >98% of the ciprofloxacin was recovered, it was assumed that hydrolysis did not occur under the low pH conditions. Ciprofloxacin was extracted using solid-phase extraction with Waters Sep-Pak tC2 cartridges. Cartridges were conditioned with 1mL methanol and rinsed with 1mL of DI water. 0.5mL of sample was loaded onto cartridge followed by a 0.5mL rinse with DI to remove all iron from cartridge. The sample was eluted under vacuum with three subsequent 1mL quantities of a methanol/0.1% formic acid solution. Extracted ciprofloxacin samples were quantified using standards prepared in methanol/0.1% formic acid. The linear dynamic range of the calibration curve was 1.1 to 83 µmol L^{-1} ciprofloxacin, which corresponds to 0.003 to 0.250 mmol L^{-1} ciprofloxacin before dilution by the extraction process. The method detection limit was 0.003 mmol L^{-1} in the original, non-dilute samples. (See additional statistical analysis in Table 3.3.)

Table 3.3. Statistical Parameters for Ciprofloxacin Calibration Curve

	Slope (absorbance unit per µmol L^{-1})	Abs.
Value	0.1148	-0.0283
Standard error	0.00164	0.0261
R^2	0.9994	

Ciprofloxacin extracts were diluted 1:25 in methanol and analyzed for intermediates and transformation by-products using a Thermo Scientific Exactive™ Plus Orbitrap LC-MS with ultimate 3000 RS pump, column compartment, autosampler, and diode array detector

(ThermoFisher, Pittsburg, PA) with scan range 50-500m/z; resolution 140,000; positive mode electrospray ionization; AGC target 3e6; max inject time 200ms. The ESI settings were: sheath gas 25, aux gas 6, sweep gas 3, capillary temp 300°C. The column temp was 30 C; UPLC with mobile phase 80:20 MeOH:H_2O with flow rate of 0.2mL/min, 10-minute run, 10 µL was injected. UV-vis at 272nm and 3D field from 200-400nm. The linear dynamic range of the calibration curve for ciprofloxacin was 1.2 µmol L^{-1} to 193 µmol L^{-1}. The limit of detection for the ciprofloxacin analysis was less than 1.2 µmol L^{-1}. See additional statistical analysis in Table 3.4.

Table 3.4. Statistical Parameters for HPLC-MS Calibration Curve

	Slope (peak area per µmol L^{-1})	Peak Area
Value	5.42E-07	n/a
Standard error	3.82E-09	n/a
R^2	0.9999	

Fluoride Ion Analysis: Fluoride ion (F^-) concentrations were analyzed using ion chromatography. In preparation, the pH of all samples was raised to 7 to precipitate iron and dissociate any hydrofluoric acid that may have formed during the degradation process. Samples were then filtered through successive 3.1, 1.2, 0.7 µM ThermoScientific™ Target 2™ glass microfiber syringe filters and 0.45 µM polypropylene hydrophilic syringe filters to remove particulates. Samples were transferred to low-density polyethylene (LDPE) IC vials in preparation for ion chromatography (IC; Thermo-Element, FL) using a Dionex 2100/1100 dual column system with background suppression. F^- ions were quantified using a standard calibration curve. The linear dynamic range of the calibration curve was 10.5 to 526 µmol L^{-1} F^- ions. The analytical

detection limit of the IC for fluoride analyte was less than 5.2 µmol L^{-1} F^- ions. See additional statistical analysis in Table 3.5.

Total Organic Carbon Analysis: Total organic carbon (TOC) was determined using a Shimadzu TOC-L analyzer with autosampler ASI-L. In preparation, the pH of all samples was raised to 7 to precipitate iron and dissociate any hydrofluoric acid that may have formed

Table 3.5. Statistical Parameters for Fluoride Ion Calibration Curve

	Slope (µS*min per µmol L^{-1})	Intercept (µS)
Value	0.007925	-0.0251
Standard error	9.27E-05	0.0210
R^2	0.9993	

during the degradation process. Samples were then filtered through successive 3.1, 1.2, 0.7 µM ThermoScientific™ Target 2™ glass microfiber syringe filters and 0.45 µM polypropylene hydrophilic syringe filters to remove particulates. The linear dynamic range of the calibration curve was 146 µmol L^{-1} to 4167 µmol L^{-1} TOC. The method detection limit for the TOC analysis was 52 µmol L^{-1} TOC. See additional statistical analysis in Table 3.6.

Table 3.6. Statistical Parameters for TOC Calibration Curve

	Slope (mV*min per µmol L^{-1})	Intercept (mV*min)
Value	2357	40.86
Standard error	1286	21.46
R^2	0.9996	

3.3 Results and Discussion

3.3.1 Persulfate Activation Experiments

Persulfate activation controlled by current applied to iron: Persulfate activation is represented by persulfate decomposition, which is inversely proportional to radical formation. Figure 3.2a shows the decrease in persulfate with time when exposed to solid iron with and without an applied current and no analyte present in solution. The R^2 correlation coefficients of >0.97 for a linear relationship between persulfate decomposition and time for all series (Table 3.7) establish that persulfate decomposes through a zero-order mechanism when exposed to a solid iron surface. For a constant surface area of 6.1 cm^2, a persulfate reaction rate constant of 4.3 x 10^{-7} mol L^{-1} s^{-1} was found, while an average maximum reaction rate constant of 7.1 x 10^{-7} mol L^{-1} s^{-1} at higher current densities was achieved. See Table 3.7 for reaction rate constants at all current densities.

The chemical corrosion of iron due to acidic conditions contributed to over 55% of the maximum persulfate decomposition rate achieved with use of applied current, based on a comparison of reaction rate constants with no current and with applied current using equation 3.3.

(3.3) Contribution to persulfate activation by chemical corrosion

$$\frac{(\text{Avg. max. reaction rate constant} - \text{Reaction rate constant with no current})}{\text{Avg. max. reaction rate constant}} \; X \; 100$$

The "average maximum reaction rate constant" is the average of all reaction rate constants for current densities greater than or equal to 8.2 mA cm^{-2}. At or above current densities of 8.2 mA cm^{-2}, all reaction rate constants are +/- 5% of a horizontal plateau, as shown in Figure 3.3b.

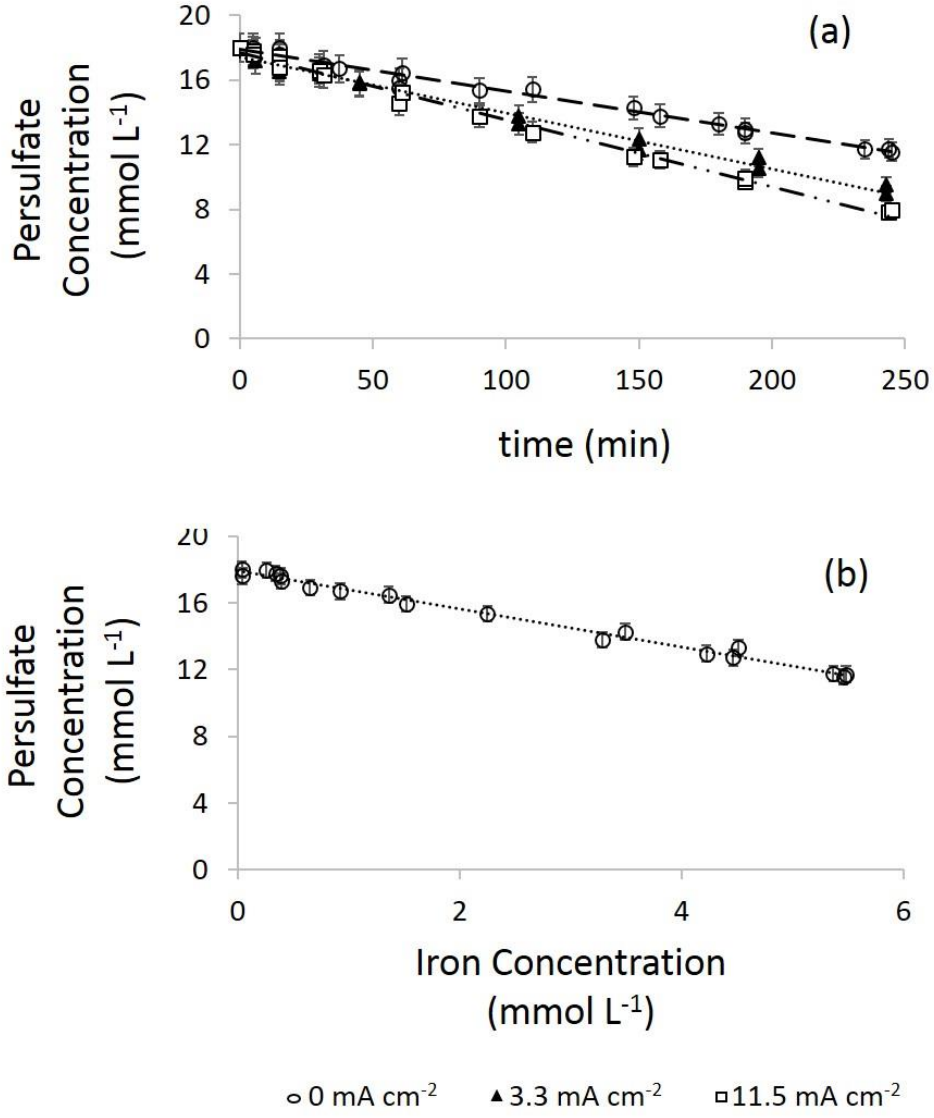

Figure 3.2. Persulfate decomposition by solid iron
(a) Persulfate decomposition by solid iron with and without applied current, as a function of time. R^2 = 0.9857 for 0 mA cm^{-2}. R^2 = 0.9838 for 3.3 mA cm^{-2} . R^2= 0.9930 for 11.5 (b) Persulfate decomposition as a function of iron production, shown at no current.cm^{-2}. The linear fits indicate a zero-order reaction mechanism between the solid iron and persulfate at all current densities. R^2 = 0.9907. The linear correlation suggests iron dissolution as the driving factor in persulfate decomposition. Initial persulfate concentrations were 18 mmol L^{-1}, iron surface area=6.1 cm^2. Error bars represent 95% interval. pH was not controlled. The final pH of all experiments at 240 minutes was 2.5.

Applied current enhanced iron production above levels achieved with the naturally occurring acidic conditions of the system. Figure 3.2b displays the relationship between iron production and persulfate decomposition without current applied. A similar linear relationship exists at all current densities tested, with R^2 values > 0.98, as shown in Table 3.8. The slope of the line elucidates the average molar decomposition of persulfate per mole of iron produced, or the persulfate to iron ratio (PS:Fe). Without electrochemical supplementation, every 1.00 mole of iron production resulted in 1.14 moles of persulfate consumed for the duration of each experiment. With equation 2.12 a proposed mechanism of ferrous iron dissolution into solution, one mole of zerovalent iron should decompose one moles of persulfate, and then the same iron, now ferrous, would decompose another mole of persulfate per equation 2.11 to generate sulfate radicals, giving an overall 2:1 PS:Fe ratio. The near 1:1 ratio can be attributed to the acidic reaction conditions of this study. In this case, the oxygen reactions with iron under acidic conditions are also a factor in iron production according to equations 3.4 and 3.5[182]. More ferrous iron is made available to generate sulfate radicals without the unproductive persulfate decomposition indicated in equation 2.12. A Fenton reaction, generating additional hydroxyl radicals to degrade the intended contaminant, may result from the reaction between H_2O_2 generated according to equation 3.5 and the ferrous iron[182].

(3.4) $Fe^0 + O_2 + 4H^+ \rightarrow 2Fe^{2+} + 2H_2O$

(3.5) $Fe^0 + O_2 + 2H^+ \rightarrow 2Fe^{2+} + H_2O_2$

Figure 3.3a shows the PS:Fe ratio as a function of current density. With applied current, there is the possibility of activating persulfate through direct electron transfer (Equation 1.3), a

Table 3.7. Statistical Parameters for Figure 3.2a.

Current Density (mA cm^{-2})	Parameter	Slope (zero-order reaction rate constant) (mmol L^{-1} persulfate min^{-1})	Intercept (mmol L^{-1} persulfate)
0.0	Value	-0.0258	17.87
	Standard error	0.00068	0.0850
	R^2	0.9857	17.45
3.3	Value	-0.0347	17.45
	Standard error	0.0010	0.123
	R^2	0.9838	
6.2*	Value	-0.0371	18.25
	Standard error	0.00086	0.130
	R^2	0.9915	17.64
8.2*	Value	-0.0407	0.318
	Standard error	0.0023	
	R^2	0.9581	
11.5	Value	-0.0415	17.72
	Standard error	0.0009	0.1065
	R^2	0.9930	

*not shown on figure

Table 3.8. Statistical Parameters for Iron Dissolution Versus Persulfate Reduction

Current Density ($mA\ cm^{-2}$)	Parameter	Slope ($mmol\ L^{-1}$ persulfate / $mmol\ L^{-1}$ iron)	Intercept ($mmol\ L^{-1}$ iron)
0.0	Value	-1.14	17.93
	Standard error	0.0254	0.0845
	R^2	0.9907	
3.3*	Value	-1.06	17.41
	Standard error	0.0316	0.121
	R^2	0.9851	
6.2*	Value	-0.977	18.42
	Standard error	0.0207	0.122
	R^2	0.9928	17.83
8.2*	Value	-0.988	0.246
	Standard error	0.0414	
	R^2	0.9760	
11.5*	Value	-1.00	17.91
	Standard error	0.0266	0.141
	R^2	0.9895	

*not shown on figure

Figure 3.3a shows the PS:Fe ratio as a function of current density. With applied current, there is the possibility of activating persulfate through direct electron transfer (Equation 1.3), as well as the possibility of regenerating Fe^{2+} from Fe^{3+} at the anode (Equation 1.20), introducing more ferrous iron into solution for persulfate activation[71, 141]. If these mechanisms play a significant role in persulfate decomposition, it would be expected that the PS:Fe ratio would increase with current. In fact, the efficiency of iron use decreased slightly with applied current, with 1.00 mole of iron production resulting in 1.00 mole of persulfate decomposed (+/- 5%), at all applied current levels. While the electrochemical activation or persulfate and ferrous ion regeneration are theoretically possible, they do not play significant roles in the overall decomposition rate.

Figure 3.3b illustrates the iron production rate and zero-order persulfate reaction rate constant as a function of current density. These inter-related variables follow the same trend, with

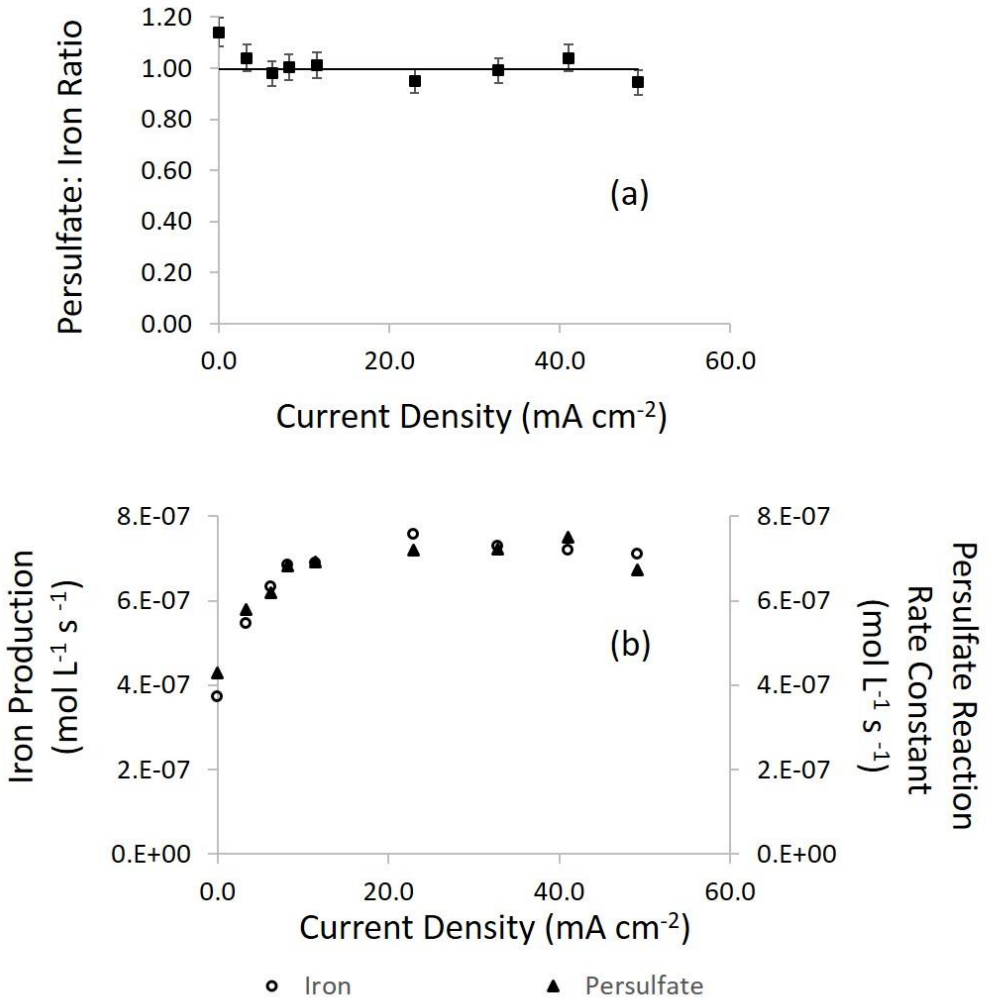

Figure 3.3. Persulfate-iron relationships as a function of current

(a) Molar ratio of persulfate decomposition to iron production as a function of current density. The solid horizontal line illustrates the average ratio. (b) Iron production rate and zero-order persulfate reaction rate constant as a function of current density. Initial persulfate concentration was 18 mmol L^{-1}, iron surface area=6.1 cm^2. Error bars represent 95% interval.

an increasing reaction rate as current density increases to 8.2 mA cm^{-2}. The plateau above 8.2mA cm^{-2} is attributed to diffusion limitations of reactants entering and leaving the surface, which is associated with the surface dominated zero-order reaction rate. Reaction rate limits are an important consideration for use of solid iron as a persulfate activator, since the limiting current density should be quantified in order to maximize persulfate activation without excess electricity used.

Persulfate decomposition controlled by iron surface area: It was postulated that manipulating the surface area of solid iron exposed to solution controls the persulfate activation. Figure 3.4 shows persulfate decomposition at iron surface areas of 3.2 cm^2, 6.1 cm^2, 9.4 cm^2 and 12.8 cm^2. The linear trends of each time series, with R^2 values >0.95 (Table 3.9), indicate that persulfate decomposes by a zero-order mechanism. Within the surface areas tested, there were no limiting conditions. The largest reaction rate constant was found at the largest surface area, with an average value of 8.4 x 10^{-7} mol L^{-1} s^{-1}. The reaction rate constant increased close to proportionally with an increase in iron surface area. Increasing the surface area by a factor of 2.1 garnered an 18% improvement in comparison the maximum reaction rate achieved with applied current. In Figure 3.5, by increasing the surface area, iron production and persulfate activation followed similar linear trends. Parameters and statistical details can be found in Table 3.10. The reaction rate constant for persulfate, as a function of iron surface area, can be modeled as shown in equation 3.6.

(3.6) $$k_{0,ps} = 7.2 \times 10^{-8} \times A - 6.1 \times 10^{-8}$$

The $k_{0,ps}$ is the persulfate reaction rate constant (mol L^{-1} s^{-1}) and A is surface area of iron (cm^2). Iron utilization was 1.14 moles of persulfate decomposed for every 1 mole of iron released.

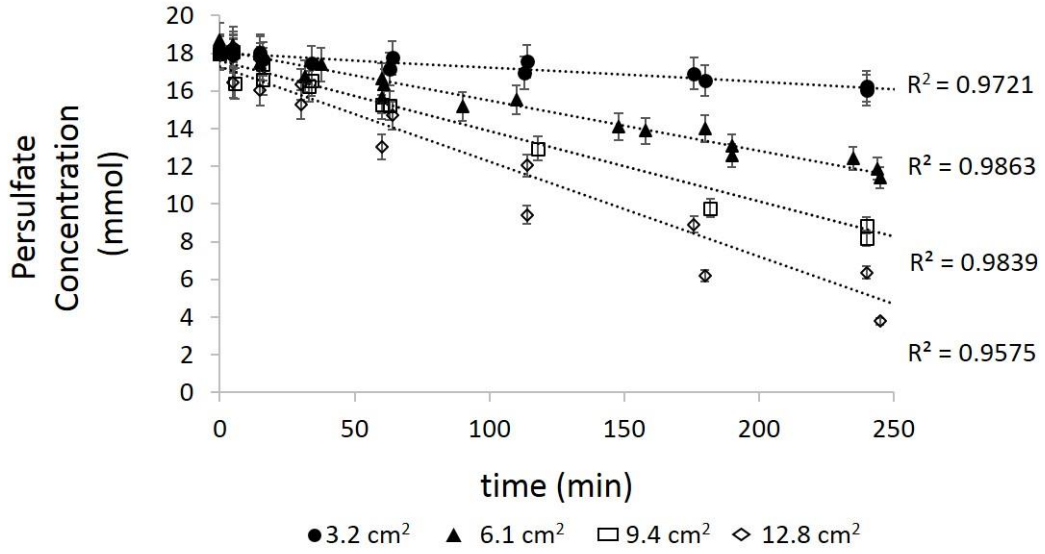

Figure 3.4. Persulfate decomposition by solid iron at different iron surface areas
Displayed as a function of time. The linear fits indicates a zero-order persulfate activation mechanism at all iron surface areas. Initial persulfate concentration was 18 mmol L^{-1}. Error bars represent 95% interval. pH was not controlled. The final pH of all experiments at 240 minutes was 2.5.

Table 3.9. Statistical Parameters for Figure 3.4.

Iron Surface Area (cm^2)	Parameter	Slope (mmol L^{-1} persulfate min^{-1})	Intercept (mmol L^{-1})
3.2	Value	-0.00757	18.00
	Standard error	0.0039	0.0644
	R^2	0.9721	
6.1	Value	-0.0259	17.88
	Standard error	0.00065	0.0798
	R^2	0.9863	
9.4	Value	-0.0373	17.58
	Standard error	0.0013	0.189
	R^2	0.9839	
12.8	Value	-0.0503	17.305
	Standard error	0.0027	0.392
	R^2	0.9575	

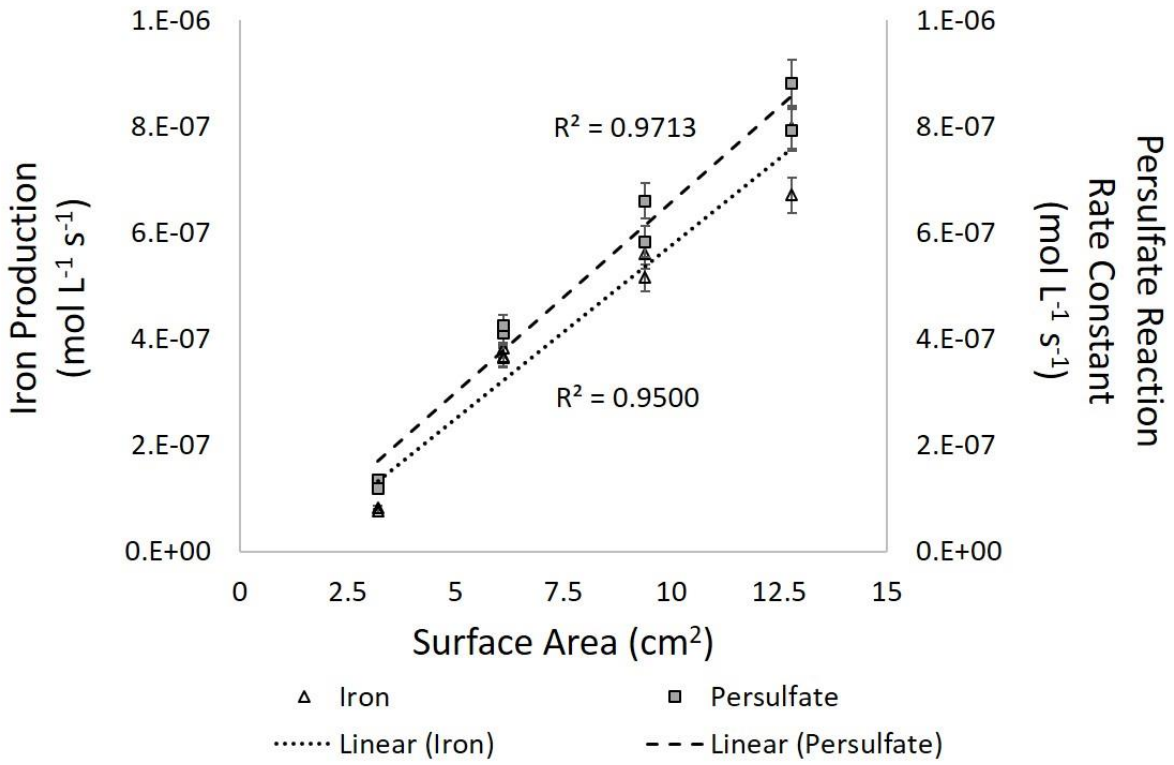

Figure 3.5. Iron production and zero-order persulfate reaction rate by iron surface area
Iron production rate and zero-order persulfate reaction rate constant as a function of solid iron surface area. The initial persulfate concentration was 18 mmol L^{-1}. Error bars represent 95% interval.

Table 3.10. Statistical Parameters for Figure 3.5.

Analyte	Parameter	Slope (mol L^{-1} s^{-1} per cm^2)	Intercept (mol L^{-1})
Iron	Value	6.526E-08	-7.663E-08
	Standard error	5.656E-09	4.757E-08
	R^2	0.9500	
Persulfate	Value	7.188E-08	-6.075E-08
	Standard error	4.670E-09	3.927E-08
	R^2	0.9713	

For surface areas and current densities, the solid iron decomposition of persulfate followed a zero-order mechanism, which is suggestive of a surface-interface dominated process. Important implications include (1) persulfate decomposition rate can be finely controlled by iron surface area, (2) persulfate decomposition can also be enhanced with the use of applied current, but diffusion limitations exist, (3) the amount of iron required to sustain the persulfate reaction can be minimized to the lower end of the PS:Fe ratio typically used to degrade contaminants with granular iron products [48, 52], and (4) solid iron can easily be removed upon reaction completion so that only the amount of iron required by the chemical reactions is introduced into the system.

3.3.2 Ciprofloxacin Experiments

Mixing phenomena: Before inserting the iron into the reaction container, a reduced ciprofloxacin concentration was noted after 5 minutes of mixing with sodium persulfate, with a significant increase in measured ciprofloxacin after 30 minutes of mixing. In a similar manner, Ji et al. (2014) noted a decrease in ciprofloxacin concentration upon mixing with persulfate, with a subsequent return to expected concentration over time [96]. Because these phenomena made it difficult to measure the true initial concentration of ciprofloxacin in solution with unactivated persulfate, the initial ciprofloxacin for all measurements was taken as the concentration of ciprofloxacin prior to mixing with persulfate, adjusted for dilution by aqueous persulfate. Ciprofloxacin concentrations as measured by HPLC-MS peaked at 30 minutes, so this was designated as the minimum time for adequate mixing, after which persulfate activation using the solid iron was initiated. At higher ciprofloxacin concentrations (0.242 mmol L^{-1} and 0.302 mmol L^{-1}), a white floc-like substance was observed to form in solution within five minutes of mixing sodium persulfate with ciprofloxacin. This floc was pH dependent and was only observed below the third pK_a (8.7) of

ciprofloxacin[96] and may be attributable to the zwitterionic characteristic of the ciprofloxacin[177]. Side-by-side comparisons did not show this effect when ciprofloxacin was mixed with potassium persulfate, potassium sulfate or sodium sulfate, which may have indicated which species (persulfate, sulfate or sodium) was responsible for the floc. The floc dissipated immediately upon addition of the iron rod and was not expected to affect results of this study.

Using HPLC-MS and IC analysis, it was determined that ciprofloxacin degradation began before persulfate activation was initiated by the iron rod, as observed by formation of expected by-products during mixing, as well as defluorination of the ciprofloxacin[44, 96, 176]. By-products with a m/z of 362, 330, and 306, as listed in Table 3.11, were observed to form in solution after 5 minutes of mixing and increase after 30 minutes of mixing. Approximately 12% defluorination was observed during the 30 minutes of mixing. Furthermore, the ciprofloxacin concentration was measure as 25% lower than expected based on ciprofloxacin concentration prior to mixing. A comparison of ciprofloxacin removal before mixing (section II) and after activation (section II) can be seen in the inset of Figure 3.6. A corresponding decrease in persulfate concentration, which would indicate persulfate activation by ciprofloxacin, was not detected.

Ciprofloxacin degradation by activated persulfate: Upon insertion of the iron rod into the ciprofloxacin-persulfate solution, ciprofloxacin degradation accelerated, as highlighted in section II of the inset of Figure 3.6. Ciprofloxacin removal increased from 20% before persulfate activation to 92% in activated persulfate after 5 minutes. Degradation plateaued at 95% removal after 15 minutes of contact with solid iron activated persulfate. These results are comparable to ferrous activated persulfate for ciprofloxacin degradation, which achieved 80% removal of ciprofloxacin in the first five minutes of the study, and overall 95.6% removal with a ciprofloxacin

Table 3.11. Primary Transformation Products

m/z	Time formed	***Time removed	Also Detected
334	*Upon activation	30 minutes	96, 176, 183
306	**Upon mixing	30 minutes	96, 183, 184
330	**Upon mixing	15 minutes	44, 60, 96, 176
362	**Upon mixing	15 minutes	96
263	*Upon activation	60 minutes	96, 183

*Upon activation indicates that this product was formed after initiation of persulfate activation by insertion of iron rod into persulfate-ciprofloxacin mixing

*Upon mixing indicates product was formed upon 5 minutes of mixing persulfate with ciprofloxacin

***Time removed indicates the time elapsed after initiation of persulfate activation

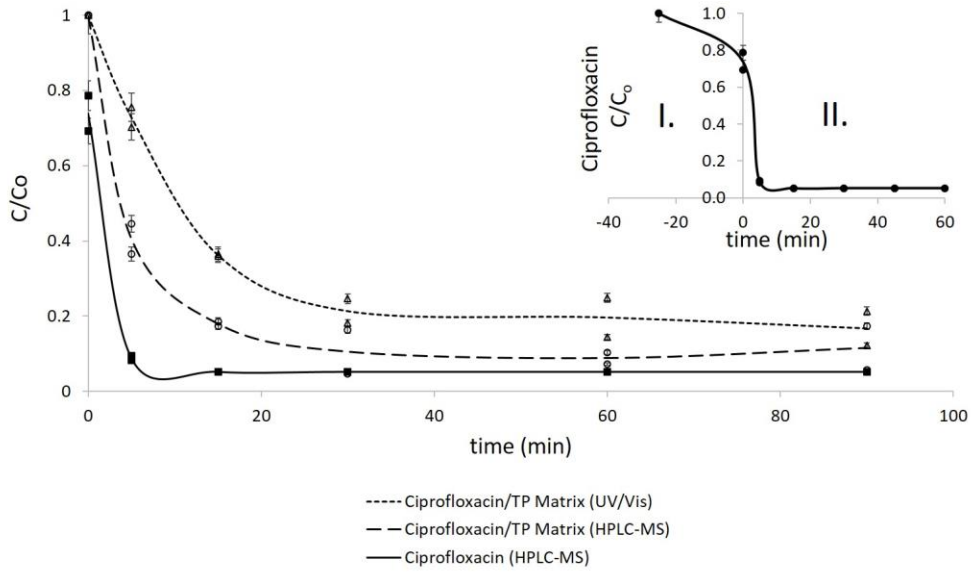

Figure 3.6. Ciprofloxacin and ciprofloxacin/TP matrix degradation as a function of time
Initial persulfate concentration was 18 mmol L^{-1}. Iron surface area=6.1 cm^2. Error bars represent 95% interval. $[Ciprofloxacin]_0$=0.121 mmol L^{-1} upon mixing with persulfate, 0.090 mmol L^{-1} upon initiation of persulfate activation at t=0. Inset: Ciprofloxacin degradation by persulfate. Section I. is ciprofloxacin removal upon mixing with persulfate, with initial concentration determined by ciprofloxacin concentration pre-mixing. Section II. is ciprofloxacin degradation upon persulfate activation by insertion of solid iron rod.

to persulfate to iron ratio of 1:20:20 [96]. Results also align with UV activated persulfate, in which 70% ciprofloxacin removal was achieved in five minutes and 98% removal overall [185]. Achieving similar removal to those established in previous studies validates solid iron as a viable method for activating persulfate to achieve contaminant removal, a key objective of this study.

While much attention has focused on removal of primary pollutants in the environmental, the formation and degradation of intermediates and by-products is gaining attention, as many of these secondary components have the potential for negative environmental impact[165, 186]. Limited information is available about the environmental effect of ciprofloxacin transformation products (TPs), but some studies have found these compounds to be mutagenic and/or genotoxic to several cell lines[187, 188]. Because of the potential environmental impact of both ciprofloxacin and its TPs, the effect of solid iron activated persulfate on generating and degrading these compounds warrants further investigation. Using HPLC-MS, this study identified the formation and removal of five TPs with the core quinolone structure intact, as well as smaller amounts of several unidentified TPs. These are listed in Table 3.11. Removal of the ciprofloxacin/TP matrix, as determined by HPLC-MS, is illustrated on the "ciprofloxacin/TP matrix (HPLC-MS)" curve on Figure 3.6. The ciprofloxacin/TP matrix undergoes removal by iron activated persulfate, albeit at a slower rate than ciprofloxacin itself. 90% of the ciprofloxacin/TP matrix was degraded in 30 minutes, with negligible removal after that time period. Because only partial mineralization occurred, as discussed in section 3.2.4, it is clear that one or more transformation products remained in solution and were not detected by the current HPLC-MS analytical methods, which is similar to the finding by Toolaram et al. (2016) in a study of photo-transformation products of ciprofloxacin [187]. It was also noted that the ciprofloxacin/TP matrix had a strong UV/Vis absorbance at 272 nm when

measured directly (without HPLC separation). The presence and removal of the matrix, determined by an examination of relative absorbance peak heights at each time point, followed a similar trend as the presence and removal measured by HPLC-MS. This trend is demonstrated on the "ciprofloxacin/TP matrix (UV/Vis)" curve in Figure 3.6.

According to UV/Vis analysis, 78% of the ciprofloxacin/TP matrix is degraded by iron activated persulfate in 45 minutes, while degradation plateaued at 83%. Although the overall removal is slightly lower than that determined by HPLC-MS, it is still higher than TOC removal discussed in Section 3.2.4. Like the HPLC-MS data, these results indicate that one or more by-products remain in solution undetected by the UV/Vis technique. Because UV/Vis provided consistent results within the range of HPLC-MS and TOC analysis, it was decided that using the UV/Vis method to compare ciprofloxacin/TP matrix removal with and without current applied to the iron anode was appropriate for the bulk solution.

Effects of applied current on ciprofloxacin/TP matrix degradation: Figures 3.7a and 3.7b show ciprofloxacin/TP matrix degradation by solid iron activated persulfate with and without an applied current. A maximum current density of 11.5 mA cm^{-2} was tested because persulfate activation plateaued at this level per Figure 3.3b. The ciprofloxacin/TP matrix was characterized to degrade in a pseudo-first-order manner with respect to the matrix. Data from the 0.121 mmol L^{-1} experiments without applied current resulted in a pseudo-first-order reaction rate constant, $k_{1,cip}$, of 6.58 x 10^{-4} s^{-1}. This pseudo-first-order reaction rate constant was independent of current, as discussed below and tabulated in Table 3.12. An average of 83% ciprofloxacin/TP matrix removal was achieved across all data sets in Figure 3.7a and a total of 1.1 mmol L^{-1} iron was added to solution to achieve this removal. Although most degradation reactions using persulfate are

characterized as pseudo-first-order with respect to the analyte, the predicted higher order nature of these reactions leads the reaction rate to vary slightly with different ratios of analyte to persulfate. In many cases, less analyte and or more persulfate will drive the reaction more quickly or vice-versa [96]. This effect is seen currently, with a pseudo-first-order reaction rate constant, $k_{1,cip}$, of 4.59×10^{-4} s^{-1} when initial ciprofloxacin concentration is doubled to 0.242 mmol L^{-1}.

In iron activated persulfate degradation studies of trichloroethylene and pentachlorophenol, increasing current applied to an iron rod enhanced removal rates[141, 142]. In contrast, the rate and extent of ciprofloxacin/TP matrix removal in this study was independent of applied current, as shown by the overlapping curves in Figures 3.7a and 3.7b. Ciprofloxacin/TP matrix removal was constant at the four current densities tested despite higher rates of persulfate decomposition as current density increased (Figure 3.8). Increased iron introduction by the applied current, and the resulting increased persulfate activation, may generate an overabundance of radical scavenging ferrous ions (equation 1.13) as well as propagate self-scavenging by sulfate and hydroxyl radicals. These effects have been noted to inhibit contaminant removal at high iron or persulfate levels in some other studies[48].

Defluorination, mineralization and degradation mechanism: Fluoride abstraction is an important outcome in the degradation of fluorinated pharmaceuticals, as it may lower their toxicity[189]. Figure 3.9a shows ciprofloxacin degradation along with fluoride generation from ciprofloxacin. Defluorination slightly lags ciprofloxacin removal, with 75% de-fluorination achieved in 5 minutes, as shown in Figure 3.9b. De-fluorination reached >95% after 15 minutes, in line with the 95% ciprofloxacin removal achieved in this same time period. This degree of fluoride removal is significantly higher than that achieved by some other ciprofloxacin degradation

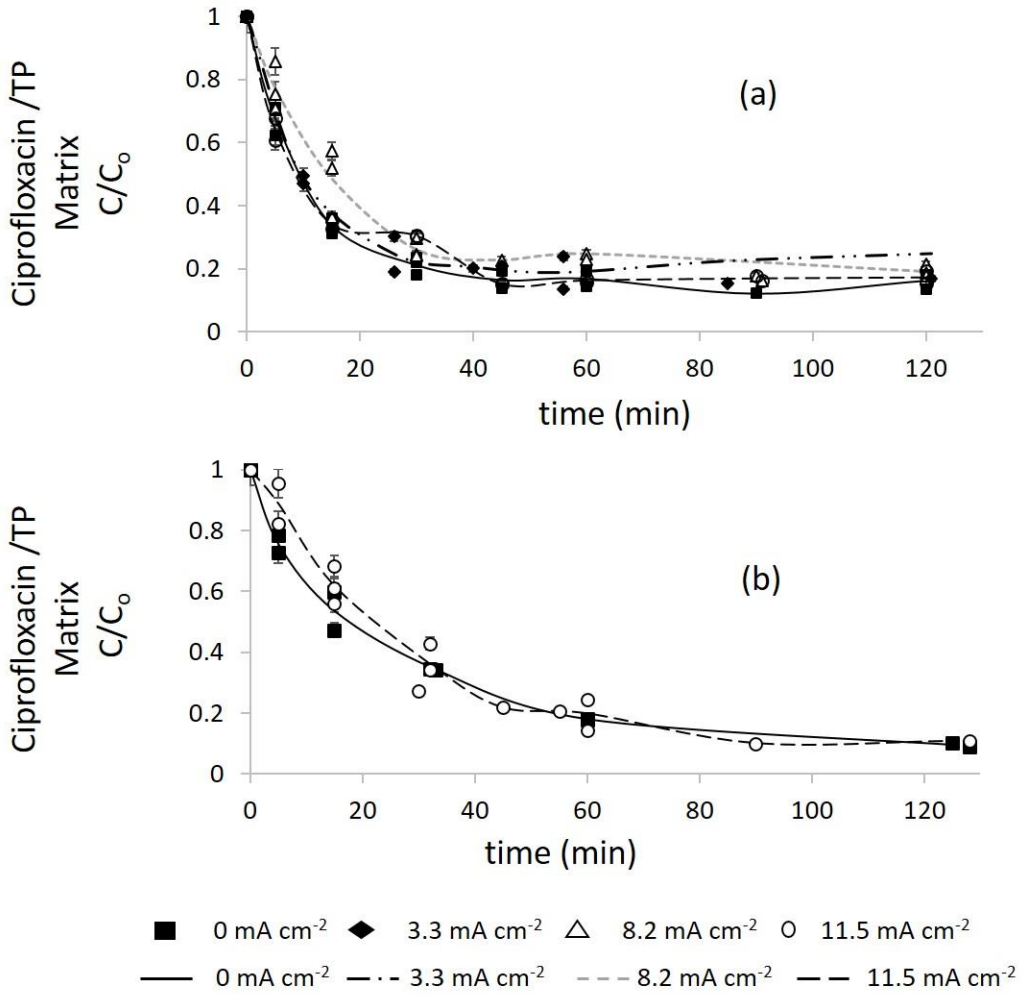

Figure 3.7. Ciprofloxacin degradation at various current densities, as a function of time
Initial persulfate concentration was 18 mmol L^{-1}. Iron surface area=6.1 cm^2. Error bars represent 95% interval. (a) $[Ciprofloxacin]_0$=0.121 mmol L^{-1} (b) $[Ciprofloxacin]_0$=0.242 mmol L^{-1}. Measured via UV/Vis absorbance.

Table 3.12. Statistical Parameters for ciprofloxacin/TP matrix pseudo-first order degradation reaction rate constants

[Ciprofloxacin]$_o$ = 0.121 mmol L^{-1}]

Current Density (mA cm^{-2})	Parameter	Slope (s^{-1})	Intercept (LN (C/C$_o$ cipro)
0.0	Value	-0.000658	-0.2129
	Standard error	0.000111	0.167
	R^2	0.9220	
3.3	Value	-0.000653	-0.18451
	Standard error	0.000136	0.199
	R^2	0.9199	
11.5	Value	-0.000628	-0.202
	Standard error	0.000104	0.157
	R^2	0.9244	
MeOH Quench	Value	-0.000115	0.0608
(no current)	Standard error	2.0E-05	0.062
	R^2	0.9138	
TBA Quench	Value	-0.000151	0.0380
(no current)	Standard error	1.3E-05	0.024
	R^2	0.9861	

[Ciprofloxacin]$_o$ = 0.242 mmol L^{-1}]

Current Density (mA cm^{-2})	Parameter	Slope (s^{-1})	Intercept (LN (C/C$_o$ cipro)
0.0	Value	-0.000460	-0.116
	Standard error	3.29E-05	0.0621
	R^2	0.9848	
11.5	Value	-0.000487	-0.0293
	Standard error	4.09E-05	0.0836
	R^2	0.9726	

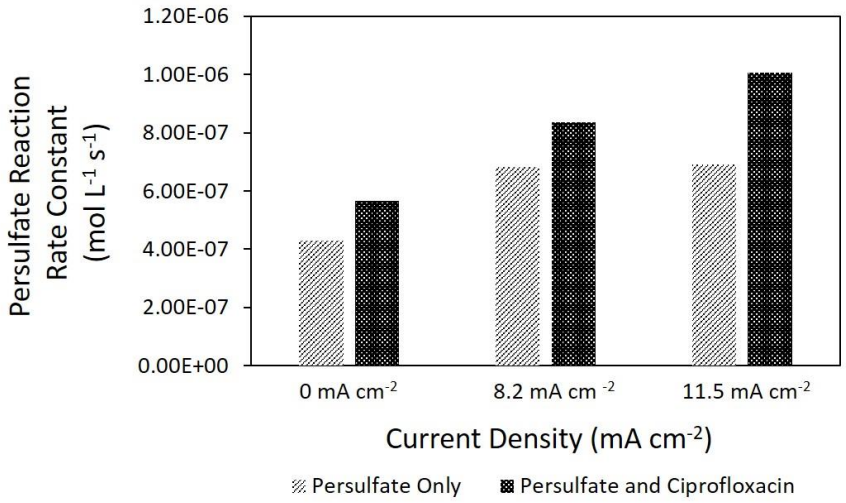

Figure 3.8. Persulfate decomposition rate with and without ciprofloxacin
Shown for three different current densities. $[Ciprofloxacin]_0$= 0.121 mmol L^{-1} $[Persulfate]_0$=18 mmol L^{-1} . Iron surface area=6.1 cm^2. Quinoline degradation intermediates are suggested to enhance persulfate activation.

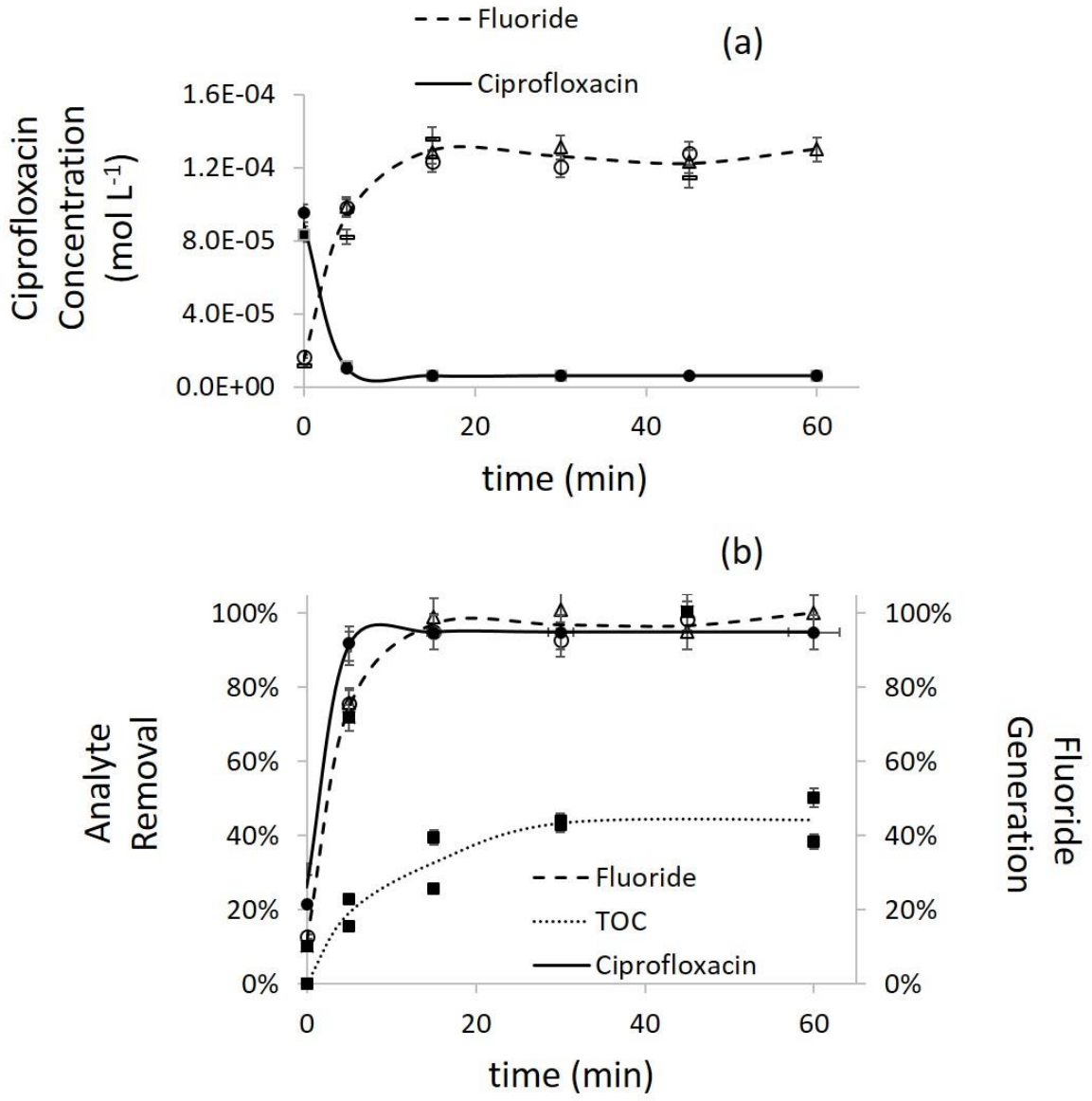

Figure 3.9. Fluoride generation and TOC removal as a function of time
(a) Ciprofloxacin degradation and fluoride generation from ciprofloxacin as a function of time. (b) Comparison of relative degrees of ciprofloxacin or TOC removal and fluoride generation as a function of time. Initial ciprofloxacin and persulfate concentrations were 0.121 mmol L^{-1} and 18 mmol L^{-1}, respectively . Iron surface area=6.1 cm^2. Error bars represent 95% interval.

studies indicating that solid iron activated persulfate may offer an advantage for removal of some fluorinated compounds[176, 183].

As mention previously, TPs with m/z of 362, 330, and 306 formed upon mixing of ciprofloxacin with persulfate. Additionally, upon activation of persulfate, compounds with m/z of 334 and 263 were detected, as outlined in supplementary table 3.11. The presence of these TPs corresponds with degradation pathways of piperazine ring cleavage and substitution described in other studies [96, 176]. The compound with m/z 330, where fluoride is replaced by a hydroxyl radical, was detected at high levels upon mixing, as well as in the initial 15 minutes of the reaction, which corresponds with the quick de-fluorination observed in the first 15 minutes. Based on these findings, substitution is suggested as the primary degradation mechanism for ciprofloxacin removal by solid iron activated persulfate. At the end of 60 minutes, the five primary TPs named in this study were non-detectable in solution, and only unidentified compounds remained.

Total organic carbon (TOC) removal is shown in Figure 3.9b. At the end of 60 minutes, an average of 44% TOC was removed from solution, afterwards which removal plateaued. Incomplete mineralization was achieved with this process and follow-up studies are recommended to identify the presence and hazards of compounds remaining in solution.

Quenching studies to determine dominant radicals: The relative contribution of the sulfate and hydroxyl radicals to ciprofloxacin degradation was studied using radical quenchers methanol and tert-butanol (TBA). Methanol has high reaction rates with both radicals, with a reaction rate constant of 1.0×10^7 M^{-1} s^{-1} for the sulfate radical and 9.7×10^8 M^{-1} s^{-1} for the hydroxyl radical [42]. TBA has a slower reaction rate with the sulfate radical, with a rate constant of $(4.0\text{-}9.1) \times 10^5$ M^{-1} s^{-1} for the sulfate radical versus a reaction rate constant of $(3.8\text{-}7.6) \times 10^8$ M^{-1} s^{-1} with the hydroxyl

radical [42]. The ciprofloxacin pseudo-first order reaction rate constants with and without quenching are illustrated in Figure 3.10. With TBA preferentially quenching hydroxyl radicals, the ciprofloxacin rate constant decreased by 77.1% (from 6.58 to 1.51 x 10^{-4} s^{-1}), indicating that hydroxyl radicals play a substantial role in the degradation process. With methanol quenching both hydroxyl and sulfate radicals, the ciprofloxacin rate constant only decreased another 5.4% to a value of 1.15 x 10^{-4} s^{-1}, suggesting that sulfate radicals play a far less significant role in the degradation mechanism than hydroxyl radicals. Some studies suggest that the hydroxyl radical is the dominant reactive species in iron-activated persulfate systems, even at acidic pH, and the current findings supports this conclusion[141, 190]. This hydroxyl dominated process may explain the primary degradation pathway of fluoride substitution by hydroxyl species noted in section 3.2.4. As noted by Yuan et al. (2014) during quenching studies of trichloroethylene degradation with iron activated persulfate, the degradation reaction was not completely quenched by the radical scavengers, which implies that other reactive species may be involved in the degradation mechanism [141]. Hydrogen peroxide, theoretically present in solution, was not detectable in this study.

Persulfate usage during ciprofloxacin degradation: Of note is the enhanced persulfate decomposition with ciprofloxacin in solution (Figure 3.8). Fang et al. (2013) demonstrated persulfate activation by quinones and compounds containing quinone structures such as ciprofloxacin[51]. Control experiments in this study did not show persulfate activation by ciprofloxacin directly, so it is theorized that, in this case, a quinone degradation intermediates enhanced the reaction. This may have broad implication for activated persulfate degradation of ciprofloxacin using other persulfate activators.

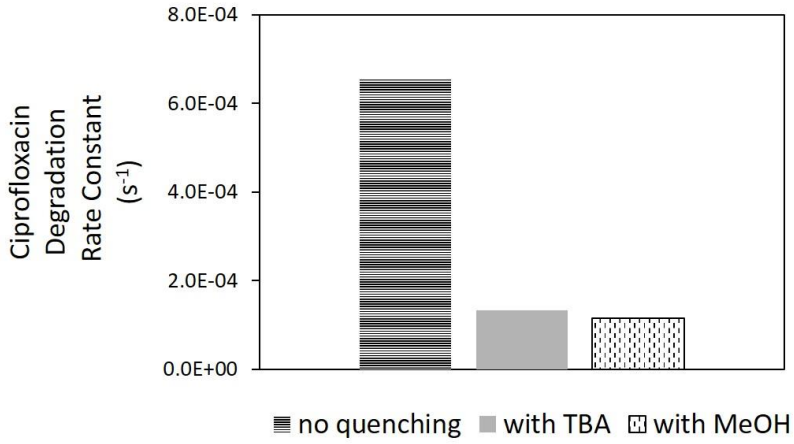

Figure 3.10. Ciprofloxacin/TP matrix pseudo-first order rate constants with quenching. Initial ciprofloxacin and persulfate concentrations were 0.121 mmol L^{-1} and 18 mmol L^{-1}, respectively . Iron surface area=6.1 cm^2. Concentration of methanol and TBA quenchers was 220 mmol L^{-1}. Measured by UV/Vis.

The reaction stoichiometric ratio (RSE) can be used to compare degradation results for different analytes and between activation techniques. It is defined as the number of moles of analyte removed divided by the number of moles of persulfate consumed, reported as a percentage [166]. The RSE for the ciprofloxacin/TP matrix for experiments without current (Figure 3.7a) was 7.7% at 30 minutes and 5.6% at 60 minutes. In comparison, the RSE for ibuprofen degradation by heat activated persulfate was 7.5% and the RSE for sulfamethoxazole removal by Fe^0 activated persulfate was 6.0%, both measured at 60 minutes[95, 165]. For sulfamethoxazole removal by micrometric Fe^0 activated persulfate, the RSE was 3.7% in 60 minutes[102]. The similar scale of pharmaceutical to persulfate ratios achieved across studies may provide guidance or expectations for future work in this area. For experiments in this study conducted with 8.2 mA cm^{-2} applied current, (Figure 3.7a), the RSE for the ciprofloxacin/TP matrix was 3.5% at 30 minutes and 1.0%

at 60 minutes. The lower RSE with applied current was a result of similar ciprofloxacin/TP matrix degradation with higher persulfate activation when current was applied.

3.4 Conclusion

Persulfate activation by solid iron is proposed to be a surface dominated mechanism. The fundamental relationships between iron surface area, applied current, iron production and persulfate activation were elucidated by experimentation without analyte in solution. Sustained persulfate activation can be accomplished with the use of solid iron, with 1.14 moles of persulfate activated for 1 mole of iron used. The surface area of the solid iron can be adjusted to control the persulfate activation rate. Applied current enhances persulfate activation until diffusion limitations are reached. Ciprofloxacin was degraded by solid iron activated persulfate, with 95% removal achieved in 15 minutes under experimental conditions. Furthermore, the corresponding transformation product matrix was also removed by 90% in 30 minutes by solid iron activated persulfate process. The ciprofloxacin/transformation product matrix degrades via a pseudo-first order mechanism with respect to the matrix, with hydroxyl radicals identified as the primary reactive species. Defluorination under the same conditions was >95%, demonstrating that solid iron activated persulfate may offer an advantageous technique for removal of fluorinated environmental contaminants. Enhancement of the ciprofloxacin degradation was not achieved by applying a current to the iron electrode despite increased persulfate activation. This is possibly due to the scavenging effect of excess ferrous ions and radical species.

CHAPTER FOUR: UNDERSTANDING ELECTROCHEMICALLY ACTIVATED PERSULFATE AND ITS APPLICATION TO CIPROFLOXACIN ABATEMENT

This chapter is revised based on a paper published as follows:

Matzek, L.W., Tipton, M.J., Farmer, A.T., Steen, A., Carter, K.E., 2018. Understanding Electrochemically Activated Persulfate and Its Application to Ciprofloxacin Abatement. Environ Sci Technology.

4.1 Introduction

Electrochemically activated persulfate (EAP) analyte removal has not been widely addressed except in cases where iron is a co-activator[48, 191]. EAP without an iron co-activator avoids the use of a sacrificial anode and the introduction of iron in systems where this would not be suitable. Studies investigating EAP without iron suggest persulfate activation, through direct electron transfer at the cathode, creates sulfate radicals (Equation 2.3)[59, 133].

Recent studies found persulfate addition to electrochemical abatement of industrial wastewater improved removal of dinitrotoluene and aniline but did not compare the effects created by sulfate addition[59, 133]. Another report indicated persulfate addition to sodium chloride electrolyte increased COD removal for malachite green and 2,4-dinitrophenol while sulfate did not, though differences between these electrolytes was not the focus[192]. Farhat et al. (2015) found that persulfate addition to nitrate electrolyte did not result in as fast of a diatrizoate removal rate as in pure sulfate[42]. However, equimolar amounts of persulfate and sulfate were not compared, and cathodic persulfate activation was not explored[42].

Other studies have examined the role of sulfate radicals (E^o = 2.5-3.1 V) in EAOP[42, 193]. Sulfate radicals form anodically using BDD electrodes (Equation 4.1) and will degrade many organic analytes[42, 48]. These radicals can also form reactive hydroxyl radicals (Equation 4.1) [48].

Higher removal rates for diatrizoate and carbamazepine were achieved in sulfate versus nitrate electrolyte, which was credited to anodic sulfate radical formation[42, 193].

(4.1) $SO_4^{2-} \rightarrow SO_4^{\cdot -} + e^-$

The purpose of this study is to explore/characterize/quantify enhanced electrochemical removal of organic species observed in sulfate and persulfate electrolytes, including the roles played by sulfate radical formation at the anode and persulfate activation at the cathode.[133, 192] Elucidating the sources and roles reactive species play in sulfate radical-based systems lends insight to appropriate application and design of electrochemical abatement systems. Finally, although fluoroquinolone removal has previously been demonstrated at a boron-doped diamond (BDD) anode in synthetic urine and a SnO_2/Sb-Ti anode in sodium sulfate, it has not been evaluated in the EAP system[44, 194]. Thus, this study aims to assess EAP's ability to remove ciprofloxacin and investigate removal mechanisms as a step in screening EAP as an appropriate point source treatment for wastewaters with high antibiotic content[22, 44].

4.2 Materials and Methods

4.2.1 Chemicals

Ciprofloxacin (98%), sodium persulfate (98%), potassium sulfate, sodium nitrate, potassium iodide (99+%), sodium bicarbonate (Acros Organic, Fair Lawn, NJ), Optima formic acid, sodium hydroxide, hydrochloric acid, Optima Methanol (MeOH), tert-butanol (TBA), dimethyl sulfoxide (DMSO), and fluoride standard were purchased from Fisher Scientific (Pittsburg, PA) and 1N sulfuric acid was from J.T. Baker. Deionized water (DI) (18.2 MΩ-cm) was produced by a Millipore Milli-Q system.

4.2.2 Experimental Setup

Rotating disk electrode (RDE) experiments were performed using a SP-150 potentiostat (Bio-Logic Science Instruments, Knoxville, TN) with a mercury-mercury sulfate reference electrode in single-cell or split-cell configuration, illustrated by Figures 4.1a and 4.1b. A multi-speed rotator (Pine Research Instrumentation, PRI, Durham, NC) was set to 2000 rpm for RDE experiments with bulk mixing with a magnetic stir-bar. Anodes (0.5 cm O.D., 0.196 cm^{-2} surface area) were a change-disk RDE tip (PRI) with BDD electrode insert (Fraunhofer Center for Coatings and Diamond Technologies, East Lansing, MI), or fixed-disk platinum (Pt) RDE tip (PRI). The potential window for the BDD was -1.2V to 2.5V vs. SHE. Cathodes were Electron Microscopy Science graphite (Gr) rods (0.30 cm O.D) (Fisher Scientific, Pittsburg, PA), or a platinum wire (0.5 mm O.D.) (PRI). Cathodic surface areas exposed to solution were 4.8 cm^2 for graphite and 3.69-4.76 cm^2 for Pt. Potential windows for cathode materials are -1.5 to 1.5 V (Gr) and -0.85 to 1.9 V (Pt) [195].

For single-cell persulfate experiments, 200 mL of 22 mmol L^{-1} persulfate was electrolyzed and sampled periodically. Single-cell ciprofloxacin experiments used 50 mL of 0.171 mmol L^{-1} ciprofloxacin (0.1% sulfuric acid to aid dissolution) mixed with 140 mL DI water. The solution was spiked with 10 mL concentrated electrolyte just before applying constant anodic current density of 76 mA cm^{-2}, unless noted otherwise. Initial concentrations were 0.043 mmol L^{-1} ciprofloxacin plus 22 mmol L^{-1} sulfate or persulfate, or 66 mmol L^{-1} nitrate, maintaining the same ionic strength for all solutions. Quenching experiments were performed by replacing some water with TBA or DMSO to achieve quencher concentration of 2200 mmol L^{-1}, which provided 100:1 a quencher to persulfate ratio[158, 185].

Split-cell experiments were performed using 300-mL anodic and 80-mL cathodic compartments. Reaction times were normalized to a 200-mL volume per Equation 4.2.

(4.2) $$\text{reaction time}_{\text{normalized}} = \text{time}_{\text{reaction}} \text{ x } \frac{\text{normalzied volume}}{\text{reactor volume}}$$

A cation-exchange Chemours 115 Nafion membrane (Fuel Cell Store, College Station, TX), separated the compartments and was experimentally confirmed not to transmit nitrate/sulfate/persulfate anions. Current density of 28.5 mA cm^{-2} was employed due to system physical limitations. For ciprofloxacin removal, outcomes are indicative of behavior in the single-cell reactor, but numerical results are not directly comparable due to current densities utilized.

Experiments were performed in duplicate at 20˚C. Initial pHs averaged 4.5 upon mixing ciprofloxacin and electrolytes. Average final pHs were 2.5, 6.5, and 8.0 in persulfate, sulfate, and nitrate, respectively. pH was not controlled in any experiments as buffer anions can significantly alter the system chemistry confounding interpretation of the results[104, 135, 141, 177, 196, 197]. As the pH range impacts the kinetics of electrochemical degradation reactions by influencing the active radical species involved (hydroxyl or sulfate)[48], this study aims to understand the natural progression of these reactions, including the possibility that different reaction kinetics may occur due to pH shifts from different species formed in the three electrolytes.

4.2.3 Analytical Methods

Persulfate and ciprofloxacin-matrix concentrations were analyzed using a ThermoScientific Evolution 600 UV/Vis spectrometer (ThermoFisher, Pittsburg, PA) at 272 and 352 nm, respectively, with methodology described in Chapter 3[180, 181, 191].

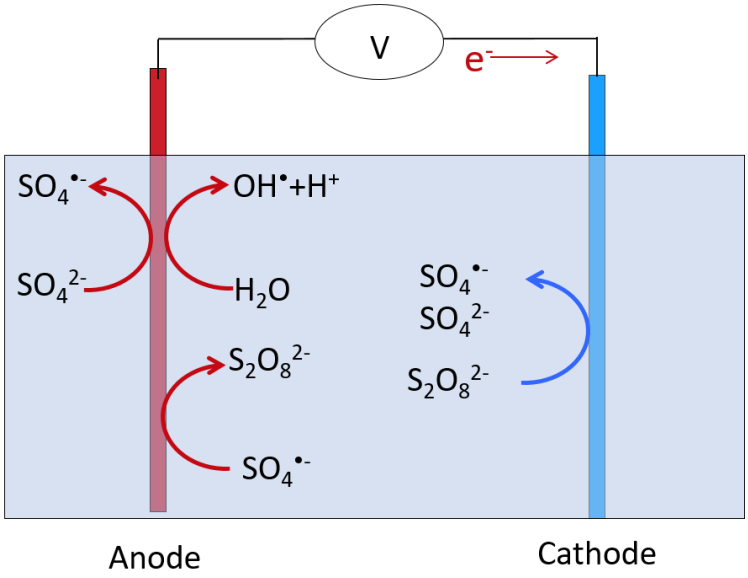

Figure 4.1a. Single-cell reactor with rotating disk electrode (RDE)
Total volume = 200 mL.

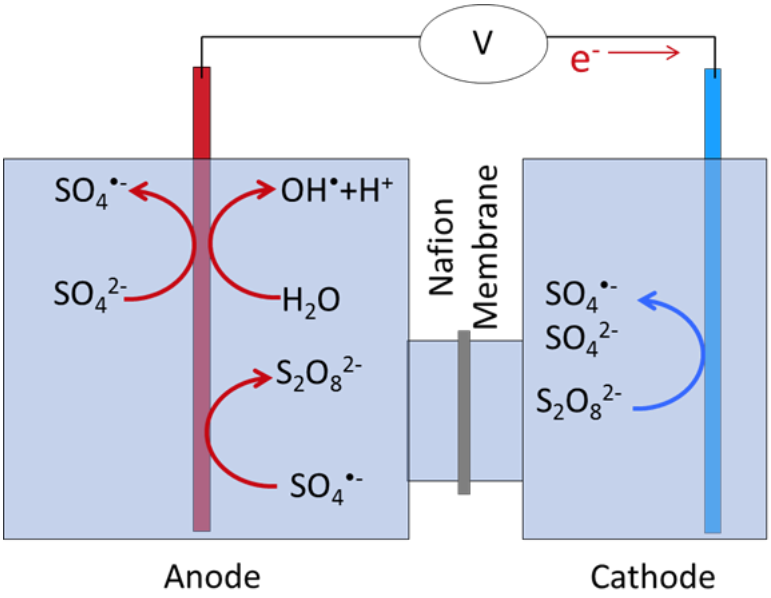

Figure 4.1b. Split-cell reactor with rotating disk electrode (RDE)
Anode Volume = 300 mL. Cathode volume = 80 mL.

In Chapter 3, it was shown that the "ciprofloxacin-matrix" concentrations measured by UV/Vis *without* HPLC separation were proportional to the total concentration determined by HPLC-MS analysis of a mixture containing ciprofloxacin and its transformation byproducts, which includes core quinolone structures with potentially negative environmental effects[187, 188, 191]. This matrix's UV/Vis absorbance is attributed to ciprofloxacin and its transformation products containing the C=C-C=C-C=C-C=0 chromophore[198]. While ciprofloxacin-matrix concentration does not account for every degradation by-product that may be generated, it is a consistently reproducible and easily modeled variable found to be proportional to actual ciprofloxacin and TOC concentrations. Because of its repeatability, proportionate relationship to TOC, and inclusion of significant by-products, the ciprofloxacin-matrix concentration is utilized in this study to compare results between experimental runs.

Waters Sep-Pak tC2 cartridges were used to extract ciprofloxacin for HPLC-UV and HPLC-MS analysis. Cartridges were conditioned with 1 mL methanol then 1mL DI water. A 0.5-mL sample was loaded then extracted using 2X1-mL quantities of methanol/0.1% formic acid.[191] The extraction efficiency was 80%, measured by comparing extracted standards to standards made in methanol/0.1% formic acid.

Extracted ciprofloxacin was quantified by separation using a Shimadzu HPLC equipped with binary pumps, a Hypersil Gold column (100 mm × 4.6 mm I.D. , 5 µm diameter) (Thermoscientific, Waltham, MA) and a SPD-M20A diode array detector. A gradient eluent separation was used with eluent "A" DI water/0.1% formic acid and eluent "B" acetonitrile/0.1% formic acid. A multi-step gradient program varied from 5% - 95% eluent A over 20 minutes (Table 4.1). Column temperature was held at 40˚C. Sample absorbance was measured at 278 nm, which

was confirmed to be the absorbance maximum of ciprofloxacin standards. Statistics for the calibration curve are provided in Table 4.2. The instrument detection limit was 0.30 µmol L^{-1} and method detection limit was 0.38 µmol L^{-1}.

Table 4.1. HPLC-UV Multi-step Gradient Program

Time (min)	% A
0	5
2	5
8	75
12	75
14	95
16	95
19	5
20	5

Table 4.2. Statistical Parameters for HPLC-UV

	Slope (peak area per µmol L^{-1})	Intercept (peak area)
Value	14004	-12353
Standard error	211	4835
R^2	0.9993	

Extracted samples were diluted with methanol and analyzed for intermediates and transformation by-products using a Thermo Scientific Exactive™ Plus Orbitrap LC-MS with ultimate 3000 RS pump, column compartment, autosampler, and diode array detector (ThermoFisher, Pittsburgh, PA). The mobile phase consisted of 80/20 methanol/water with flow rate 0.2mL min^{-1}, 10-minute run time, and 10-µL sample injection. UV/Vis was used to detect the antibiotic and byproduct species at 275 nm and 3D field from 200-400nm[199]. A mass to charge (m/z) scan range of 50-500 m/z with resolution of 140,000 was performed using positive mode

electrospray ionization and data was analyzed to determine masses of both the parent compounds and the degradation/transformation byproducts[199-201].

TOC was analyzed using a Shimadzu TOC-L analyzer with an ASI-L autosampler. Samples were diluted 1:4 with acidified DI water (pH 3.0 with HCl). Statistical parameters for the method were described in Chapter 3[191].

Hydrogen peroxide concentrations were determined by reacting equal volumes of sample with ammonium metavanadate. The metavanadate solution was prepared with 1-part ammonium metavanadate in 9.5 parts 1N sulfuric acid at 50˚C, then diluted with DI water to a final concentration of 12 mM and 114 mM, respectively. Absorbance was measured using the Evolution 600 UV-Vis (wavelength 450 nm) [42, 202]. Absorbance was compared to solutions of known hydrogen peroxide concentrations.

Ion chromatography used to analyze fluoride (F^-) concentrations using a Dionex 2100/1100 dual column system with background suppression. pH of all samples was raised to 6, dissociating any potential hydrofluoric acid. Fluoride detection limit was less than 5.2 µmol L^{-1} F^- ions as described in Chapter 3.

4.3 Results and Discussion

4.3.1 Electrochemical persulfate decomposition and regeneration

Persulfate behavior was investigated without an analyte using a single-cell RDE system for three anode/cathode combinations: Pt/Gr, BDD/Gr and BDD/Pt. The persulfate removal rate was measured to demonstrate the maximum potential persulfate activation rate based on equation 1.3. For persulfate formation at the anode, this removal rate becomes the net rate of persulfate reduction (or activation) at the cathode and persulfate generation at the anode (Equation 4.3). Similar results

were obtained for all electrode combinations with R^2>0.95 linear relationship of persulfate decomposition with time. Plots for BDD/Gr (Figure 4.2a) illustrate these findings. The zero-order mechanism indicates a surface-dominated reaction with the net persulfate reaction rate a function of current density (Figure 4.3a and 4.3b). Persulfate reaction rates were independent of anode material but were higher using a Gr-cathode compared to a Pt-cathode, as shown in Figures 4.3a and b. Additional experiments investigating the effects of cathode material for ciprofloxacin removal using EAP are described in *Ciprofloxacin Degradation* section.

To further explore the role of sulfate radicals in EAOP, electrochemical persulfate removal and generation were examined using split-cell RDE experiments with a BDD/Gr anode/cathode combination. Anodic persulfate generation from sulfate, shown to be a zero-order mechanism in Figure 4.2c, was used to demonstrate the presence of sulfate radicals, as sulfate-radical based reactions (Equation 4.3) have been shown to be the dominant mechanism of persulfate production at BDD anodes.[203]

(4.3) $SO_4^{\cdot -} + SO_4^{\cdot -} \rightarrow S_2O_8^{2-}$

During this process, persulfate becomes available in sulfate solution to initiate non-radical degradation or degradation through persulfate activation at the cathode[42, 133, 203]. As expected, no persulfate was formed in the sulfate solution from cathodic reactions (Figure 4.2c) and no hydrogen peroxide was detected in any of the solutions. Further evaluation of H_2O_2 suggests that reaction potentials used were outside the ideal range for H_2O_2 formation[204]. As the solution was not oxygenated, which aids H_2O_2 production (Equation 4.4)[204], this species was determined to have no significant influence in the current EAP system[204].

(4.4) $O_2 + 2H^+ + 2e^- \rightarrow H_2O_2$

Figure 4.2b shows the persulfate concentration remained constant at the anode, thus persulfate activation by anodically generated hydroxyl radicals was ruled out. Persulfate decomposition at the cathode followed a zero-order mechanism. The zero-order persulfate reaction rate constant of 1.85 x 10^{-7} mol L^{-1} s^{-1} at a cathodic current density of 1.2 mA cm^{-2} corresponds to the potential sulfate radical formation rate. When the anodic persulfate formation rate of 3.40 x 10^{-9} mol L^{-1} s^{-1} was subtracted from the cathodic persulfate decomposition rate, the net reaction rate change in the divided cell was 1.82 x 10^{-7} mol L^{-1} s^{-1}, higher than the 1.5 x 10^{-7} mol L^{-1} s^{-1} predicted by the single-cell curve in Figures 4.3a and b at the same current densities (28.5/1.2 mA cm^{-2} anode/cathode, respectively). Differences in single-cell and split-cell reaction rate constants imply the persulfate activation and generation processes may be dependent on one another and are influenced by reactions occurring at the opposite electrode. Experiments determining whether cathodic persulfate decomposition corresponds to sulfate radical formation at the cathode are discussed in *Cyclic voltammetry* and *Using ciprofloxacin to evaluate persulfate activation* sections.

4.3.2 Ciprofloxacin Degradation

Removal of ciprofloxacin (extracted and separated by HPLC), ciprofloxacin-matrix (measured by UV-Vis; see *Analytical Methods*) and TOC was compared for BDD/Pt and BDD/Gr electrode pairs in a single-cell RDE system to establish how cathode materials affect EAP during analyte removal. The pseudo-first order rate constants (and relevant statistics) for the ciprofloxacin, ciprofloxacin-matrix and TOC removal (with respect to these variables) by cathode type are shown in Tables 4.3a, b and c.

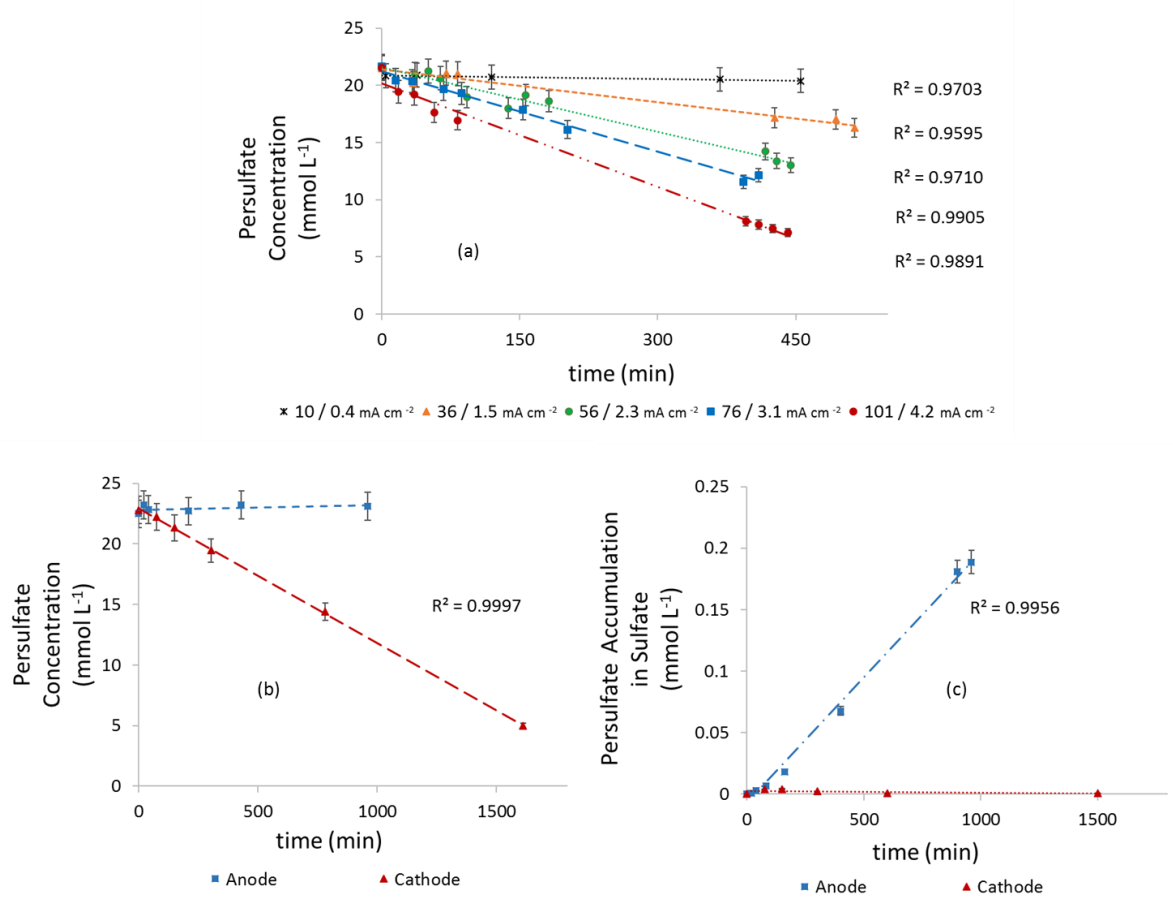

Figure 4.2. Persulfate concentration with time in an electrochemical reactor
(a) Zero-order persulfate removal over time in a single-cell reactor with $[Persulfate]_0$= 22 mmol L^{-1}. Legend values denote anodic / cathodic current densities. (b) Persulfate concentration versus time with $[Persulfate]_0$= 22 mmol L^{-1} in a split cell reactor. Anodic current density =28.5 mA cm^{-2} and cathodic current density = 1.2 mA cm^{-2}. (c) Persulfate concentration versus time with $[Sulfate]_0$ =22 mmol L^{-1} in a split cell reactor. Anodic current density =28.5 mA cm^{-2} and cathodic current density = 1.2 mA cm^{-2}. (a-c) BDD/Gr anode/cathode pairs. No organic analyte. Error bars represent the 95% interval.

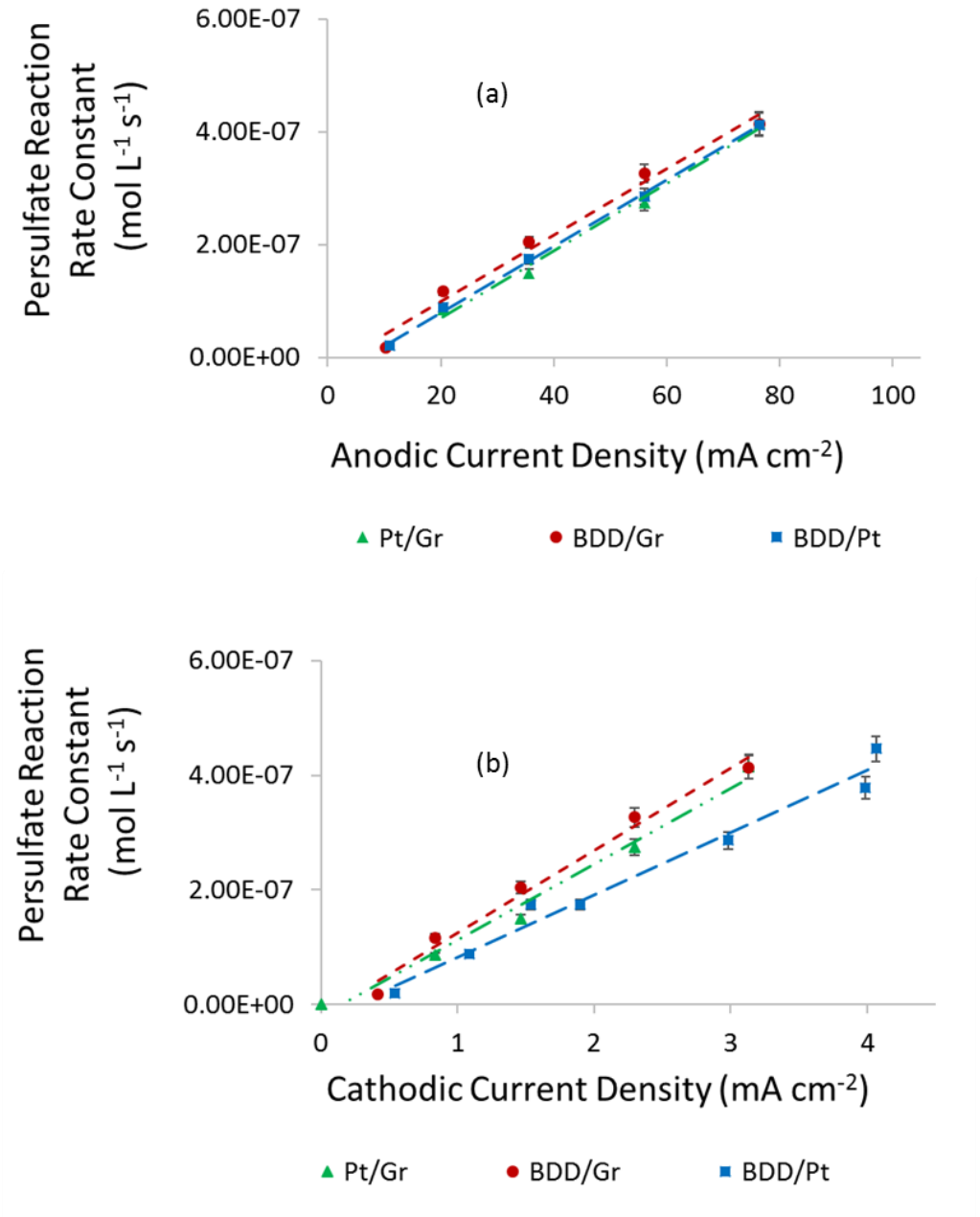

Figure 4.3. Persulfate reaction rate as a function of current density
(a) Persulfate zero-order reaction rate constant as a function of anodic current density. (b) Persulfate zero-order reaction rate constant as a function of cathodic current density. Error bars represent the 95% interval.

Table 4.3a. Effects of Cathodes on Removal Rates of Ciprofloxacin

Electrolyte	Cathode	Ciprofloxacin pseudo-first order rate constant (s^{-1} x 10^{-5})	Pseudo-first order fit (r^2)	Difference (%)	Statistical significance of difference
Persulfate	Pt	1.92 ± 0.21	0.9907	8%	0.5902
	Gr	2.08 ± 0.58	0.9112		(not significant)

Table 4.3b. Effects of Cathodes on Removal Rates of Ciprofloxacin-Matrix

Electrolyte	Cathode	Ciprofloxacin pseudo-first order rate constant (s^{-1} x 10^{-5})	Pseudo-first order fit (r^2)	Difference (%)	Statistical significance of difference
Persulfate	Pt	4.52 ± 0.22	0.9954	5%	0.5769
	Gr	4.28 ± 0.18	0.9907		(not significant)
Sulfate	Pt	2.28 ± 0.22	0.9849	4%	0.6663
	Gr	2.31 ± 0.09	0.9892		(not significant)
Nitrate	Pt	0.54 ± 0.16	0.7624	19%	0.3029
	Gr	0.44 ± 0.12	0.7691		(not significant)

Table 4.3c. Effects of Cathodes on Removal Rates of TOC

Electrolyte	Cathode	TOC pseudo-first order rate constant (s^{-1} x 10^{-5})	Pseudo-first order fit (r^2)	Difference (%)	Statistical significance of difference
Persulfate	Pt	0.86 ± 0.21	0.9465	6%	0.6735
	Gr	0.81 ± 0.24	0.9270		(not significant)
Sulfate	Pt	0.42 ± 0.13	0.8723	-5%	0.7871
	Gr	0.44 ± 0.17	0.9047		(not significant)
Nitrate	Pt	0.099 ± 0.34	0.0787	75%	0.6930
	Gr	0.025 ± 0.28	0.0059		(not significant)

Differences in ciprofloxacin, ciprofloxacin-matrix and TOC degradation rates were statistically insignificant with Pt- and Gr-cathodes. It was concluded that graphite is a suitable substitute for platinum for ciprofloxacin removal using EAP.

Electrolyte effects on ciprofloxacin, ciprofloxacin-matrix and TOC removal were compared using the single-cell RDE with nitrate, sulfate or persulfate. The ciprofloxacin decay mechanism was pseudo-first order with respect to ciprofloxacin in all electrolytes, as shown in Figures 4.4 and 4.5a. The pseudo-first order rate constants (and relevant statistics) for are shown in Table 4.4. Ciprofloxacin degraded rapidly upon electrolysis in persulfate (Figures 4.4), reaching 84% of the initial concentration after 120 minutes and plateauing at 90% after 240 minutes. The removal rate in sulfate was 33% slower, although similar degrees of removal were achieved within 240 minutes. Much slower removal was observed in nitrate, reaching 90% in 24 hours (Figure 4.5a). A sixfold increase in the overall reaction rate constant was observed using sulfate in place of nitrate electrolyte. This is similar to Radjenovic et al. (2016) findings where using sulfate instead of nitrate electrolyte resulted in a sevenfold increase in reaction rates for iopromide and diatrizoate removal.[193]

Ciprofloxacin-matrix removal is shown in Figure 4.5b, with pseudo-first order modeling with respect to the matrix illustrated in Figure 4.6. The initial stages of removal are shown in Figure 4.7. The overall pseudo-first order rate constants (and relevant statistics) for are in Table 4.5a. Rate-constants for each electrode pairs (BDD/Pt and BDD/Gr) are also shown. A fourfold increase in the overall reaction rate constant was observed using sulfate in place of nitrate electrolyte. The current findings for ciprofloxacin and the ciprofloxacin-matrix, in conjunction with the previously described persulfate experiments, confirm that sulfate does not act as an inert

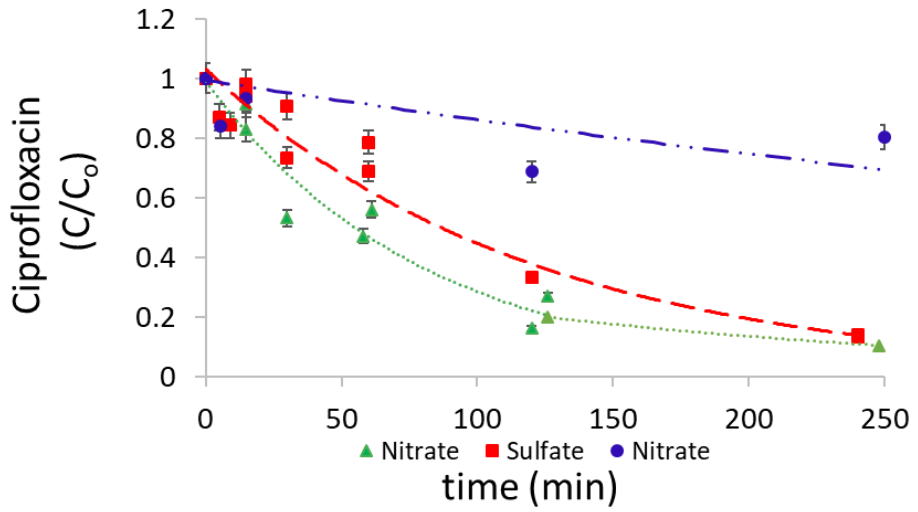

Figure 4.4. Removal of ciprofloxacin with time
(a) Removal of ciprofloxacin versus time, as measured by HPLC-UV. $[Persulfate]_0$ or $[Sulfate]_0$ = 22 mmol L^{-1}. $[Nitrate]_0$ = 66 mmol L^{-1}. $[Ciprofloxacin]_0$ = 0.043 mmol L^{-1}. Experiments completed in a single-cell RDE reactor at 76 mA cm^{-2} anodic current density,

Table 4.4. Effects of Electrolytes on Removal Rates of Ciprofloxacin

Analyte	Electrolyte	Ciprofloxacin Pseudo-first order rate constant (s^{-1} x 10^{-4})	Pseudo-first order fit (R^2)	Rate Constant Difference from Persulfate (%)	Statistical Significance of Difference from Persulfate
Ciprofloxacin	persulfate	2.08 ± 0.58	0.9112		
	sulfate	1.39 ± 0.14	0.9717	33%	>99%(p<0.0039)
	nitrate	0.24 ± 0.05	0.9517	88%	>99%(p<0.0001)

± *denotes 95% confidence intervals*

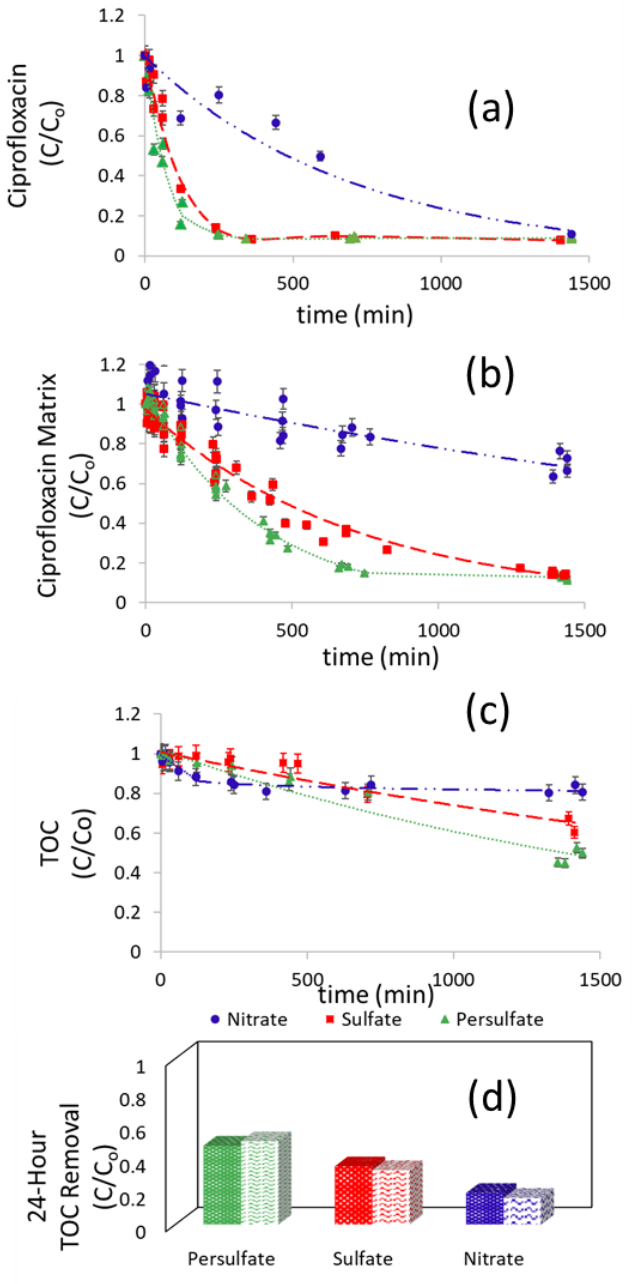

Figure 4.5. Removal of ciprofloxacin with time

(a) Removal of ciprofloxacin versus time, as measured by HPLC-UV. (b) Removal of ciprofloxacin-matrix versus time, as measured on UV/Vis (c) Total organic carbon removal versus time (d) Total organic carbon removal from ciprofloxacin after 24 hours. $[Persulfate]_0$ or $[Sulfate]_0$ = 22 mmol L^{-1}. $[Nitrate]_0$ = 66 mmol L^{-1}. $[Ciprofloxacin]_0$ = 0.043 mmol L^{-1}. Experiments completed in a single-cell RDE reactor at 76 mA cm^{-2} anodic current density and 1.33 mA cm^{-2} cathodic current density. BDD anode, data included for Gr or Pt cathodes.

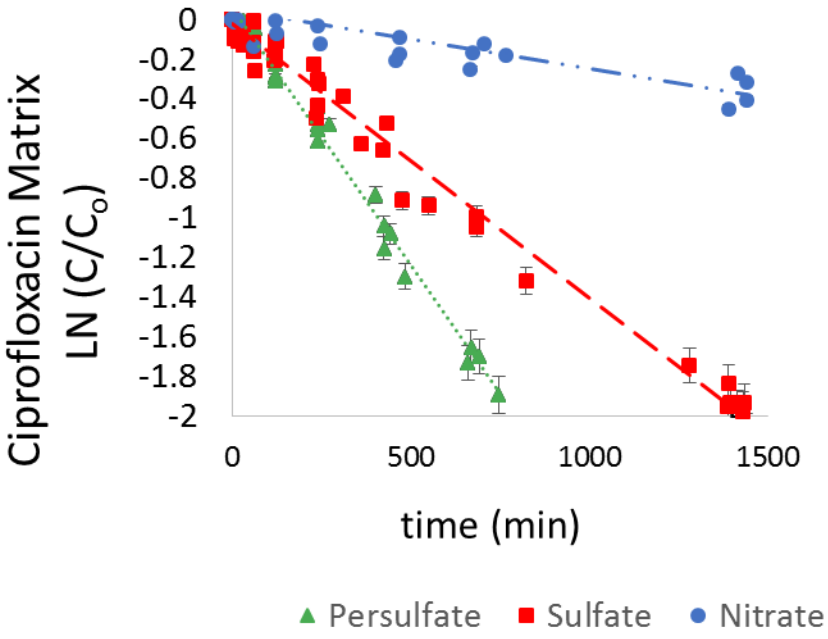

Figure 4.6. Pseudo-first order kinetics for degradation of ciprofloxacin-matrix
Data from Figure 4.5b. Single-cell RDE, BDD anode with graphite or platinum cathode. Anodic current density = 76 mA cm^{-2} and cathodic current density = 1.33 mA cm^{-2}. $[Persulfate]_0$ = 22 mmol L^{-1} OR $[Sulfate]_0$ = 22 mmol L^{-1} OR $[Nitrate]_0$ = 66 mmol L^{-1}.

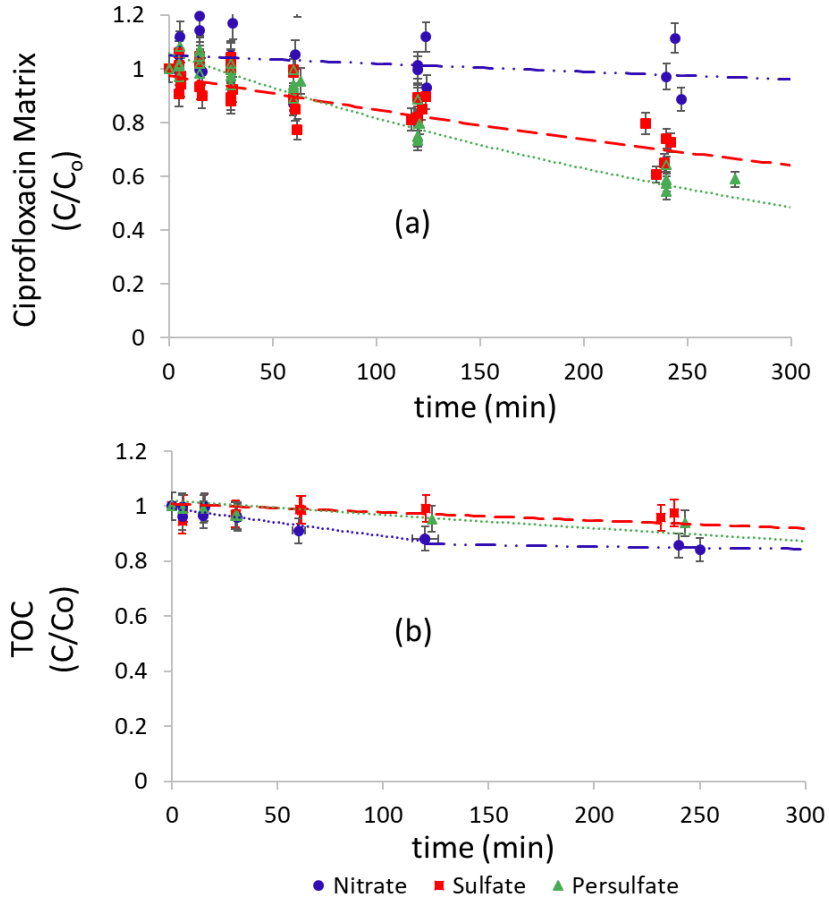

Figure 4.7. Initial stages of ciprofloxacin removal
Data from Figure 4.5. (a) Removal of ciprofloxacin matrix versus time, as measured on UV/Vis (b) Total organic carbon removal versus time. $[Persulfate]_0$ or $[Sulfate]_0$ = 22 mmol L^{-1}. $[Nitrate]_0$ = 66 mmol L^{-1}. $[Ciprofloxacin]_0$ = 0.043 mmol L^{-1}. Experiments completed in a single-cell RDE reactor at 76 mA cm^{-2} anodic current density and 1.33 mA cm^{-2} cathodic current density. BDD anode, data included for Gr or Pt cathodes.

Table 4.5a. Effects of Electrolytes on Removal Rates of Ciprofloxacin Matrix

Electrode Combination	Electrolyte	Ciprofloxacin pseudo-first order rate constant (s^{-1} x 10^{-5})	Ciprofloxacin pseudo-first order fit (R^2)	Rate Constant Difference from Persulfate (%)	Statistical Significance of Difference
BDD-Pt	persulfate	4.52 ± 0.22	0.9954		
	sulfate	2.31 ± 0.09	0.9892	49%	>99% (p<0.0001)
	nitrate	0.54 ± 0.16	0.7624	88%	>99% (p<0.0001)
BDD-Gr	persulfate	4.28 ± 0.18	0.9907		
	sulfate	2.28 ± 0.22	0.9849	47%	>99% (p<0.0001)
	nitrate	0.44 ± 0.12	0.7691	90%	>99% (p<0.0001)
Overall	persulfate	4.33 ± 0.14	0.9891		
	sulfate	2.29 ± 0.08	0.9823	47%	>99%(p<0.0001)
	nitrate	0.48 ± 0.09	0.7530	91%	>99%(p<0.0001)

Table 4.5b. Effects of Electrolytes on Removal Rates of TOC from Ciprofloxacin Matrix

Electrode Combination	Electrolyte	TOC pseudo-first order rate constant (s^{-1} x 10^{-5})	Pseudo-first order fit (R^2)	Rate Constant Difference from Persulfate (%)	Statistical Significance of Difference
BDD-Pt	persulfate	0.86 ± 0.21	0.9465		
	sulfate	0.42 ± 0.13	0.8723	51%	>99% (p=0.0008)
	nitrate	0.099 ± 0.34	0.0787	88%	>99% (p<0.0001)
BDD-Gr	persulfate	0.81 ± 0.24	0.9270		
	sulfate	0.44 ± 0.17	0.9047	46%	> 99% (p=0.0091)
	nitrate	0.025 ± 0.28	0.0059	97%	>99% (p<0.0001)
Overall	persulfate	0.83 ± 0.13	0.9396		
	sulfate	0.43 ± 0.10	0.8582	48%	>99% (p<0.0001)
	nitrate	0.061 ± 0.18	0.317	93%	>99% (p<0.0001)

± *denotes 95% confidence intervals*

electrolyte when using BDD anodes, rather it participates in degradation reactions, likely through sulfate radical formation. A significant increase of 47% was achieved for the ciprofloxacin-matrix reaction rate constant using persulfate instead of sulfate electrolyte, which may be attributed to cathodic persulfate activation, as described in *Cyclic voltammetry* and *Using ciprofloxacin to evaluate persulfate activation* sections. While the matrix removal reached ~85% for both persulfate and sulfate, persulfate attained this removal in ~12 hours versus ~24 hours for sulfate.

TOC removal followed pseudo-first order kinetics in sulfate and persulfate (Figure 4.5c, Table 4.5b), with respect to TOC concentration. Results by cathode type are provided in Table 4.3b. Degradation was proportional to but less than ciprofloxacin-matrix removal. Although the pseudo-first order fit for nitrate was poor, this model aided quantitative comparison. Nitrate initially produced more rapid TOC degradation than sulfate or persulfate electrolytes, and similar removal was observed for sulfate and persulfate during this initial timeframe (Figure 4.7). However, TOC removal in nitrate quickly plateaued and little removal was observed after the two-hour mark, while persulfate began to show better removal than sulfate. The effect of sulfate over nitrate produced a sevenfold increase in TOC removal rate ($p<0.0001$). For the time series, the additional TOC removal rate for persulfate versus sulfate was 48%, slightly larger than that observed for the ciprofloxacin relationship (Table 4.4) and similar to that for the ciprofloxacin-matrix relationship (Table 4.5b). Comparison of 24-hour removal rates is shown in Figure 4.5d. For both environmentally relevant parameters, ciprofloxacin and TOC removal, EAP offers an advantage for degradation and may be the best approach for some EAOP applications.

Figure 4.8 shows the specific energy consumption for the data in Figure 4.5. Energy consumption per unit mass of TOC removed was calculated using Equation 4.5 and presented in

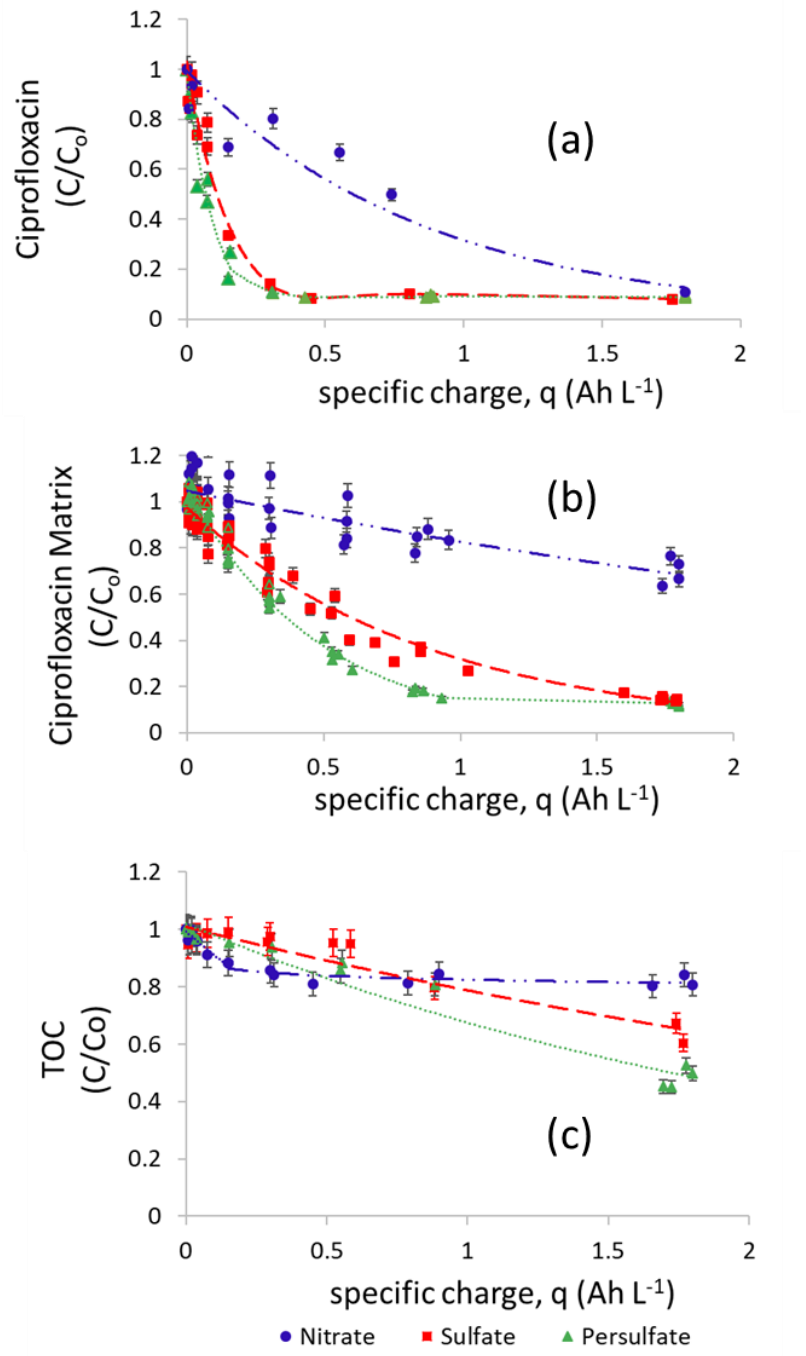

Figure 4.8. Removal of ciprofloxacin versus specific electrical charge
(a) Removal of ciprofloxacin versus specific electrical charge, as measured by HPLC-MS. (b) Removal of ciprofloxacin matrix versus specific electrical charge, as measured on UV/Vis. (c) Removal of TOC versus specific electrical charge. $[Persulfate]_0$ or $[Sulfate]_0$ = 22 mmol L^{-1}. $[Nitrate]_0$ = 66 mmol L^{-1}. $[Ciprofloxacin]_0$ = 0.043 mmol L^{-1}. Experiments completed in a single-cell RDE reactor at 76 mA cm^{-2} anodic current density and 1.33 mA cm^{-2} cathodic current density.

Table 4.6.

(4.5) Energy consumption (EC) per unit mass[205] (kWh (g)$^{-1}$) = $\frac{\text{Ecell} * \text{I} * \text{t}}{V*([A]-[A]_0)}$

For Equation 4.5, E_{cell} = average cell voltage, I = current, V = cell volume, t= time and A= TOC concentration, OR ciprofloxacin matrix concentration. Energy consumption for persulfate and sulfate electrolytes was in line with that determined for electro-Fenton degradation of enrofloxacin using a BDD anode[205].

Faraday's law was used to calculate the Coulombic efficiency for ciprofloxacin removal in all three electrolytes. From Figure 4.4, 120 minutes was used as the timepoint to calculate coulombs based on a constant 15 mA current. Faraday's law establishes that 1.12 mmoles of ciprofloxacin should be degraded under theoretical 100% current efficiency. In nitrate, 0.013 mmoles were degraded, giving a 1.2% coulombic efficiency. In sulfate, 0.029 mmoles ciprofloxacin were degraded, giving a 2.6% efficiency. In persulfate, 0.034 mmoles were degraded, giving a 3.1% efficiency.

Table 4.6. Energy consumption during removal of TOC from Ciprofloxacin

Analyte	Electrolyte	TOC Pseudo-first order rate constant (s^{-1} x 10^{-5})	Pseudo-first order fit (R^2)	Rate Constant Difference from Persulfate	Energy Consumption per Unit Mass (kWh (g^{-1}))
TOC	persulfate	0.83 ± 0.13	0.9396		0.428
	sulfate	0.43 ± 0.10	0.8582	48%	0.578
	nitrate	0.061 ± 0.18	0.317	93%	1.60

± *denotes 95% confidence intervals*

Persulfate was measured during ciprofloxacin reactions in both sulfate and persulfate electrolytes (Figure 4.9). Ultimately, persulfate reduced to sulfate (Figure 4.10), with 1.99 moles

sulfate formed for every mole persulfate decomposed. In ciprofloxacin-persulfate solutions, persulfate did not follow the same kinetics as in experiments without organic analyte. Persulfate decayed following a pseudo-first order mechanism with respect to persulfate with R^2=0.99 (Figure 4.9). The pseudo-first order kinetics indicates that, in addition to surface-based persulfate decomposition and generation, there are bulk persulfate reactions that depend on the persulfate concentration, which include possible interactions between persulfate and ciprofloxacin or persulfate and organic radicals. In fact, although both ciprofloxacin decay and persulfate decomposition model well as pseudo-first order mechanisms with respect to themselves, (the typical kinetic model used in environmental remediation studies[48]), there is a second-order relationship at play between the persulfate and ciprofloxacin-matrix, shown in Figure 4.11. The second-order reaction rate constant, calculated by Equation 4.6, is 2.1 x 10^{-2} L mol^{-1} s^{-1} with R^2=0.95[206], indicating a slow reaction rate between persulfate and the ciprofloxacin[206].

(4.6) Second-order kinetics model[206]

$$\ln \frac{[A]_0\ [B]}{[A]\ [B]_0} = ([B]_0\ -\ [A]_0\ )\ k\ t$$

In Equation 4.6, [A]= [Ciprofloxacin] and $[A]_0$ = 0.043 mmol L^{-1}, [B] = [Persulfate] and $[B]_0$ = 22 mmol L^{-1}, t = time (seconds) and k = second order reaction rate constant. The second-order rate constant for persulfate and ciprofloxacin was determined by graphing the left-hand term versus time (Figure 4.11). The slope was then set equal to $([B]_0\ -\ [A]_0\ )$ k and the reaction rate, k, calculated. In sulfate, persulfate level increased in a non-uniform fashion, likely due to the complex set of reactions including sulfate radicals degrading ciprofloxacin, persulfate activation, and interaction between ciprofloxacin and persulfate.

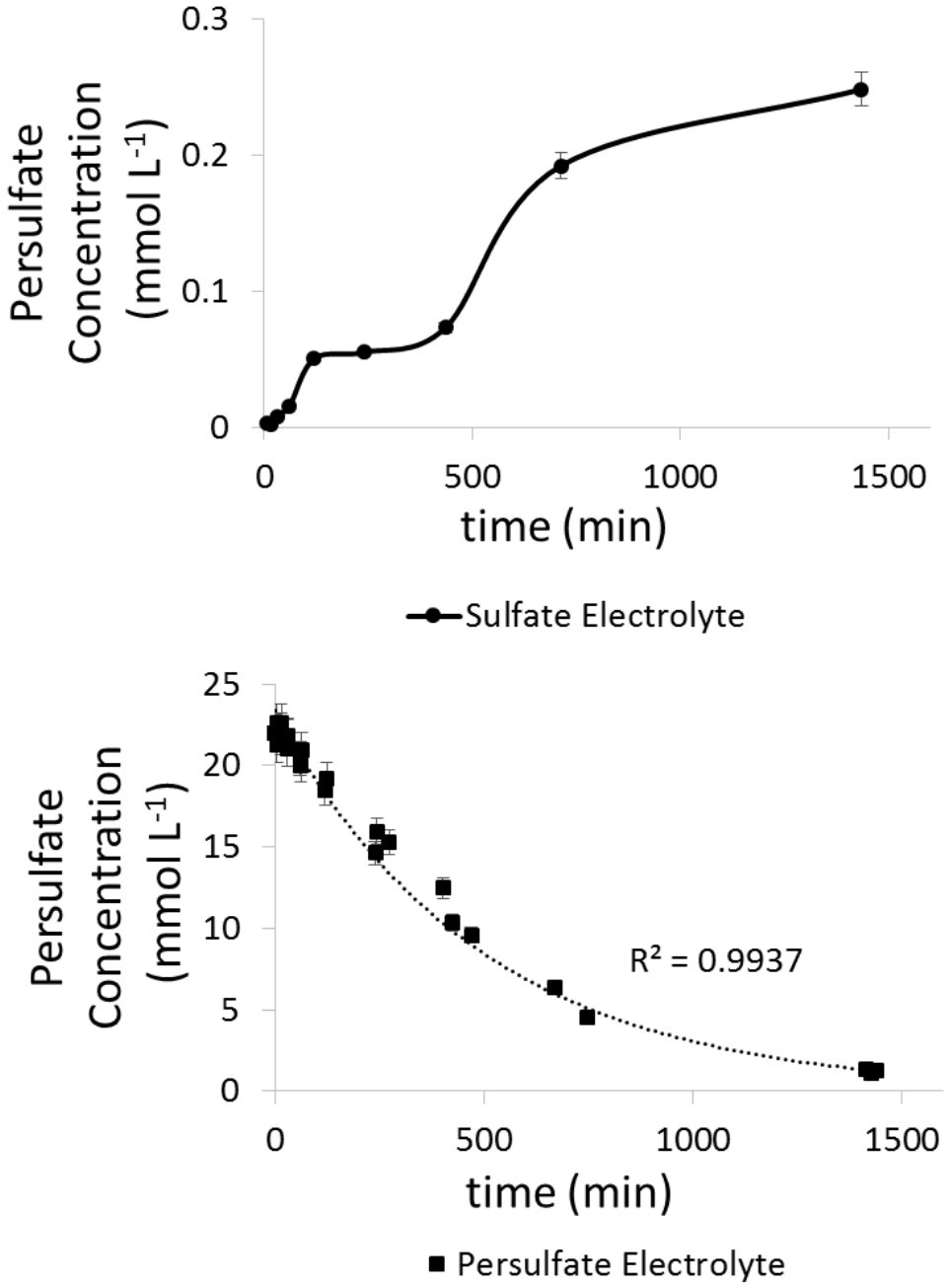

Figure 4.9. Persulfate behavior during ciprofloxacin degradation
Single-cell RDE with anodic current density = 76 mA cm^{-2} and cathodic current density = 1.33 mA cm^{-2}.

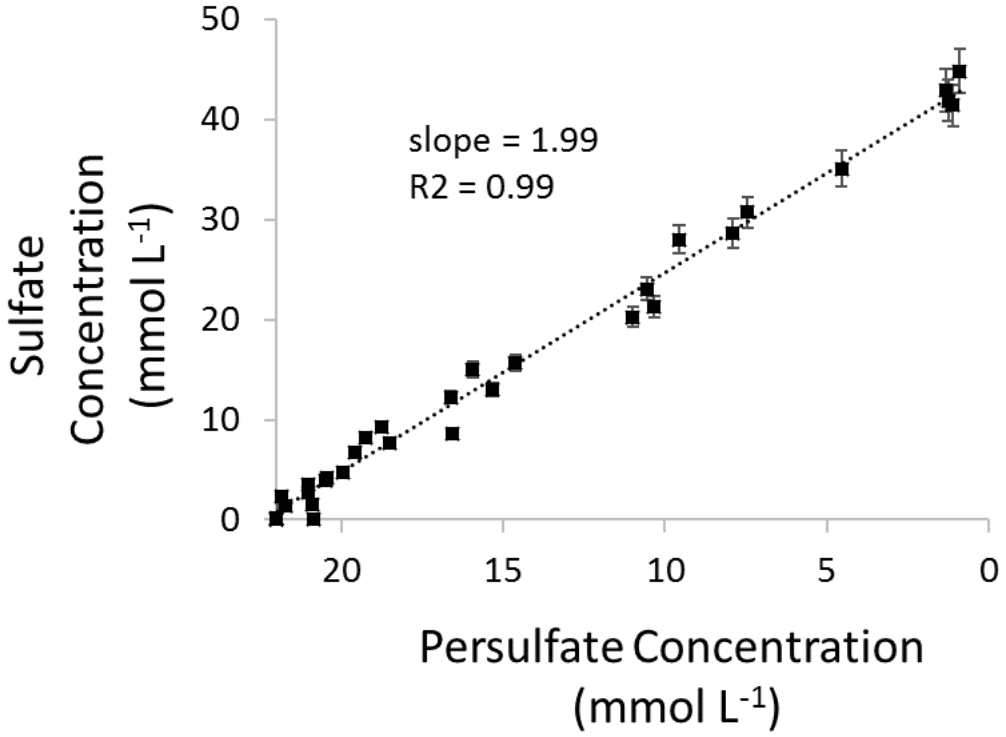

Figure 4.10. Persulfate reduction to sulfate
$[Persulfate]_0$ = 22 mmol L^{-1} and $[Ciprofloxacin]_0$ =0.043 mmol L^{-1}. Single-cell RDE with anodic current density = 76 mA cm^{-2} and cathodic current density = 1.33 mA cm^{-2}. BDD anode, combined data for Gr and Pt cathodes.

4.3.3 Radical roles in ciprofloxacin degradation

Quenching studies examined hydroxyl and sulfate radical roles in ciprofloxacin removal. Rate constants for quenchers or ciprofloxacin with radicals are outlined in Table 4.7.

Table 4.7. Reaction Rate Constants for Quenching Experiments

Reactant	Reaction Rate Constant with Hydroxyl Radicals (M^{-1} s^{-1})	Reaction Rate Constant with Sulfate Radicals (M^{-1} s^{-1})
DMSO	6.7×10^9 [207]	3.0×10^9 [208]
TBA	6.0×10^8 [158,42]	4.0×10^5 [158,42]
Ciprofloxacin	$(4.1 - 5.0) \times 10^9$ [38, 209]	*est. $10^6 - 10^9$ [76, 210]

**estimate based on reaction rate of sulfate radical with many organic compounds*

During DMSO quenching, virtually all radicals were predicted to react with DMSO over ciprofloxacin (Equation 4.7a-b)[211].

(4.7) Competition kinetics for ciprofloxacin in quenchers[211]

(a) $f_{OH-DMSO} = \frac{kOH\_cip\ [Cip]}{kOH\_cip\ [Cip]+kOH\_DMSO\ [DMSO]}$ = 1.3×10^{-5}

(b) $f_{SO4-DSM0} = \frac{kSO4\_cip\ [Cip]}{kSO4\_cip\ [Cip]+kSO4\_DMSO[DMSO]}$ = 6.5×10^{-7}

(c) $f_{OH-TBA} = \frac{kOH\_cip\ [Cip]}{kOH\_cip[Cip]+kOH\_TBA\ [TBA]}$ = 1.5×10^{-4}

(d) $f_{SO4-TBA} = \frac{kSO4\_cip\ [Cip]}{kSO4\_cip\ [Cip]+kSO4\_TBA\ [TBA]}$ = 4.9×10^{-3}

For Equation 4.7: $f_{OH-DMSO}$ represents the fraction of hydroxyl radicals preferentially reacting with ciprofloxacin instead of reacting with (being quenched by) DMSO, $f_{SO4-DSM0}$ represents the fraction of sulfate radicals preferentially reacting with ciprofloxacin instead of reacting with (being quenched by) DMSO, f_{OH-TBA} represents the fraction of hydroxyl

radicals preferentially reacting with ciprofloxacin instead of reacting with (being quenched by) TBA, $f_{SO4-TBA}$ represents the fraction of hydroxyl radicals preferentially reacting with ciprofloxacin instead of reacting with (being quenched by) TBA, [Cip] = concentration of ciprofloxacin (0.043 mmol L^{-1}), [TBA] = concentration of tert-butanol quencher (2200 mmol L^{-1}), [DMSO] = concentration of dimethyl sulfoxide quencher (2200 mmol L^{-1}), kOH_cip = hydroxyl radical-ciprofloxacin second order reaction rate constant listed in Table 4.7 (median value of 4.55 x 10^9 used for calculations), kSO4_cip = sulfate radical-ciprofloxacin second order reaction rate constant listed in Table 4.7 (a value of 10^8 used for calculations based on those found for many aromatic compounds)[76], kOH_DMSO hydroxyl radical-DMSO second order reaction rate constant listed in Table 4.7, kSO4_DMSO sulfate radical-DMSO second order reaction rate constant listed in Table 4.7, kOH_TBA hydroxyl radical-TBA second order reaction rate constant listed in Table 4.7 and kSO4_TBA sulfate radical-TBA second order reaction rate constant listed in Table 4.7.

With DMSO addition, only 12% removal was observed in the nitrate solution (Figure 4.12). Therefore, a portion of the removal in the nitrate solution, under non-quenched conditions, was attributed to hydroxyl radicals, with electrode surface reactions, such as direct oxidation, contributing the remaining portion. In sulfate or persulfate, a substantial reduction in removal was also observed during DMSO quenching. However, in these cases a significant portion of degradation under non-quenched conditions was attributed to both hydroxyl and sulfate radicals. While TBA is typically used to distinguish between sulfate and hydroxyl radicals, calculations (Equations 4.7a-d) did not predict a significant difference in its ability to preferentially quench sulfate radicals over hydroxyl radicals under current experimental conditions. Differences in removal with the two quenchers may be attributable to actual differences in hydroxyl versus sulfate

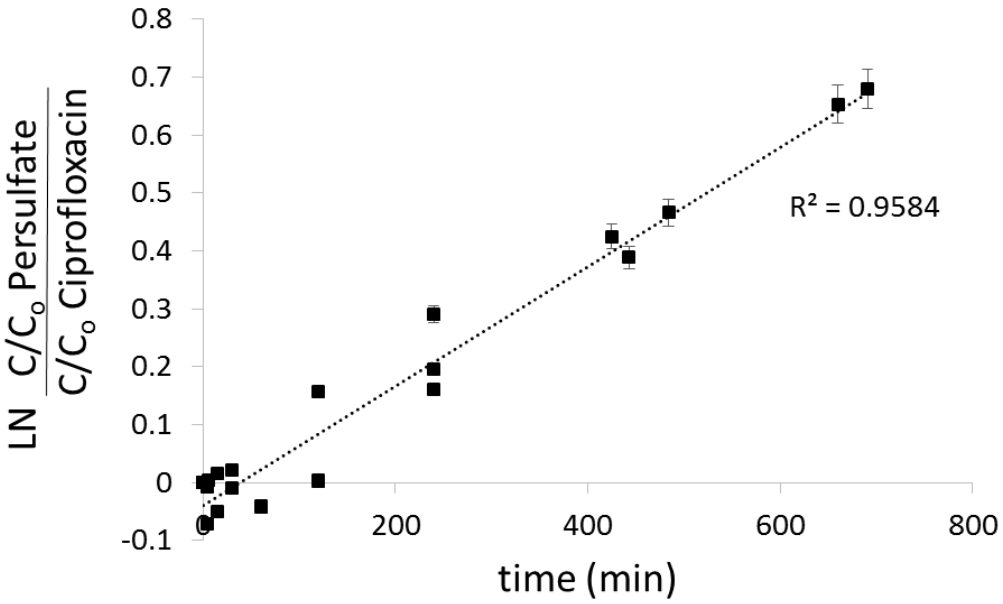

Figure 4.11. Second-order reaction modeling of ciprofloxacin and persulfate
Initial 0.043 mmol L^{-1} ciprofloxacin and 22 mmol L^{-1} persulfate. Single-cell RDE with anodic current density = 76 mA cm^{-2} and cathodic current density = 1.33 mA cm^{-2}.

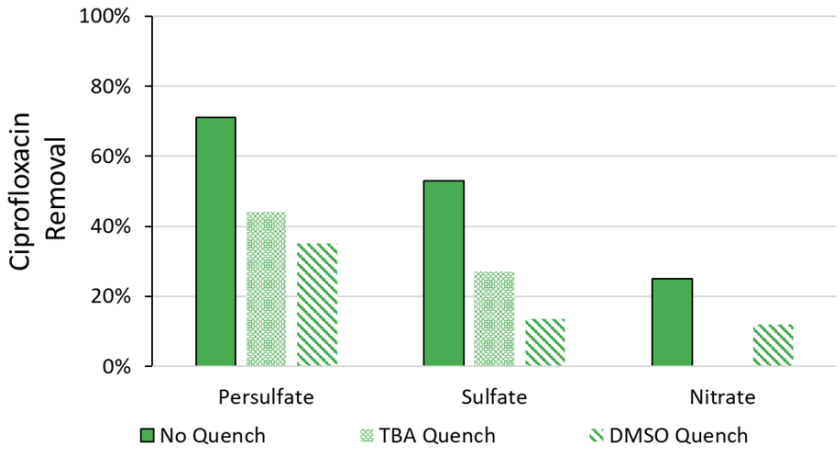

Figure 4.12. Quenching Experiments
Quenching Experiments. $[Persulfate]_0$ or $[Sulfate]_0$ = 22 mmol L^{-1}. $[Nitrate]_0$ = 66 mmol L^{-1}. $[Ciprofloxacin]_0$ = 0.043 mmol L^{-1}. Experiments completed in a single-cell RDE reactor at 76 mA cm^{-2} anodic current density with a BDD anode and Gr or Pt cathode (data is averaged for cathodes since no significant difference was found between cathodes). 2200 mmol L^{-1} TBA used to quench hydroxyl radicals. 2200 mmol L^{-1}DMSO used to quench hydroxyl and sulfate radicals. Time point of 120 minutes used to compare all samples.

radical reactivity, or may be due to differences in the ability of quenchers to suppress radicals, as established by the competition kinetics fractional calculations (Equations 4.7c-d). Overall, the decreasing ciprofloxacin degradation under quenched conditions suggests that one or both radicals play a significant role in ciprofloxacin degradation using EAP. Of note is the ~35% removal achieved in persulfate with primary radicals quenched. Radicals such as persulfate ($S_2O_8^{2-}\cdot$), R· (organic) and ROO· (organo-peroxide) may propagate from sulfate and hydroxyl radicals but have limited potential to form because their parent radical is quenched[96, 135, 151, 212]. It is suggested that non-radical based persulfate activation at the BDD anode is partially responsible for enhanced ciprofloxacin removal in persulfate, which has recently been observed in other persulfate-based systems[42, 84, 213].

4.3.4 Cyclic voltammetry

Cyclic voltammograms (C-V) were performed to clarify differences between electrolytes for persulfate activation and ciprofloxacin abatement. Two distinct oxidation peaks for ciprofloxacin were observed at the BDD anode (Figure 4.13) in all electrolytes, demonstrating that surface-based oxidation of ciprofloxacin is likely partially responsible for the ciprofloxacin removal seen in Figure 4.4. A third oxidation peak was marginally visible in sulfate and nitrate, but was more prominent in persulfate, revealing that persulfate electrolyte may drive oxidation at a lower voltage. Full C-Vs are shown in Figure 4.14. Multi-cycle C-Vs, displayed in Figure 4.15, demonstrate ciprofloxacin oxidation is quasi-irreversible process, as there are no symmetric reduction peaks and the oxidation peaks almost disappear after the first cycle. C-Vs were also completed for graphite and platinum material (Figure 4.16), with focus on the reductive reactions occurring at these cathodes (Figure 4.17). For nitrate and sulfate electrolytes, there were no significant differences between cathode materials. Direct reduction of ciprofloxacin was not observed in the potential range evaluated. An irreversible reduction peak at both cathodes is observed when persulfate and ciprofloxacin are present in solution together. This indicates a surface-based reaction between persulfate and ciprofloxacin, i.e., direct electrochemical persulfate activation.

4.3.5 Using ciprofloxacin to evaluate persulfate activation

Further verification of electrochemical persulfate activation was established with ciprofloxacin electrolysis in a split-cell RDE with BDD/Gr electrodes. Figure 4.18 shows a well-defined difference in ciprofloxacin removal at the cathode in persulfate with pseudo-first order (R^2=0.9215) degradation, with respect to ciprofloxacin, in persulfate and 55% removal within 300

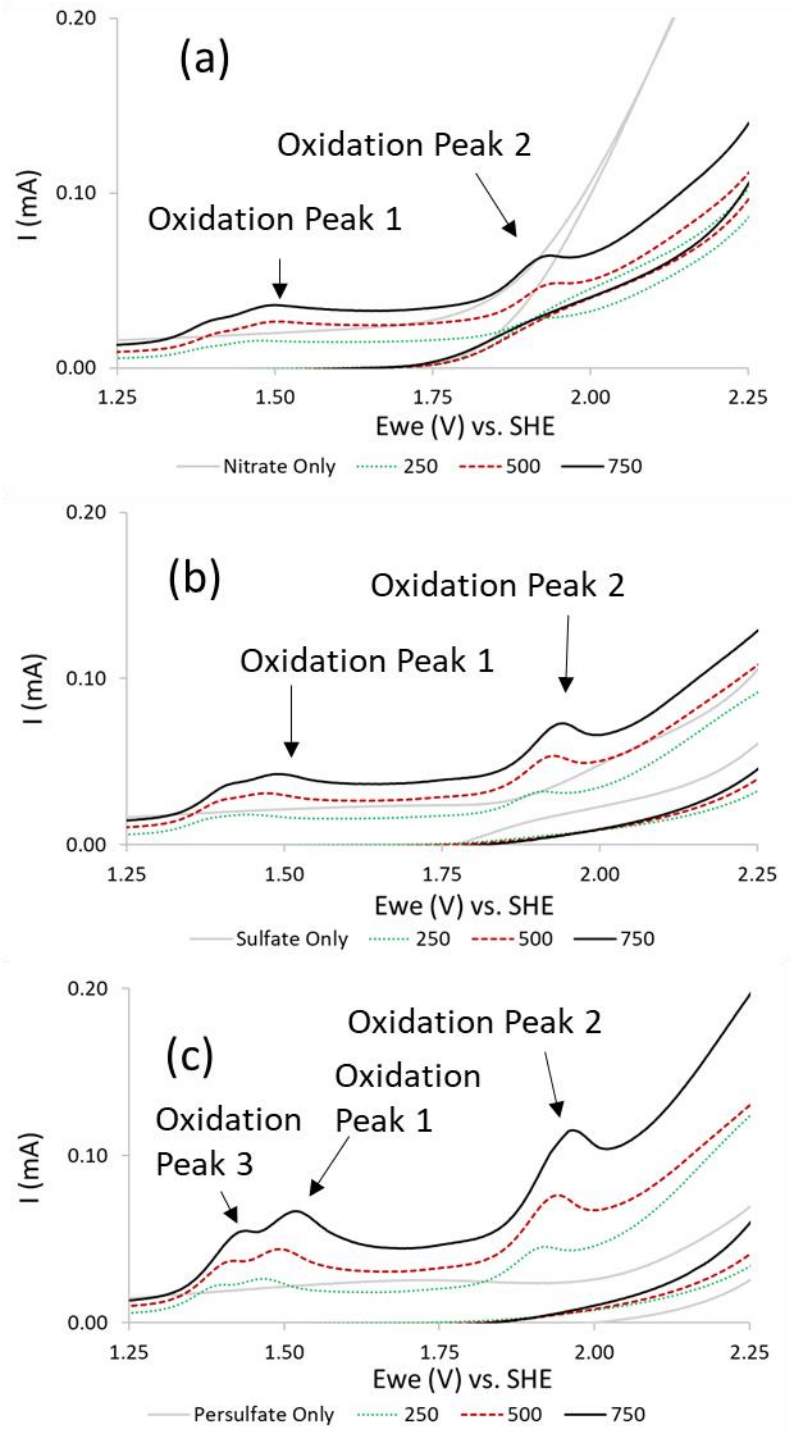

Figure 4.13. Ciprofloxacin oxidation peaks during cyclic voltammetry using a BDD anode
C-Vs were run with multiple cycles to determine reversibility but only the first cycle is pictured for clarity. "electrolyte only" are controls; other C-Vs with the addition of 0.043 mmol L^{-1} ciprofloxacin at 250, 500 and 750 mV s^{-1} scan rates. All C-Vs with 22 mmol L^{-1} sulfate or persulfate, or 66 mmol L^{-1} nitrate.

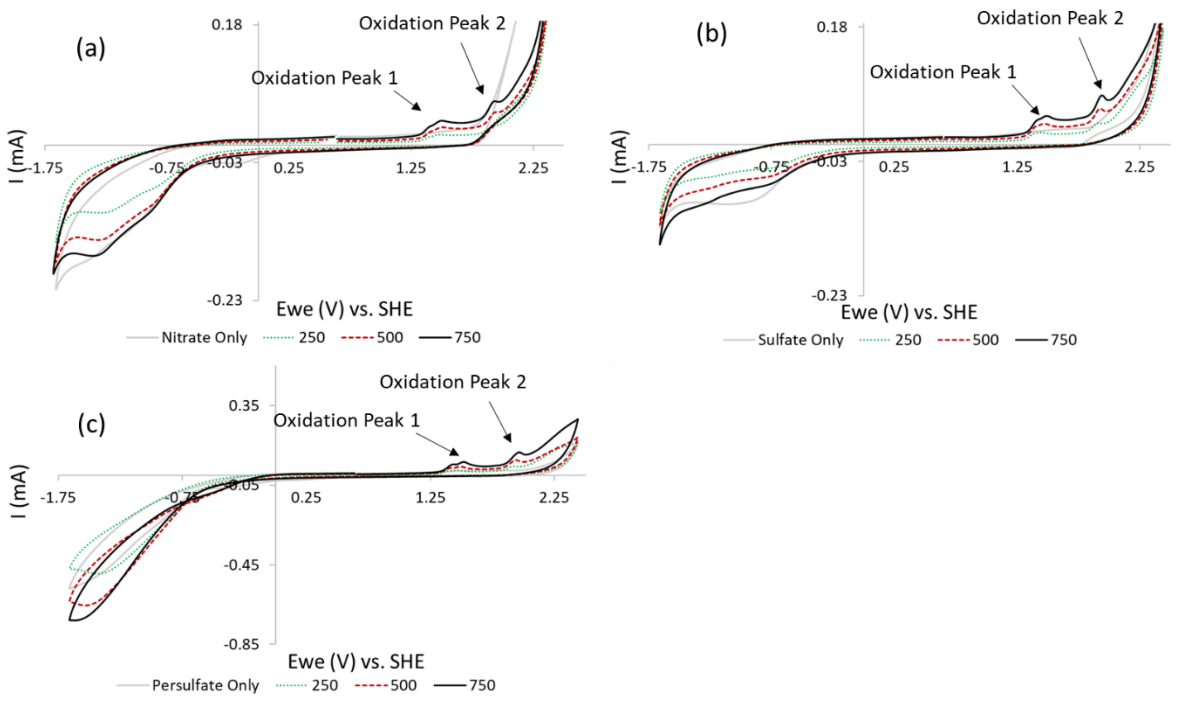

Figure 4.14. Complete cyclic voltammograms of ciprofloxacin using BDD anode
0.043 mmol L^{-1} ciprofloxacin in (a) 66 mmol L^{-1} nitrate b) 22 mmol L^{-1} sulfate or (c) 22 mmol L^{-1} persulfate using a BDD anode at different scan rates. Numerical legend values are scan rates in mV s^{-1}. Electrolyte only baselines are scanned at 750 mV s^{-1}.

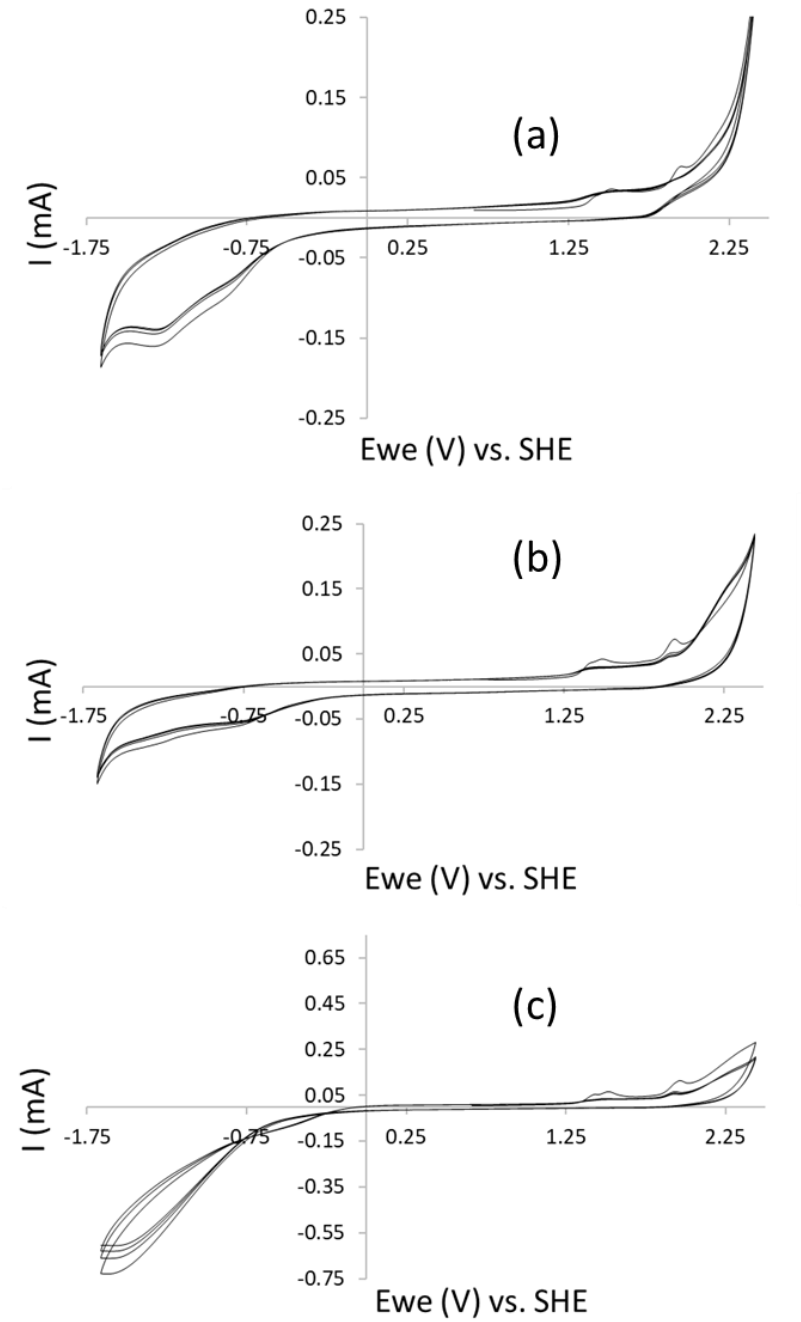

Figure 4.15. Multiple-cycle cyclic voltammograms of ciprofloxacin
0.043 mmol L^{-1} ciprofloxacin in (a) 66 mmol L^{-1} nitrate b) 22 mmol L^{-1} sulfate or (c) 22 mmol L^{-1} persulfate using a BDD anode at a scan rate of 750 mV s^{-1}. Prominent oxidation peaks are present in the first cycle in all electrolytes. No oxidation peaks are present in nitrate after the first cycle. In persulfate, a slight oxidation peak appears in subsequent cycles for sulfate and persulfate. These voltammograms were similar at lower scan rates as well and illustrate the irreversible nature of the ciprofloxacin oxidations.

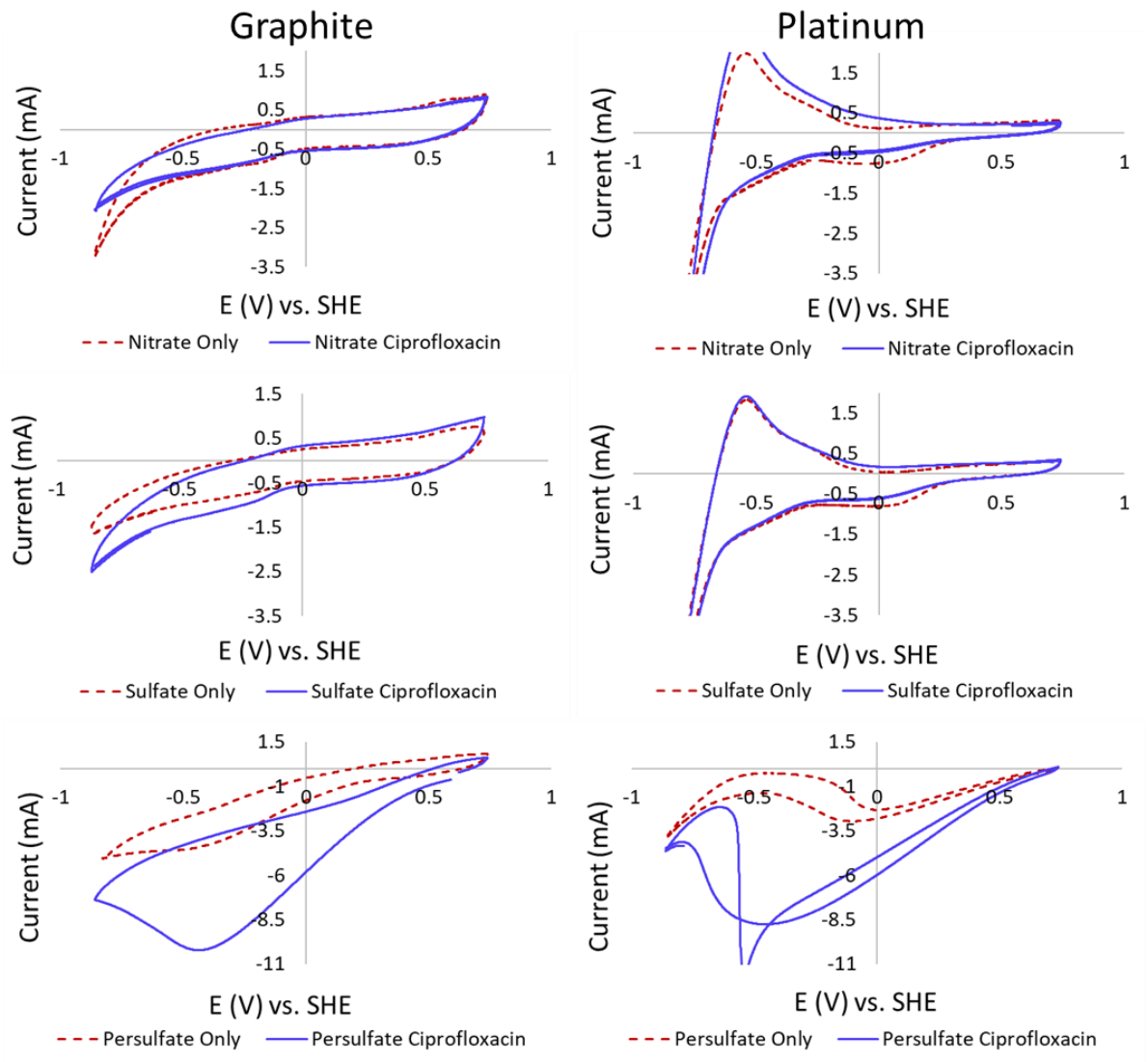

Figure 4.16. Cyclic voltammograms of ciprofloxacin using Pt or Gr anodes
All C-Vs with 22 mmol L^{-1} sulfate or persulfate, or 66 mmol L^{-1} nitrate. 0.043 mmol L^{-1} ciprofloxacin where indicated in legend.

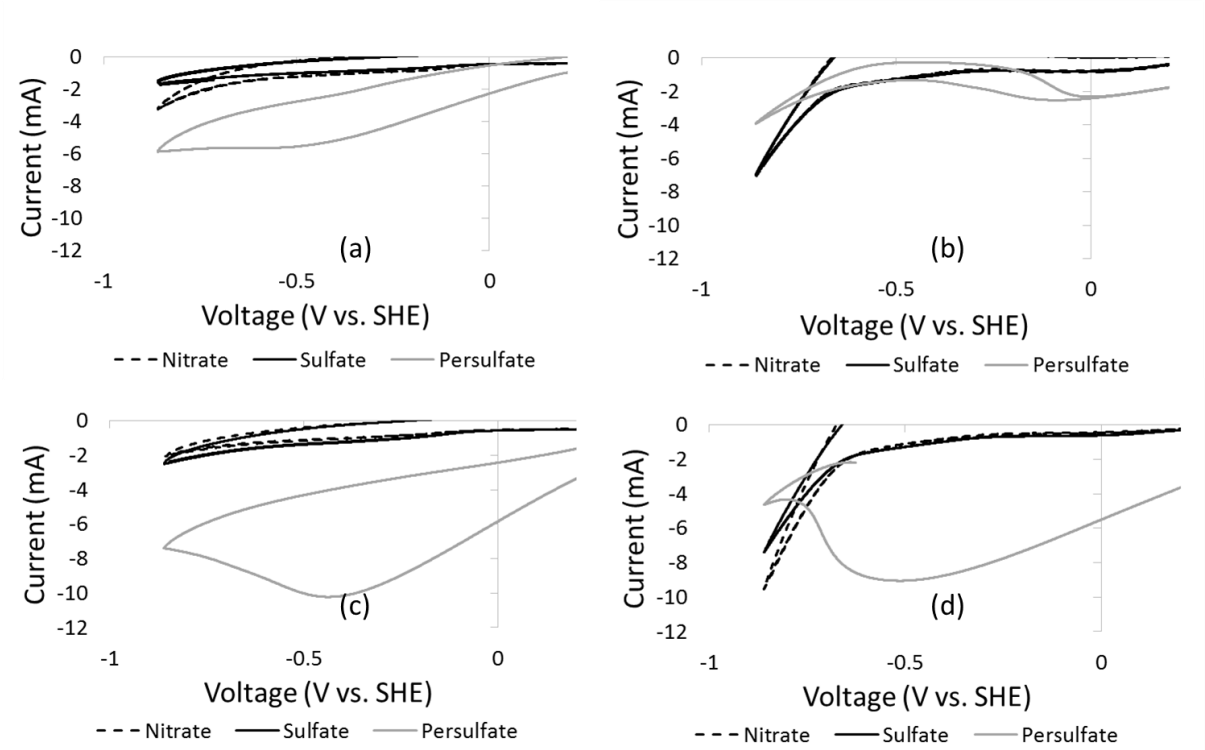

Figure 4.17. Reduction peak during cyclic voltammetry of cathode materials
Figures 4.17a and c: C-Vs of (a) electrolyte control and (c) electrolyte with ciprofloxacin, both completed with graphite electrode. Figure 4.17 b and d: C-Vs of (b) electrolyte control and (d) electrolyte with ciprofloxacin, both completed with platinum electrode. All C-Vs with 22 mmol L^{-1} sulfate or persulfate, or 66 mmol L^{-1} nitrate. C-Vs c. and d. include the addition of 0.043 mmol L^{-1} ciprofloxacin.

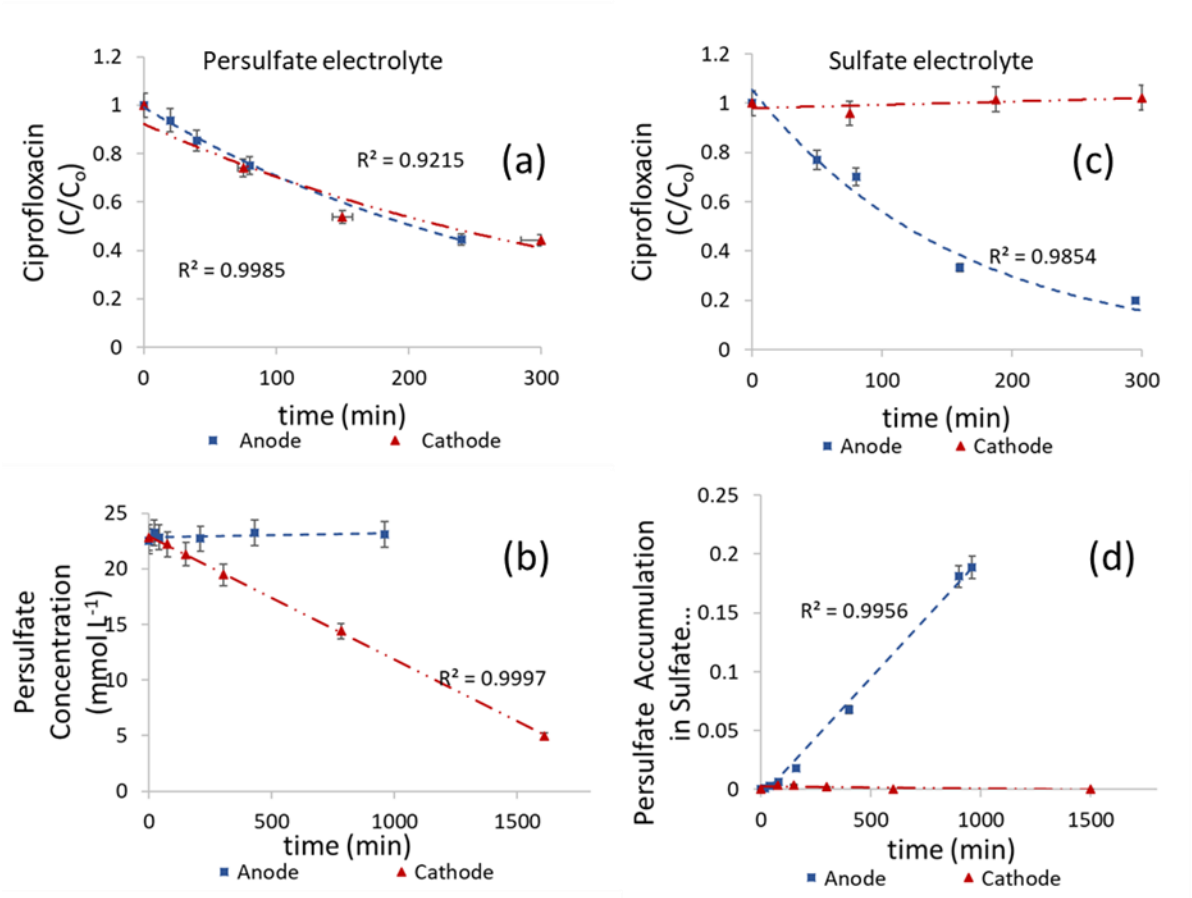

Figure 4.18. Ciprofloxacin removal in a split-cell reactor
Ciprofloxacin removal and corresponding persulfate concentration in a split-cell RDE. Anodic current density = 28.5 mA cm^{-2}. Cathodic current density = 1.33 mA cm^{-2}. [Ciprofloxacin]$_0$ = 0.043 mol L^{-1}. (a-b) [Persulfate]$_0$ 22 mmol L^{-1}. (c-d) [Sulfate]$_0$ = 22 mmol L^{-1}.

minutes (Figure 4.18a) versus no removal in sulfate electrolyte (Figure 4.18c). These results, combined with C-V analysis, provide strong experimental evidence of persulfate activation at the cathode, verifying what other studies have previously postulated[59, 133]. While persulfate transformation at the anode did not occur (Figure 4.18b) and sulfate was not available to form sulfate radicals, some ciprofloxacin removal was still observed at the anode in persulfate, with reaction rates of 1.1x10-4 s-1 and 5.1x10-5 s-1 in sulfate and persulfate, respectively. Quenching results suggested that non-radical persulfate activation at the BDD anode may account for ciprofloxacin removal in the anode cell.

Persulfate activation and regeneration were observed with organic analyte in solution (Figures 4.18b and d) as without organic analyte (Figure 4.2b and c). Persulfate decomposition at the cathode (Figure 4.18b) did not exhibit pseudo-first order decay with respect to persulfate as seen in the single-cell solution even though ciprofloxacin was present. This pseudo-first order mechanism may result from a synergistic effect between reactions at the anode and cathode.

4.3.6 Ciprofloxacin transformation

Ciprofloxacin transformation pathways were examined in the three electrolytes, as shown in Figure 4.19. Mass spectra corresponding to by-products shown in Figure 4.19 are presented in Appendix Figures A13a-u. In persulfate, rapid defluorination occurred within 15 minutes (Figure 4.20), corresponding to the rapid ciprofloxacin removal observed in Figure 4.4. A multi-point hydroxylation with fluoride substitution (Figure 4.19), through m/z 362, was identified as a dominant route for ciprofloxacin breakdown in persulfate. Similar mechanisms involving hydroxylation and/or defluorination were observed in multiple studies[44,96,176,184,194]. Ciprofloxacin defluorination (Figure 4.20) reached >90% in both persulfate and sulfate, which is important

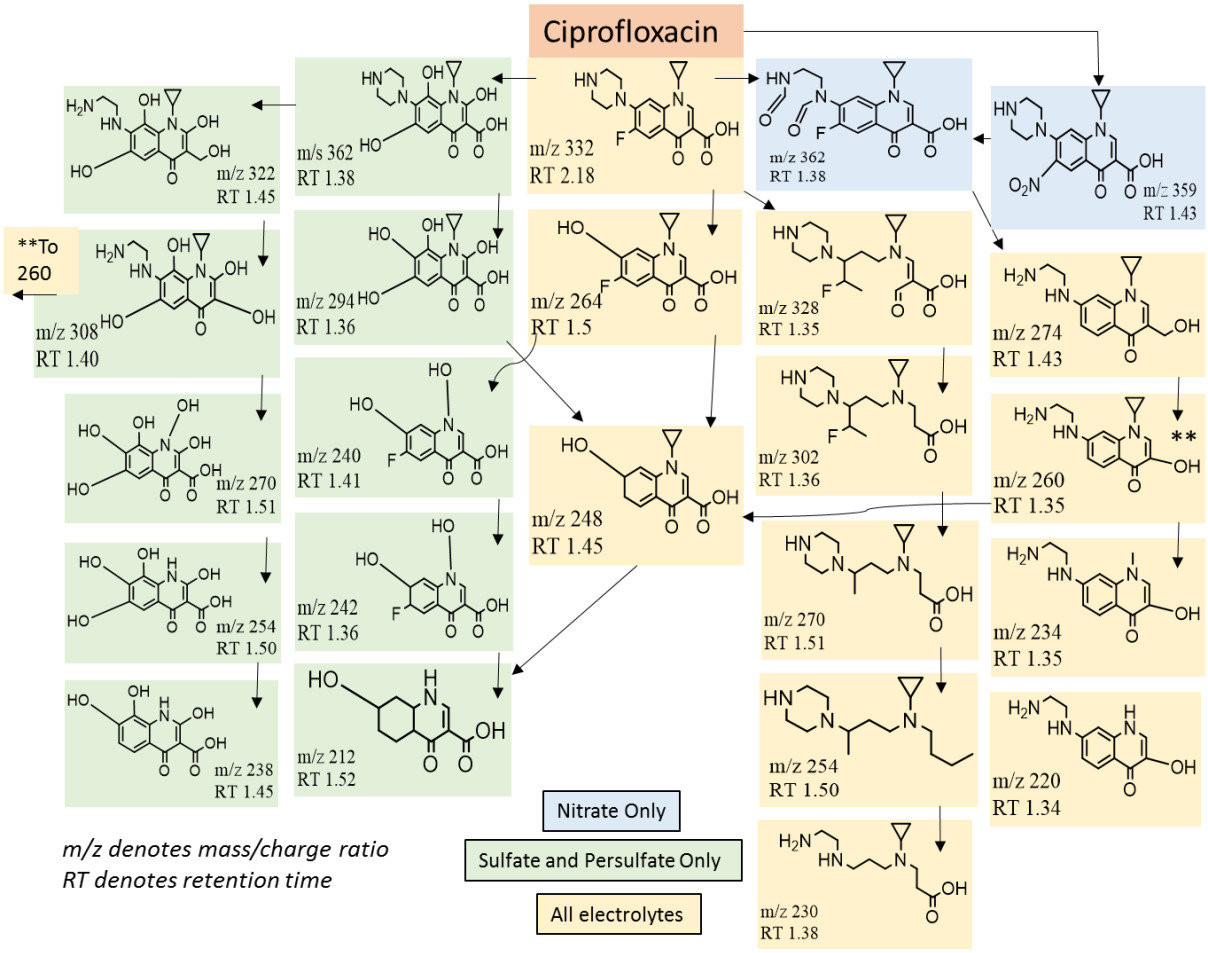

Figure 4.19. Ciprofloxacin Transformation Pathways
Primary persulfate pathways through m/z 362 and 264. Primary sulfate pathway through m/z 264. Primary nitrate pathways through m/z 264 and 362. Secondary pathway in all three electrolytes through m/z 328.

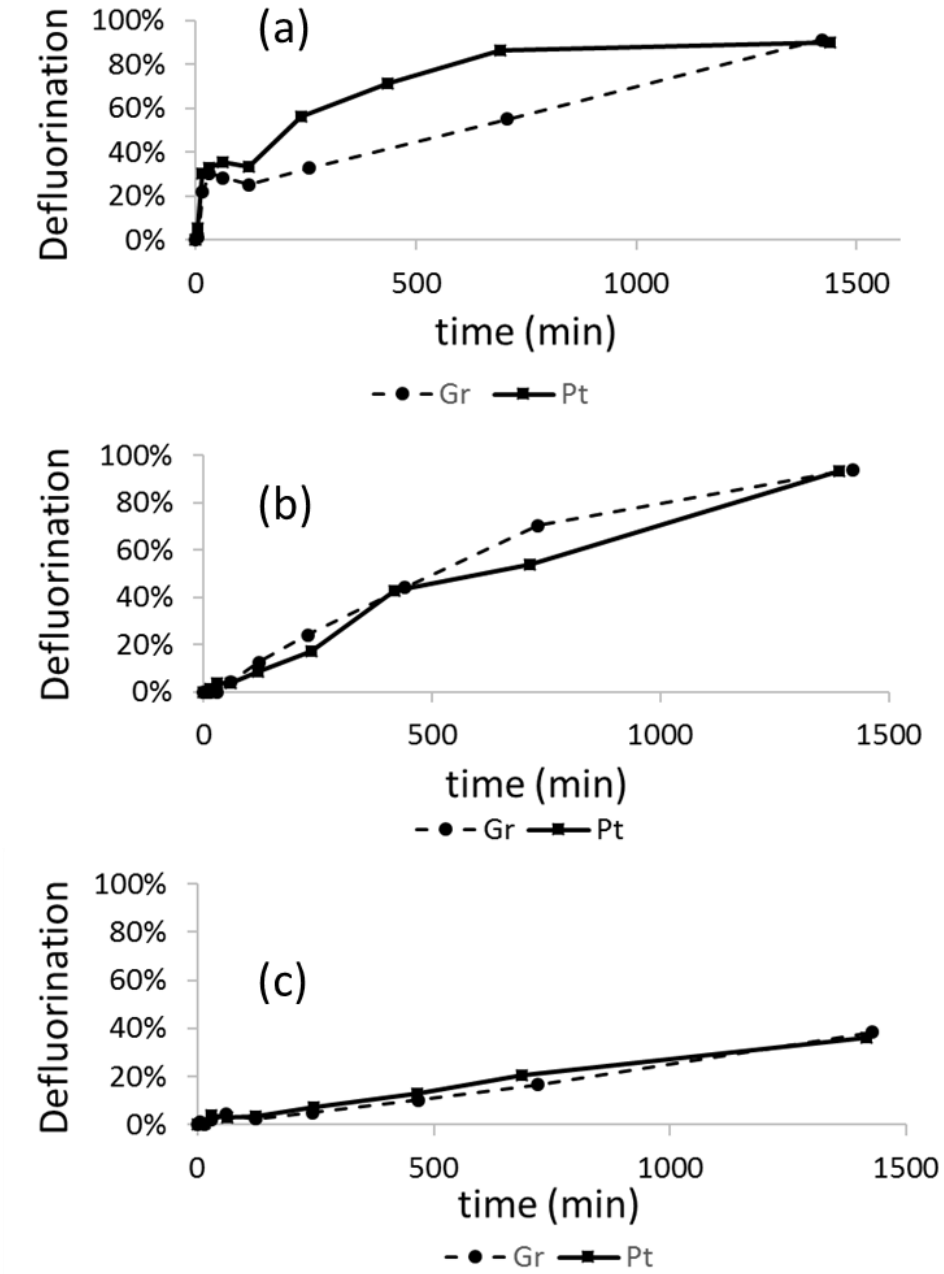

Figure 4.20. Defluorination of ciprofloxacin

Defluorination of 0.043 mmol L^{-1} ciprofloxacin with a BDD anode and graphite or platinum cathode. Single-cell RDE with anodic current density = 76 mA cm^{-2} and cathodic current density = 1.33 mA cm^{-2}. (a) $[Persulfate]_0$ = 22 mmol L^{-1} (b) $[Sulfate]_0$ = 22 mmol L^{-1} (c) $[Nitrate]_0$ = 66 mmol L^{-1}.

because defluorination may lower toxic effects of fluorinated contaminants[176]. Defluorination in nitrate only reached 36%. Fluoride removal in sulfate and nitrate was almost linear, indicating a surface-dominated mechanism. Hydroxylation without defluorination, through m/z 264, was a major degradation route in all electrolytes and the dominant pathway in nitrate and sulfate. A third pathway, breakdown of the core quinolone structure through m/z 328, was comparable to results observed in other studies[44, 96].

Additional key mechanisms here and other ciprofloxacin studies include: 1) piperazine-ring cleavage[44, 96, 176, 184, 194, 214], 2) cyclo-propyl group breakdown [44], 3) loss of amines[44, 184], and 4) decarboxylation[96, 184, 214]. No significant differences were noted between cathode materials. While no sulfate-adducts were observed, possible nitrate-adduct formation indicates potential nitrate radical evolution at the BDD anode in nitrate. Overall, electrochemically generated sulfate radicals resulted in additional degradation pathways corresponding to the enhanced ciprofloxacin and TOC removal observed in sulfate and persulfate solutions.

4.4 Conclusion

Based on this study's results, anodic sulfate radical formation, anodic non-radical persulfate activation and cathodic persulfate activation are expected to contribute to accelerated removal rates of organic analytes susceptible to activated persulfate reactions. This study screened EAP as a viable candidate for point source treatment of wastewaters contaminated by fluoroquinilone antibiotics like ciprofloxacin. Future work should include analysis of reactions in real-water matrices (including presence of inorganic ions and high TOC levels) and application to other analytes. Reactor design must also be considered, including flow-through single-cell reactors, where mass transfer limitations to electrode surface might impact the system's ability to effectively

activate persulfate and subsequently degrade antibiotics. Further investigation is warranted in determining the efficacy of EAP for real-world application.

CHAPTER FIVE: CIPROFLOXACIN DEGRADATION IN SYNTHETIC HOSPITAL EFFLUENT

5.1 Introduction

For scale-up of EAP from laboratory to practical application, more must be understood about variables affecting EAP degradation results. These include effects of persulfate concentration, reactor configuration, sizes of electrodes and how the system performs when applied to complex wastewaters.

A significant concern with the use of electrochemical treatment of organic effluents is the formation of organic and inorganic disinfection by-products (DBPs), which can occur in reactive systems that contain both halogens and organic matter[46, 215]. During electrochemical treatment of water using a BDD anode, hydroxyl radicals formed at the BDD surface reacted with halogens to create halogenated radical species[135]. These halogenated radical species have the potential to react with organics in solution to create trihalomethanes and halo-acetic acids[216]. Hydroxyl radicals also can oxidize chloride ions to progressively form hypochlorite, chlorite, chlorate and perchlorate ions[135, 215, 217]. One study generated significant levels (1-2 mg L^{-1}) of chlorate and perchlorate during the electrochemical post-treatment of chlorinated drinking water[217]. Another study treating clofibric acid in synthetic secondary wastewater effluent generated over 100 mg L^{-1} perchlorate using a BDD anode, well above the US EPA's drinking water health advisory of 15 µg L^{-1} [218]. Finally, the inorganic DBP nitrite can form by oxidation of nitrate at the anode surface in slightly basic solutions[219].

In an activated persulfate system, the same hydroxyl-based radicals that are active in electrochemical systems can create organic and inorganic DBPs[216, 220]. The accelerated organic

degradation found by combing electrochemical reactions with activated persulfate reactions in an EAP system may compound the effect. It is imperative that DBP formation in EAP systems is understood to prove the feasibility of using persulfate addition as a means for treating complex wastewater matrices.

Ciprofloxacin is a fluoroquinolone antibiotic that is known to degrade electrochemically in sulfate and persulfate solutions, as shown in Chapter 4[194]. Because of its high environmental risk factor[29], ciprofloxacin was chosen as a model compound for this study and will be used to explore parameters influencing EAP for environmental contaminant removal.

The first objective of this study is to evaluate reactor configurations for use with EAP. Ciprofloxacin removal during the EAP process was studied in a rotating-disk electrode (RDE) reactor, a batch reactor, and a flow-through reactor (FTR). The second objective of the study is to establish effects of variable persulfate concentration and cathode size on ciprofloxacin removal using EAP. Third, ciprofloxacin degradation will be analyzed using EAP in a "real-world" matrix. To accomplish this objective, EAP was applied to ciprofloxacin removal from synthetic hospital effluent. Kinetics of ciprofloxacin decay were compared to that in pure electrolyte. Finally, this study aims to evaluate inorganic DBP formation during treatment of ciprofloxacin in synthetic hospital effluent. This step was completed for FTR and RDE reactor configurations.

5.2 Materials and Methods

5.2.1 Chemicals

Ciprofloxacin (98%), sodium persulfate (98%), potassium sulfate, sodium nitrate, potassium iodide (99+%), urea, uric acid, DL-tyrosine (98%), creatinine (99+%), sodium bicarbonate (Acros Organic), Optima formic acid, Optima Methanol (MeOH), magnesium perchlorate, RICCA

sodium chlorite (80%), sodium chloride, ammonia chloride, potassium phosphate monobasic, and fluoride standard were purchased from Fisher Scientific (Pittsburg, PA) and 1N sulfuric acid was from J.T. Baker. Deionized water (DI) (18.2 MΩ-cm) was produced by a Millipore Milli-Q system.

5.2.2 Experimental Setup

Initial ciprofloxacin concentrations were 0.043 mmol L^{-1} for all experiments (after addition of electrolyte and effluent as noted below), with ciprofloxacin preparation as described in Chapter 4. All experiments were spiked with concentrated electrolyte to the desired concentration just before applying current, as described in Chapter 4.

For hospital effluent experiments, concentrated hospital effluent was prepared in advance, with components shown in Table 5.1. The synthetic effluent was mixed with ciprofloxacin before electrolyte was added. Synthetic hospital effluent composition for all experiments is shown in Table 5.1 and is based on values determined experimentally in other publications[28, 221]. Total organic carbon, at a level of 221 mg/L, consisted of ciprofloxacin plus a mixture of urea, uric acid, creatinine and tyrosine as outlined in Table 5.1. Tyrosine has been shown to react with chlorine to form various organic chlorinated by-products[222]. Urea and creatinine are major constituents of human urine, and uric acid is a minor constituent; all three are expected to be present in hospital wastewater[223].

FTR experiments were conducted using apparatus depicted in Figure 5.1. A boron-doped diamond (BDD) anode and graphite cathode were used (both surface areas 18 cm^2). Recirculation was maintained at 16mL min^{-1}. The effective treatment time was calculated by equation 5.1[132]:

$$t_{eff} = t_{actual} * \frac{reactor\ volume}{total\ volume} \quad (5.1)$$

Table 5.1. Synthetic Hospital Effluent Composition for EAP Degradation of Ciprofloxacin

Compound	Ion/Molecule	Formula	Ion Concentration (mg L^{-1})
Potassium Sulfate	Sulfate	SO_4^{2-}	34.6
Potassium Nitrate	Nitrate	NO^{3-}	18.0
Ammonium Chloride	Ammonium	NH^{4+}	30.7
Potassium Phosphate Monobasic	Phosphate	$HPO4^{-}$	81.5
(Ammonium-, Sodium-) Chloride	Chloride	Cl^{-}	150.2
Sodium (-Chloride, -Bicarbonate)	Sodium	Na^{+}	85.5
Potassium (-Phosphate Monobasic, -Sulfate, -Nitrate)	Potassium	K^{+}	74.4
Sodium Bicarbonate	Bicarbonate	HCO_3^{-}	73.0
Total Organic Carbon		TOC	221
Urea	Urea	CH_4N_2O	800 (160 mg L^{-1} TOC)
Uric Acid	Uric Acid	C5H4N4O3	2.0 (0.71 mg L^{-1} TOC)
Tyrosine	Tyrosine	C9H11NO34	2.0 (1.2 mg L^{-1} TOC)
Creatinine	Creatinine	C4H7N3O	118 (50 mg L^{-1} TOC)
Ciprofloxacin	Ciprofloxacin	$C_{17}H_{18}FN_3O_3$	14 (8.6 mg L^{-1} TOC)

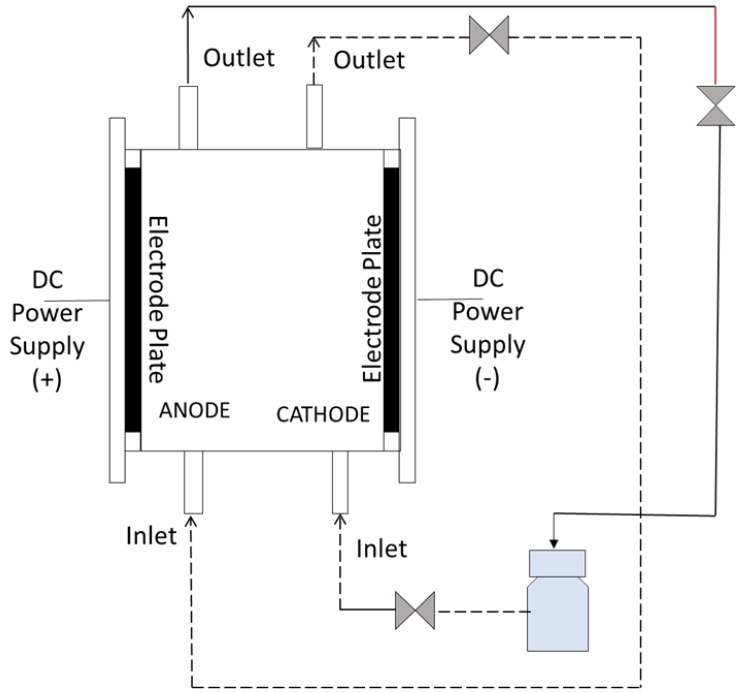

Figure 5.1. Schematic of the flow-through cell
Valves are used to allow for sampling.

The reactor volume was 36.5 mL and initial solution volume was 1000 mL. A BK Precision 1761 DC power supply purchased from Cole Parmer was used to maintain a current of 125 mA (current density = 6.9 mA cm^{-2}) for all FTR experiments.

Batch reactor experiments were conducted using the apparatus depicted in Figure 5.2. A BDD anode and graphite cathode were used (both surface areas 18 cm^2). Stirring was maintained with a magnetic stir bar. Initial solution volume was 500 mL. The same BK Precision power supply was used to maintain a current of 125 mA (current density 6.9 mA cm^{-2}) for all batch experiments. An SP-150 potentiostat (Bio-Logic Science Instruments, Knoxville, TN) with a mercury-mercury sulfate reference electrode was used to perform rotating disk electrode (RDE) experiments with schematic provided in Chapter 4 (Figure 4.1a). A multi-speed rotator (Pine

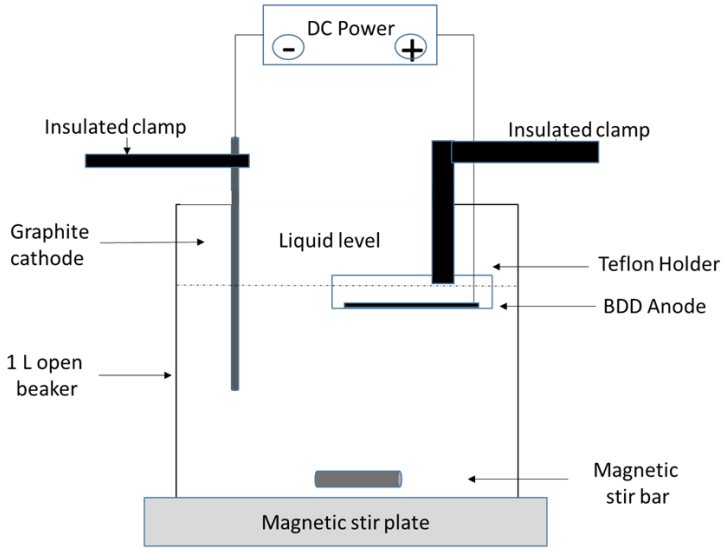

Figure 5.2. Schematic of batch reactor

Research Instrumentation, PRI, Durham, NC) set to 2000 rpm was used for the RDE experiments and bulk mixing was maintained using a magnetic stir-bar. The anode was a change-disk RDE tip (PRI) with BDD electrode insert of 0.196 cm^{-2} surface area (Fraunhofer Center for Coatings and Diamond Technologies, East Lansing, MI). The cathodes were Electron Microscopy Science graphite (Gr) rods (Fisher Scientific, Pittsburg, PA) with 4.8 cm^2 exposed to solution except as noted. Experiments were conducted with 200-mL solution volumes with a constant current of 15 mA (76 mA cm^{-2} current density).

Experiments were completed at 20˚C with an initial pH of 4.0 for experiments in the pure electrolyte and 7.05 for experiments in the synthetic hospital effluent. pH was not buffered in these experiments to prevent impacts due to buffering ions[141]. Average final pHs were consistently 2.15-2.5 in persulfate electrolyte, with or without effluent. In sulfate electrolyte, pH did not change during the reactions in the batch reactor. In the FTR and RDE reactors, pH increased during

reactions in pure sulfate electrolyte, ending at 8.0 in the FTR and 6.5 in the RDE reactor. With sulfate in the effluent, average final pHs were 2.5-3.0 for both reactor configurations.

5.2.3 Analytical Methods

Persulfate and ciprofloxacin-matrix concentrations were analyzed using a ThermoScientific Evolution 600 UV/Vis spectrometer (ThermoFisher, Pittsburg, PA) at 272 and 352 nm, respectively, with methodology described in Chapter 3[180, 181, 191].

HPLC-UV was used for direct ciprofloxacin analysis. Samples were prepared by extraction with Waters Sep-Pak tC2 cartridges as follows: conditioning with 1-mL methanol/1-mL DI water; loading 1-mL sample; extracting with 2x1-mL quantities of methanol/0.1% formic acid[191]. Extraction efficiency was 80%. Detailed methodology and statistical parameters were described in Chapter 4 and applied in this study.

A Shimadzu HPLC with Hypersil Gold column (100 mm long, 4.6 I.D., 5-micron particles) and detection by a SPD-M20A diode array detector at 278 nm was used to quantify ciprofloxacin, as described in Chapter 4.

A Shimadzu TOC-L analyzer with an ASI-L autosampler was used to analyze TOC. Statistical parameters for the method were described in Chapter 3[191].

A ThermoFisher fluoride ion selective probe was used to analyze fluoride (F^-) concentrations. TISAB II was added in equal amounts to samples and standards, to act as an ionic strength buffer and dissociate potential hydrofluoric acid. Statistical parameters for the calibration curve are found in Table 5.2. The method detection limit was 0.012 mmol L^{-1}.

Ion chromatography was used to analyze the inorganic disinfection by-products chlorite, chlorate, perchlorate and nitrite. A Dionex 2100/1100 dual column system with background

suppression was used. Statistical parameters for the calibration curves for these ions are found in Tables 5.3-5.6. The method detection limit for chlorite was 4.7×10^{-3}, chlorate was 1.7×10^{-4}mmol L^{-1}, perchlorate was 1.7×10^{-2} mmol L^{-1} and nitrite was 3.8×10^{-4} mmol L^{-1}.

Table 5.2. Statistical Parameters for Fluoride Calibration Curve

	Slope (mV per LN (mmol L^{-1} F^-))	Intercept (mV)
Value	-22.0	28.0
Standard error	0.50	1.86
R^2	0.9979	

Table 5.3. Statistical Parameters for Chlorite Calibration Curve

	Slope (peak area per mmol L^{-1})	Intercept (peak area)
Value	8.32	0.017
Standard error	0.22	0.034
R^2	0.9971	

Table 5.4. Statistical Parameters for Chlorate Calibration Curve

	Slope (peak area per mmol L^{-1})	Intercept (peak area)
Value	9.44	-0.065
Standard error	0.01	0.029
R^2	0.9996	

Table 5.5. Statistical Parameters for Perchlorate Calibration Curve

	Slope (peak area per mol L^{-1})	Intercept (peak area)
Value	7.23	-0.040
Standard error	0.13	0.016
R^2	0.9989	

Table 5.6. Statistical Parameters for Nitrite Calibration Curve

	Slope (peak area per mol L^{-1})	Intercept (peak area)
Value	8.40	-0.031
Standard error	0.11	0.011
R^2	0.9992	

5.3 Results

5.3.1 FTR experiments

In Chapter 4, persulfate addition was shown to enhance removal of ciprofloxacin in a RDE reactor. To better assess reactor configuration for practical application, experiments to electrochemically degrade ciprofloxacin in a FTR and batch reactor were performed in sulfate and persulfate electrolytes. At the same time, different levels of persulfate electrolyte were evaluated to optimize the amount of persulfate recommended for these systems.

FTR results are shown in Figure 5.3. Based on Chapter 4 results, it was expected that persulfate would offer an advantage over sulfate for electrochemical ciprofloxacin removal, due to persulfate activation at the cathode. In 11 mmol L^{-1} persulfate, 95% of ciprofloxacin and 66% of TOC were removed in t_{eff} = 60 minutes. Degradation followed pseudo-first-order kinetics, with ciprofloxacin-matrix k_{eff} = 9.53 +/- 1.03 x 10^{-4} s^{-1} and TOC k_{eff} = 3.16 +/- 0.45 x 10^{-4} s^{-1}. The fit for pseudo-first order was R^2 = 0.9549 for ciprofloxacin-matrix and R^2 = 0.9276 for TOC. Similar results were found in 11 mmol L^{-1} sulfate electrolyte with 92% removal of ciprofloxacin-matrix and 61% removal of TOC in t_{eff} = 60 minutes. Removal in sulfate also followed first-order kinetics with ciprofloxacin-matrix k_{eff} = 7.68 +/- 0.57 10^{-4} s^{-1} (R^2=0.9768) and TOC k_{eff} = 2.64 +/- 0.65 x 10^{-4} s^{-1} (R^2=0.8259). Removal of the ciprofloxacin-matrix was a statistically significant 19% faster in persulfate than sulfate (p=0.0016). TOC removal was not statistically different (p=0.1631).

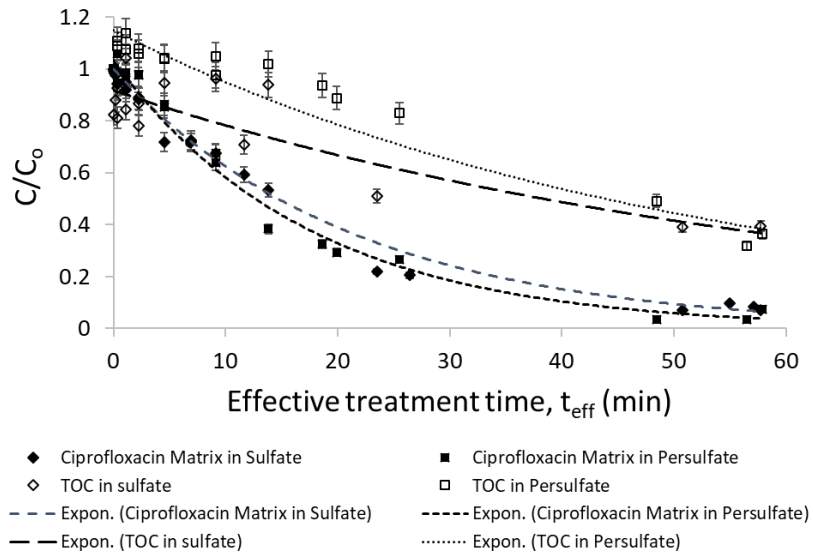

Figure 5.3. Degradation of ciprofloxacin-matrix and TOC in a flow-through reactor
$Sulfate_0$ = $Persulfate_0$ = 11 mmol L^{-1}. $Ciprofloxacin_0$ = 0.043 mmol L^{-1}. Current density 6.9 mA cm^{-2}.

Defluorination, shown in Figure 5.4, reached 100% and was similar in both electrolytes. After an initial spike of defluorination with the addition of electrolyte, the ciprofloxacin defluorinated linearly with the square root of time (Figure 5.4b). Because fluoride removal may lower the toxicity of fluorinated pharmaceuticals, defluorination is a significant outcome in the treatment of such compounds [189].

Persulfate reduction, determined in Chapter 4 to indicate persulfate activation in an RDE system, was confirmed to occur in the FTR (Figure 5.5a) via a pseudo-first order (Figure5.5b) mechanism with respect to persulfate. Persulfate generation from sulfate, previously established in an RDE system, was also confirmed in the FTR (Figure 5.5a). Because of the small difference in ciprofloxacin removal and lack of difference in TOC removal between no persulfate (sulfate only) and a high level of persulfate (11 mmol L^{-1}), intermediate levels were not tested.

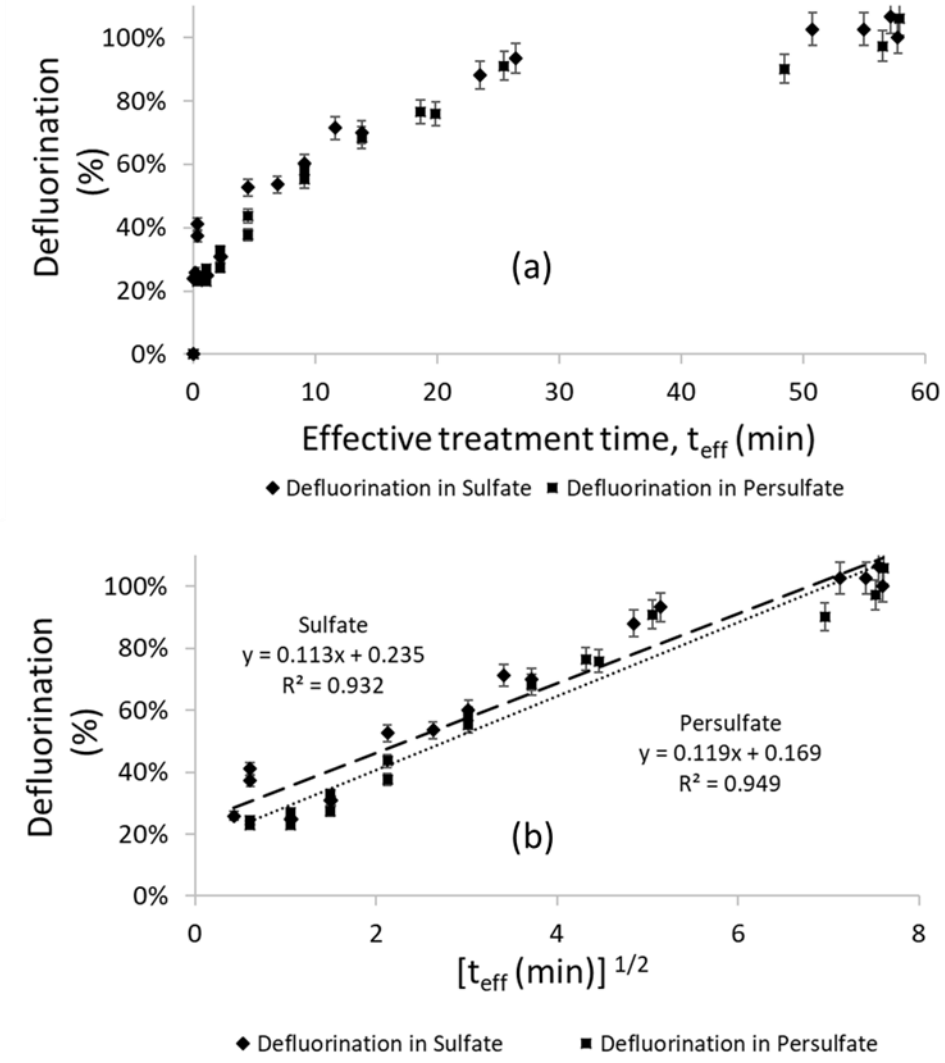

Figure 5.4. Defluorination of ciprofloxacin in a FTR
(a) Defluorination of ciprofloxacin in persulfate and sulfate electrolytes in an electrochemical FTR. (b) Modeling for Figure 5.4a. (a-b) $Sulfate_0 = Persulfate_0 = 11$ mmol L^{-1}. $Ciprofloxacin_0 = 0.043$ mmol L^{-1}. Current density 6.9 mA cm^{-2}.

5.3.2 Batch Reactor Experiments

Batch reactor results for electrochemical ciprofloxacin degradation are shown in Figure 5.6. Several levels of persulfate concentration were employed to better understand the limited difference in ciprofloxacin removal between persulfate levels on the FTR. Ciprofloxacin-matrix and TOC removal both followed pseudo-first order kinetics with respect to themselves, as illustrated in Figures 5.6a and 5.6b respectively. Reaction rate constants and statistics for the curves in Figure 5.6 are shown in Table 5.7. Ciprofloxacin-matrix removal ranged from 92.5% without persulfate to 94% at 3.1 mmol L^{-1} persulfate to 96.5% in 11 mmol L^{-1} persulfate, all in 300 minutes. The removal rate with the high level of persulfate ($k = 1.83 +/- 0.13\ 10^{-4}\ s^{-1}$) was a statistically significant 25% greater than with sulfate alone ($k = 1.37 +/- 0.12\ 10^{-4}\ s^{-1}$), at $p<0.0001$. With less persulfate (3.1 mmol L^{-1}) the 11% increase in rate was also significant ($p=0.0325$). TOC removal in the same timeframe averaged 78% and was not statistically significant without or with persulfate. As shown in Figure 5.6c, the ciprofloxacin-matrix reaction rate constant increased linearly ($R^2=0.9360$) with increasing persulfate concentration (Figure 5.6c). The pseudo-first order reaction rate constant (r) vs. persulfate concentration was modeled as $r=(3.94x10^{-6})\ x\ c + (1.36x10^{-4})$, where c is mmol L^{-1} persulfate.

Defluorination (Figure 5.7) was similar without persulfate and with high persulfate (11 mmol L^{-1}) and reached ~85%, so intermediate levels were not evaluated. Defluorination increases linearly with the square root of time, as shown in Figure 5.7b, so the provided equations on Figure 5.7b can be used to predict defluorination in this system.

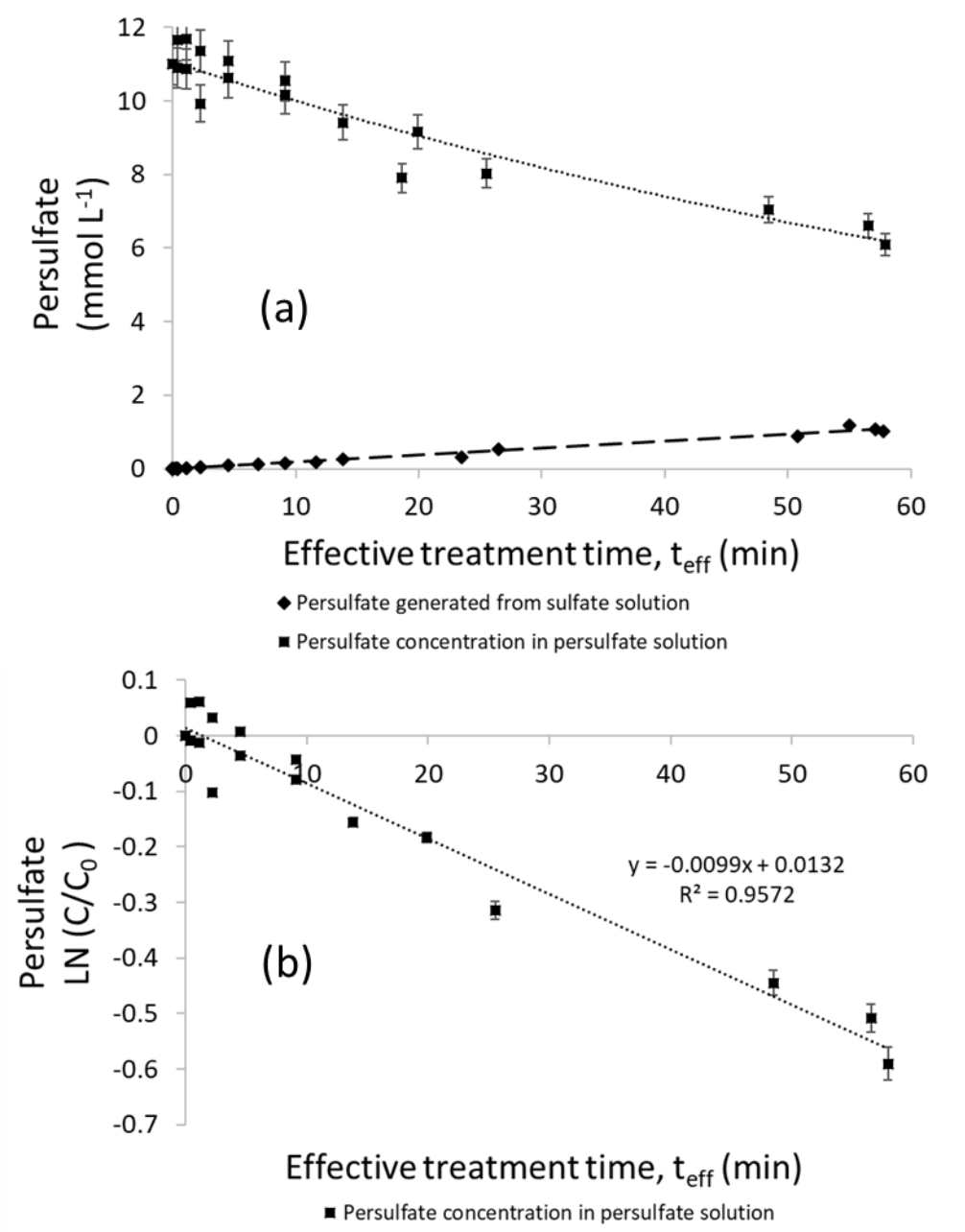

Figure 5.5. Persulfate behavior during ciprofloxacin removal in a FTR
(a) Persulfate concentration over time during ciprofloxacin removal in an electrochemical FTR. (b) Modeling for Figure 5.5a. (a-b) $Sulfate_0$ = $Persulfate_0$ = 11 mmol L^{-1}. $Ciprofloxacin_0$ = 0.043 mmol L^{-1}. Current density 6.9 mA cm^{-2}.

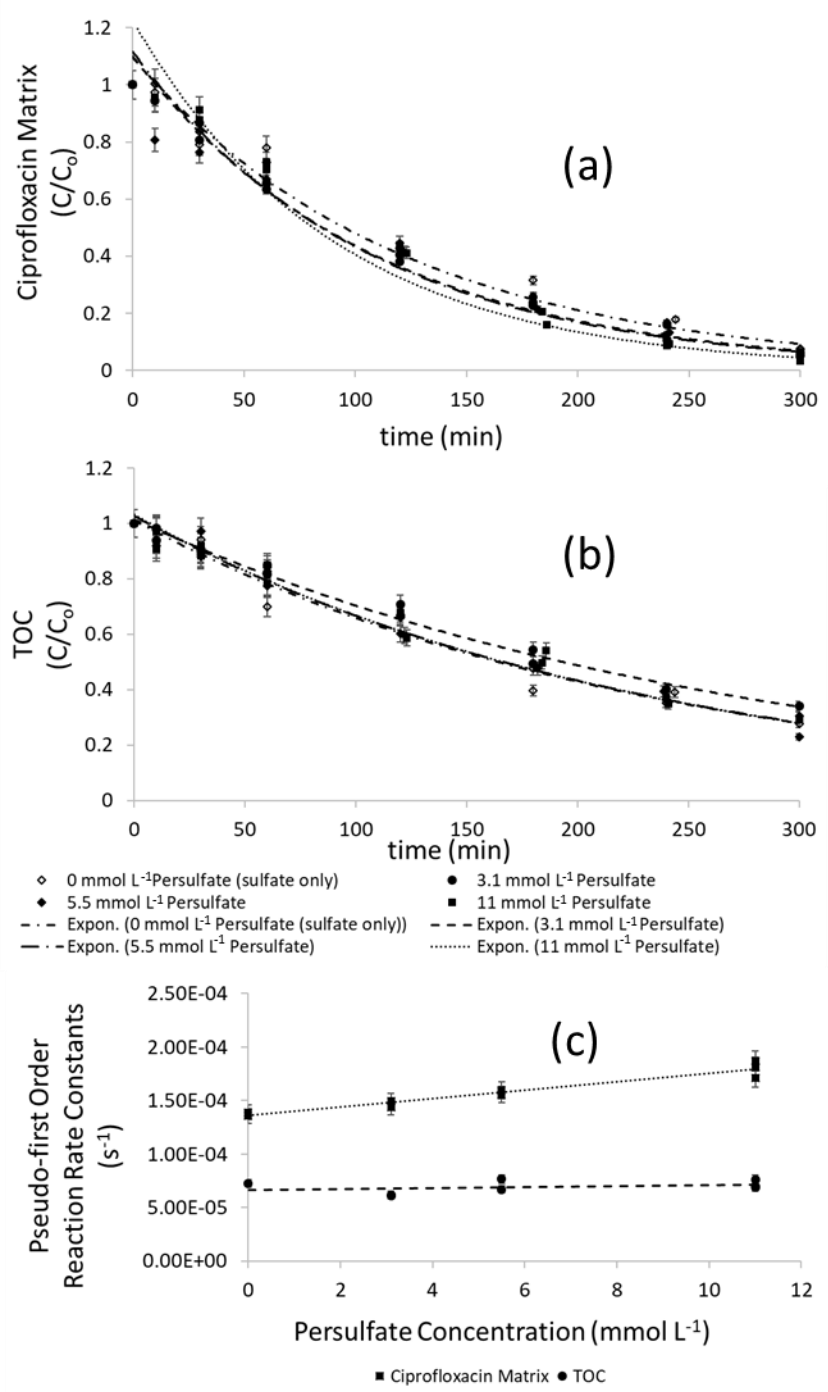

Figure 5.6. Degradation of ciprofloxacin-matrix and TOC in in a batch reactor
Sulfate$_0$ or Persulfate$_0$ shown on legend. Ciprofloxacin$_0$ = 0.043 mmol L^{-1}. Current density 6.9 mA cm^{-2}.

Table 5.7. Reaction rate constants and statistics for batch reactor with varying persulfate levels

Persulfate (mmol L^{-1})	Pseudo-first order reaction rate constant X 10^{-4} (s^{-1})	+/-	R^2 first-order fit	% difference from sulfate	Statistical significance of difference from sulfate
Ciprofloxacin-matrix					
11*	1.83	0.13	.9790	25%	$p < 0.0001$
5.5*	1.58	0.16	.9722	13%	p=0.0325
3.1	1.54	0.12	.9843	11%	p=0.037
0	1.37	0.12	.9794	n/a	n/a
TOC					
11	0.70	0.08	.9519	3%	p=0.8305 (not sig.)
5.5	0.72	0.06	.9771	0%	p=0.9041 (not sig.)
3.1	0.70	0.40	.9855	3%	p=0.7471 (not sig.)
0	0.72	0.07	.9755	n/a	n/a

**Difference between 11 and 3.1 was also a statistically significant 16% with p=0.0032; difference between 11 and 5.5 was also a statistically significant 14% with p=0.0217.*

Persulfate reduction and persulfate generation from sulfate is shown in Figure 5.8. Persulfate reduction occurred via a first-order mechanism as shown in Figure 5.8b.

It was suspected that the 1:1 anode:cathode ratio utilized in the batch and flow-through reactor make these anode dominant processes, so that persulfate activation at the cathode is not a significant contributor to degradation, especially for TOC removal. Chapter 4, in which cathodic persulfate activation influenced degradation, had an anode:cathode size ratio of 1:24 with an RDE setup, much different than the 1:1 ratio for experiments described thus far in the current study. It was also hypothesized that mass transfer limitations, minimized in the previous study through use of an RDE, inhibited the ability of radicals formed at the anode or cathode to be effective in solution. Mass transfer limitations would increase going from an RDE configuration with anode rotation at 2000 rpm, to a batch reactor with stirring maintained in the vessel, to a flow-through reactor with flow parallel to the reactor plate. This expectation follows the observed decrease in persulfate effectiveness from RDE (Chapter 4) to batch to FTR.

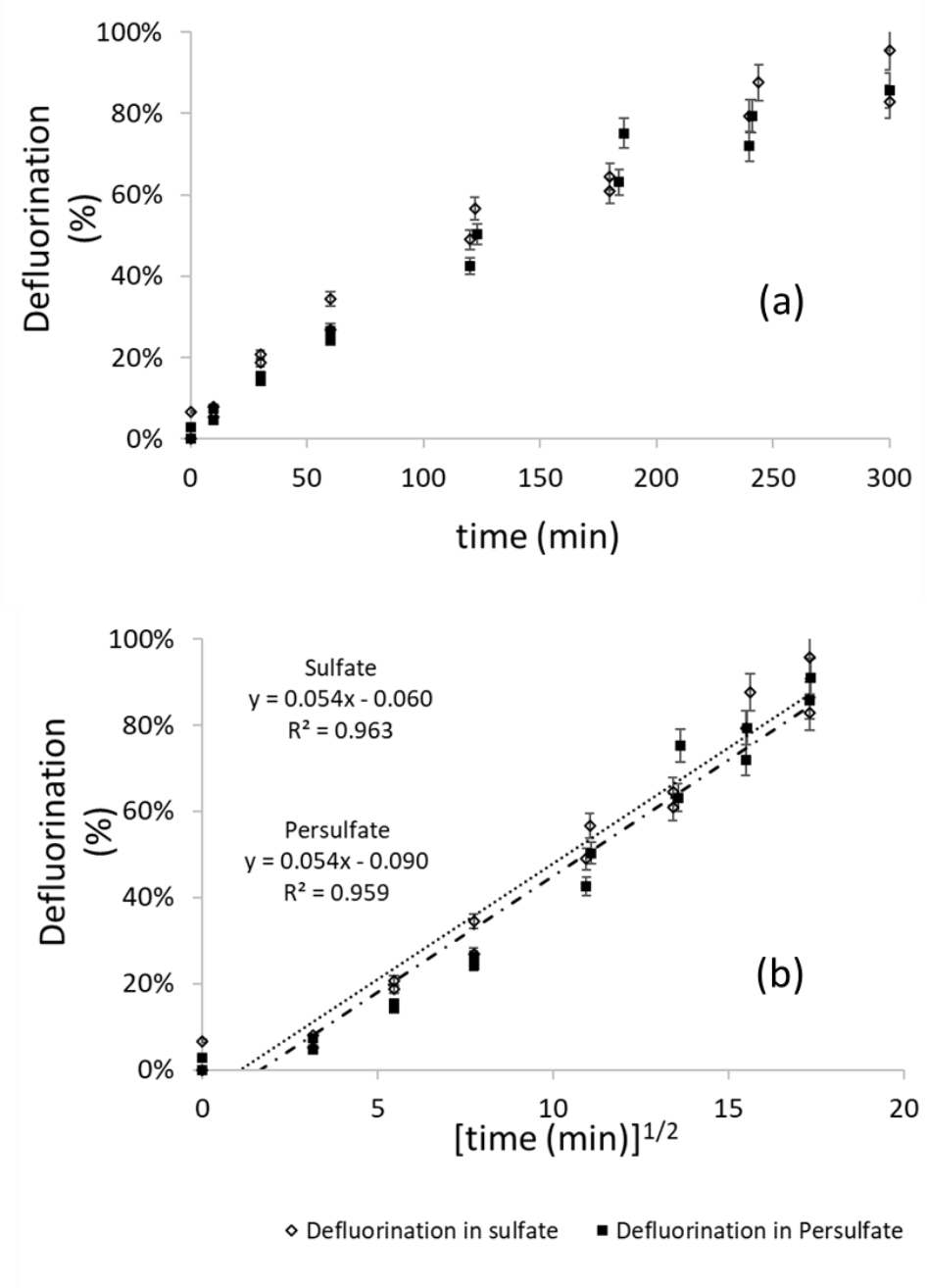

Figure 5.7. Defluorination of ciprofloxacin in a batch reactor
(a) Defluorination of ciprofloxacin in persulfate and sulfate electrolytes in an electrochemical batch reactor. (b) Modeling for Figure 5.7a. (a-b) $Sulfate_0$ or $Persulfate_0$ = 11 mmol L^{-1}. $Ciprofloxacin_0$ = 0.043 mmol L^{-1}. Current density 6.9 mA cm^{-2}.

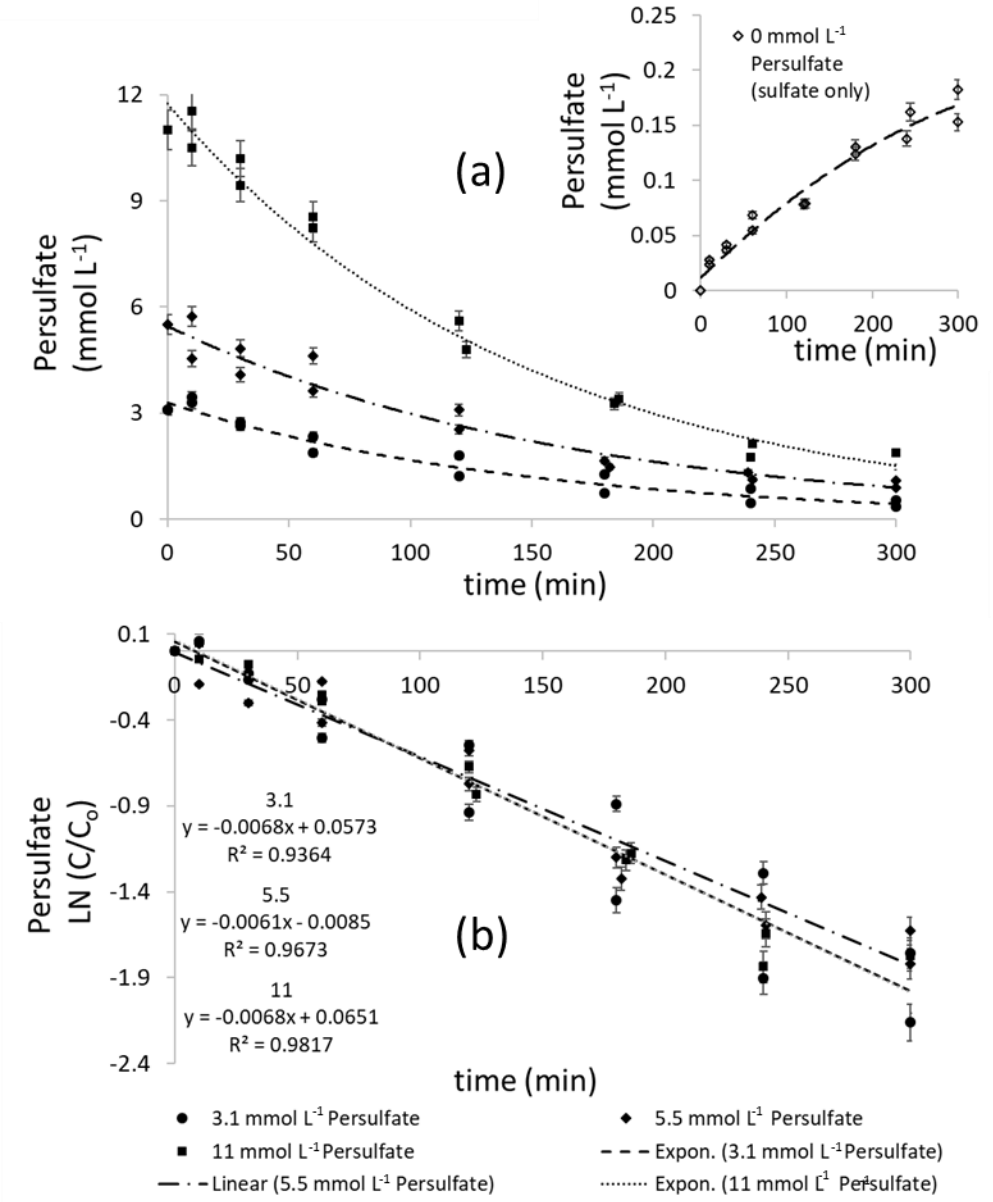

Figure 5.8. Persulfate behavior during ciprofloxacin removal in a batch reactor
(a) Persulfate concentration over time for ciprofloxacin removal in a batch reactor. (b) Modeling for Figure 5.8a. (a-b) $Persulfate_0$ indicated on legend. $Sulfate_0$ =11 mmol L^{-1} (Figure 5.8a inset). $Ciprofloxacin_0$ = 0.043 mmol L^{-1}. Current density 6.9 mA cm^{-2}.

5.3.3 RDE reactor experiments

To understand fundamental effects of cathode size, experiments were completed with an RDE while varying anode:cathode ratios (Figure 5.9). Pseudo-first order reaction rate constants and related statistics are provided in Table 5.8. Ciprofloxacin-matrix removal rate was significantly inhibited with an anode:cathode ratio of 1:1. There was a statistically significant 32% increase in reaction rate going from a ratio of 1:1 to 1:10, with further increases in cathode size having negligible effect on the ciprofloxacin-matrix. For TOC, reaction rates had a statistically significant 26% increase when cathode size increased to a ratio of 1:20 and continued to increase slightly up at a 1:40 ratio. In comparison, changing the anode:cathode from 1:1 to 1:30 for removal in nitrate electrolyte (an anode dominant process) did not change removal rates. It is clear that anode:cathode ratio must be considered when designing an EAP process, and that a smaller, more expensive and brittle BDD can be used relative to a larger, less expensive graphite material. To optimize removal time for both ciprofloxacin-matrix and TOC, a minimum of 1:20 anode: cathode size is recommended for use with a BDD/Gr pair.

Persulfate activation, measured by net persulfate reduction, was also evaluated. Increasing persulfate activation was observed for increasing cathode size (Figure 5.10). Persulfate increased with the square root of increasing cathode:anode ratio, as shown on Figure 5.10d.

Ciprofloxacin removal versus varying persulfate concentration was next evaluated on the RDE to understand the fundamentals effects of increasing persulfate levels when mass transfer limitations are minimized. Ciprofloxacin-matrix and TOC removal are shown in Figure 5.11. Both degraded via pseudo-first order mechanisms with respect to themselves, with reaction rates and related statistics shown in Table 5.9. The maximum degradation rate occurred in 11 mmol L^{-}

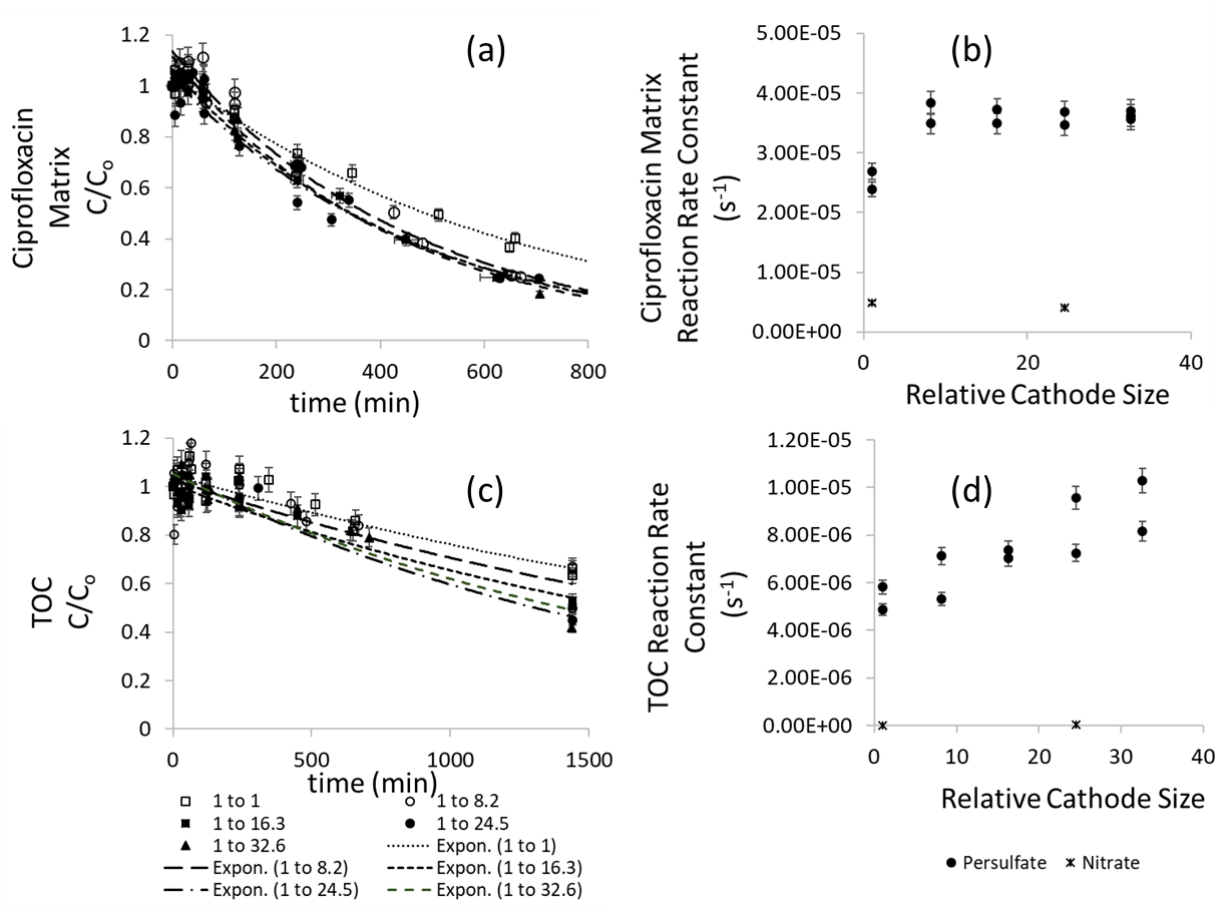

Figure 5.9. Ciprofloxacin-matrix and TOC removal with varying anode:cathode ratios
(a-b) Degradation of ciprofloxacin-matrix and TOC in an RDE over time in persulfate electrolyte with various anode:cathode ratios as noted in legend. (c-d) Reaction rate constants versus relative cathode size for curves shown in (a-b). Persulfate$_0$ = 22 mmol L^{-1}. Ciprofloxacin$_0$ = 0.043 mmol L^{-1}. Current density mA cm^{-2}. Also shown, reaction rate constants for degradation of ciprofloxacin-matrix and TOC in an RDE over time in nitrate electrolyte under same conditions and nitrate$_0$ = 22 mmol L^{-1}.

Table 5.8. Reaction rate constants and statistics for RDE with varying anode:cathode size

Ratio of size (anode:cathode)	Pseudo-first order reaction rate constant X 10^{-5} (s^{-1})	+/-	R^2 for first-order fit	% difference from 1:1	Statistical significance of difference from 1:1
*Ciprofloxacin-matrix/persulfate**					
1:40	3.93	0.29	.9850	36%	p<0.0001
1:30	3.57	0.38	.9635	32%	p<0.0001
1:20	3.67	0.25	.9843	32%	p<0.0001
1:10	3.65	0.33	.9774	32%	p<0.0001
1:1	2.51	0.20	.9782	n/a	n/a
*TOC from Ciprofloxacin/persulfate**					
1:40	0.88	0.14	.9211	40%	p<0.0001
1:30	0.82	0.21	.8424	35%	p=0.0109
1:20	0.72	0.11	.9303	26%	p=0.0136
1:10	0.63	0.21	.7291	16%	p=0.3861 (not sig.)
1:1	0.53	0.11	.8623	n/a	n/a
*Ciprofloxacin-matrix/nitrate**					
1:30	0.40	0.10	0.8094	-22%	p=0.9753 (not sig.)
1:1	0.49	0.23	0.5996	n/a	n/a
*TOC from Ciprofloxacin/nitrate**					
1:30	0.036	0.036	0.1260**	67%	p=0.3297 (not sig.)
1:1	0.012	0.12	0.0795**	n/a	n/a

**Experiments conducted in 22 mmol L^{-1} electrolyte*

***Poor statistics due to almost no removal in 24-hours for either case*

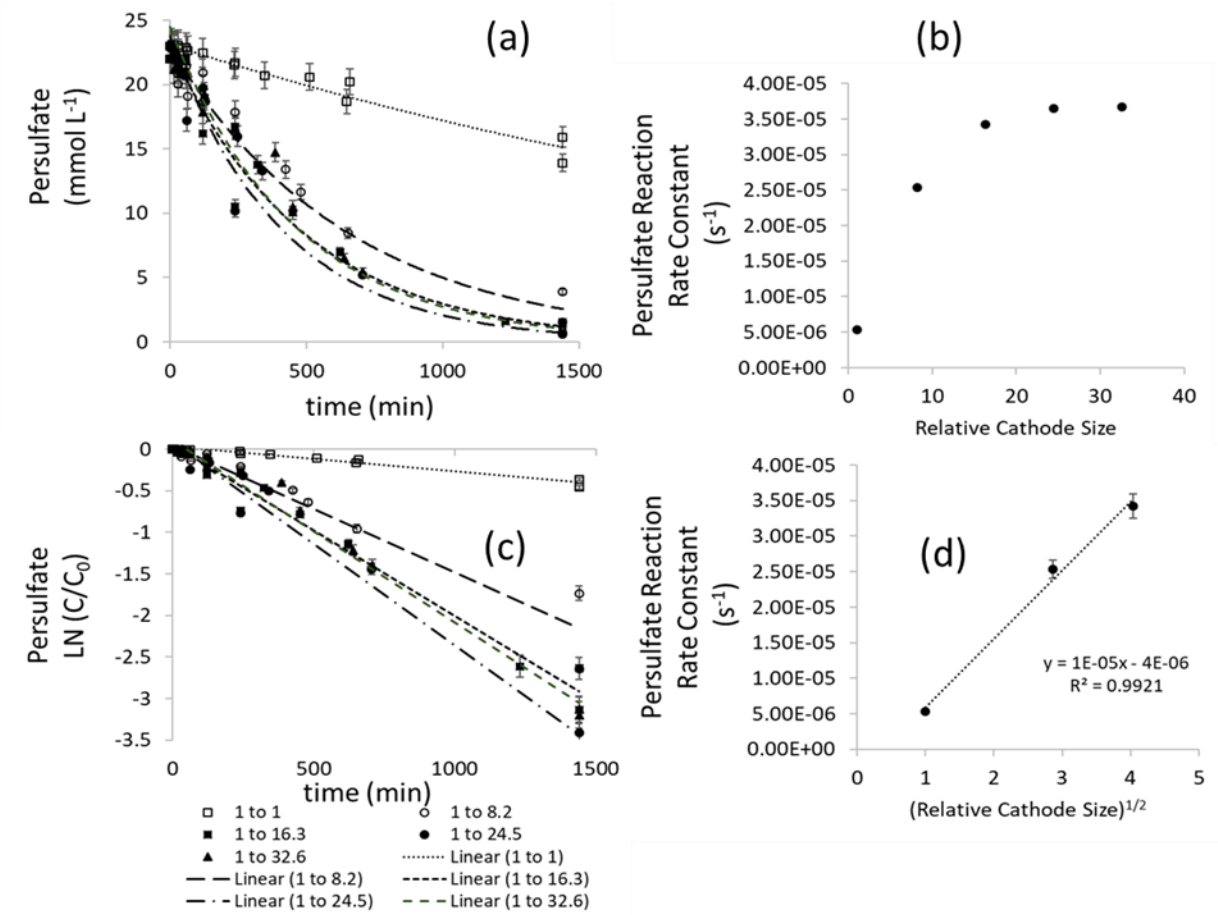

Figure 5.10. Persulfate behavior with different cathode sizes during ciprofloxacin removal in a RDE reactor

(a) Persulfate versus cathode size cathode sizes (b) Persulfate pseudo-first order reaction rate constant versus cathode size (relative to anode size) (c) Modeling for Figure 5.10a. (a-b) $Persulfate_0$ = 11 mmol L^{-1}. $Ciprofloxacin_0$ = 0.043 mmol L^{-1}. Current density 15 mA cm^{-2}.

persulfate electrolyte, with 80% ciprofloxacin-matrix removal achieved in 10 hours, and 65% TOC removal achieved in 24 hours. The ciprofloxacin removal rate constant of k = 4.5 +/- 0.28 10^{-5} s^{-1} in 11 mmol L^{-1} persulfate was 44% greater than the rate without persulfate, at $p<0.0001$. The TOC removal rate constant of k = 1.20 +/- 0.13 in 11 mmol L^{-1} persulfate showed even greater gains, with a statistically significant 53% increase versus no persulfate. The removal rate declined when doubling the persulfate from 11 to 22 mmol L^{-1}. A maximum persulfate level beyond which degradation plateaus or decreases has been shown in other studies and is likely due to sulfate radicals scavenging themselves [48]. At a lower 3.1 mmol L^{-1} persulfate, 30% faster removal rates for both ciprofloxacin-matrix (k = 3.67 +/- 0.13) and TOC (k = 0.82 +/- 0.13) were achieved, resulting in statistically significant great improvements over no persulfate for the ciprofloxacin-matrix degradation rate ($p<0.0001$) and the TOC degradation rate (at $p=0.0410$). Using 3.1 mmol L^{-1} persulfate offers the benefits of enhanced analyte removal while limiting the addition of sulfate to the system to 6.2 mmol L^{-1} (600 mg L^{-1}) from persulfate reduction (as demonstrated in Figure 4.10) and may be considered an optimum level for this system. The fundamental relationship of ciprofloxacin-matrix removal versus varying persulfate concentration was elucidated in Figure 5.11c. The reaction rate constants of ciprofloxacin-matrix and TOC both increased with the square root of persulfate concentration up to 11 mmol L^{-1}, with R^2 values of 0.8933 and 0.9325 respectively.

The smaller, or in some cases lack of, difference between ciprofloxacin-matrix and TOC removal rates at higher and lower persulfate levels in the batch and flow-through reactors are attributed to the use of a 1:1 anode:cathode ratio as well as mass transfer limitations. For EAP,

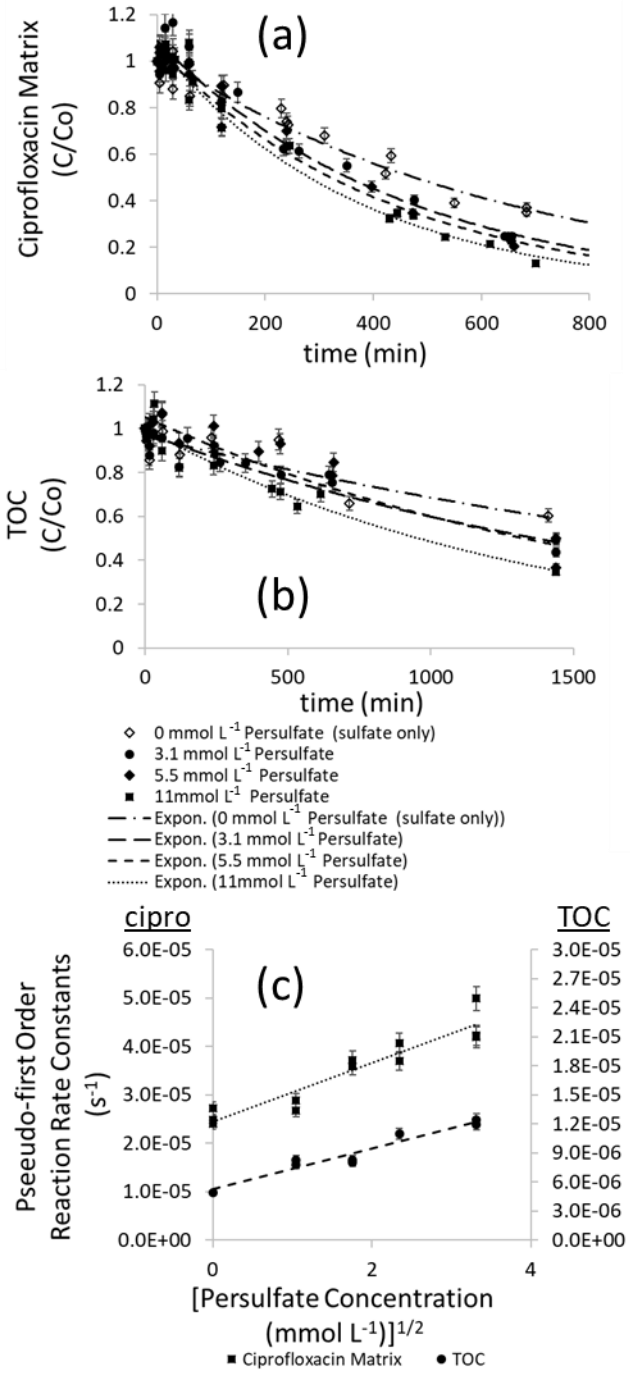

Figure 5.11. Ciprofloxacin-matrix and TOC removal with varying persulfate levels
(a-b) Degradation of ciprofloxacin-matrix and TOC in an RDE over time in varying levels of persulfate electrolyte. (c) Reaction rate constants versus square root of persulfate concentration (*1.1 mmol L^{-1} persulfate level not shown in a-b for clarity but included in trend on c). $Persulfate_0$ = 22 mmol L^{-1}. $Ciprofloxacin_0$ = 0.043 mmol L^{-1}. Current density 15 mA cm^{-2}.

Table 5.9. Reaction rate constants and statistics for RDE reactor with varying persulfate levels

Persulfate (mmol L^{-1})	Pseudo-first order reaction rate constant X 10^{-5} (s^{-1})	+/-	R^2 for first-order fit	% difference from sulfate	Statistical significance of difference from sulfate	Statistical significance from previous increment (i.e. 3.1 vs 1.1)
Ciprofloxacin-matrix						
22*	3.58	0.17	.9626	29%	$p < 0.0001$	
11	4.50	0.28	.9801	44%	$p < 0.0001$	p=0.0184
5.5	3.90	0.30	.9808	35%	$p < 0.0001$	p=0.2958
3.1	3.67	0.35	.9724	31%	$p < 0.0001$	p=0.8838
1.1*	2.82	0.18	.9868	10%	p=0.0588	p=0.0588
0	2.53	0.22	.9635	n/a	n/a	n/a
TOC						
22*	0.96	0.19	.9648	41%	p=0.0138	
11	1.20	0.13	.9686	53%	$p < 0.0001$	p=0.0001
5.5	0.93	0.18	.8725	39%	p=0.0206	p=0.2844
3.1	0.82	0.13	.9377	30%	p=0.0410	p=0.0001
1.1*	0.83	0.13	.9361	30%	p=0.0344	p=0.0344
0	0.57	0.25	.7764	n/a	n/a	n/a

**Not shown on Figure 5.11*

reactor design plays a critical role in the effectiveness of the system, as mass transfer must be maximized and anode:cathode ratio must be optimized. As in the flow-through and batch reactors, defluorination was not statistically different between 0 and 11 mmol L^{-1} (Figure 5.12). There was also no effect by cathode size. Defluorination increased linearly with time, demonstrative of a surface-based reaction. It was concluded that defluorination is dominated by an anodic electrochemical mechanism versus an EAP or cathodic mechanism.

Persulfate activation, demonstrated by persulfate reduction, occurred through a first-order mechanism, as shown in Figure 5.13a-b. Persulfate generation from sulfate is demonstrated in the inset. The persulfate curves in Figures 5.5b, 5.8b and 5.13b for FTR, batch and RDE respectively, all show a linear relationship between LN (C/C_0) with time, so it was concluded that persulfate

activates by a pseudo-first order mechanism, with respect to persulfate, across reactor configurations.

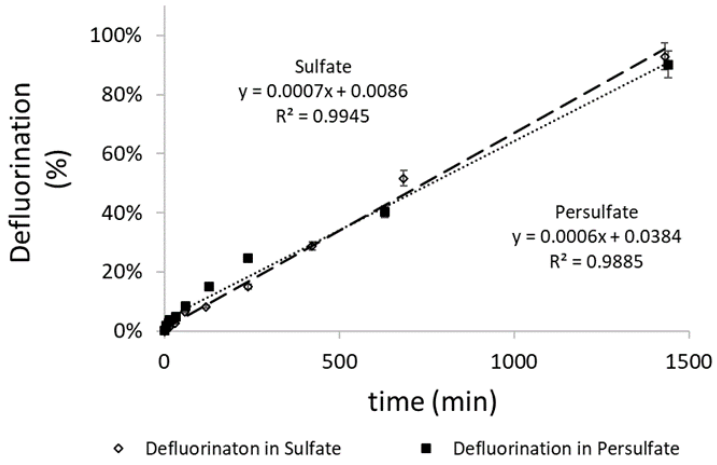

Figure 5.12. Defluorination of ciprofloxacin in a RDE reactor
(a) Defluorination of ciprofloxacin in persulfate and sulfate electrolytes in a RDE reactor. $Sulfate_0$ or $Persulfate_0$ = 11 mmol L^{-1}. $Ciprofloxacin_0$ = 0.043 mmol L^{-1}. Current density 15 mA cm^{-2}.

5.3.4 Second-order mechanisms

Although environmental contaminant degradation research relies almost solely on establishing pseudo-first order rate constants with respect to the analyte being degraded, evaluating second-order relationships may be useful for truly understanding fundamental mechanisms of decay. The second-order relationships between persulfate and pure ciprofloxacin (extracted by SPE and evaluated on HPLC/UV) was evaluated for the RDE configurations using equation 4.6. Results are shown in Figure 5.14 and indicate a second-order mechanism between ciprofloxacin decay and persulfate removal. Second-order rate constants calculated from the 11 and 3.1 mmol L^{-1} persulfate curves were 1.67 and 4.09 $x10^{-2}$ L mol^{-1} s^{-1}, respectively. These values are the same

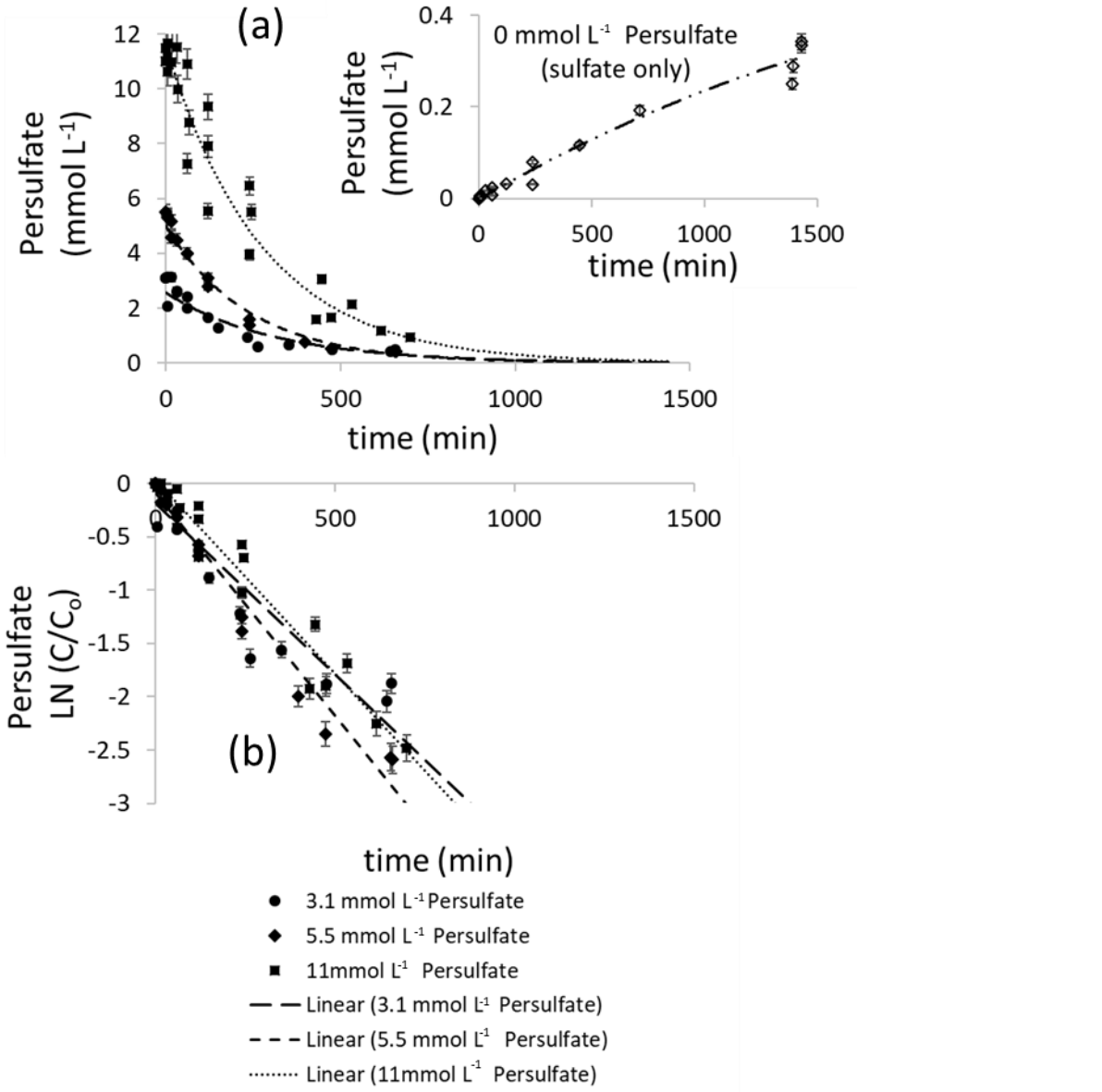

Figure 5.13. Persulfate behavior during ciprofloxacin removal in a RDE reactor
(a) Persulfate concentration with time. (b) Modeling for Figure 5.13a. (a-b) $Persulfate_0$ indicated on legend. $Sulfate_0$ =11 mmol L^{-1} (Figure S9a inset). $Ciprofloxacin_0$ = 0.043 mmol L^{-1}. Current density 15 mA cm^{-2}.

magnitude as the rate constant (2.10 x10^{-2} L mol^{-1} s^{-1}) calculated for the 22 mmol L^{-1} persulfate curve in Chapter 4. Combining the three curves gives a ciprofloxacin-persulfate second-order rate constant of 2.62 +/- 1.46 x 10^{-2} L mol^{-1} s^{-1} in the RDE reactor.

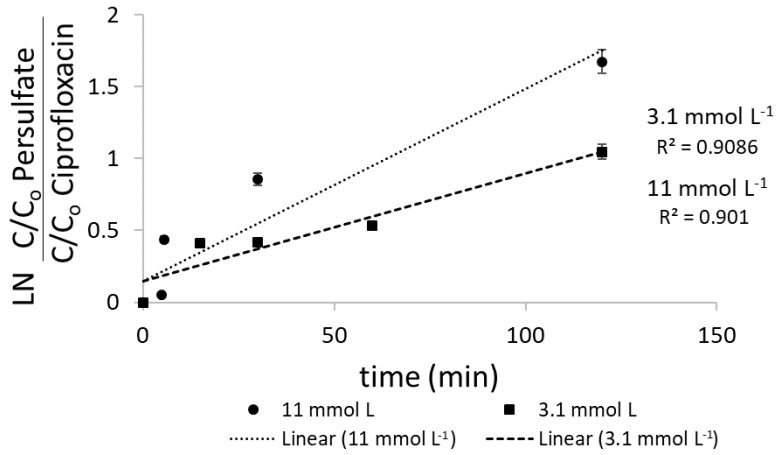

Figure 5.14. Second-order modeling for the reaction of Ciprofloxacin and Persulfate
$Persulfate_0$ = 3.1 and 11 mmol L^{-1} indicated on legend. $Ciprofloxacin_0$ = 0.043 mmol L^{-1}. Current density 15 mA cm^{-2}.

5.3.5 Ciprofloxacin degradation in synthetic hospital effluent

An important consideration when evaluating EAP for practical application is the system's performance for analyte removal in a "real-world" matrix. EAP was applied to ciprofloxacin removal from synthetic hospital effluent using the FTR and RDE reactor configurations. The FTR was utilized to demonstrate a reactor configuration that might be used in the field, while the RDE was employed to elucidate fundamentals of EAP in a complex matrix. Results for ciprofloxacin degradation in synthetic effluent in the FTR were compared to results obtained in pure electrolyte, as shown in Figure 5.15. A pseudo-first order mechanism (with respect to listed analytes) for decay of ciprofloxacin-matrix and TOC was found in the effluent as in pure electrolyte, with rate

constants and related statistics shown in Table 5.10. Removal rates for ciprofloxacin-matric decreased by 41% in the persulfate-effluent system and by 32% in the sulfate-effluent system. The difference in removal rates previously seen between sulfate and persulfate was not found in the effluent, so that persulfate did not offer an advantage for ciprofloxacin-matrix removal in the synthetic effluent. While TOC removal rates in both electrolyte/effluent systems declined by just over 50% versus pure electrolyte, of note is the 25x increase in TOC added by the effluent matrix. The decrease in performance was much less than the TOC added and it was concluded that the electrochemical FTR is capable of removing relatively high levels of TOC. This experiment was unable to discern differences in TOC removal from ciprofloxacin versus the other organics in solution. Persulfate provided a statistically significant ($p=0.0010$) 24% faster rate than sulfate for TOC removal from effluent. EAP in an FTR may offer an advantage over sulfate for TOC removal in complex matrices such as hospital effluent.

Defluorination in the effluent solution using the FTR followed the same pattern as in pure electrolyte, with defluorination increasing with the square root of effective time, as seen in Figure 5.16. Less defluorination was achieved in effluent, in keeping with the lower rate of ciprofloxacin-matrix removal achieved. Defluorination in the sulfate-effluent system was higher than that in the persulfate-effluent system, with 80% removal versus 62% in 60 minutes of effective time, respectively. It may be the interactions of persulfate and effluent at the anode interfered with the anode-dominated defluorination mechanism previously described.

Persulfate reduction in the effluent (Figure 5.17) followed the same trend as reduction in pure persulfate (Figure 5.5). On the other hand, persulfate generation from sulfate was much less in the effluent, with only 0.10 mmol L^{-1} detected over the 60-minute effective treatment time in

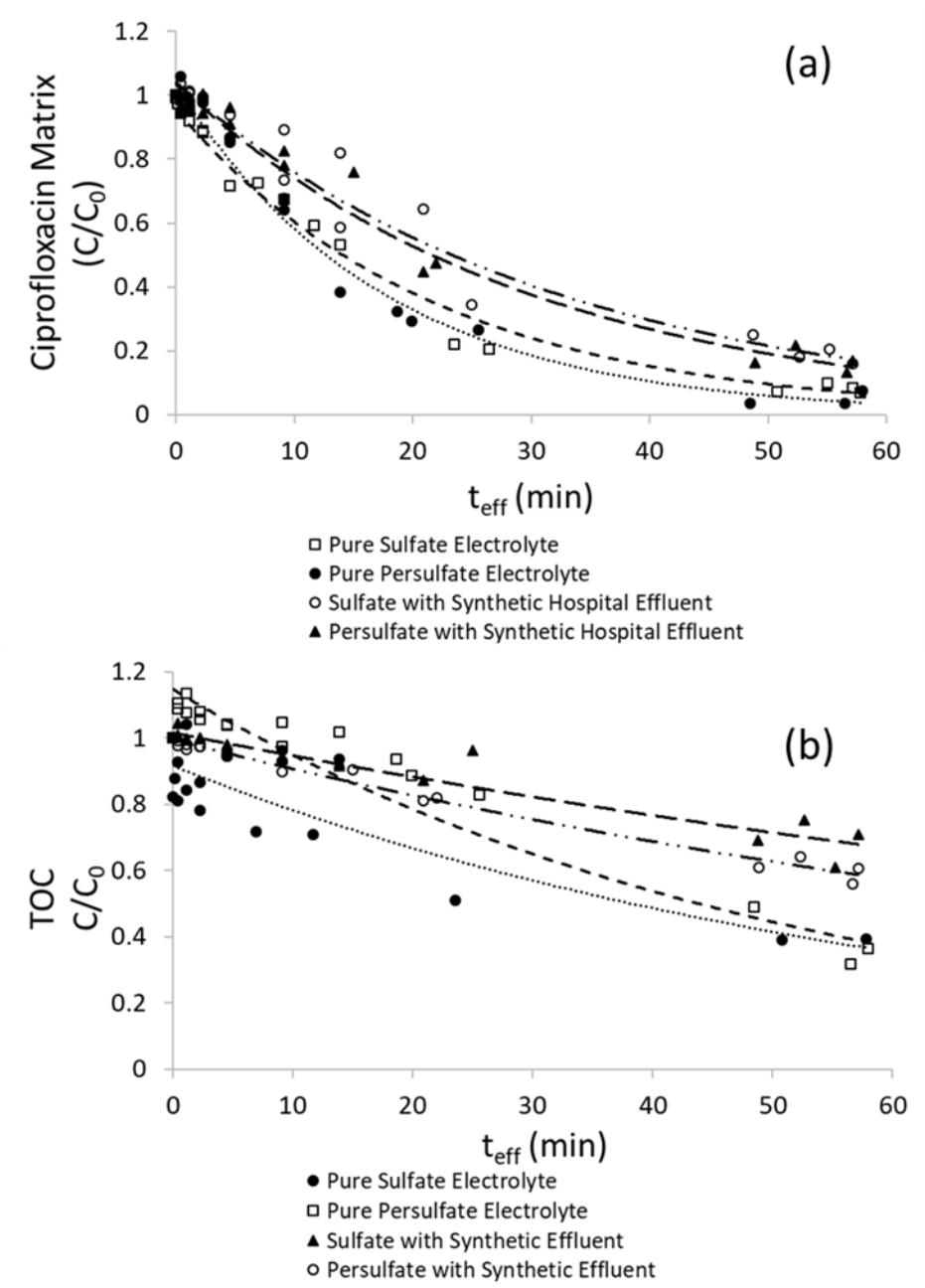

Figure 5.15. Degradation of ciprofloxacin-matrix and TOC in synthetic hospital effluent in a FTR.

$Sulfate_0$ = $Persulfate_0$ = 11 mmol L^{-1}. TOC_0=221 mg L^{-1} in effluent and 8.6 mg L^{-1} in pure electrolyte. $Ciprofloxacin_0$ = 0.043 mmol L^{-1}. Current density 6.9 mA cm^{-2}.

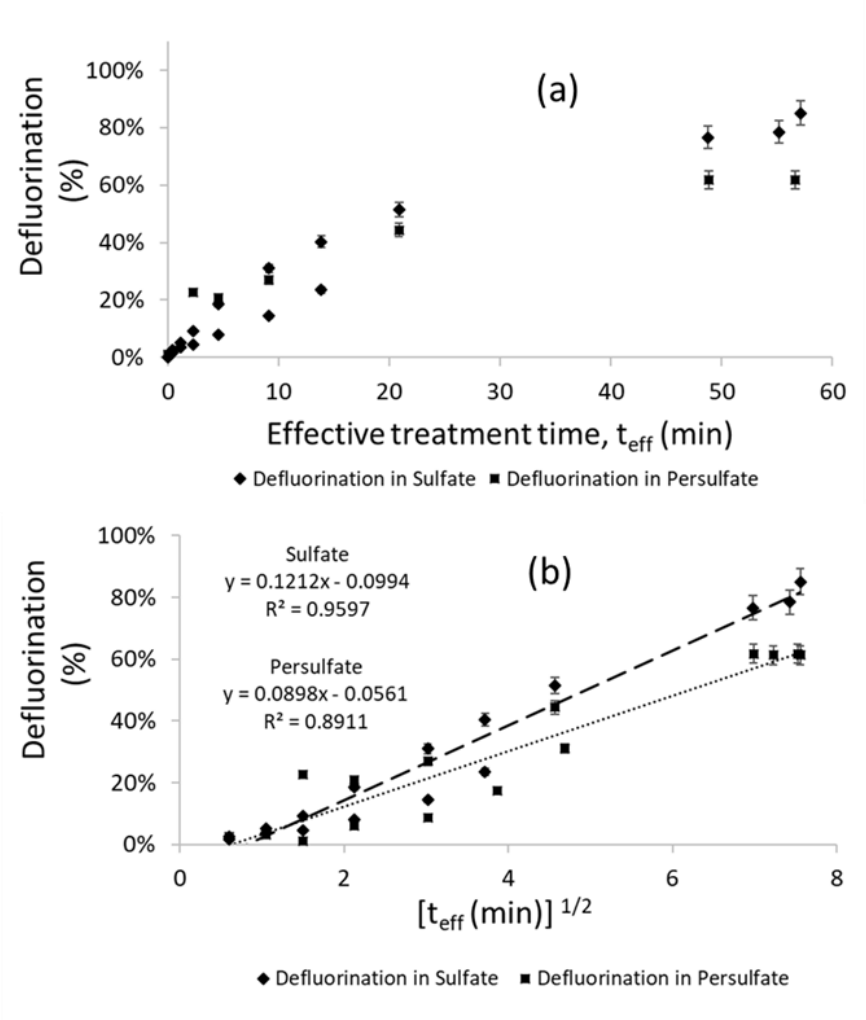

Figure 5.16. Defluorination of ciprofloxacin in synthetic hospital effluent in a FTR
(a) Defluorination with time. (b) Modeling for Figure 5.16a. (a-b) $Sulfate_0$ or $Persulfate_0$ = 11 mmol L^{-1}. $Ciprofloxacin_0$ = 0.043 mmol L^{-1}. Current density 6.9 mA cm^{-2}.

Table 5.10. Reaction rate constants and statistics for FTR experiments in hospital effluent

Persulfate (mmol L^{-1})	Pseudo-first order reaction rate constant X 10^{-4} (s^{-1})	+/-	R^2 for first-order fit	% difference in effluent versus electrolyte	Statistical significance of difference in electrolyte versus effluent
Ciprofloxacin-matrix/persulfate					
Synthetic Effluent	5.65	0.42	.9791	-41%	$p < 0.0001$
Pure electrolyte	9.53	1.03	.9549		
**TOC/persulfate*					
Synthetic Effluent	1.54	0.10	.9847	-51%	$p < 0.0001$
Pure electrolyte	3.16	0.45	.9276		
Ciprofloxacin-matrix/sulfate					
Synthetic Effluent	5.25	0.47	.9681	-32%	$p < 0.0001$
Pure electrolyte	7.68	0.57	.9768		
**TOC/sulfate*					
Synthetic Effluent	1.17	0.19	.9058	-56%	$p < 0.0001$
Pure electrolyte	2.64	0.65	.8259		

**Note that starting TOC was significantly higher in the effluent, going from 8.6 mg L^{-1} in pure electrolyte to 221 mg L^{-1} in effluent*

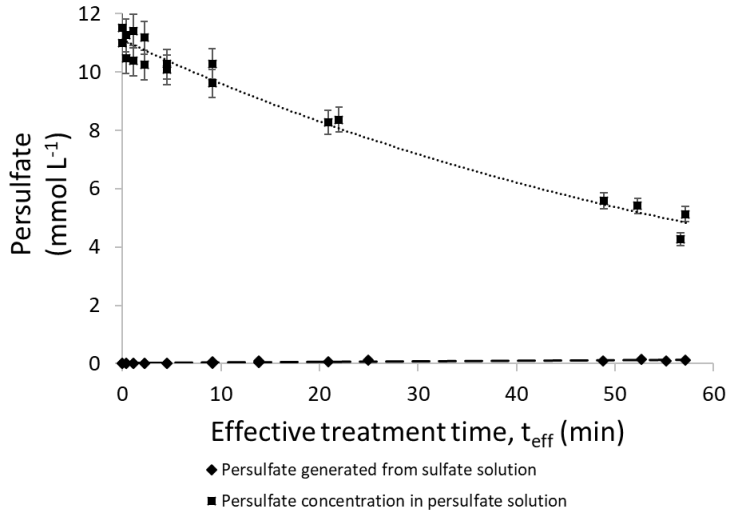

Figure 5.17. Persulfate behavior during ciprofloxacin removal in synthetic hospital effluent in a FTR
$Sulfate_0$ or $Persulfate_0$ =11 mmol L^{-1}. $Ciprofloxacin_0$ = 0.043 mmol L^{-1}. Current density 6.9 mA cm^{-2}.

effluent versus the accumulation of 1.0 mmol L^{-1} in the same time in pure sulfate electrolyte. Similar to defluorination, the interaction of the effluent at the anode may interfere with formation of persulfate from sulfate at the anode.

During experiments using the RDE, extracted ciprofloxacin (separated by SPE and measured by HPLC) was measured in addition to ciprofloxacin-matrix to study differences that may occur in molecular ciprofloxacin removal versus the ciprofloxacin-matrix. Extracted ciprofloxacin was analyzed in pure electrolyte and effluent. The pure ciprofloxacin degraded via pseudo-first order mechanisms, with respect to ciprofloxacin concentration, in all solutions, with reaction rate constants and statistics provided in Table 5.11. In pure electrolyte, differences in removal between persulfate levels was similar for molecular ciprofloxacin as for the ciprofloxacin-matrix, although molecular ciprofloxacin removal rates were an order of magnitude higher than those for the ciprofloxacin-matrix. It is clear from comparing Figure 5.18a and b that pure

ciprofloxacin removal slowed dramatically in synthetic hospital effluent, unlike ciprofloxacin matrix or TOC in the effluent. For pure ciprofloxacin and TOC, differences in removal rates by persulfate level, observed in pure electrolyte, did not translate to differences in removal in effluent. In fact, the ciprofloxacin removal rate from effluent with 3.1 mmol L^{-1} persulfate was actually slower than with no persulfate. The only variable that was positively influenced by persulfate addition to the effluent system was the ciprofloxacin-matrix, in which 80% and 88% faster removal was obtained with the addition of 3.1 and 11 mmol L^{-1} persulfate, respectively. As with the FTR, TOC rates between pure electrolyte and effluent only dropped between 21% and 43%, despite a 25 times increase in the initial amount of TOC. This confirms findings from the FTR that this electrochemical process is capable of removing relatively high levels of organics from a complex matrix such as hospital effluent.

Defluorination of ciprofloxacin in the effluent followed a similar linear trend to that in pure electrolyte, although lower amounts of defluorination were achieved (Figure 5.19). There was also a greater difference in the defluorination rate between 11 mmol L^{-1} persulfate and sulfate only solutions when the effluent was present. This was correlated with the greater difference in ciprofloxacin-matrix removal, where the ciprofloxacin-matrix was found in Chapter 4 to be partially comprised of large fluorinated chromophores.

Persulfate behavior in the synthetic effluent was also evaluated, as shown in Figure 5.20. While persulfate reduction was similar to that in pure electrolyte, persulfate generation from sulfate was not observed. This matches findings in the FTR and further indicates an interfering effect at the anode from the effluent.

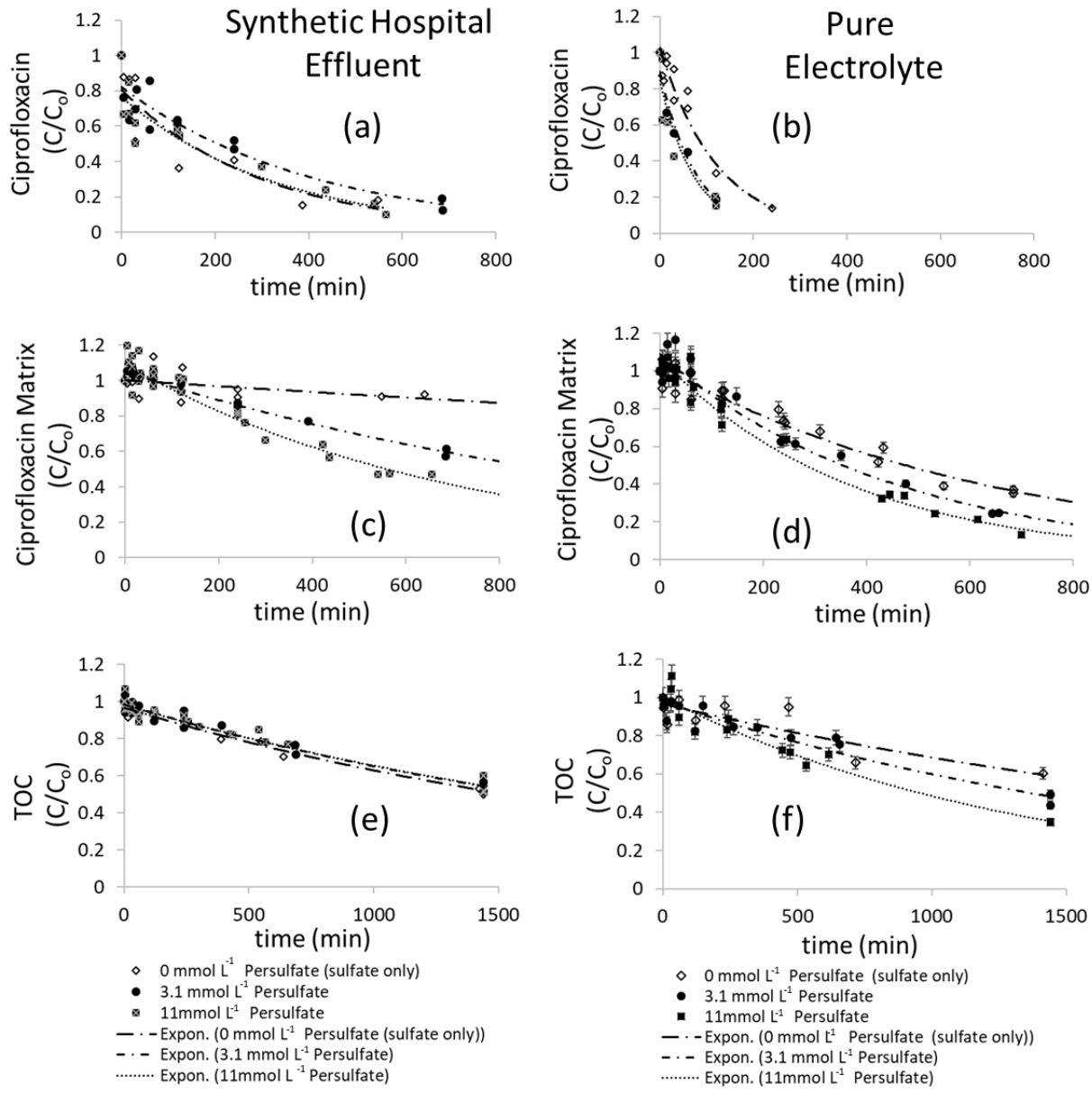

Figure 5.18. Ciprofloxacin degradation over time in pure electrolyte and synthetic hospital effluent in a RDE reactor

Persulfate$_0$ indicated on legend. Sulfate$_0$ = 11 mmol L^{-1}. TOC$_0$=221 mg L^{-1} in effluent and 8.6 mg L^{-1} in pure electrolyte. Ciprofloxacin$_0$ = 0.043 mmol L^{-1}. Current density 15 mA cm^{-2}.

Table 5.11. Reaction rate constants and statistics for RDE experiments in hospital effluent

Persulfate (mmol L^{-1})	Pseudo-first order reaction rate constant X 10^{-5} (s^{-1})	+/-	R^2 for first-order fit	% difference from sulfate	Statistical significance of difference from sulfate
Ciprofloxacin in pure electrolyte					
11	23.3	6.5	.9251	41%	p=0.0013
3.1	21.7	6.5	.9742	37%	p=0.0039
0	13.7	1.8	.9622	n/a	n/a
Ciprofloxacin in effluent					
11	5.00	1.0	.9134	-10%	p=0.6220 (not sig.)
3.1	4.00	0.67	.9308	-38%	p=0.0747
0	5.50	1.8	.8446	n/a	n/a
Ciprofloxacin-matrix in pure electrolyte: see Table 5.8					
Ciprofloxacin-matrix in effluent					
11	2.33	0.25	.9389	88%	p < 0.0001
3.1	1.38	0.12	.9775	80%	p < 0.0001
0	0.28	0.28	.2288	n/a	n/a
TOC in pure electrolyte: see Table 5.8					
TOC in effluent					
11	0.68	0.06	.9535	6%	p=0.3127 (not sig.)
3.1	0.68	0.07	.9638	6%	p=0.4917 (not sig.)
0	0.72	0.06	.9834	n/a	n/a

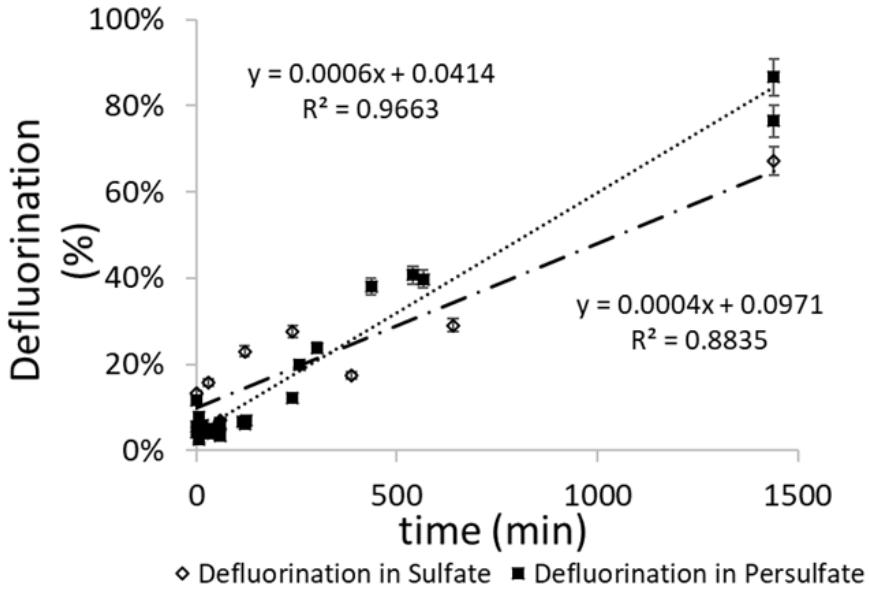

Figure 5.19. Defluorination of ciprofloxacin in synthetic hospital effluent in a RDE reactor $Sulfate_0$ or $Persulfate_0$ = 11 mmol L^{-1}. $Ciprofloxacin_0$ = 0.043 mmol L^{-1}. Current density 15 mA cm^{-2}.

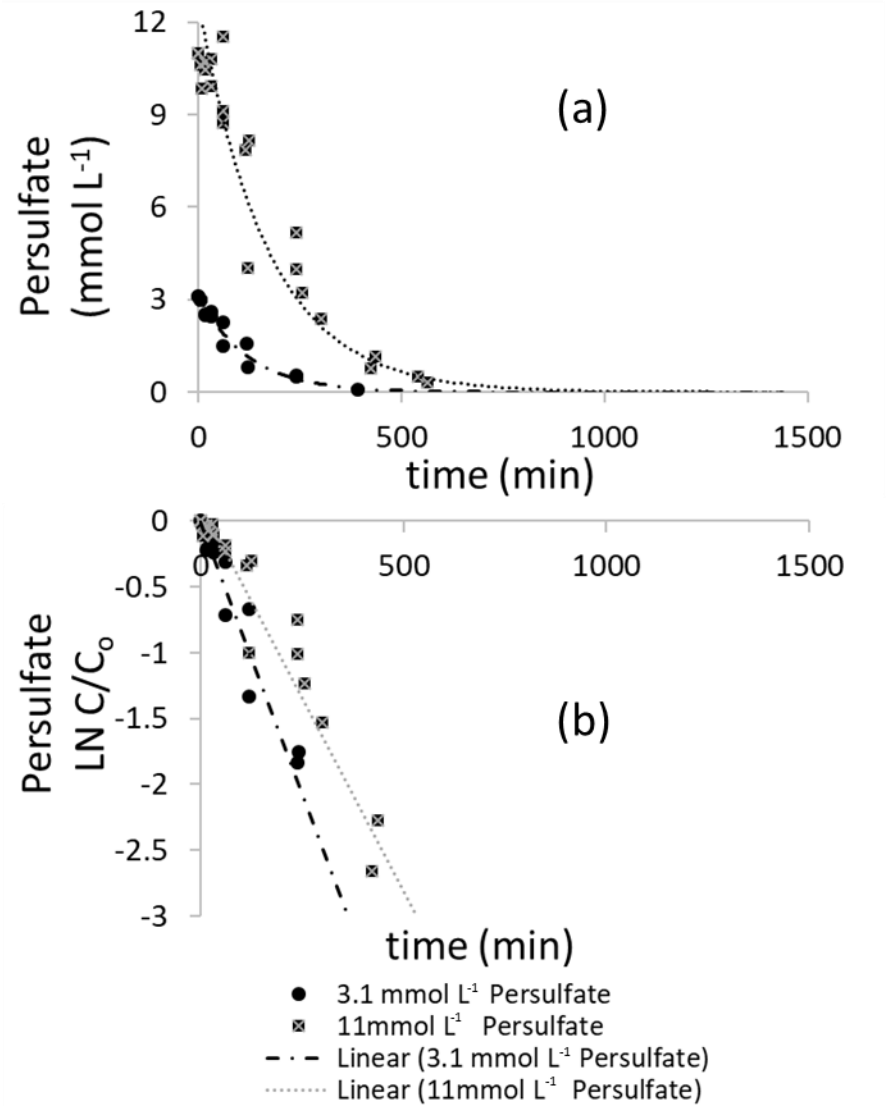

Figure 5.20. Persulfate behavior during ciprofloxacin removal in synthetic hospital effluent in a RDE reactor

(a) Persulfate concentration with time. (b) Modeling for Figure 5.20. (a-b) $Persulfate_0$ indicated on legend. $Ciprofloxacin_0$ = 0.043 mmol L^{-1}. Current density 15 mA cm^{-2}. Persulfate generation from sulfate did not occur and is not pictured.

5.3.6 Inorganic disinfection by-products

The inorganic DBPs chlorite, chlorate, perchlorate and nitrite were evaluated to screen EAP for practical application. This study was conducted on both the FTR and RDE reactor, and formation amounts were compared between sulfate and persulfate electrolytes. The variable mg L^{-1} DBP formed per mg L^{-1} TOC removed was utilized. Figure 5.21 shows that the formation of inorganic DBPs in the FTR is mostly independent of the presence of persulfate. Slightly more chlorate was formed in the FTR in the presence of persulfate.

Figure 5.22 shows that, like the FTR, formation of inorganic DBPs in the RDE is mostly independent of the presence of persulfate. Slightly more nitrite was formed in the RDE experiments with persulfate than without persulfate.

While the persulfate independence shows that use of EAP does not provide *additional potential for* inorganic DBP formation, the overall level of inorganic DBPS formed during the time to achieve significant TOC removal is of concern for both electrochemical setups, as shown in Table 5.12. The FTR generated over 200 mg L^{-1} perchlorate during the 60-minute effective treatment time and the RDE generate over 29 mg L^{-1} perchlorate in a 24-hour treatment time.

Perchlorate is chemically stable because of its high activation energy (120 kJ mol^{-1}) and is not removed or destroyed by most traditional wastewater treatment processes[224]. With use of EAP as a pre-treatment for release of hospital effluent to a WWTP, perchlorate may pass through the system unchanged and enter the environment. The FTR-EAP system is not recommended in its current design as a stand-alone treatment system. It may be best coupled with a successful perchlorate removal technique, such as ion-exchange, which would serve to remove organic components in the EAP phase and inorganic DBP through ion-exchange resin[224].

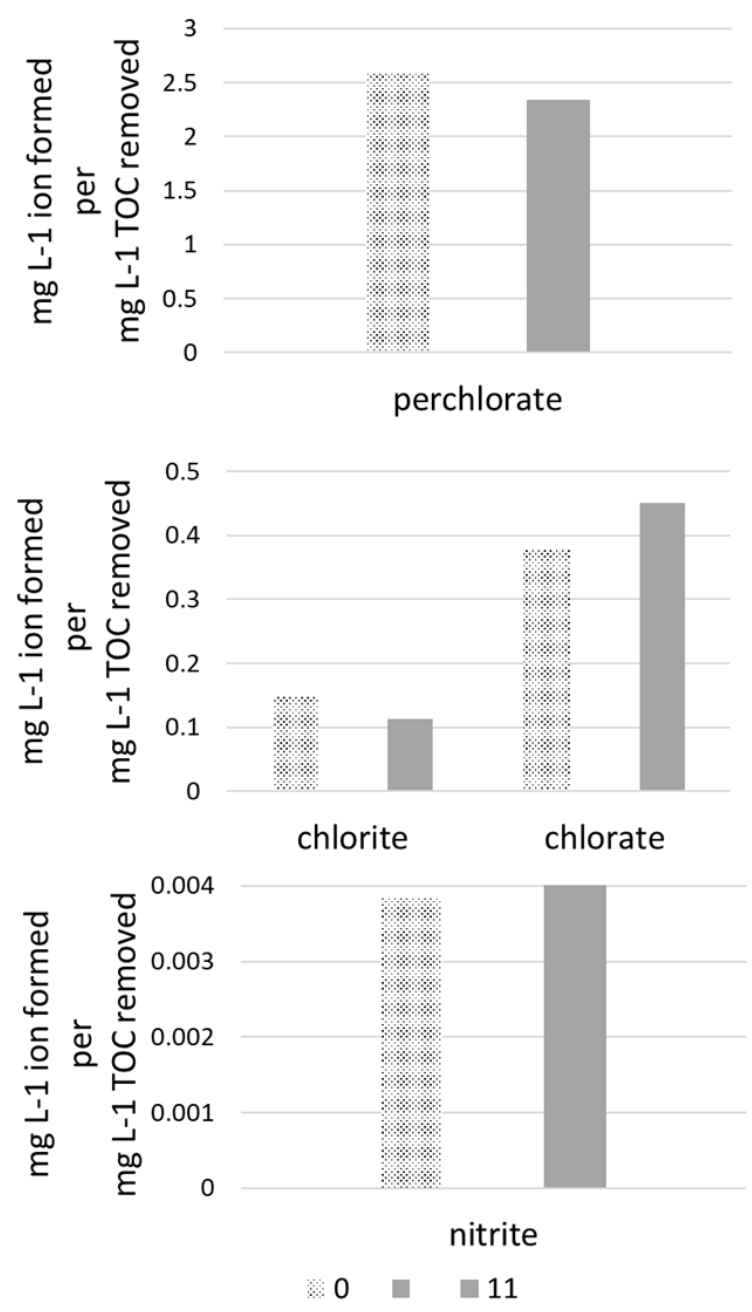

Figure 5.21. Formation of inorganic disinfection by-products in synthetic hospital effluent in a FTR

Persulfate$_0$ indicated on legend. Sulfate$_0$ = 11 mmol L^{-1}. TOC$_0$=221 mg L^{-1}. Current density = 6.9 mA cm^{-2} on FTR.

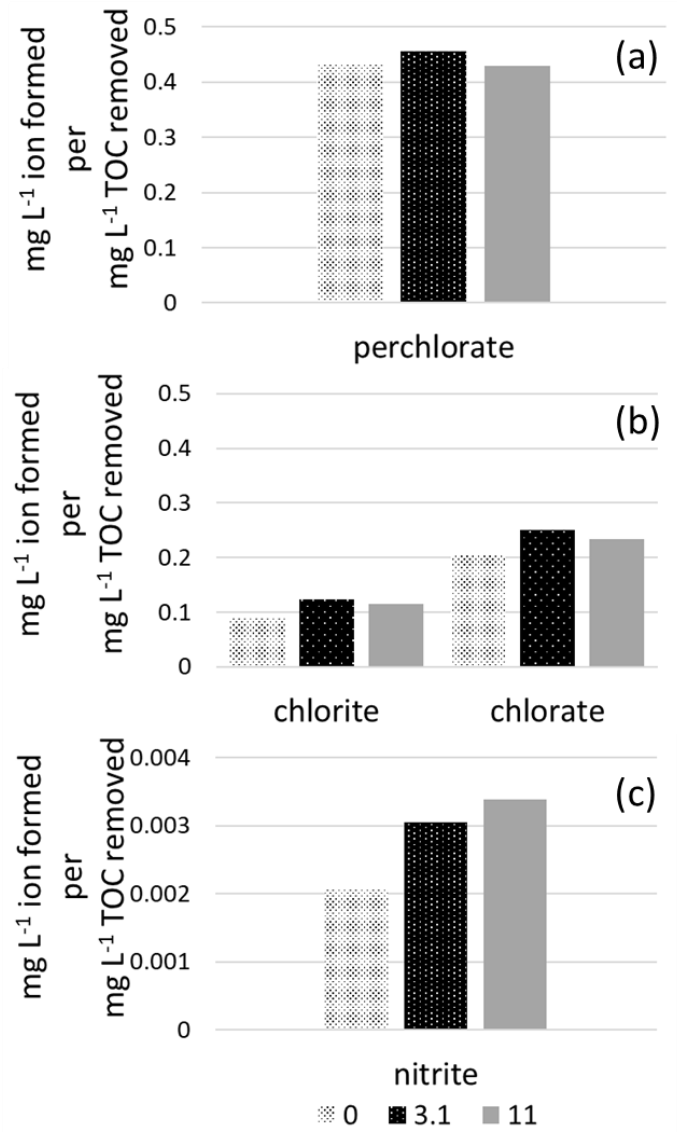

Figure 5.22. Formation of inorganic disinfection by-products in synthetic hospital effluent in a RDE reactor

Persulfate$_0$ indicated on legend. Sulfate$_0$ = 11 mmol L^{-1}. TOC_0=221 mg L^{-1}. Current density = 15 mA cm^{-2}.

Table 5.12. Inorganic Disinfection By-product Formation During Electrochemical Treatment of Ciprofloxacin

Disinfection By-product	Persulfate (mmol L^{-1})	mg L^{-1} in RDE*	mg L^{-1} in FTR**
Nitrite	11	0.33	0.35
	3.1	0.32	
	0	0.24	0.30
Chlorite	11	11.8	9.8
	3.1	12.9	
	0	10.2	10.8
Chlorate	11	26.3	39.0
	3.1	26.3	
	0	23.1	29.0
Perchlorate	11	39.0	203.0
	3.1	48.4	
	0	42.8	245.8

5.4 Conclusion

Overall, this study demonstrated successful electrochemical degradation of ciprofloxacin using flow-through, batch and RDE reactors. Electrochemically activated persulfate demonstrated improvement over sulfate in some cases in pure electrolyte, but showed limited benefit when applied to a more complex matrix such as synthetic hospital effluent. Relative cathode size and mass transfer effects were both suggested to influence the effectiveness of the systems, with at least a 1:20 anode to cathode size ratio recommended to optimize contaminant removal. The electrochemical systems showed efficacy for TOC removal even when TOC content was greatly increased by addition of synthetic hospital effluent components; however, these systems also generated high levels of perchlorate during TOC removal. Further work is recommended to study multi-step treatment trains. Such systems might consist of electrochemical treatment with sulfate or persulfate electrolyte, and a stage such as ion exchange to remove the generated inorganic DBPs.

CHAPTER SIX: CONCLUSIONS

The research described in Chapters 3 and 4 provides fundamentals of electrochemical persulfate activation, while Chapters 3, 4 and 5 examine application of EAP to ciprofloxacin degradation. Throughout these studies, ciprofloxacin removal is analyzed in detail, while ciprofloxacin is also used as a model compound to better understand EAP.

Chapters 3 and 4 assessed electrochemical persulfate activation without analyte in solution, an important step to understand the fundamentals of EAP systems. In chapter 3, persulfate activation by solid iron was proposed to be a surface dominated mechanism. The relationships between iron surface area, applied current, iron production and persulfate activation were elucidated. Sustained persulfate activation was accomplished with the use of solid iron, with 1.14 moles of persulfate activated for 1 mole of iron used. It was found that the surface area of the solid iron could be adjusted to control the persulfate activation rate. Applied current enhanced persulfate activation until diffusion limitations were reached. In Chapter 4, anodic sulfate radical formation, anodic non-radical persulfate activation and cathodic persulfate activation were discovered to be persulfate activation mechanisms. Cathodic activation was found to be the same for graphite and platinum materials. Persulfate generation from sulfate at a BDD anode was also confirmed. Net persulfate activation increased linearly with increased current density, within the range tested.

Chapters 3, 4 and 5 examined parameters affecting ciprofloxacin removal using EAP. In Chapter 3, EAP using an iron anode and graphite cathode was evaluated without current and at three levels of applied current. Although applied current did not enhance ciprofloxacin removal, significant defluorination and ciprofloxacin-matrix removal was attained from the chemical activation of persulafte by the solid iron rod. Sustained persulfate activation and minimal iron

usage was achieved. In Chapter 4, ciprofloxacin degradation was accomplished with applied current using a BDD/Gr anode/cathode pair without the addition of iron. Significant improvements in removal rates were achieved by using sulfate instead of nitrate electrolyte, and even more benefit was gained through the use of persulfate electrolyte, in other words, EAP. Pathways of ciprofloxacin transformation were elucidated. Chapter 5 evaluated effects of persulfate concentration, anode:cathode size ratio, and reactor configuration. It was found that at least a 1:20 anode:cathode size ratio was needed to benefit from EAP. In the flow-through reator configuration, increasing persulfate concentration only offered moderate improvements for ciprofloxacin removal, likely due to mass-transfer limitations and the sub-optimal anode:cathode size ratio used. EAP was slightly more effective in a batch reactor. The RDE reactor provided the most effective use of activated persulfate with increasing removal rates seen as persulfate concentration was increased. This was attributed to the larger relative cathode size (at least 1:20 anode:cathode was found to be optimal) and minimization of mass-transfer limitations.

Chapter 5 evaluted the use of EAP for ciprofloxacin removal from synthetic hospital effluent. Removal slowed down significantly in the effluent solution versus using pure electrolyte. There were no differences in removal of ciprofloxacin or TOC when using EAP or sulfate electrolyte for effluent treatment in the FTR. Overall, the system was successful in removing high amounts of TOC from the effluent. On the RDE, EAP increased removal rates of the ciprofloxacin-matrix but did not increase the removal of the ciprofloxacin itself or TOC. Again, high levels of TOC removal from the effluent was achieved. During ciprofloxacin treatment in effluent in the FTR and RDE reactors, high levels of disinfection by-products were formed. It was recommended that future studies incude pairing EAP with another treatment step, such as ion exchange, to

remove combine TOC removal with DBP removal. It is also recommended to assess EAP with other organic analytes, where enhancements seen with ciprofloxacin in the pure electrolyte on the RDE may better translate to a flow-through reactor design in a complex matrix.

BIBLIOGRAPHY

1. Papageorgiou, M.; Kosma, C.; Lambropoulou, D., Seasonal occurrence, removal, mass loading and environmental risk assessment of 55 pharmaceuticals and personal care products in a municipal wastewater treatment plant in Central Greece. *Sci Total Environ* **2016,** *543*, 547-569.
2. der Beek, T. A.; Weber, F. A.; Bergmann, A.; Hickmann, S.; Ebert, I.; Hein, A.; Kuster, A., Pharmaceuticals in the Environment-Global Occurrences and Perspectives. *Environ Toxicol Chem* **2016,** *35*, (4), 823-835.
3. Zuccato, E.; Castiglioni, S.; Bagnati, R.; Melis, M.; Fanelli, R., Source, occurrence and fate of antibiotics in the Italian aquatic environment. *J Hazard Mater* **2010,** *179*, (1-3), 1042-1048.
4. He, K.; Soares, A. D.; Adejumo, H.; McDiarmid, M.; Squibb, K.; Blaney, L., Detection of a wide variety of human and veterinary fluoroquinolone antibiotics in municipal wastewater and wastewater-impacted surface water. *J Pharmaceut Biomed* **2015,** *106*, 136-143.
5. Chen, K.; Zhou, J. L., Occurrence and behavior of antibiotics in water and sediments from the Huangpu River, Shanghai, China. *Chemosphere* **2014,** *95*, 604-612.
6. Kolpin, D. W.; Furlong, E. T.; Meyer, M. T.; Thurman, E. M.; Zaugg, S. D.; Barber, L. B.; Buxton, H. T., Pharmaceuticals, hormones, and other organic wastewater contaminants in US streams, 1999-2000: A national reconnaissance. *Environ Sci Technol* **2002,** *36*, (6), 1202-1211.
7. Flaherty, C. M.; Dodson, S. I., Effects of pharmaceuticals on Daphnia survival, growth, and reproduction. *Chemosphere* **2005,** *61*, (2), 200-207.
8. Wollenberger, L.; Halling-Sorensen, B.; Kusk, K. O., Acute and chronic toxicity of veterinary antibiotics to Daphnia magna. *Chemosphere* **2000,** *40*, (7), 723-730.
9. Migliore, L.; Civitareale, C.; Brambilla, G.; DiDelupis, G. D., Toxicity of several important agricultural antibiotics to Artemia. *Water Res* **1997,** *31*, (7), 1801-1806.
10. Klaver, A. L.; Matthews, R. A., EFFECTS OF OXYTETRACYCLINE ON NITRIFICATION IN A MODEL AQUATIC SYSTEM. *Aquaculture* **1994,** *123*, (3-4), 237-247.
11. Yang, L. H.; Ying, G. G.; Su, H. C.; Stauber, J. L.; Adams, M. S.; Binet, M. T., Growth-inhibiting effects of 12 antibacterial agents and their mixtures on the freshwater microalga Pseudokirchneriella subcapitata. *Environ Toxicol Chem* **2008,** *27*, (5), 1201-1208.
12. Jiang, L.; Hu, X. L.; Xu, T.; Zhang, H. C.; Sheng, D.; Yin, D. Q., Prevalence of antibiotic resistance genes and their relationship with antibiotics in the Huangpu River and the drinking water sources, Shanghai, China. *Sci Total Environ* **2013,** *458*, 267-272.
13. Robinson, A. A.; Belden, J. B.; Lydy, M. J., Toxicity of fluoroquinolone antibiotics to aquatic organisms. *Environ Toxicol Chem* **2005,** *24*, (2), 423-430.
14. Johansson, C. H.; Janmar, L.; Backhaus, T., Toxicity of ciprofloxacin and sulfamethoxazole to marine periphytic algae and bacteria. *Aquat Toxicol* **2014,** *156*, 248-258.
15. Schoenfuss, H. L.; Furlong, E. T.; Phillips, P. J.; Scott, T. M.; Kolpin, D. W.; Cetkovic-Cvrlje, M.; Lesteberg, K. E.; Rearick, D. C., Complex Mixtures, Complex Responses: Assessing Pharmaceutical Mixtures Using Field and Laboratory Approaches. *Environ Toxicol Chem* **2016,** *35*, (4), 953-965.
16. Chen, H.; Liu, S.; Xu, X. R.; Zhou, G. J.; Liu, S. S.; Yue, W. Z.; Sun, K. F.; Ying, G. G., Antibiotics in the coastal environment of the Hailing Bay region, South China Sea: Spatial distribution, source analysis and ecological risks. *Mar Pollut Bull* **2015,** *95*, (1), 365-373.
17. Andrieu, M.; Rico, A.; Phu, T. M.; Huong, D. T. T.; Phuong, N. T.; Van den Brink, P. J., Ecological risk assessment of the antibiotic enrofloxacin applied to Pangasius catfish farms in the Mekong Delta, Vietnam. *Chemosphere* **2015,** *119*, 407-414.

18. Coutu, S.; Pouchon, T.; Queloz, P.; Vernaz, N., Integrated stochastic modeling of pharmaceuticals in sewage networks. *Stoch Env Res Risk A* **2016,** *30*, (4), 1087-1097.
19. Kummerer, K., Antibiotics in the aquatic environment - A review - Part I. *Chemosphere* **2009,** *75*, (4), 417-434.
20. Batt, A. L.; Bruce, I. B.; Aga, D. S., Evaluating the vulnerability of surface waters to antibiotic contamination from varying wastewater treatment plant discharges. *Environ Pollut* **2006,** *142*, (2), 295-302.
21. Watkinson, A. J.; Micalizzi, G. R.; Bates, J. R.; Costanzo, S. D., Novel method for rapid assessment of antibiotic resistance in Escherichia coli isolates from environmental waters by use of a modified chromogenic agar. *Appl Environ Microb* **2007,** *73*, (7), 2224-2229.
22. Mackul'ak, T.; Vojs, M.; Grabic, R.; Golovko, O.; Stanova, A. V.; Birosova, L.; Medved'ova, A.; Hives, J.; Gal, M.; Kromka, A.; Hanusova, A., Occurrence of pharmaceuticals, illicit drugs, and resistant types of bacteria in hospital effluent and their effective degradation by boron-doped diamond electrodes. *Monatsh Chem* **2016,** *147*, (1), 97-103.
23. Beier, S.; Cramer, C.; Koster, S.; Mauer, C.; Palmowski, L.; Schroder, H. F.; Pinnekamp, J., Full scale membrane bioreactor treatment of hospital wastewater as forerunner for hot-spot wastewater treatment solutions in high density urban areas. *Water Sci Technol* **2011,** *63*, (1), 66-71.
24. Beier, S.; Cramer, C.; Mauer, C.; Koster, S.; Schroder, H. F.; Pinnekamp, J., MBR technology: a promising approach for the (pre-)treatment of hospital wastewater. *Water Sci Technol* **2012,** *65*, (9), 1648-1653.
25. Santos, L. H. M. L. M.; Gros, M.; Rodriguez-Mozaz, S.; Delerue-Matos, C.; Pena, A.; Barceló, D.; Montenegro, M. C. B. S. M., Contribution of hospital effluents to the load of pharmaceuticals in urban wastewaters: Identification of ecologically relevant pharmaceuticals. *Sci Total Environ* **2013,** *461–462*, 302-316.
26. Phillips, P. J.; Smith, S. G.; Kolpin, D. W.; Zaugg, S. D.; Buxton, H. T.; Furlong, E. T.; Esposito, K.; Stinson, B., Pharmaceutical Formulation Facilities as Sources of Opioids and Other Pharmaceuticals to Wastewater Treatment Plant Effluents. *Environmental Science & Technology* **2010,** *44*, (13), 4910-4916.
27. Yuan, X. J.; Qiang, Z. M.; Ben, W. W.; Zhu, B.; Qu, J. H., Distribution, mass load and environmental impact of multiple-class pharmaceuticals in conventional and upgraded municipal wastewater treatment plants in East China. *Environ Sci-Proc Imp* **2015,** *17*, (3), 596-605.
28. Ory, J.; Bricheux, G.; Togola, A.; Bonnet, J. L.; Donnadieu-Bernard, F.; Nakusi, L.; Forestier, C.; Traore, O., Ciprofloxacin residue and antibiotic-resistant biofilm bacteria in hospital effluent. *Environ Pollut* **2016,** *214*, 635-645.
29. Helwig, K.; Hunter, C.; McNaughtan, M.; Roberts, J.; Pahl, O., Ranking Prescribed Pharmaceuticals in Terms of Environmental Risk: Inclusion of Hospital Data and the Importance of Regular Review. *Environ Toxicol Chem* **2016,** *35*, (4), 1043-1050.
30. Ji, K.; Han, E. J.; Back, S.; Park, J.; Ryu, J.; Choi, K., Prioritizing Human Pharmaceuticals for Ecological Risks in the Freshwater Environment of Korea. *Environ Toxicol Chem* **2016,** *35*, (4), 1028-1036.
31. Mutiyar, P. K.; Mittal, A. K., Risk assessment of antibiotic residues in different water matrices in India: key issues and challenges. *Environ Sci Pollut R* **2014,** *21*, (12), 7723-7736.

32. Klancar, A.; Trontelj, J.; Kristl, A.; Justin, M. Z.; Roskar, R., Levels of pharmaceuticals in Slovene municipal and hospital wastewaters: a preliminary study. *Arh Hig Rada Toksiko* **2016,** *67*, (2), 106-115.
33. Du, L. F.; Liu, W. K., Occurrence, fate, and ecotoxicity of antibiotics in agro-ecosystems. A review. *Agron Sustain Dev* **2012,** *32*, (2), 309-327.
34. Hartmann, A.; Alder, A. C.; Koller, T.; Widmer, R. M., Identification of fluoroquinolone antibiotics as the main source of umuC genotoxicity in native hospital wastewater. *Environ Toxicol Chem* **1998,** *17*, (3), 377-382.
35. Verlicchi, P.; Al Aukidy, M.; Zambello, E., What have we learned from worldwide experiences on the management and treatment of hospital effluent? — An overview and a discussion on perspectives. *Sci Total Environ* **2015,** *514*, 467-491.
36. Ou, H. S.; Ye, J. S.; Ma, S.; Wei, C. H.; Gao, N. Y.; He, J. Z., Degradation of ciprofloxacin by UV and UV/H2O2 via multiple-wavelength ultraviolet light-emitting diodes: Effectiveness, intermediates and antibacterial activity. *Chem Eng J* **2016,** *289*, 391-401.
37. Ammar, H. B., Sono-Fenton process for metranidazole degradation in aqueous solution: Effect of acoustic cavitation and peroxydisulfate anion. *Ultrason Sonochem* **2016,** *33*, 164-169.
38. Lester, Y.; Avisar, D.; Gozlan, I.; Mamane, H., Removal of pharmaceuticals using combination of UV/H2O2/O-3 advanced oxidation process. *Water Sci Technol* **2011,** *64*, (11), 2230-2238.
39. Nasuhoglu, D.; Rodayan, A.; Berk, D.; Yargeau, V., Removal of the antibiotic levofloxacin (LEVO) in water by ozonation and TiO2 photocatalysis. *Chem Eng J* **2012,** *189*, 41-48.
40. Wigh, A.; Devaux, A.; Brosselin, V.; Gonzalez-Ospina, A.; Domenjoud, B.; Ait-Aissa, S.; Creusot, N.; Gosset, A.; Bazin, C.; Bony, S., Proposal to optimize ecotoxicological evaluation of wastewater treated by conventional biological and ozonation processes. *Environ Sci Pollut R* **2016,** *23*, (4), 3008-3017.
41. Jara, C. C.; Fino, D.; Specchia, V.; Saracco, G.; Spinelli, R., Electrochemical removal of antibiotics from wastewaters. *Appl Catal B-Environ* **2007,** *70*, (1-4), 479-487.
42. Farhat, A.; Keller, J.; Tait, S.; Radjenovic, J., Removal of Persistent Organic Contaminants by Electrochemically Activated Sulfate. *Environ Sci Technol* **2015,** *49*, (24), 14326-14333.
43. Miyata, M.; Ihara, I.; Yoshid, G.; Toyod, K.; Umetsu, K., Electrochemical oxidation of tetracycline antibiotics using a Ti/IrO₂ anode for wastewater treatment of animal husbandry. *Water Sci Technol* **2011,** *63*, (3), 456-461.
44. Antonin, V. S.; Santos, M. C.; Garcia-Segura, S.; Brillas, E., Electrochemical incineration of the antibiotic ciprofloxacin in sulfate medium and synthetic urine matrix. *Water Res* **2015,** *83*, 31-41.
45. Sirés, I.; Brillas, E., Remediation of water pollution caused by pharmaceutical residues based on electrochemical separation and degradation technologies: A review. *Environ Int* **2012,** *40*, 212-229.
46. Radjenovic, J.; Sedlak, D. L., Challenges and Opportunities for Electrochemical Processes as Next-Generation Technologies for the Treatment of Contaminated Water. *Environ Sci Technol* **2015,** *49*, (19), 11292-11302.
47. Garcia-Segura, S.; Keller, J.; Brillas, E.; Radjenovic, J., Removal of organic contaminants from secondary effluent by anodic oxidation with a boron-doped diamond anode as tertiary treatment. *J Hazard Mater* **2015,** *283*, 551-557.

48. Matzek, L. W.; Carter, K. E., Activated persulfate for organic chemical degradation: A review. *Chemosphere* **2016,** *151*, 178-188.
49. Zhao, L.; Hou, H.; Fujii, A.; Hosomi, M.; Li, F. S., Degradation of 1,4-dioxane in water with heat- and Fe2+-activated persulfate oxidation. *Environ Sci Pollut R* **2014,** *21*, (12), 7457-7465.
50. Chen, W. S.; Huang, C. P., Mineralization of aniline in aqueous solution by electrochemical activation of persulfate. *Chemosphere* **2015**.
51. Fang, G. D.; Gao, J.; Dionysiou, D. D.; Liu, C.; Zhou, D. M., Activation of Persulfate by Quinones: Free Radical Reactions and Implication for the Degradation of PCBs. *Environ Sci Technol* **2013,** *47*, (9), 4605-4611.
52. Zhang, B. T.; Zhang, Y.; Teng, Y. H.; Fan, M. H., Sulfate Radical and Its Application in Decontamination Technologies. *Crit Rev Env Sci Tec* **2015,** *45*, (16), 1756-1800.
53. He, X.; Mezyk, S. P.; Michael, I.; Fatta-Kassinos, D.; Dionysiou, D. D., Degradation kinetics and mechanism of beta-lactam antibiotics by the activation of H2O2 and Na2S2O8 under UV-254 nm irradiation. *J Hazard Mater* **2014,** *279*, 375-383.
54. Schwarz, H. A.; Dodson, R. W., Equilibrium between Hydroxyl Radicals and Thallium(Ii) and the Oxidation Potential of Oh(Aq). *J Phys Chem-Us* **1984,** *88*, (16), 3643-3647.
55. Eberson, L., *Electron Transfer Reactions in Organic Chemistry*. Springer: Berlin, 1987.
56. Hao, F. F.; Guo, L. L.; Wang, A. Q.; Leng, Y. Q.; Li, H. L., Intensification of sonochemical degradation of ammonium perfluorooctanoate by persulfate oxidant. *Ultrason Sonochem* **2014,** *21*, (2), 554-558.
57. Huang, K. C.; Couttenye, R. A.; Hoag, G. E., Kinetics of heat-assisted persulfate oxidation of methyl tert-butyl ether (MTBE). *Chemosphere* **2002,** *49*, (4), 413-420.
58. Wang, X.; Wang, L. G.; Li, J. B.; Qiu, J. J.; Cai, C.; Zhang, H., Degradation of Acid Orange 7 by persulfate activated with zero valent iron in the presence of ultrasonic irradiation. *Sep Purif Technol* **2014,** *122*, 41-46.
59. Chen, W. S.; Jhou, Y. C.; Huang, C. P., Mineralization of dinitrotoluenes in industrial wastewater by electro-activated persulfate oxidation. *Chem Eng J* **2014,** *252*, 166-172.
60. Paul, J.; Naik, D. B.; Bhardwaj, Y. K.; Varshney, L., Studies on oxidative radiolysis of ibuprofen in presence of potassium persulfate. *Radiat Phys Chem* **2014,** *100*, 38-44.
61. Zhang, M.; Chen, X. Q.; Zhou, H.; Murugananthan, M.; Zhang, Y. R., Degradation of p-nitrophenol by heat and metal ions co-activated persulfate. *Chem Eng J* **2015,** *264*, 39-47.
62. Wang, C. W.; Liang, C. J., Oxidative degradation of TMAH solution with UV persulfate activation. *Chem Eng J* **2014,** *254*, 472-478.
63. Waldemer, R. H.; Tratnyek, P. G.; Johnson, R. L.; Nurmi, J. T., Oxidation of chlorinated ethenes by heat-activated persulfate: Kinetics and products. *Environ Sci Technol* **2007,** *41*, (3), 1010-1015.
64. Yan, N.; Liu, F.; Huang, W. Y., Interaction of oxidants in siderite catalyzed hydrogen peroxide and persulfate system using trichloroethylene as a target contaminant. *Chem Eng J* **2013,** *219*, 149-154.
65. Tsitonaki, A.; Petri, B.; Crimi, M.; Mosbaek, H.; Siegrist, R. L.; Bjerg, P. L., In Situ Chemical Oxidation of Contaminated Soil and Groundwater Using Persulfate: A Review. *Crit Rev Env Sci Tec* **2010,** *40*, (1), 55-91.

66. Criquet, J.; Leitner, N. K. V., Reaction pathway of the degradation of the p-hydroxybenzoic acid by sulfate radical generated by ionizing radiations. *Radiat Phys Chem* **2015,** *106*, 307-314.
67. Lee, Y. C.; Lo, S. L.; Kuo, J.; Huang, C. P., Promoted degradation of perfluorooctanic acid by persulfate when adding activated carbon. *J Hazard Mater* **2013,** *261*, 463-469.
68. Sun, H. Q.; Kwan, C.; Suvorova, A.; Ang, H. M.; Tade, M. O.; Wang, S. B., Catalytic oxidation of organic pollutants on pristine and surface nitrogen-modified carbon nanotubes with sulfate radicals. *Appl Catal B-Environ* **2014,** *154*, 134-141.
69. Kolthoff, I. M.; Miller, I. K., The Chemistry of Persulfate .1. The Kinetics and Mechanism of the Decomposition of the Persulfate Ion in Aqueous Medium. *J Am Chem Soc* **1951,** *73*, (7), 3055-3059.
70. Anipsitakis, G. P.; Dionysiou, D. D., Radical generation by the interaction of transition metals with common oxidants. *Environ Sci Technol* **2004,** *38*, (13), 3705-3712.
71. Hayon, E.; Treinin, A.; Wilf, J., Electronic-Spectra, Photochemistry, and Autoxidation Mechanism of Sulfite-Bisulfite-Pyrosulfite Systems - So2-, So3-, So4-, and So5- Radicals. *J Am Chem Soc* **1972,** *94*, (1), 47-&.
72. Johnson, R. L.; Tratnyek, P. G.; Johnson, R. O., Persulfate Persistence under Thermal Activation Conditions. *Environ Sci Technol* **2008,** *42*, (24), 9350-9356.
73. Liang, C. J.; Su, H. W., Identification of Sulfate and Hydroxyl Radicals in Thermally Activated Persulfate. *Ind Eng Chem Res* **2009,** *48*, (11), 5558-5562.
74. Petri, B. G.; Watts, R. J.; Teel, A. L.; Huling, S. G.; Brown, R. A., Fundamentals of Isco Using Hydrogen Peroxide. *Serdp Estcp Remediat* **2011**, 33-88.
75. Anipsitakis, G. P.; Dionysiou, D. D., Transition metal/UV-based advanced oxidation technologies for water decontamination. *Appl Catal B-Environ* **2004,** *54*, (3), 155-163.
76. Neta, P.; Madhavan, V.; Zemel, H.; Fessenden, R. W., Rate Constants and Mechanism of Reaction of So4.- with Aromatic-Compounds. *J Am Chem Soc* **1977,** *99*, (1), 163-164.
77. Tanner, D. D.; Osman, S. A. A., Oxidative Decarboxylation - on the Mechanism of the Potassium Persulfate Promoted Decarboxylation Reaction. *J Org Chem* **1987,** *52*, (21), 4689-4693.
78. Evseev, A. K.; Khubutiya, M. S.; Gol'din, M. M.; Volkov, A. G.; Koldaev, A. A., Electrochemical synthesis of peroxodisulfates from dilute sulfate solutions for detoxification of biological media. *Russ J Electrochem+* **2008,** *44*, (8), 901-909.
79. Oh, S. Y.; Kang, S. G.; Chiu, P. C., Degradation of 2,4-dinitrotoluene by persulfate activated with zero-valent iron. *Sci Total Environ* **2010,** *408*, (16), 3464-3468.
80. Le, C.; Wu, J. H.; Li, P.; Wang, X. D.; Zhu, N. W.; Wu, P. X.; Yang, B., Decolorization of anthraquinone dye Reactive Blue 19 by the combination of persulfate and zero-valent iron. *Water Sci Technol* **2011,** *64*, (3), 754-759.
81. Lee, Y.; Lo, S. L.; Kuo, J.; Hsieh, C. H., Decomposition of perfluorooctanoic acid by microwaveactivated persulfate: Effects of temperature, pH, and chloride ions. *Front Env Sci Eng* **2012,** *6*, (1), 17-25.
82. Shih, Y. J.; Putra, W. N.; Huang, Y. H.; Tsai, J. C., Mineralization and deflourization of 2,2,3,3-tetrafluoro-1-propanol (TFP) by UV/persulfate oxidation and sequential adsorption. *Chemosphere* **2012,** *89*, (10), 1262-1266.
83. Latimer, W. M., *Oxidation Potentials*. Prentice-Hall, Inc.: Englewood Cliffs, NJ, 1952.

84. Zhang, T.; Chen, Y.; Wang, Y. R.; Le Roux, J.; Yang, Y.; Croue, J. P., Efficient Peroxydisulfate Activation Process Not Relying on Sulfate Radical Generation for Water Pollutant Degradation. *Environ Sci Technol* **2014,** *48*, (10), 5868-5875.
85. Zhou, Z.; Jiang, J. Q., Reaction kinetics and oxidation products formation in the degradation of ciprofloxacin and ibuprofen by ferrate(VI). *Chemosphere* **2015,** *119*, S95-S100.
86. Xiong, X. M.; Sun, B.; Zhang, J.; Gao, N. Y.; Shen, J. M.; Li, J. L.; Guan, X. H., Activating persulfate by Fe-0 coupling with weak magnetic field: Performance and mechanism. *Water Res* **2014,** *62*, 53-62.
87. House, D. A., Kinetics and Mechanism of Oxidations by Peroxydisulfate. *Chem Rev* **1962,** *62*, (3), 185-&.
88. Buxton, G. V.; Malone, T. N.; Salmon, G. A., Reaction of SO4.- with Fe2+, Mn2+ and Cu2+ in aqueous solution. *J Chem Soc Faraday T* **1997,** *93*, (16), 2893-2897.
89. Rastogi, A.; Al-Abed, S. R.; Dionysiou, D. D., Effect of inorganic, synthetic and naturally occurring chelating agents on Fe(II) mediated advanced oxidation of chlorophenols. *Water Res* **2009,** *43*, (3), 684-694.
90. Fordham, J. W. L.; Williams, H. L., The Persulfate Iron(Ii) Initiator System for Free Radical Polymerizations. *J Am Chem Soc* **1951,** *73*, (10), 4855-4859.
91. Liang, C.; Lee, I. L.; Hsu, I. Y.; Liang, C. P.; Lin, Y. L., Persulfate oxidation of trichloroethylene with and without iron activation in porous media. *Chemosphere* **2008,** *70*, (3), 426-435.
92. Oh, S. Y.; Kim, H. W.; Park, J. M.; Park, H. S.; Yoon, C., Oxidation of polyvinyl alcohol by persulfate activated with heat, Fe2+, and zero-valent iron. *J Hazard Mater* **2009,** *168*, (1), 346-351.
93. Lee, Y. C.; Lo, S. L.; Chiueh, P. T.; Chang, D. G., Efficient decomposition of perfluorocarboxylic acids in aqueous solution using microwave-induced persulfate. *Water Res* **2009,** *43*, (11), 2811-2816.
94. Vicente, F.; Santos, A.; Romero, A.; Rodriguez, S., Kinetic study of diuron oxidation and mineralization by persulphate: Effects of temperature, oxidant concentration and iron dosage method. *Chem Eng J* **2011,** *170*, (1), 127-135.
95. Ayoub, G.; Ghauch, A., Assessment of bimetallic and trimetallic iron-based systems for persulfate activation: Application to sulfamethoxazole degradation. *Chem Eng J* **2014,** *256*, 280-292.
96. Ji, Y. F.; Ferronato, C.; Salvador, A.; Yang, X.; Chovelon, J. M., Degradation of ciprofloxacin and sulfamethoxazole by ferrous-activated persulfate: Implications for remediation of groundwater contaminated by antibiotics. *Sci Total Environ* **2014,** *472*, 800-808.
97. Rodriguez, S.; Santos, A.; Romero, A.; Vicente, F., Kinetic of oxidation and mineralization of priority and emerging pollutants by activated persulfate. *Chem Eng J* **2012,** *213*, 225-234.
98. Al-Shamsi, M. A.; Thomson, N. R., Treatment of Organic Compounds by Activated Persulfate Using Nanoscale Zerovalent Iron. *Ind Eng Chem Res* **2013,** *52*, (38), 13564-13571.
99. Jiang, X. X.; Wu, Y. L.; Wang, P.; Li, H. J.; Dong, W. B., Degradation of bisphenol A in aqueous solution by persulfate activated with ferrous ion. *Environ Sci Pollut R* **2013,** *20*, (7), 4947-4953.
100. Hussain, I.; Zhang, Y. Q.; Huang, S. B., Degradation of aniline with zero-valent iron as an activator of persulfate in aqueous solution. *Rsc Adv* **2014,** *4*, (7), 3502-3511.

101. Rodriguez, S.; Vasquez, L.; Romero, A.; Santos, A., Dye Oxidation in Aqueous Phase by Using Zero-Valent Iron as Persulfate Activator: Kinetic Model and Effect of Particle Size. *Ind Eng Chem Res* **2014,** *53*, (31), 12288-12294.
102. Ghauch, A.; Ayoub, G.; Naim, S., Degradation of sulfamethoxazole by persulfate assisted micrometric Fe0 in aqueous solution. *Chem Eng J* **2013,** *228*, 1168-1181.
103. Naim, S.; Ghauch, A., Ranitidine abatement in chemically activated persulfate systems: Assessment of industrial iron waste for sustainable applications. *Chem Eng J* **2016,** *288*, 276-288.
104. Liang, C. J.; Bruell, C. J.; Marley, M. C.; Sperry, K. L., Persulfate oxidation for in situ remediation of TCE. II. Activated by chelated ferrous ion. *Chemosphere* **2004,** *55*, (9), 1225-1233.
105. Furman, O. S.; Teel, A. L.; Watts, R. J., Mechanism of Base Activation of Persulfate. *Environmental Science & Technology* **2010,** *44*, (16), 6423-6428.
106. Zhang, Y. Q.; Xie, X. F.; Huang, S. B.; Liang, H. Y., Effect of chelating agent on oxidation rate of aniline in ferrous ion activated persulfate system at neutral pH. *J Cent South Univ* **2014,** *21*, (4), 1441-1447.
107. Zhou, L.; Zheng, W.; Ji, Y. F.; Zhang, J. F.; Zeng, C.; Zhang, Y.; Wang, Q.; Yang, X., Ferrous-activated persulfate oxidation of arsenic(III) and diuron in aquatic system. *J Hazard Mater* **2013,** *263*, 422-430.
108. Fang, G. D.; Dionysiou, D. D.; Al-Abed, S. R.; Zhou, D. M., Superoxide radical driving the activation of persulfate by magnetite nanoparticles: Implications for the degradation of PCBs. *Appl Catal B-Environ* **2013,** *129*, 325-332.
109. Zhao, Y. S.; Sun, C.; Sun, J. Q.; Zhou, R., Kinetic modeling and efficiency of sulfate radical-based oxidation to remove p-nitroaniline from wastewater by persulfate/Fe3O4 nanoparticles process. *Sep Purif Technol* **2015,** *142*, 182-188.
110. Ahmad, M.; Teel, A. L.; Watts, R. J., Persulfate activation by subsurface minerals. *J Contam Hydrol* **2010,** *115*, (1-4), 34-45.
111. Teel, A. L.; Ahmad, M.; Watts, R. J., Persulfate activation by naturally occurring trace minerals. *J Hazard Mater* **2011,** *196*, 153-159.
112. Liu, H. Z.; Bruton, T. A.; Doyle, F. M.; Sedlak, D. L., In Situ Chemical Oxidation of Contaminated Groundwater by Persulfate: Decomposition by Fe(III)- and Mn(IV)-Containing Oxides and Aquifer Materials. *Environ Sci Technol* **2014,** *48*, (17), 10330-10336.
113. Huang, K. C.; Zhao, Z. Q.; Hoag, G. E.; Dahmani, A.; Block, P. A., Degradation of volatile organic compounds with thermally activated persulfate oxidation. *Chemosphere* **2005,** *61*, (4), 551-560.
114. Tan, C. Q.; Gao, N. Y.; Deng, Y.; Li, L.; Deng, J.; Zhou, S. Q., Kinetic oxidation of antipyrine in heat-activated persulfate. *Desalin Water Treat* **2015,** *53*, (1), 263-271.
115. Qi, C. D.; Liu, X. T.; Zhao, W.; Lin, C. Y.; Ma, J.; Shi, W. X.; Sun, Q.; Xiao, H., Degradation and dechlorination of pentachlorophenol by microwave-activated persulfate. *Environ Sci Pollut R* **2015,** *22*, (6), 4670-4679.
116. Wang, Z.; Deng, D. Y.; Yang, L. L., Degradation of dimethyl phthalate in solutions and soil slurries by persulfate at ambient temperature. *J Hazard Mater* **2014,** *271*, 202-209.
117. Costanza, J.; Otano, G.; Callaghan, J.; Pennell, K. D., PCE Oxidation by Sodium Persulfate in the Presence of Solids. *Environ Sci Technol* **2010,** *44*, (24), 9445-9450.

118. Qi, C. D.; Liu, X. T.; Lin, C. Y.; Zhang, X. H.; Ma, J.; Tan, H. B.; Ye, W., Degradation of sulfamethoxazole by microwave-activated persulfate: Kinetics, mechanism and acute toxicity. *Chem Eng J* **2014,** *249*, 6-14.
119. Teel, A. L.; Cutler, L. M.; Watts, R. J., Effect of sorption on contaminant oxidation in activated persulfate systems. *J Environ Sci Heal A* **2009,** *44*, (11), 1098-1103.
120. Drzewicz, P.; Perez-Estrada, L.; Alpatova, A.; Martin, J. W.; El-Din, M. G., Impact of Peroxydisulfate in the Presence of Zero Valent Iron on the Oxidation of Cyclohexanoic Acid and Naphthenic Acids from Oil Sands Process-Affected Water. *Environ Sci Technol* **2012,** *46*, (16), 8984-8991.
121. Li, R. C.; Jin, X. Y.; Megharaj, M.; Naidu, R.; Chen, Z. L., Heterogeneous Fenton oxidation of 2,4-dichlorophenol using iron-based nanoparticles and persulfate system. *Chem Eng J* **2015,** *264*, 587-594.
122. Berlin, A. A., Kinetics of Radical-Chain Decomposition of Persulfate in Aqueous-Solutions of Organic-Compounds. *Kinet Catal+* **1986,** *27*, (1), 34-39.
123. Dogliott.L; Hayon, E., Flash Photolysis of Persulfate Ions in Aqueous Solutions . Study of Sulfate and Ozonide Radical Anions. *J Phys Chem-Us* **1967,** *71*, (8), 2511-&.
124. Heidt, L. J., The photolysis of persulfate. *J Chem Phys* **1942,** *10*, (5), 297-302.
125. Lin, C. C.; Wu, M. S., UV/S2O82- process for degrading polyvinyl alcohol in aqueous solutions. *Chem Eng Process* **2014,** *85*, 209-215.
126. Shu, H. Y.; Chang, M. C.; Huang, S. W., UV irradiation catalyzed persulfate advanced oxidation process for decolorization of Acid Blue 113 wastewater. *Desalin Water Treat* **2015,** *54*, (4-5), 1013-1021.
127. Guo, Y. G.; Zhou, J.; Lou, X. Y.; Liu, R. L.; Xiao, D. X.; Fang, C. L.; Wang, Z. H.; Liu, J. S., Enhanced degradation of Tetrabromobisphenol A in water by a UV/base/persulfate system: Kinetics and intermediates. *Chem Eng J* **2014,** *254*, 538-544.
128. Ahmed, M. M.; Chiron, S., Solar photo-Fenton like using persulphate for carbamazepine removal from domestic wastewater. *Water Res* **2014,** *48*, 229-236.
129. Avetta, P.; Pensato, A.; Minella, M.; Malandrino, M.; Maurino, V.; Minero, C.; Hanna, K.; Vione, D., Activation of Persulfate by Irradiated Magnetite: Implications for the Degradation of Phenol under Heterogeneous Photo-Fenton-Like Conditions. *Environ Sci Technol* **2015,** *49*, (2), 1043-1050.
130. Petri, B. G.; Watts, R. J.; Tsitonaki, A.; Crimi, M.; Thomson, N. R.; Teel, A. L., Fundamentals of Isco Using Persulfate. *Serdp Estcp Remediat* **2011**, 147-191.
131. Furman, O. S.; Teel, A. L.; Ahmad, M.; Merker, M. C.; Watts, R. J., Effect of Basicity on Persulfate Reactivity. *J Environ Eng-Asce* **2011,** *137*, (4), 241-247.
132. Carter, K. E.; Farrell, J., Oxidative Destruction of Perfluorooctane Sulfonate Using Boron-Doped Diamond Film Electrodes. *Environ Sci Technol* **2008,** *42*, (16), 6111-6115.
133. Chen, W.-S.; Huang, C.-P., Mineralization of aniline in aqueous solution by electrochemical activation of persulfate. *Chemosphere* **2015,** *125*, 175-181.
134. Weiss, E.; Groenen-Serrano, K.; Savall, A., Electrochemical mineralization of sodium dodecylbenzenesulfonate at boron doped diamond anodes. *J Appl Electrochem* **2007,** *37*, (11), 1337-1344.

135. Sirés, I.; Brillas, E.; Oturan, M. A.; Rodrigo, M. A.; Panizza, M., Electrochemical advanced oxidation processes: today and tomorrow. A review. *Environ Sci Pollut R* **2014,** *21*, (14), 8336-8367.
136. Carter, K. E.; Farrell, J., Electrochemical Oxidation of Trichloroethylene Using Boron-Doped Diamond Film Electrodes. *Environ Sci Technol* **2009,** *43*, (21), 8350-8354.
137. Balazs, G. B.; Cooper, J. F.; Shell, T. E., Effect of trace additives on the efficiency of peroxydisulfate regeneration. *J Appl Electrochem* **1999,** *29*, (3), 285-292.
138. Serrano, K.; Michaud, P. A.; Comninellis, C.; Savall, A., Electrochemical preparation of peroxodisulfuric acid using boron doped diamond thin film electrodes. *Electrochim Acta* **2002,** *48*, (4), 431-436.
139. Davis, J. R.; Baygents, J. C.; Farrell, J., Effect of current density and sulfuric acid concentration on persulfuric acid generation by boron-doped diamond film anodes. *J Appl Electrochem* **2014,** *44*, (7), 841-848.
140. Goldin, M. M.; Khubutiya, M. S.; Kolesnikov, V. A.; Abakumov, M. M.; Evseev, A. K.; Volkov, A. G., Indirect electrochemical synthesis of active oxygen in dilute sulfate solutions. *J Appl Electrochem* **2009,** *39*, (2), 185-189.
141. Yuan, S. H.; Liao, P.; Alshawabkeh, A. N., Electrolytic Manipulation of Persulfate Reactivity by Iron Electrodes for Trichloroethylene Degradation in Groundwater. *Environ Sci Technol* **2014,** *48*, (1), 656-663.
142. Govindan, K.; Raja, M.; Noel, M.; James, E. J., Degradation of pentachlorophenol by hydroxyl radicals and sulfate radicals using electrochemical activation of peroxomonosulfate, peroxodisulfate and hydrogen peroxide. *J Hazard Mater* **2014,** *272*, 42-51.
143. Lin, H.; Wu, J.; Zhang, H., Degradation of bisphenol A in aqueous solution by a novel electro/Fe3+/peroxydisulfate process. *Sep Purif Technol* **2013,** *117*, 18-23.
144. Zou, X. L.; Zhou, T.; Mao, J.; Wu, X. H., Synergistic degradation of antibiotic sulfadiazine in a heterogeneous ultrasound-enhanced Fe-0/persulfate Fenton-like system. *Chem Eng J* **2014,** *257*, 36-44.
145. Liang, C. J.; Lin, Y. T.; Shih, W. H., Treatment of Trichloroethylene by Adsorption and Persulfate Oxidation in Batch Studies. *Ind Eng Chem Res* **2009,** *48*, (18), 8373-8380.
146. Yang, S. Y.; Yang, X.; Shao, X. T.; Niu, R.; Wang, L. L., Activated carbon catalyzed persulfate oxidation of Azo dye acid orange 7 at ambient temperature. *J Hazard Mater* **2011,** *186*, (1), 659-666.
147. Yang, S. Y.; Xiao, T.; Zhang, J.; Chen, Y. Y.; Li, L., Activated carbon fiber as heterogeneous catalyst of peroxymonosulfate activation for efficient degradation of Acid Orange 7 in aqueous solution. *Sep Purif Technol* **2015,** *143*, 19-26.
148. Ji, Y. F.; Dong, C. X.; Kong, D. Y.; Lu, J. H.; Zhou, Q. S., Heat-activated persulfate oxidation of atrazine: Implications for remediation of groundwater contaminated by herbicides. *Chem Eng J* **2015,** *263*, 45-54.
149. Rao, Y. F.; Qu, L.; Yang, H. S.; Chu, W., Degradation of carbamazepine by Fe(II)-activated persulfate process. *J Hazard Mater* **2014,** *268*, 23-32.
150. Moghaddam, S. K.; Rasoulifard, M.; Vahedpour, M.; Eskandarian, M., Removal of tylosin from aqueous solution by UV/nano Ag/S2O82- process : Influence of operational parameters and kinetic study. *Korean J Chem Eng* **2014,** *31*, (9), 1577-1581.

151. Yu, X. Y.; Bao, Z. C.; Barker, J. R., Free radical reactions involving Cl-center dot, Cl-2(-center dot), and SO4-center dot in the 248 nm photolysis of aqueous solutions containing S2O82- and Cl-. *J Phys Chem A* **2004,** *108*, (2), 295-308.
152. Lin, C. C.; Lee, L. T.; Hsu, L. J., Degradation of polyvinyl alcohol in aqueous solutions using UV-365 nm/S2O8 (2-) process. *Int J Environ Sci Te* **2014,** *11*, (3), 831-838.
153. Zhao, J. Y.; Zhang, Y. B.; Quan, X.; Chen, S., Enhanced oxidation of 4-chlorophenol using sulfate radicals generated from zero-valent iron and peroxydisulfate at ambient temperature. *Sep Purif Technol* **2010,** *71*, (3), 302-307.
154. Xie, X. F.; Zhang, Y. Q.; Huang, W. L.; Huang, S. B., Degradation kinetics and mechanism of aniline by heat-assisted persulfate oxidation. *J Environ Sci-China* **2012,** *24*, (5), 821-826.
155. Zhang, Y. Q.; Xie, X. F.; Huang, W. L.; Huang, S. B., Degradation of aniline by Fe2+-activated persulfate oxidation at ambient temperature. *J Cent South Univ* **2013,** *20*, (4), 1010-1014.
156. Li, B. Z.; Li, L.; Lin, K. F.; Zhang, W.; Lu, S. G.; Luo, Q. S., Removal of 1,1,1-trichloroethane from aqueous solution by a sono-activated persulfate process. *Ultrason Sonochem* **2013,** *20*, (3), 855-863.
157. Bennedsen, L. R.; Muff, J.; Sogaard, E. G., Influence of chloride and carbonates on the reactivity of activated persulfate. *Chemosphere* **2012,** *86*, (11), 1092-1097.
158. Tan, C. Q.; Gao, N. Y.; Zhou, S. Q.; Xiao, Y. L.; Zhuang, Z. Z., Kinetic study of acetaminophen degradation by UV-based advanced oxidation processes. *Chem Eng J* **2014,** *253*, 229-236.
159. Wu, X. L.; Gu, X. G.; Lu, S. G.; Xu, M. H.; Zang, X. K.; Miao, Z. W.; Qiu, Z. F.; Sui, Q., Degradation of trichloroethylene in aqueous solution by persulfate activated with citric acid chelated ferrous ion. *Chem Eng J* **2014,** *255*, 585-592.
160. Xie, P. C.; Ma, J.; Liu, W.; Zou, J.; Yue, S. Y. C.; Li, X.; Wiesner, M. R.; Fang, J. Y., Removal of 2-MIB and geosmin using UV/persulfate: Contributions of hydroxyl and sulfate radicals. *Water Res* **2015,** *69*, 223-233.
161. Gao, Y. Q.; Gao, N. Y.; Deng, Y.; Yin, D. Q.; Zhang, Y. S., Degradation of florfenicol in water by UV/Na2S2O8 process. *Environ Sci Pollut R* **2015,** *22*, (11), 8693-8701.
162. Boni, M. R.; Sbaffoni, S., Chemical Oxidation by Sodium Persulphate for the Treatment of Contaminated Groundwater. Laboratory Tests. *Bosicon 2012: 3rd International Conference on Contaminated Sites Remediation* **2012,** *28*, 157-162.
163. Chou, Y. C.; Lo, S. L.; Kuo, J.; Yeh, C. J., Microwave-enhanced persulfate oxidation to treat mature landfill leachate. *J Hazard Mater* **2015,** *284*, 83-91.
164. Zhang, H.; Wang, Z.; Liu, C. C.; Guo, Y. Z.; Shan, N.; Meng, C. X.; Sun, L. Y., Removal of COD from landfill leachate by an electro/Fe2+/peroxydisulfate process. *Chem Eng J* **2014,** *250*, 76-82.
165. Ghauch, A.; Tuqan, A. M.; Kibbi, N., Ibuprofen removal by heated persulfate in aqueous solution: A kinetics study. *Chem Eng J* **2012,** *197*, 483-492.
166. Ghauch, A.; Tuqan, A. M., Oxidation of bisoprolol in heated persulfate/H2O systems: Kinetics and products. *Chem Eng J* **2012,** *183*, 162-171.
167. Yan, J. C.; Han, L.; Gao, W. G.; Xue, S.; Chen, M. F., Biochar supported nanoscale zerovalent iron composite used as persulfate activator for removing trichloroethylene. *Bioresource Technol* **2015,** *175*, 269-274.

168. Kusic, H.; Peternel, I.; Koprivanac, N.; Bozic, A. L., Iron-Activated Persulfate Oxidation of an Azo Dye in Model Wastewater: Influence of Iron Activator Type on Process Optimization. *J Environ Eng-Asce* **2011,** *137*, (6), 454-463.
169. Cai, C.; Zhang, H.; Zhong, X.; Hou, L. W., Electrochemical enhanced heterogeneous activation of peroxydisulfate by Fe-Co/SBA-15 catalyst for the degradation of Orange II in water. *Water Res* **2014,** *66*, 473-485.
170. Sra, K. S.; Thomson, N. R.; Barker, J. F., Stability of Activated Persulfate in the Presence of Aquifer Solids. *Soil Sediment Contam* **2014,** *23*, (8), 820-837.
171. Ahmad, M.; Teel, A. L.; Watts, R. J., Mechanism of Persulfate Activation by Phenols. *Environ Sci Technol* **2013,** *47*, (11), 5864-5871.
172. Chen, J.; Qian, Y.; Liu, H.; Huang, T., Oxidative Destruction of Diclofenac by Thermally Activated Persulfate: Implication for ISCO. *Environmental Science Pollution Research* **2015**.
173. Wu, X. L.; Gu, X. G.; Lu, S. G.; Qiu, Z. F.; Sui, Q.; Zang, X. K.; Miao, Z. W.; Xu, M. H., Strong enhancement of trichloroethylene degradation in ferrous ion activated persulfate system by promoting ferric and ferrous ion cycles with hydroxylamine. *Sep Purif Technol* **2015,** *147*, 186-193.
174. Liang, S. H.; Kao, C. M.; Kuo, Y. C.; Chen, K. F., Application of persulfate-releasing barrier to remediate MTBE and benzene contaminated groundwater. *J Hazard Mater* **2011,** *185*, (2-3), 1162-1168.
175. Kambhu, A.; Comfort, S.; Chokejaroenrat, C.; Sakulthaew, C., Developing slow-release persulfate candles to treat BTEX contaminated groundwater. *Chemosphere* **2012,** *89*, (6), 656-664.
176. Perini, J. A. D.; Silva, B. F.; Nogueira, R. F. P., Zero-valent iron mediated degradation of ciprofloxacin - Assessment of adsorption, operational parameters and degradation products. *Chemosphere* **2014,** *117*, 345-352.
177. Oncu, N. B.; Mercan, N.; Balcioglu, I. A., The impact of ferrous iron/heat-activated persulfate treatment on waste sewage sludge constituents and sorbed antimicrobial micropollutants. *Chem Eng J* **2015,** *259*, 972-980.
178. Lin, H.; Wu, J.; Zhang, H., Degradation of clofibric acid in aqueous solution by an EC/Fe3+/PMS process. *Chem Eng J* **2014,** *244*, 514-521.
179. Liang, C. J.; Guo, Y. Y., Mass Transfer and Chemical Oxidation of Naphthalene Particles with Zerovalent Iron Activated Persulfate. *Environmental Science & Technology* **2010,** *44*, (21), 8203-8208.
180. Liang, C. J.; Huang, C. F.; Mohanty, N.; Kurakalva, R. M., A rapid spectrophotometric determination of persulfate anion in ISCO. *Chemosphere* **2008,** *73*, (9), 1540-1543.
181. Kolthoff, I. M.; Carr, E. M., Volumetric Determination of Persulfate in the Presence of Organic Substances. *Anal Chem* **1953,** *25*, (2), 298-301.
182. Keenan, C. R.; Sedlak, D. L., Factors affecting the yield of oxidants from the reaction of manoparticulate zero-valent iron and oxygen. *Environ Sci Technol* **2008,** *42*, (4), 1262-1267.
183. Paul, T.; Dodd, M. C.; Strathmann, T. J., Photolytic and photocatalytic decomposition of aqueous ciprofloxacin: Transformation products and residual antibacterial activity. *Water Res* **2010,** *44*, (10), 3121-3132.
184. Yahya, M. S.; Oturan, N.; El Kacemi, K.; El Karbane, M.; Aravindakumar, C. T.; Oturan, M. A., Oxidative degradation study on antimicrobial agent ciprofloxacin by electro-fenton process: Kinetics and oxidation products. *Chemosphere* **2014,** *117*, 447-454.

185. Lin, C. C.; Wu, M. S., Degradation of ciprofloxacin by UV/S2O82- process in a large photoreactor. *J Photoch Photobio A* **2014,** *285*, 1-6.
186. Yan, N.; Liu, F.; Xue, Q.; Brusseau, M. L.; Liu, Y. L.; Wang, J. J., Degradation of trichloroethene by siderite-catalyzed hydrogen peroxide and persulfate: Investigation of reaction mechanisms and degradation products. *Chem Eng J* **2015,** *274*, 61-68.
187. Toolaram, A. P.; Haddad, T.; Leder, C.; Kummerer, K., Initial hazard screening for genotoxicity of photo-transformation products of ciprofloxacin by applying a combination of experimental and in-silico testing. *Environ Pollut* **2016,** *211*, 148-156.
188. Haddad, T.; Kummerer, K., Characterization of photo-transformation products of the antibiotic drug Ciprofloxacin with liquid chromatography-tandem mass spectrometry in combination with accurate mass determination using an LTQ-Orbitrap. *Chemosphere* **2014,** *115*, 40-46.
189. Purser, S.; Moore, P. R.; Swallow, S.; Gouverneur, V., Fluorine in medicinal chemistry. *Chemical Society Reviews* **2008,** *37*, (2), 320-330.
190. Ahmad, M.; Teel, A. L.; Furman, O. S.; Reed, J. I.; Watts, R. J., Oxidative and Reductive Pathways in Iron-Ethylenediaminetetraacetic Acid-Activated Persulfate Systems. *J Environ Eng-Asce* **2012,** *138*, (4), 411-418.
191. Matzek, L. W.; Carter, K. E., Sustained persulfate activation using solid iron: Kinetics and application to ciprofloxacin degradation. *Chem Eng J* **2017,** *307*, 650-660.
192. Pillai, I. M. S.; Gupta, A. K., Effect of inorganic anions and oxidizing agents on electrochemical oxidation of methyl orange, malachite green and 2,4-dinitrophenol. *J Electroanal Chem* **2016,** *762*, 66-72.
193. Radjenovic, J.; Petrovic, M., Sulfate-mediated electrooxidation of X-ray contrast media on boron doped diamond anode. *Water Res* **2016,** *94*, 128-135.
194. Wang, Y.; Shen, C. C.; Zhang, M. M.; Zhang, B. T.; Yu, Y. G., The electrochemical degradation of ciprofloxacin using a SnO2-Sb/Ti anode: Influencing factors, reaction pathways and energy demand. *Chem Eng J* **2016,** *296*, 79-89.
195. Menegazzo, N.; Jin, C. M.; Narayan, R. J.; Mizaikoff, B., Compositional and electrochemical characterization of noble metal-diamondlike carbon nanocomposite thin films. *Langmuir* **2007,** *23*, (12), 6812-6818.
196. Cañizares, P.; Sáez, C.; Sánchez-Carretero, A.; Rodrigo, M., Synthesis of novel oxidants by electrochemical technology. *J Appl Electrochem* **2009,** *39*, (11), 2143-2149.
197. Guinea, E.; Centellas, F.; Brillas, E.; Cañizares, P.; Sáez, C.; Rodrigo, M. A., Electrocatalytic properties of diamond in the oxidation of a persistant pollutant. *Applied Catalysis B: Environmental* **2009,** *89*, (3), 645-650.
198. Georgeta, S.; Renata, Z., Antibacterial Quinolones: Ciprofloxacin. *Analele Universităţii din Oradea, Fascicula: Ecotoxicologie, Zootehnie şi Tehnologii de Industrie Alimentară* **2014,** *XIII*, (A), 247-252.
199. Sturini, M.; Speltini, A.; Maraschi, F.; Pretali, L.; Profumo, A.; Fasani, E.; Albini, A.; Migliavacca, R.; Nucleo, E., Photodegradation of fluoroquinolones in surface water and antimicrobial activity of the photoproducts. *Water Res* **2012,** *46*, (17), 5575-5582.
200. Watkinson, A. J.; Murby, E. J.; Costanzo, S. D., Removal of antibiotics in conventional and advanced wastewater treatment: Implications for environmental discharge and wastewater recycling. *Water Res* **2007,** *41*, (18), 4164-4176.

201. Xu, Y. P.; Chen, T.; Wang, Y.; Tao, H.; Liu, S. Y.; Shi, W. X., The occurrence and removal of selected fluoroquinolones in urban drinking water treatment plants. *Environ Monit Assess* **2015,** *187*, (12).
202. Nogueira, R. F. P.; Oliveira, M. C.; Paterlini, W. C., Simple and fast spectrophotometric determination of H2O2 in photo-Fenton reactions using metavanadate. *Talanta* **2005,** *66*, (1), 86-91.
203. Davis, J.; Baygents, J. C.; Farrell, J., Understanding Persulfate Production at Boron Doped Diamond Film Anodes. *Electrochim Acta* **2014,** *150*, 68-74.
204. Figueroa, S.; Vazquez, L.; Alvarez-Gallegos, A., Decolorizing textile wastewater with Fenton's reagent electrogenerated with a solar photovoltaic cell. *Water Res* **2009,** *43*, (2), 283-294.
205. Guinea, E.; Garrido, J. A.; Rodriguez, R. M.; Cabot, P. L.; Arias, C.; Centellas, F.; Brillas, E., Degradation of the fluoroquinolone enrofloxacin by electrochemical advanced oxidation processes based on hydrogen peroxide electrogeneration. *Electrochim Acta* **2010,** *55*, (6), 2101-2115.
206. Clark, M. M., *Transport modeling for environmental engineers and scientists*. John Wiley & Sons: 2011.
207. Stoyanovsky, D. A.; Melnikov, Z.; Cederbaum, A. I., ESR and HPLC analysis of the interaction of hydroxyl radical with DMSO: Rapid reduction and quantification of POBN and PBN nitroxides. *Anal Chem* **1999,** *71*, (3), 715-721.
208. Zhu, L.; Nicovich, J. M.; Wine, P. H., Temperature-dependent kinetics studies of aqueous phase reactions of SO4- radicals with dimethylsulfoxide, dimethylsulfone, and methanesulfonate. *J Photoch Photobio A* **2003,** *157*, (2-3), 311-319.
209. Dodd, M. C.; Buffle, M. O.; Von Gunten, U., Oxidation of antibacterial molecules by aqueous ozone: Moiety-specific reaction kinetics and application to ozone-based wastewater treatment. *Environ Sci Technol* **2006,** *40*, (6), 1969-1977.
210. Neta, P.; Huie, R. E.; Ross, A. B., Rate Constants for Reactions of Inorganic Radicals in Aqueous-Solution. *J Phys Chem Ref Data* **1988,** *17*, (3), 1027-1284.
211. von Gunten, U., Ozonation of drinking water: Part I. Oxidation kinetics and product formation. *Water Res* **2003,** *37*, (7), 1443-1467.
212. Petri, B. G.; Watts, R. J.; Tsitonaki, A.; Crimi, M.; Thomson, N. R.; Teel, A. L., Fundamentals of Isco Using Persulfate. *Serdp Estcp Remediat* **2011,** *3*, 147-191.
213. Lee, H.; Lee, H.-J.; Jeong, J.; Lee, J.; Park, N.-B.; Lee, C., Activation of persulfates by carbon nanotubes: Oxidation of organic compounds by nonradical mechanism. *Chem Eng J* **2015,** *266*, 28-33.
214. Guo, H. G.; Gao, N. Y.; Yang, Y.; Zhang, Y. L., Kinetics and transformation pathways on oxidation of fluoroquinolones with thermally activated persulfate. *Chem Eng J* **2016,** *292*, 82-91.
215. Polcaro, A. M.; Vacca, A.; Mascia, M.; Palmas, S.; Ruiz, J. R., Electrochemical treatment of waters with BDD anodes: kinetics of the reactions involving chlorides. *J Appl Electrochem* **2009,** *39*, (11), 2083-2092.
216. Lou, X. Y.; Xiao, D. X.; Fang, C. L.; Wang, Z. H.; Liu, J. S.; Guo, Y. G.; Lu, S. Y., Comparison of UV/hydrogen peroxide and UV/peroxydisulfate processes for the degradation of humic acid in the presence of halide ions. *Environ Sci Pollut R* **2016,** *23*, (5), 4778-4785.

217. Bergmann, M. E. H.; Rollin, J., Product and by-product formation in laboratory studies on disinfection electrolysis of water using boron-doped diamond anodes. *Catal Today* **2007,** *124*, (3-4), 198-203.
218. Abdessalem, A. K.; Oturan, M. A.; Oturan, N.; Bellakhal, N.; Dachraoui, M., Treatment of an aqueous pesticides mixture solution by direct and indirect electrochemical advanced oxidation processes. *Int J Environ an Ch* **2010,** *90*, (3-6), 468-477.
219. Bergmann, M. E. H.; Koparal, A. S., Studies on electrochemical disinfectant production using anodes containing RuO2. *J Appl Electrochem* **2005,** *35*, (12), 1321-1329.
220. Xie, W. P.; Dong, W.; Kong, D. Y.; Ji, Y. F.; Lu, J. H.; Yin, X. M., Formation of halogenated disinfection by-products in cobalt-catalyzed peroxymonosulfate oxidation processes in the presence of halides. *Chemosphere* **2016,** *154*, 613-619.
221. Verlicchi, P.; Zambello, E., Predicted and measured concentrations of pharmaceuticals in hospital effluents. Examination of the strengths and weaknesses of the two approaches through the analysis of a case study. *Sci Total Environ* **2016,** *565*, 82-94.
222. Chu, W. H.; Li, D. M.; Gao, N. Y.; Yin, D. Q.; Zhang, Y. S.; Zhu, Y. P., Comparison of free amino acids and short oligopeptides for the formation of trihalomethanes and haloacetonitriles during chlorination: Effect of peptide bond and pre-oxidation. *Chem Eng J* **2015,** *281*, 623-631.
223. Dbira, S.; Bensalah, N.; Cañizares, P.; Rodrigo, M. A.; Bedoui, A., The electrolytic treatment of synthetic urine using DSA electrodes. *J Electroanal Chem* **2015,** *744*, 62-68.
224. Srinivasan, R.; Sorial, G. A., Treatment of perchlorate in drinking water: A critical review. *Sep Purif Technol* **2009,** *69*, (1), 7-21.
225. Rodriguez, S.; Vasquez, L.; Costa, D.; Romero, A.; Santos, A., Oxidation of Orange G by persulfate activated by Fe(II), Fe(III) and zero valent iron (ZVI). *Chemosphere* **2014,** *101*, 86-92.
226. Luo, Q. S., Oxidative treatment of aqueous monochlorobenzene with thermally-activated persulfate. *Front Env Sci Eng* **2014,** *8*, (2), 188-194.
227. Khan, J. A.; He, X.; Shah, N. S.; Khan, H. M.; Hapeshi, E.; Fatta-Kassinos, D.; Dionysiou, D. D., Kinetic and mechanism investigation on the photochemical degradation of atrazine with activated H2O2, S2O82- and HSO5-. *Chem Eng J* **2014,** *252*, 393-403.
228. Liang, C. J.; Huang, C. F.; Chen, Y. J., Potential for activated persulfate degradation of BTEX contamination. *Water Res* **2008,** *42*, (15), 4091-4100.
229. Long, A. H.; Lei, Y.; Zhang, H., Degradation of Toluene by a Selective Ferrous Ion Activated Persulfate Oxidation Process. *Ind Eng Chem Res* **2014,** *53*, (3), 1033-1039.
230. Nfodzo, P.; Choi, H., Sulfate Radicals Destroy Pharmaceuticals and Personal Care Products. *Environ Eng Sci* **2011,** *28*, (8), 605-609.
231. Tan, C. Q.; Gao, N. Y.; Chu, W. H.; Li, C.; Templeton, M. R., Degradation of diuron by persulfate activated with ferrous ion. *Sep Purif Technol* **2012,** *95*, 44-48.
232. Hussain, I.; Zhang, Y. Q.; Huang, S. B.; Du, X. Z., Degradation of p-chloroaniline by persulfate activated with zero-valent iron. *Chem Eng J* **2012,** *203*, 269-276.
233. Romero, A.; Santos, A.; Vicente, F.; Gonzalez, C., Diuron abatement using activated persulphate: Effect of pH, Fe(II) and oxidant dosage. *Chem Eng J* **2010,** *162*, (1), 257-265.
234. Xu, M. H.; Du, H. Z.; Gu, X. G.; Lu, S. G.; Qiu, Z. F.; Sui, Q., Generation and intensity of active oxygen species in thermally activated persulfate systems for the degradation of trichloroethylene. *Rsc Adv* **2014,** *4*, (76), 40511-40517.

235. Nie, M. H.; Yang, Y.; Zhang, Z. J.; Yan, C. X.; Wang, X. N.; Li, H. J.; Dong, W. B., Degradation of chloramphenicol by thermally activated persulfate in aqueous solution. *Chem Eng J* **2014,** *246*, 373-382.
236. Lee, Y. C.; Lo, S. L.; Kuo, J.; Lin, Y. L., Persulfate oxidation of perfluorooctanoic acid under the temperatures of 20-40 degrees C. *Chem Eng J* **2012,** *198*, 27-32.
237. Lee, Y. C.; Lo, S. L.; Chiueh, P. T.; Liou, Y. H.; Chen, M. L., Microwave-hydrothermal decomposition of perfluorooctanoic acid in water by iron-activated persulfate oxidation. *Water Res* **2010,** *44*, (3), 886-892.
238. Liu, C. S.; Higgins, C. P.; Wang, F.; Shih, K., Effect of temperature on oxidative transformation of perfluorooctanoic acid (PFOA) by persulfate activation in water. *Sep Purif Technol* **2012,** *91*, 46-51.
239. Oh, S. Y.; Shin, D. S., Degradation of spent caustic by Fenton and persulfate oxidation with zero-valent iron. *J Chem Technol Biot* **2013,** *88*, (1), 145-152.
240. Wu, J. T.; Wu, C. H.; Liu, C. Y.; Huang, W. J., Photodegradation of sulfonamide antimicrobial compounds (sulfadiazine, sulfamethizole, sulfamethoxazole and sulfathiazole) in various UV/oxidant systems. *Water Sci Technol* **2015,** *71*, (3), 412-417.
241. Rasoulifard, M. H.; Mohammadi, S. M. M. D.; Heidari, A.; Shahverdizadeh, G. H., Photocatalytic degradation of acid red 14 from contaminated water using immobilized TiO2 nanoparticles on glass beads activated by UV/peroxydisulfate. *Desalin Water Treat* **2014,** *52*, (28-30), 5479-5484.
242. Wang, D. G.; Li, Y. F.; Yang, M.; Han, M., Decomposition of polycyclic aromatic hydrocarbons in atmospheric aqueous droplets through sulfate anion radicals: An experimental and theoretical study. *Sci Total Environ* **2008,** *393*, (1), 64-71.
243. Hazime, R.; Nguyen, Q. H.; Ferronato, C.; Salvador, A.; Jaber, F.; Chovelon, J. M., Comparative study of imazalil degradation in three systems: UV/TiO2, UV/K2S2O8 and UV/TiO2/K2S2O8. *Appl Catal B-Environ* **2014,** *144*, 286-291.
244. Hori, H. Y., Ari; Hayakawa, Etsuko; Taniyasu, Sachi; Tamashita, Nobuyoshi; Kutsuna, Shuzo, Efficient Decomposition of Environmentally Persistant PerfluorocarboxylicAcids by the Use of Persulfate as a Photochemical Oxidant. *Environ Sci Technol* **2005,** *39*, (7), 2383-2388.
245. Lin, C. C.; Lee, L. T., Degradation of polyvinyl alcohol in aqueous solutions using UV/oxidant process. *J Ind Eng Chem* **2015,** *21*, 569-574.
246. Wu, J.; Zhang, H.; Qiu, J. J., Degradation of Acid Orange 7 in aqueous solution by a novel electro/Fe2+/peroxydisulfate process. *J Hazard Mater* **2012,** *215*, 138-145.
247. Yang, S. W.; Sun, J.; Hu, Y. Y.; Cheng, J. H.; Liang, X. Y., Effect of vacuum ultraviolet on ultrasonic defluorination of aqueous perfluorooctanesulfonate. *Chem Eng J* **2013,** *234*, 106-114.

APPENDIX

Table A1. Iron, Heat and Ultraviolet Light Activated Persulfate Degradation of Various Organics

Iron-Activated Degradation	Analyte (mmol L^{-1})	Persulfate (mmol L^{-1})	Maximum Analyte Removal	Rxn Time (min)	Optimal Molar Ratio	Form of Iron	
Aniline[100]	0.05	2.5	100%	10	1:50:100	Fe^0	
Aniline[106]	0.05	2.5	73%	240	1:125:25	Fe^{2+}	
Bisphenol A[99]	80	2	100%	45	1:5:4	Fe^0	
Bisphenol A[99]	80	2	100%	30	1:5:4	Fe^{2+} Continuous addition	
Bisphenol A[99]	80	2	97%	30	1:5:4	Fe^{2+} Sequential addition	
-Nitroaniline[109]	0.2	8	100%	270	1:40:115	nano-Fe_3O_4	
2,4-Dichlorophenol[121]	0.184	12	93%	60	1:65:197	nano-Fe^0	
Orange G[225]	0.1	1	100%	30	1:10:10	Fe^{2+} or Fe^{3+}	
Trichloroethene[225]	0.1	1	100%	120	1:10:10	Fe^0	
Trichloroethene[167]	0.15	4.5	>99%	5	1:30:30:150	Fe^0, biochar support	
Trichloroethane[173]	0.15	2.25	>99%	30	1:15:2:10	Fe^{2+}, hydroxylamine	
Heat-Activated Degradation					**Optimal Temp. (C)**	**Synergistic Effects**	
Aniline[100]	0.05	2.5	100%	60	80	+5mM Fe^0	
Atrazine[148]	0.05	1	100%	90	60	none	
2,4-Dichlorophenol[121]	0.184	12	100%	60	50	+36mM Fe^0	
Dimethyl Phthalate[116]	0.0515	10.8	100%	1080	40	none	
1,4-Dioxane[49]	1.135	26	100%	180	60	none	
1,4-Dioxane[49]	1.136	26	100%	240	60	+18mM Fe^{2+}	
Monochlorobenzene[226]	0.00179	179	100%	120	60	none	
UV Light-Activated Degradation					**Fluence Rate (mW cm^{-2})**	**Synergistic Effects**	**Wavelength/Power (nm/W)**
Acid Blue 113[126]	0.073	6.3	97.70%	120	-	no pH effect	254 / 14
Atrazine[227]	0.00464	1	50%	-	-	pH=7.4	254 / -
2-Methylisoborneol[160]	0.238	0.01	86%	10	1.29	no pH effect	254 / 60
Phenol[129]	0.1	0.5	95%	900	0.18	+0.2 g/L Fe^3O^4	295-400 / 20

Table A2. Degradation of BTEX and Phenols by Iron-Activated Persulfate

Analyte	Analyte (mmol L^{-1})	Persulfate (mmol L^{-1})	*Form of Iron	**Optimal Molar Ratio	Maximum Analyte Removal	Rxn Time (min)
Benzene [228]	1	20	Chelated (Citric Acid) Fe^{2+}	1:20:5:5	100%	70
	1	100	Fe^{2+}	1:100:4	60%	5
Ethylbenzene[228]	1	100	Fe^{2+}	1:100:5	63%	5
Toluene[229]	1	27.3	Fe^{2+}	1:27:08	84%	60
Toluene[228]	1	100	Fe^{2+}	1:100:5	50%	5
Xylene[228]	1	100	Fe^{2+}	1:100:5	60%	5
4-Chlorophenol[153]	0.156	0.78	Fe^{0}	1:5:23	88%	60
	0.156	0.78	Fe^{2+}	1:5:20	31%	240
	0.156	0.78	Fe^{3+}	1:5:20	17%	240
p-Nitrophenol[61]	0.72	30	Fe^{2+}	1:42:42	20%	180
	0.72	30	Cu^{2+}	1:42:42	15%	180

**granular batch addition unless otherwise noted **Molar Ratio of Organic: Persulfate: Fe or Organic: Persulfate: Fe:Other Component*

Table A3. Degradation of Various Organics by Iron-Activated Persulfate

Analyte	Analyte Conc. (mmol L^{-1})	Persulfate Conc. (mmol L^{-1})	*Form of Iron	**Optimal Molar Ratio	Maximum Analyte Removal	Rxn Time (min)
Chlorobenzene[98]	2.665	53	nano-Fe^0	1:20:20	97%	1200
	2.665	53	Fe^{2+}	1:20:20	97%	1200
	2.665	53	Fe^0	1:20:20	71%	1200
Cyclohexanoic acid[120]	0.039	10.4	nano-Fe^0	1:266:4590	82%	8640
2,4-Dinitrotoluene[79]	0.275	1.3	Fe^0	1:5:623	100%	120
	0.275	1.3	Fe^{2+}	1:5:623	22%	240
Methyl tert-Butyl Ether[98]	3.523	70.5	nano-Fe^0	1:20:20	40%	960
	3.523	70.5	Fe^{2+}	1:20:20	28%	960
	3.523	70.5	Fe^0	1:20:20	28%	960
Napthalene[179]	0.078	42	Fe^0, sequential addition	1:538:231	>99%	7
Napthalene[98]	0.101	2.02	nano-Fe^0	1:20:20	>99%	1080
	0.101	2.02	Fe^{2+}	1:20:20	>99%	1140
	0.101	2.02	Fe^0	1:20:20	>99%	1200
Polyvinyl Alcohol[92]	0.581	1.3	Fe^{2+}	1:2:2	100%	240
	0.581	1.3	Fe^0	1:2:2	70%	240
Trichloroethene[98]	2.854	57	nano-Fe^0	1:20:20	94%	1440
	2.854	57	Fe^0	1:20:20	80%	1440
	2.854	57	Fe^{2+}	1:20:20	78%	1440

Table A4. Degradation of Pharmaceuticals by Iron-Activated Persulfate

Analyte	Analyte (mmol L^{-1})	Persulfate (mmol L^{-1})	*Form of Iron	**Optimal Molar Ratio	Maximum Analyte Removal	Rxn Time (min)
Acetaminophen[230]	0.060	4.8	Fe^0	1:80:80	60%	240
Caffeine[97]	0.0258	7.36	Fe^{2+} Continuous addition	1:285:285	100%	15
	0.0258	7.36	Fe^{2+}	1:285:285	90%	15
Carbemazepine[149]	0.150	6	Fe^{2+}, Cl- addition	1:40:5	100%	10
	0.150	6	Fe^{2+}	1:40:5	50%	40
	0.050	0.2	Fe^{2+}	1:4:2	30%	60
Ciprofloxacin[96]	0.030	2.4	Fe^{2+}	1:80:80	96%	30
	0.030	0.3	Fe^{2+} or Chelated (Citric Acid) Fe^{2+}	1:10:10:10	70%	30
Ibuprofen[97]	0.0236	7.36	Fe^{2+} or Fe^{2+} Continuous addition	1:312:312	100%	15
Nicotine[97]	0.0309	7.36	Fe^{2+} or Fe^{2+} Continuous addition	1:238:238	100%	15
Phenacetin[97]	0.0279	7.36	Fe^{2+} Continuous addition	1:264:264	100%	30
	0.0279	7.36	Fe^{2+}	1:264:264	47%	30
Sulfadiazine [144]	0.008	1.8	Fe^0	1:225:225	46%	60
Sulfamethoxazole[95]	0.039	1.0	Fe^0	1:25:56	95%	20
	0.039	1.0	CoAgFe	1:25:56	95%	30
	0.039	1.0	CoFe, AgFe, AgCoFe	1:25:56	95%	50
	0.039	1.0	Fe^{2+} Sequential addition	1:25:56	80%	120
	0.030	2.4	Fe^{2+}	1:80:80	75%	30
	0.036	2.9	Fe^0	1:80:80	60%	5
	0.030	0.3	Chelated (EDTA) Fe^{2+}	1:10:10:10	50%	30
	0.039	1.0	Fe^{2+}	1:25:56	40%	120
	0.030	0.3	Chelated (Citric Acid) Fe^{2+}	1:10:10:10	35%	30
	0.030	0.3	Fe^{2+}	1:10:10	30%	30
Triclosan[230]	0.031	2.5	Fe^0	1:80:80	60%	5

**granular batch addition unless otherwise noted **Molar Ratio of Organic: Persulfate: Fe or Organic: Persulfate: Fe:Other Component*

Table A5. Degradation of Phenyls and Dyes by Iron-Activated Persulfate

Analyte	Analyte (mmol L^{-1})	Persulfate (mmol L^{-1})	*Form of Iron	**Optimal Molar Ratio	Maximum Analyte Removal	Rxn Time (min)
Aniline[106]	0.050	2.5	Chelated (Citric Acid) Fe^{2+}	1:50:25:25	60%	240
Aniline[155]	0.10	2.5	Fe^{2+}	1:25:0.5	55%	10
Aniline[106]	0.050	2.5	Chelated (EDTA) Fe^{2+}	1:50:25:25	50%	240
	0.050	2.5	Fe^{2+}	1:50:25	45%	240
	0.050	2.5	Chelated (Oxalic) Fe^{2+}	1:50:25:25	45%	240
Diuron[94]	0.0215	7.36	Fe^{2+} Continuous addition	1:340:340	100%	15
Diuron[94]	0.0858	3.1	Fe^{2+} Continuous addition	1:36:36	100%	30
	0.0858	3.1	Fe^{2+}	1:36:36	100%	30
Diuron	0.0215	7.36	Fe^{2+}	1:340:340	90%	15
Diuron[231]	0.010	0.2	Chelated (Citric Acid) Fe^{2+}	1:20:20	90%	240
PCB28[108]	0.025	2	nano-Fe_3O_4, air purge	1:80:720	100%	200
	0.025	2	nano-Fe_3O_4-Fe^{2+}	1:80:720	95%	120
	0.025	2	nano-Fe_3O_4	1:80:720	90%	240
p-Chloroaniline[232]	0.050	2.5	Fe^0	1:50:1700	100%	12
Reactive Blue 19[80]	0.1	10	Fe^0	1:100:143	100%	45
Congo Red[178]	0.287	0.4	Zerovalent zinc	20mM	60%	180

**granular batch addition unless otherwise noted **Molar Ratio of Organic: Persulfate: Fe or Organic: Persulfate: Fe:OtherComponent*

Table A6. Degradation of Ethenes, Phenols and Phenyls by Thermally Activated Persulfate

Analyte	Analyte (mmol L^{-1})	Persulfate (mmol L^{-1})	Heating Method	Optimal Temp. (C)	Synergistic Effects	Reaction pH	Maximum Analyte Removal	Rxn Time (min)	Reaction Rate Constant (min^{-1})
Aniline[154]	0.030	100	conventional	50	none	7	75%	180	-
Diuron[94, 233]	0.0858	3.1	conventional	50	+0.90 mM Fe^{2+}	3-9	100%	30	-
	0.09	2.1	conventional	50	+0.72 mM Fe^{2+}	2.5	100%	180	0.00451
p-Chloroaniline[232]	0.050	2.5	conventional	50	+12.5 mM Fe^{0}	7	85%	300	-
	0.050	2.5	conventional	50	none	7	58%	300	-
Pentachlorophenol[115]	0.0375	0.75	microwave	90	none	-	100%	40	0.1526
	0.0375	0.75	conventional	90	none	-	94%	40	0.0707
	0.0375	0.112	microwave	130	none	-	90%	1	rapid
p-Nitroaniline[109]	0.200	8	conventional	55	+23mM nano-Fe_3O_4	7	98%	20	0.19
p-Nitrophenol[61]	0.720	30	conventional	70	Fe^{2+},Cu^{2+} did not increase degradation	-	100%	180	0.0276
	0.720	30	conventional	90		-	100%	20	0.2942
Tetrachloroethene[63]	0.045	0.45	conventional	60	none	-	94%	60	0.0332
Trichloroethene[234]	0.150	300	conventional	50	none	-	100%	9	-

Table A7. Degradation of Pharmaceuticals by Thermally Activated Persulfate

Analyte	Analyte (mmol L^{-1})	Persulfate (mmol L^{-1})	Heating Method	Optimal Temp. (C)	Synergistic Effects	Reaction pH	Maximum Analyte Removal	Rxn Time (min)	Reaction Rate Constant (min^{-1})
Antipyrine[114]	0.0265	1.855	conventional	70	none	7.1	94.0%	40	0.0854
	0.0265	2.65	conventional	60	none	4	71.4%	120	0.0092
Chloramphenicol[235]	0.200	4	conventional	80	none	5.4	>99%	40	0.0593
	0.200	4	conventional	50	none	5.4	31%	160	0.0024
Diclofenac[172]	0.047	0.47	Conventional	70	None	7	>90%	120	0.0162
Ibuprofen[165]	0.0204	1	conventional	70	none	7	100%	20	0.183
	0.0204	1	conventional	60	none	4	85%	60	0.0161
Sulfamethoxazole[118]	0.050	2.5	conventional	90	none	4.7	80%	60	0.0271
	0.050	2.5	microwave	90	none	4.7	100%	16	0.291
	0.050	2.5	microwave	130	none	4.7	100%	1	rapid

Table A8. Degradation of Various Organics by Thermally Activated Persulfate

Analyte	Analyte (mmol L^{-1})	Persulfate (mmol L^{-1})	Heating Method	Optimal Temp. (C)	Synergistic Effects	Maximum Analyte Removal	Rxn Time (min)	Reaction Rate Constant (min^{-1})
Cyclohexanoic acid[120]	0.039	10.4	microwave	80	Fe^0 did not increase degradation	100%	120	-
Dimethyl Phthalate[116]	0.0515	10.8	conventional	40	none	100%	1080	0.00172
Methyl tert-Butyl Ether[57]	0.060	31.5	conventional	50	none	100%	150	0.0348
Perfluorooctanoic Acid [81, 92, 93, 236-238]	0.2415	200	conventional	40	none	100%	4320	0.00086
	0.254	50	microwave	90	none	99.3%	240	0.01633
	0.254	10	microwave	90	none	77%	120	0.00122
	0.254	5	microwave	90	+3.6 mM Fe^0	67.60%	120	0.0417
	0.254	5	microwave	90	none	62.60%	240	0.0008
	0.0005	10	conventional	85	none	93.50%	3060	0.00158
Polyvinyl Alcohol[92]	0.581	1.00	conventional	80	Fe^{2+},Fe^0 did not increase degradation	100%	10	0.4238
	0.581	1.00	conventional	60	Fe^{2+},Fe^0 did not increase degradation	100%	30	0.0846
Landfill Leachate[163]	2090mg/L TOC	22	microwave	85	none	79.4	30	0.0099
Spent Caustic[239]	2090mg/L TOC	45	conventional	80	Fe^{2+},Fe^0 did not increase degradation +9mM Fe^0	95%	120	0.0134

Table A9. Degradation of Pharmaceuticals by Ultraviolet Light Activated Persulfate

Analyte	Analyte (mmol L^{-1})	Persulfate (mmol L^{-1})	UV Wavelength/Power (nm/W)	Fluence Rate (mW/cm^2)	Synergistic Effects	Maximum Analyte Removal	Rxn Time (min)	Reaction Constant (min^{-1})	Rate
Ciprofloxacin[185]	0.0302	8	254 / 8	1		95%	30	0.2988	
Acetaminophen[158]	0.017	0.132	253.7 / 75	0.114	-	100%	60	0.0453	
Ampicillin[53]	0.050	1	254 / 50 (two lamps)	0.1	-	75%			
Carbemazepine[128]	0.050	0.2	290 max / 1800	-	+0.1mMol/L Fe^{2+}	100%	30	0.109	
	0.050	0.2	290 max / 1800	-	-	60%	60	0.0051	
Cephalothin[53]	0.050	1	254 / 50 (two lamps)	0.1	-	91%			
Florfenicol[161]	0.02	2	254 / -	-	-	100%	60	0.0325	
Sulfadiazine[240]	0.080	0.5	254 / 8	0.112	-	93%	180	0.0245	
Sulfamethizole[240]	0.074	0.5	254 / 8	0.112	-	97%	180	0.0096	
Sulfamethoxazole[240]	0.079	0.5	254 / 8	0.112	-	98%	180	0.0283	
Sulfathiazole[240]	0.078	0.5	254 / 8	0.112	-	99%	180	0.0141	
Tylosin[150]	0.0055	2	- / 30W	-	+93uM nano-Ag	90.90%	35	-	

Table A10. Degradation of Various Organics by Ultraviolet Light Activated Persulfate

Analyte	Analyte \(mmol L^{-1})	Persulfate (mmol L^{-1})	UV Wavelength/ Power (nm / W)	Fluence Rate (mW cm^{-2})	Synergistic Effects	Maximum Analyte Removal	Rxn Time (min)	Reaction Rate Constant (min^{-1})
2,2,3,3-tetrafluoro-1-propanol[82]	1.390	20	254 / -	2.04	pH=3.0	100%	60	-
Acid Red 14[241]	0.040	5.0	200-280 / 30	-	Nano-TiO_2 on glass beads	75%	15	
Anthracene[242]	0.004	0.08	300 / -	-	-	90%	6	0.35
Geosmin[160]	0.219	0.01	254 / 60	1.29	no pH effect	94.50%	10	$7.6*10^8$ $L(mol\text{-}s)^{-1}$
Imazalil[243]	0.084	42.2	365 / 125	31	pH=6.5	100%	120	0.596
	0.084	21.1	365 / 125	31	pH=3.0; +2.5 g/L TiO_2	100%	240	0.501
Nitrobenzene[53]	0.050	1	254 / 50	0.1	pH=2.0	75%		-
Perfluorononanoic Acid[244]	0.0148	1.1	220-460 / 200	-	0.48 MPa O_2	100%	720	-
Perfluorooctanoic Acid	0.0296	1.1	220-460 / 200	-	0.48 MPa O_2	100%	240	-
Phenol[129]	0.100	50	295-400 / 20	0.18	-	95%	300	-
Polyvinyl Alcohol[125, 245]	20 mg L^{-1}	0.325	254 / 8	-	pH=3.0	100%	<5 min	1.5509
	20 mg L^{-1}	0.5	254 / 8	-	-	100%	<5 min	2.3438
	20 mg L^{-1}	0.5	365 / 8	-	-	93%	30	0.0275
Tetrabromobisphenol A[127]	0.100	20	365 max / 100	-	pH=13.0	99%	180	-

Table A11. Degradation of Various Organics by Electrochemically Activated Persulfate

Analyte	Analyte (mmol L^{-1})	Persulfate (mmol L^{-1})	Anode	Cathode	Synergistic Effects	Electrical Properties	pH	Max Analyte Removal	Reaction duration (min)
Acid Orange 7[246]	0.1	12	Ti/RuO_2/IrO_2	stainless steel	1 mM Fe^{2+}	16.8 mA cm^{-2}	3	95.7%	60
	0.1	12	Ti/RuO_2/IrO_2	stainless steel	none	16.8 mA cm^{-2}	3	65.8%	60
	64	3% by wt.	Pt	Pt	150mL/min N2	6 V	3.7	100%	420
Aniline[50]									
Bisphenol A[143]	220	10	Ti/RuO_2/IrO_2	stainless steel	2mM Fe3+	16.8 mA cm^{-2}	3	>99%	120
Dinitrotoluene[59]	25 mg L^{-1} TOC	1% by wt.	Pt	Pt	150mL/min N2	6 V	0.5	98%	480
Orange II[169]	100 mg L^{-1}	8.4	Ti/RuO_2/IrO_2	stainless steel	1g/L Fe-Co/SBA-15 catalyst	16.8 mA cm^{-2}	6	95.6%	60
	100 mg L^{-1}	8.4	Ti/RuO_2/IrO_2	stainless steel	1g/L Fe-Co/SBA-15 catalyst	8.4 mA cm^{-2}	6	90.5%	60
	100mg/L	8.4	Ti/RuO_2/IrO_2	stainless steel	none	8.4 mA cm^2	6	89.4%	60
Pentachlorophenol[142]	50	0.115	Fe	Fe	Fe from electrodes	90 mA cm^2	4.5	38%	20
Trichloroethene[141]	400	5	Fe	Mixed Metal Oxide	up to 1.8mM Fe from Fe anode	100 mA	5.6	100%	90
Landfill leachate[164]	1900 mg L^{-1} COD	62.5	Ti/IrO_2-RuO_2-TiO_2	Ti	15.6 mM Fe^{2+}	13.9 mA cm^{-2}	3	62.2%	60

Table A12. Degradation of Various Organics Using Unique Methods of Persulfate Activation

Analyte	Analyte Conc. (mmol L^{-1})	Persulfate Conc. (mmol L^{-1})	Activator	Activator Properties	Maximum Analyte Removal	Optimization	Reaction Rate Constant (min^{-1})
Benzotriazole[86]	0.02	0.5	Weak magnetic field with Fe^0	+0.5mM Fe^0; pH=7.0	>90%	WMF resulted in increase in removal	0.0126
Caffeine[86]	0.02	0.5	Same as above	Same as above	100%	Same as above	0.0175
Diuron[86]	0.02	0.5	Same as above	Same as above	100%	Same as above	0.0291
4-nitrophenol[86]	0.02	0.5	Same as above	Same as above	>95%	Same as above	0.0189
Ammonia Perfluorooctanoate[56]	0.0464	10	Ultrasonication	300W, 20kHz	51.20%	persulfate increased removal 15%	
Acid Orange 7[58]		1.3	Ultrasonication plus Fe^0	60W; +2.1mM Fe^0;	96.40%	Increased removal 35% with US; pH=5.8	
Sulfadiazine[144]	0.008	1.84	Ultrasonication	90 Watts; +0.2mM Fe^0	99.10%		
Perfluorooctanoic-sulphonic Acid[247]	0.0185	18.5	Heat, UV , Fe^{2+} or Utrasonication	UV=254nm,15W; US=2W/cm^2 ,40kHz; Fe_2=3mM	22.5% with temp	pH = 3.0	heat>UV>Fe2+> US
Ibuprofen[60]	1	20	gamma irradiation	80 kGy dose	97%	Addition of persulfate required less dose	
PCB28[51]	0.002	5	1,4-benzoquinone	0.1mM	88%	pH = 7.4	0.0097
Phenol[68]	0.213	6.2	carbon nanotubes	0.2g/L catalyst	100%		0.0439
p-Hydroxybenzoic Acid[66]	0.1	2	electron beam	3MeV vertical scan beam; 600 Gy dose	80%	Persulfate did not affect removal	
Acid Orange 7[146]	0.057	5.7	activated carbon	5g/L (adsorbent and catalyst)	>97%	Rate constant reported for 1g/L AC (82% rem.)	0.000347
Perfluorooctanoic Acid[67]	0.1206	6.3	activated carbon	10g/L (adsorbent and catalyst)	68.20%	persulfate increased reaction rate 50%	0.00437
Trichloroethene[145]	0.076	8.4	activated carbon	adsorbent and catalyst	97%	Addition of persulfate increased TCE degradation	0.0329

Figure A1. Mass spectra for byproducts are shown for a-h) nitrate, i) sulfate, and j-u) persulfate at various time points during the degradation of ciprofloxacin.

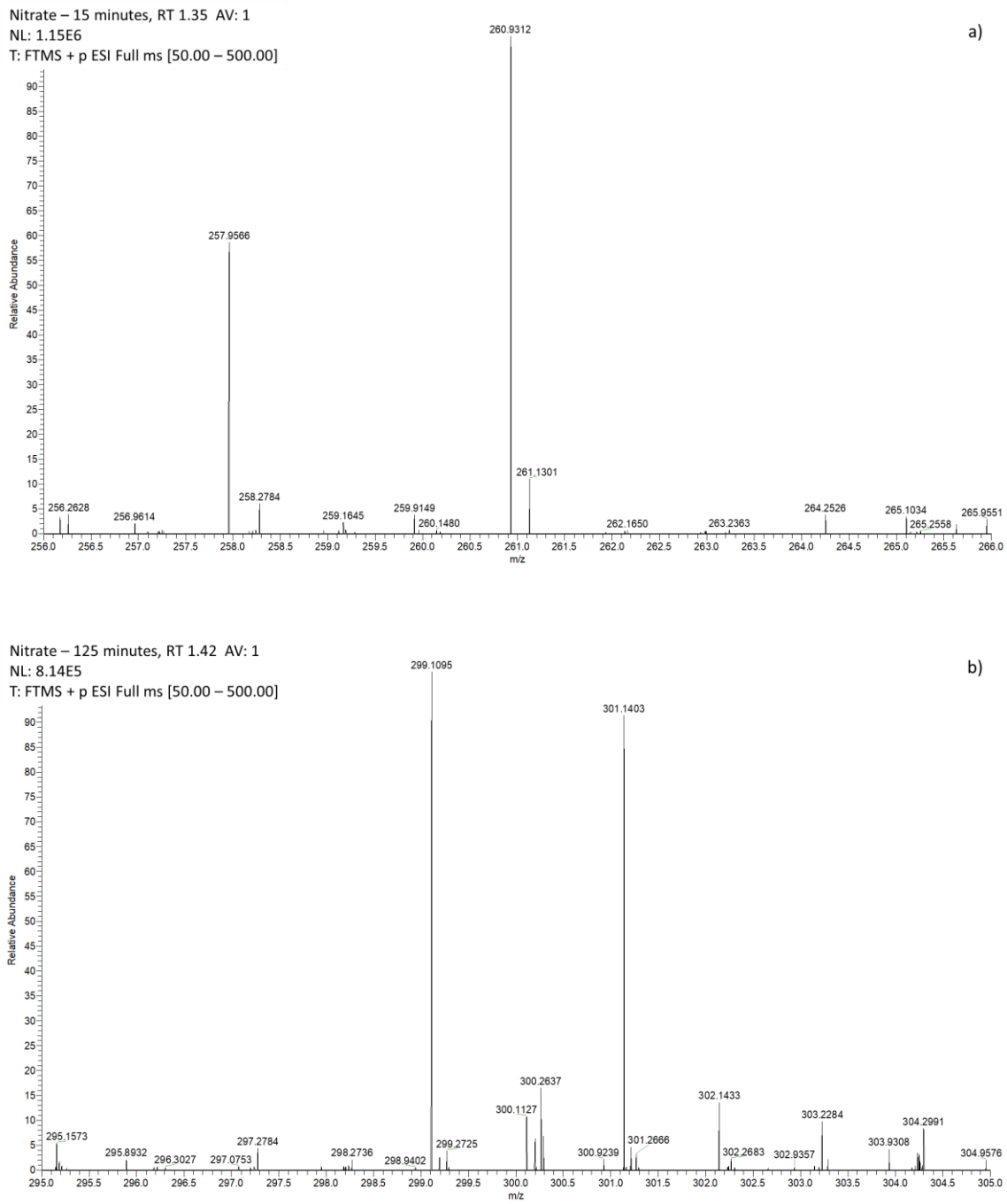

Figure A1. Continued

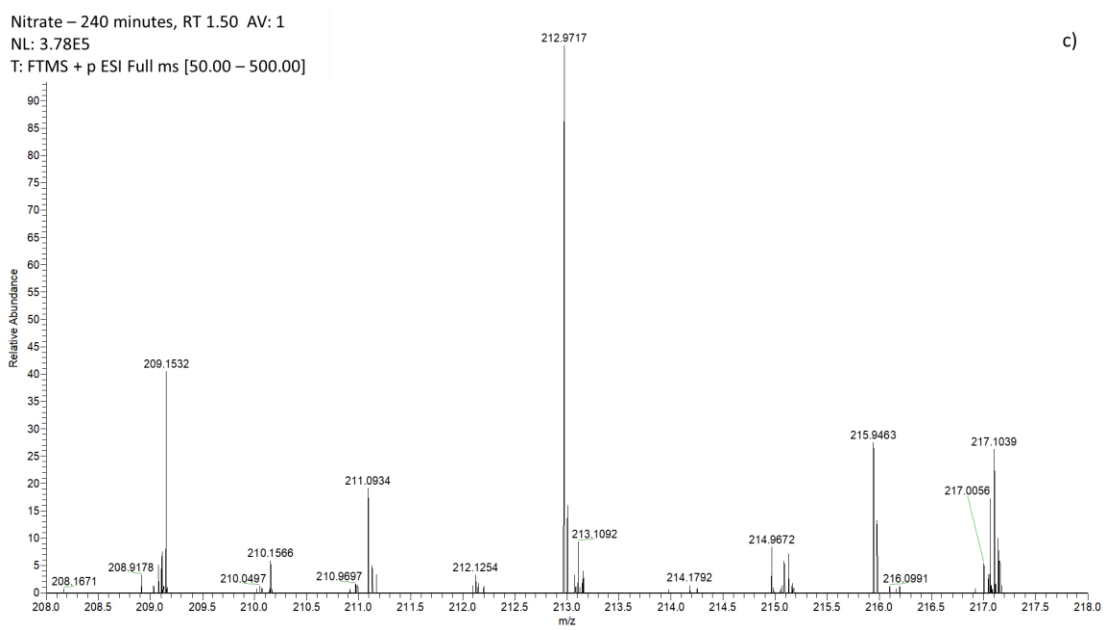

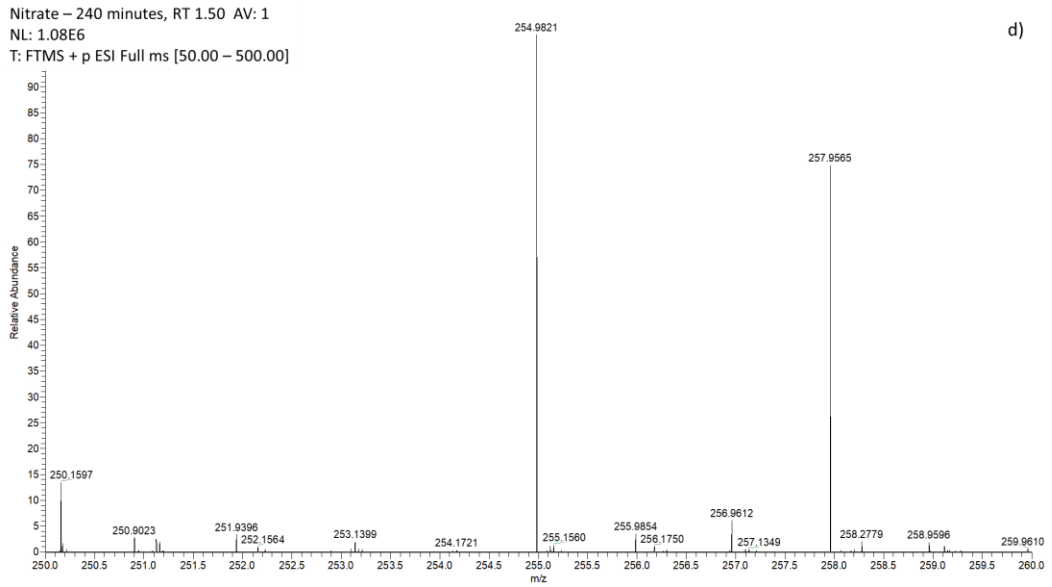

Figure A1. Continued

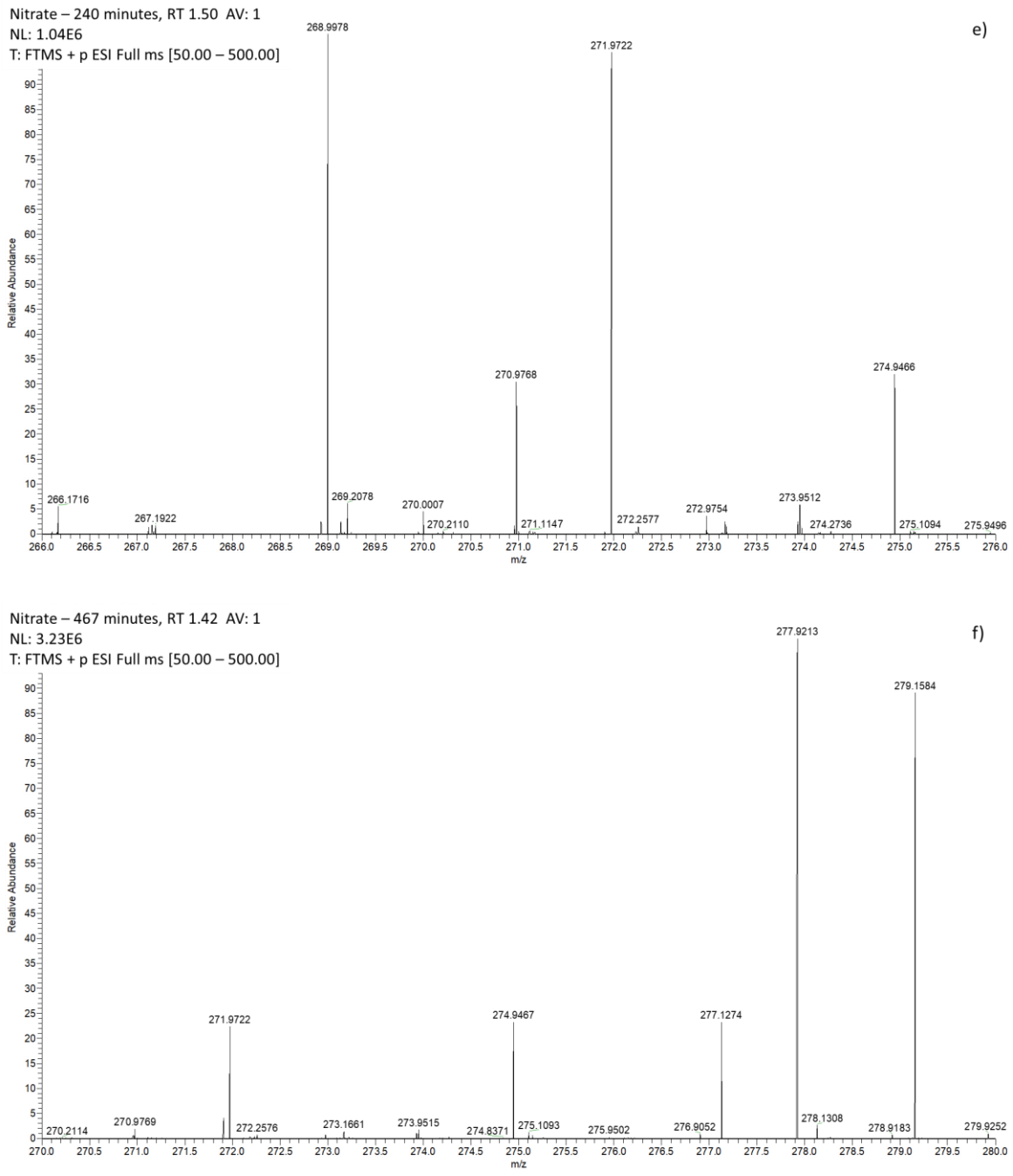

Figure A1. Continued

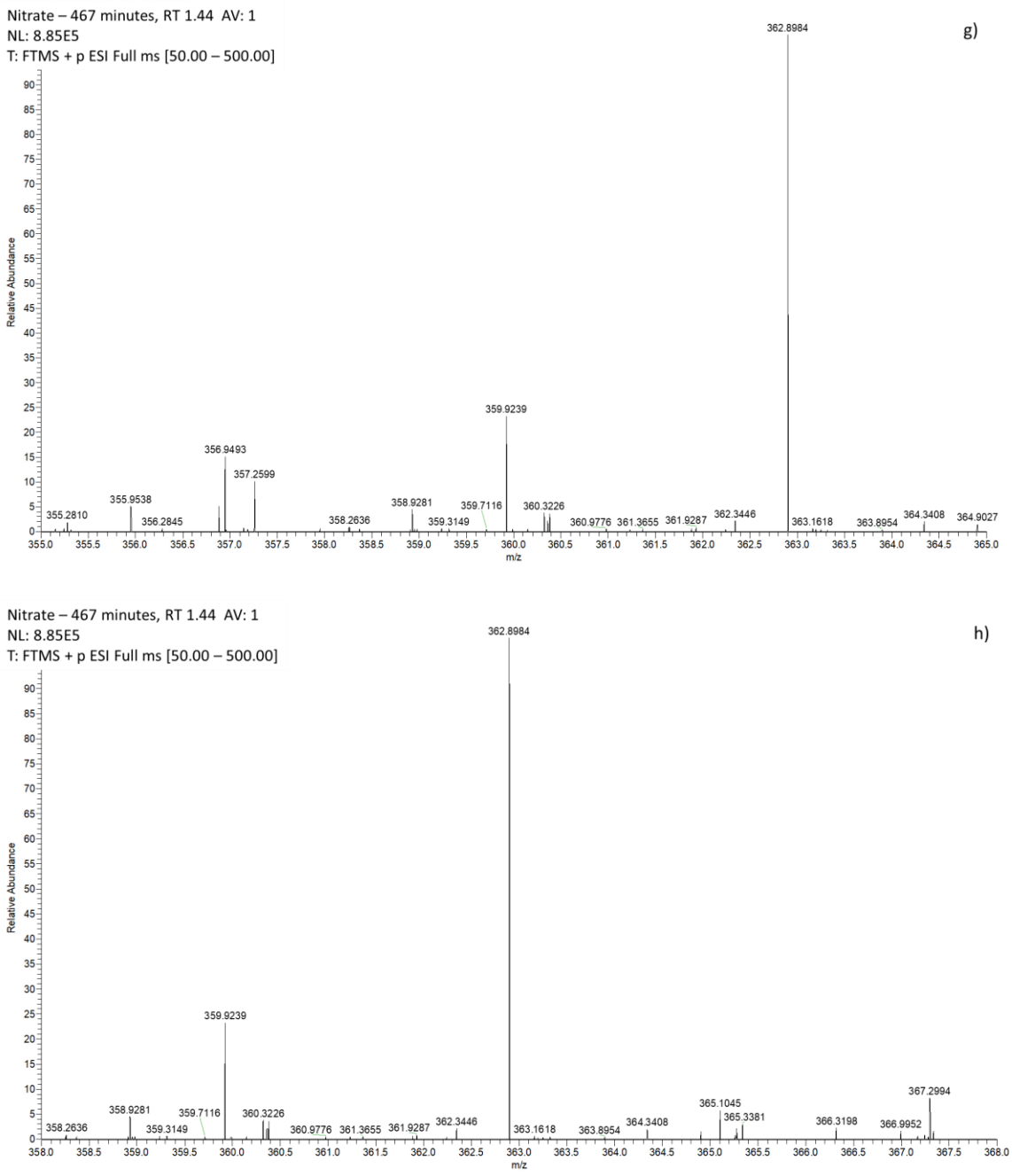

Figure A1. Continued

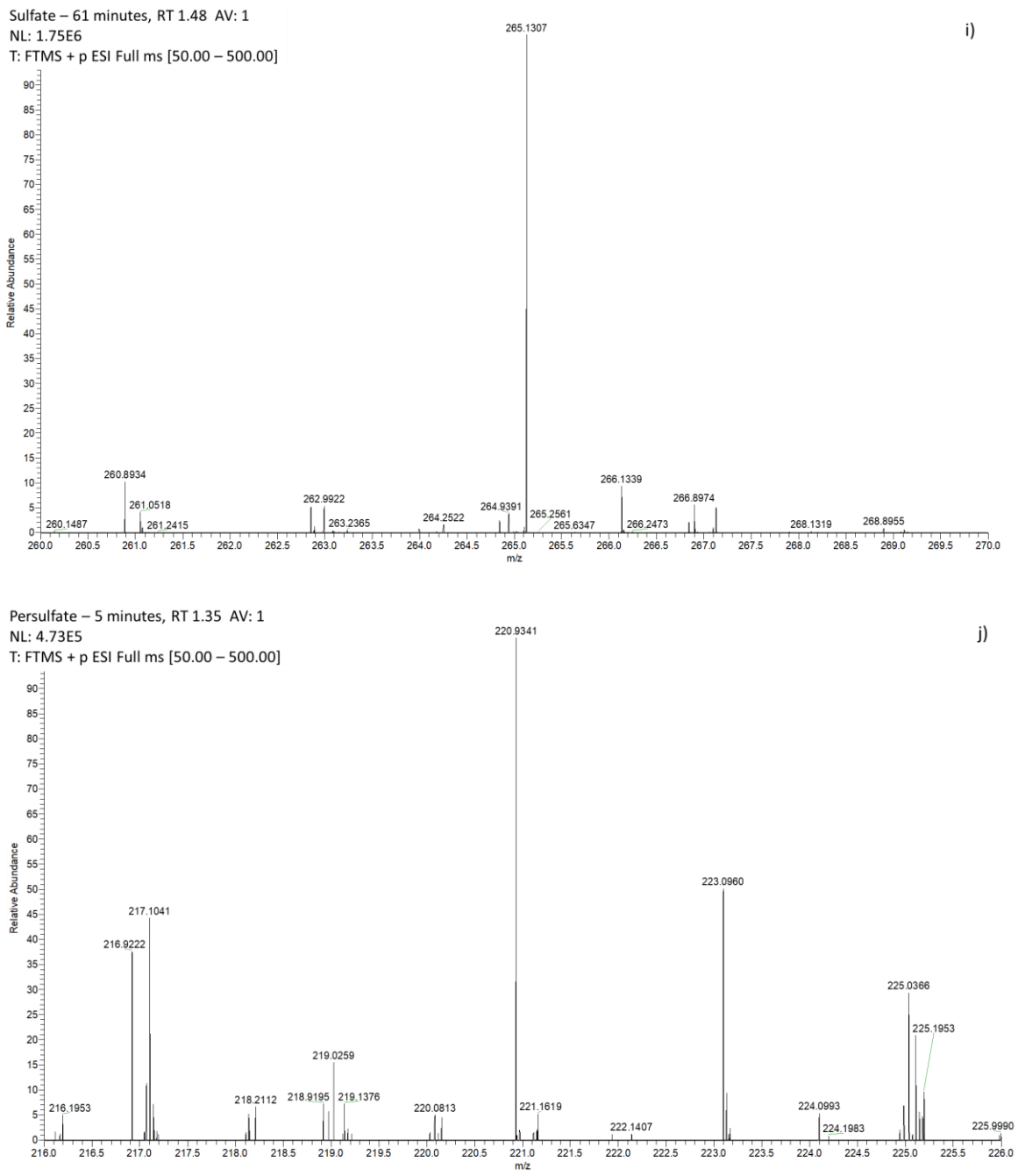

Figure A1. Continued

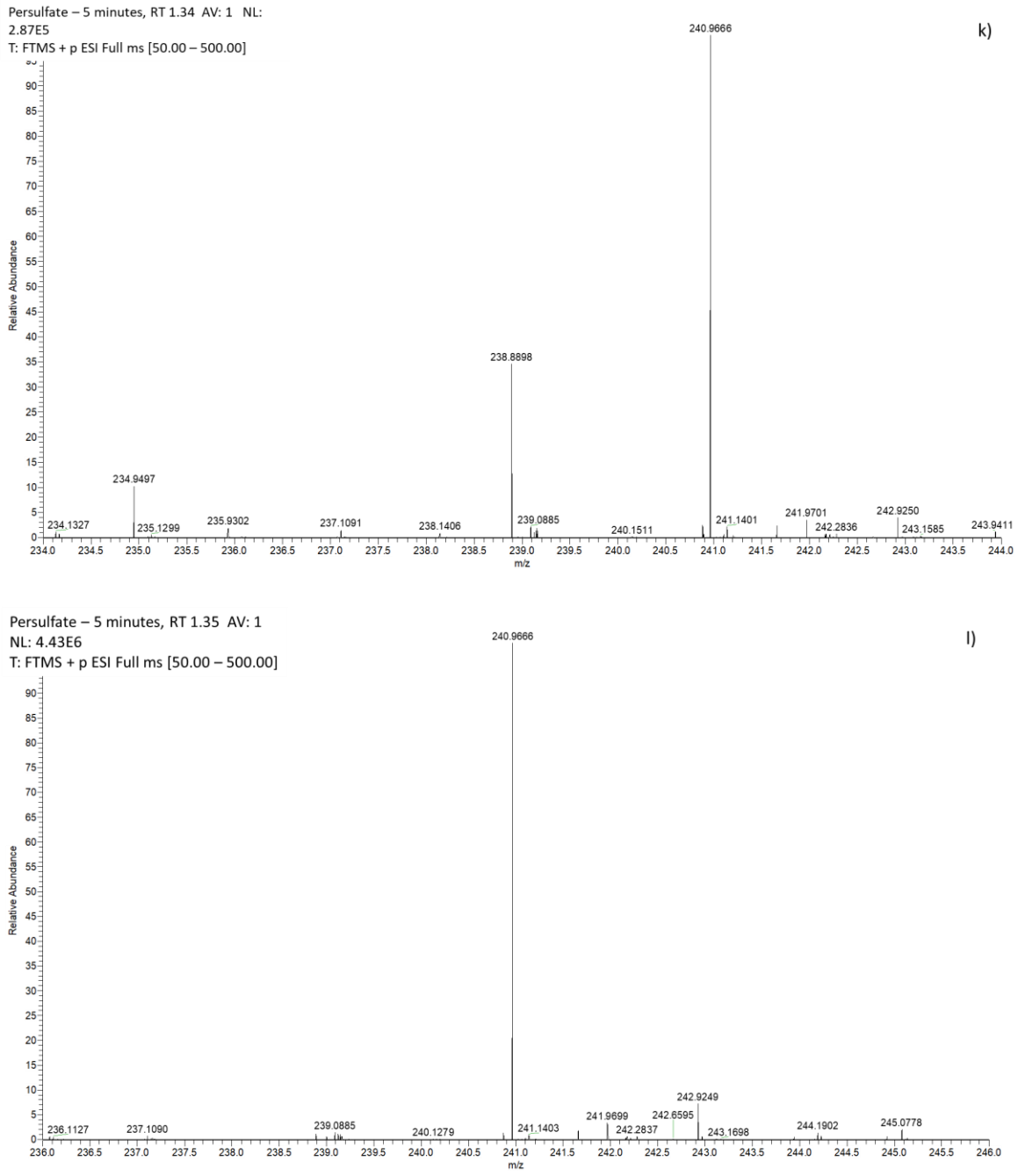

Figure A1. Continued

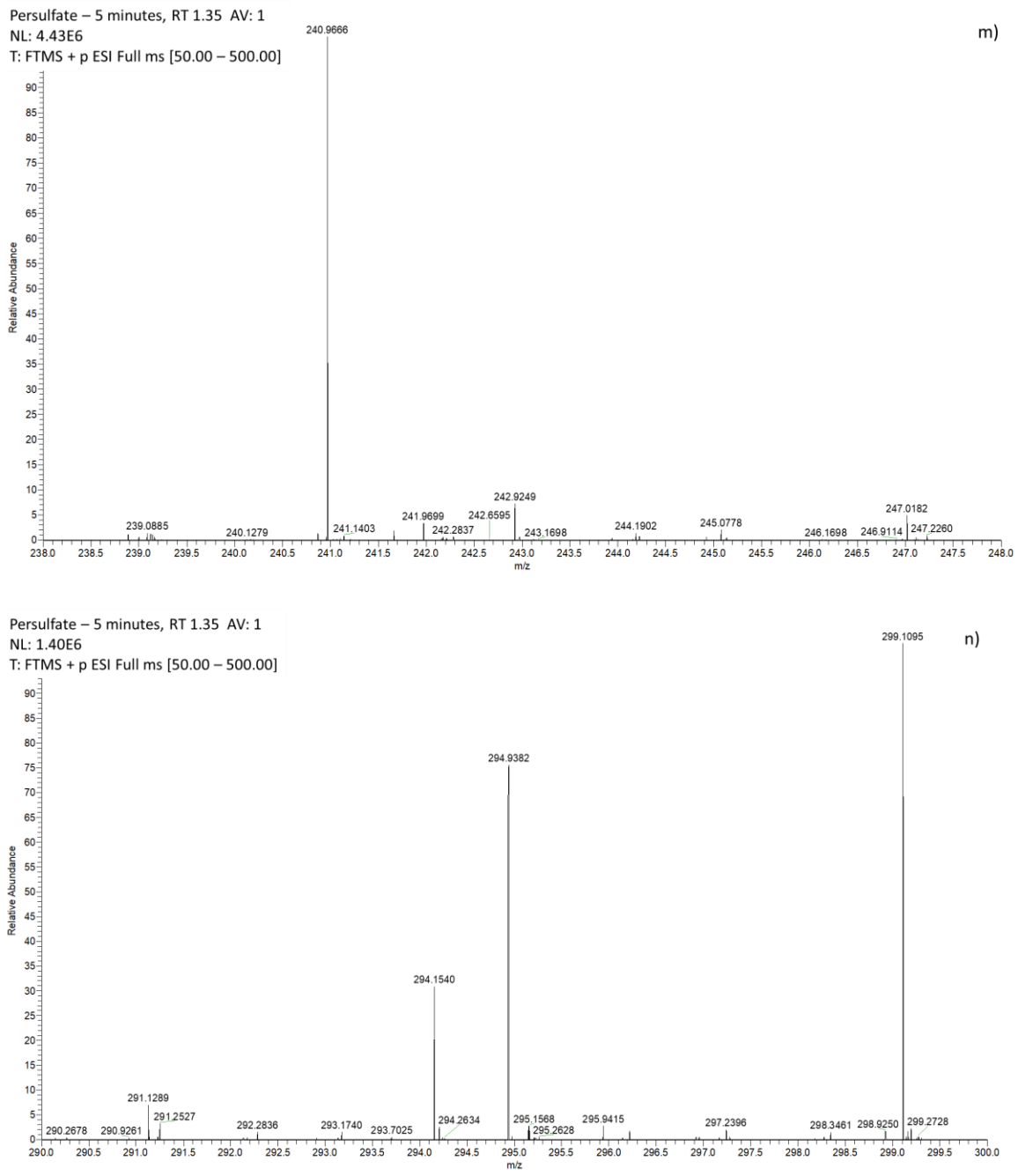

Figure A1. Continued

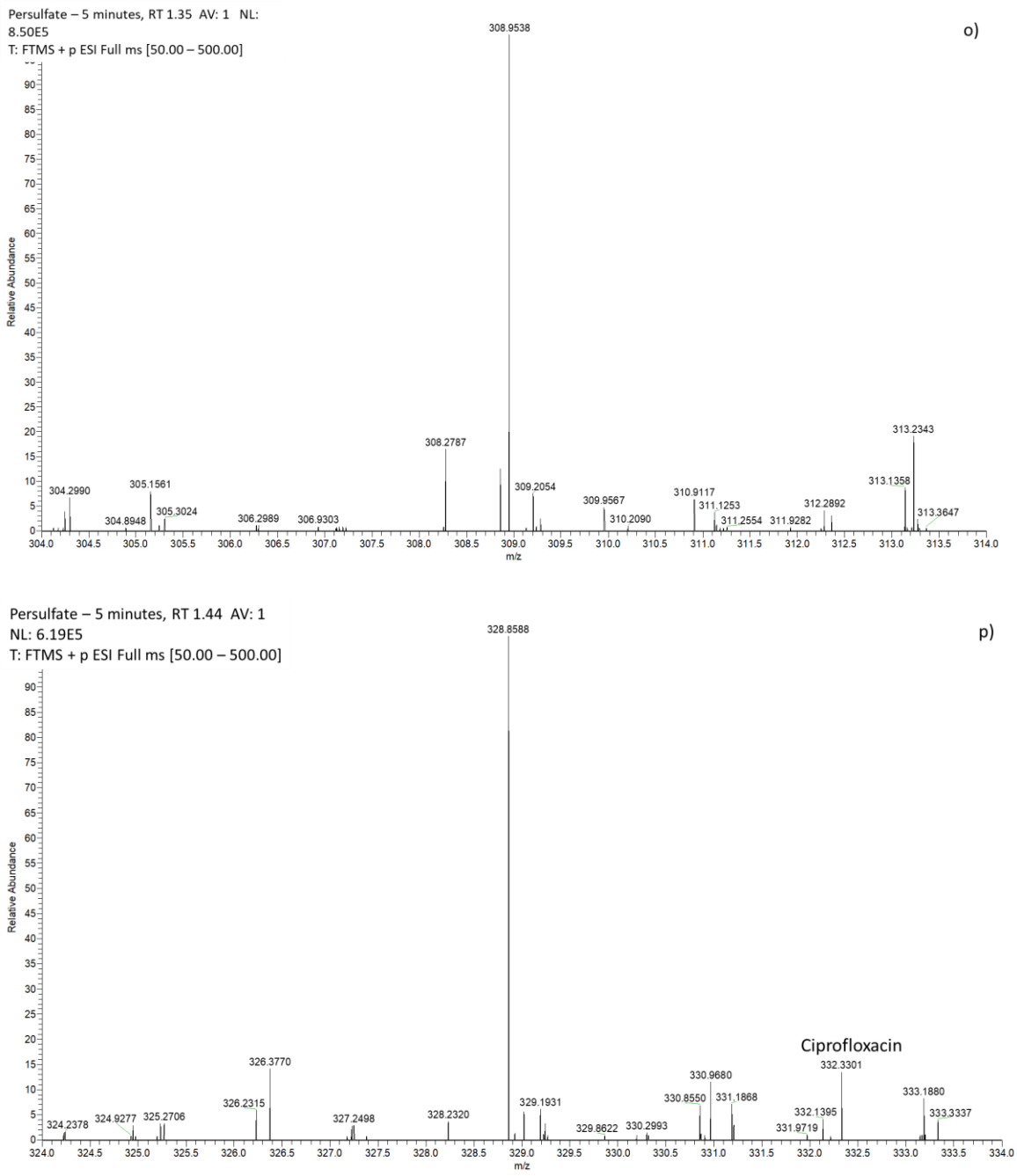

Figure A1. Continued

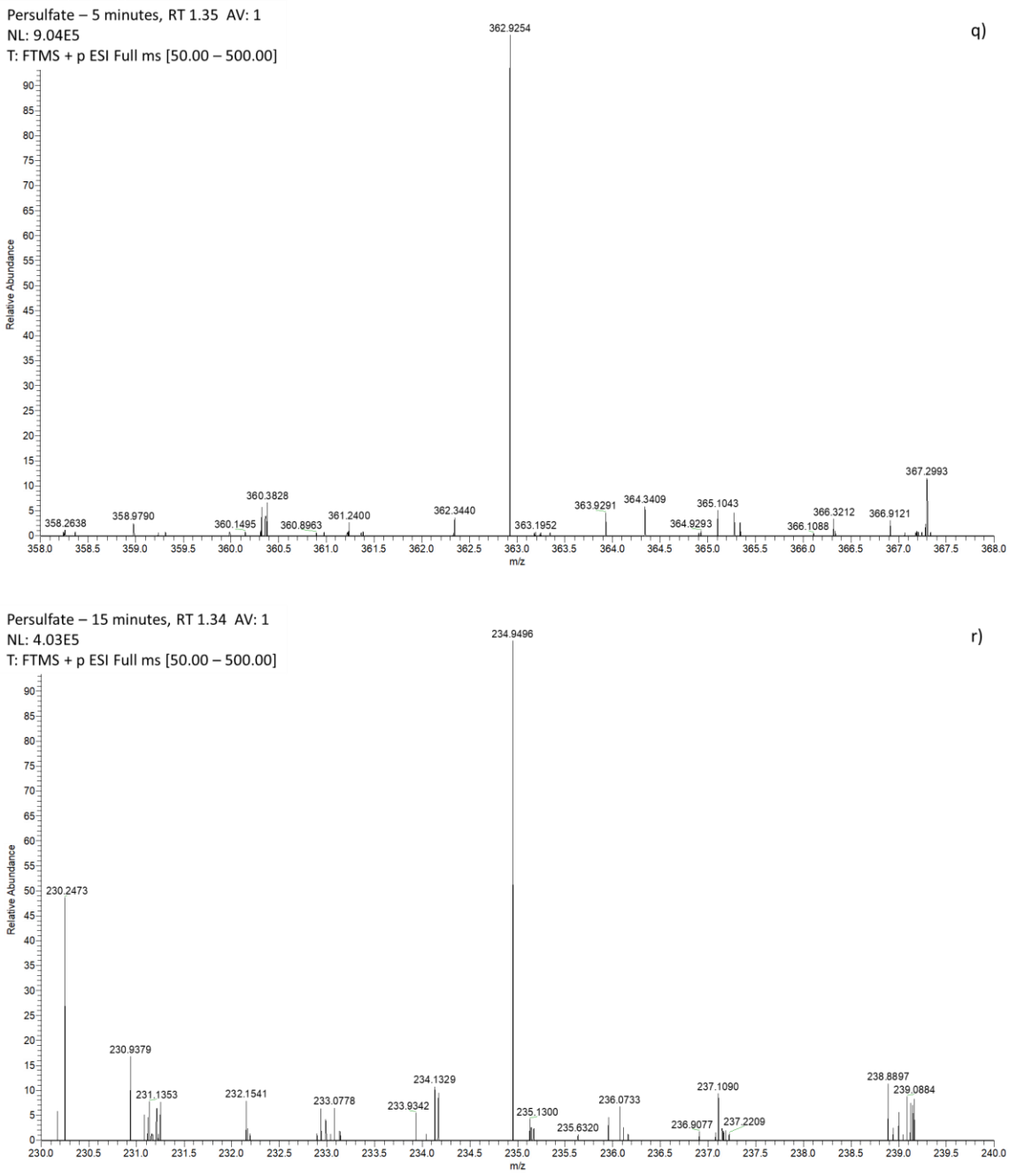

Figure A1. Continued

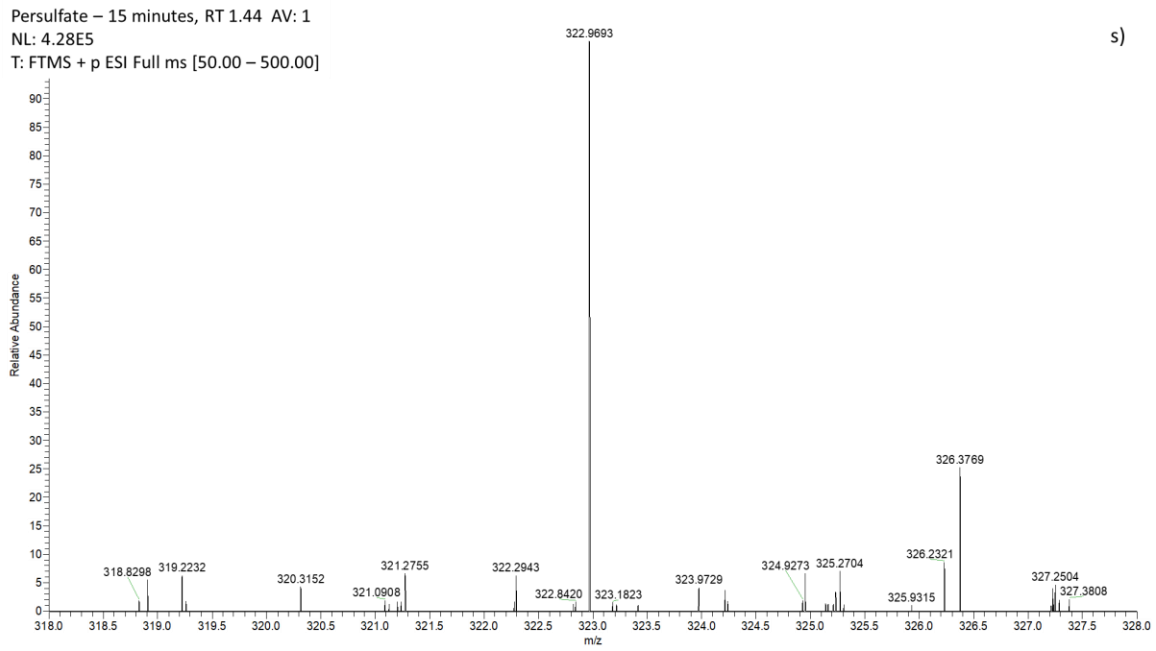

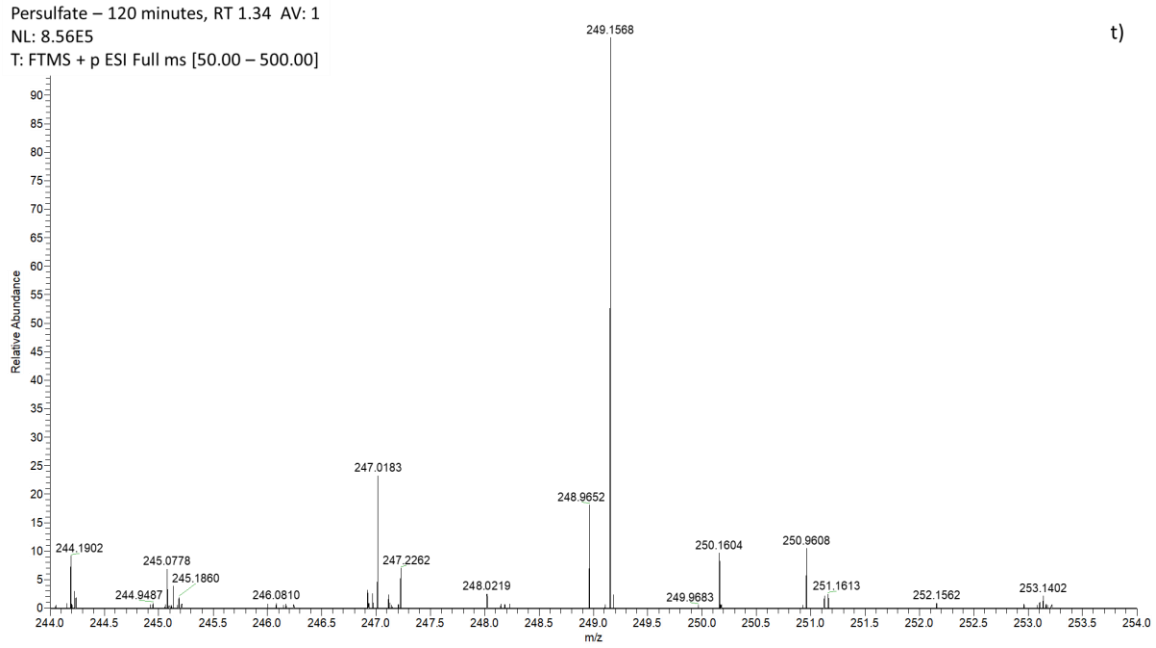

Figure A1. Continued

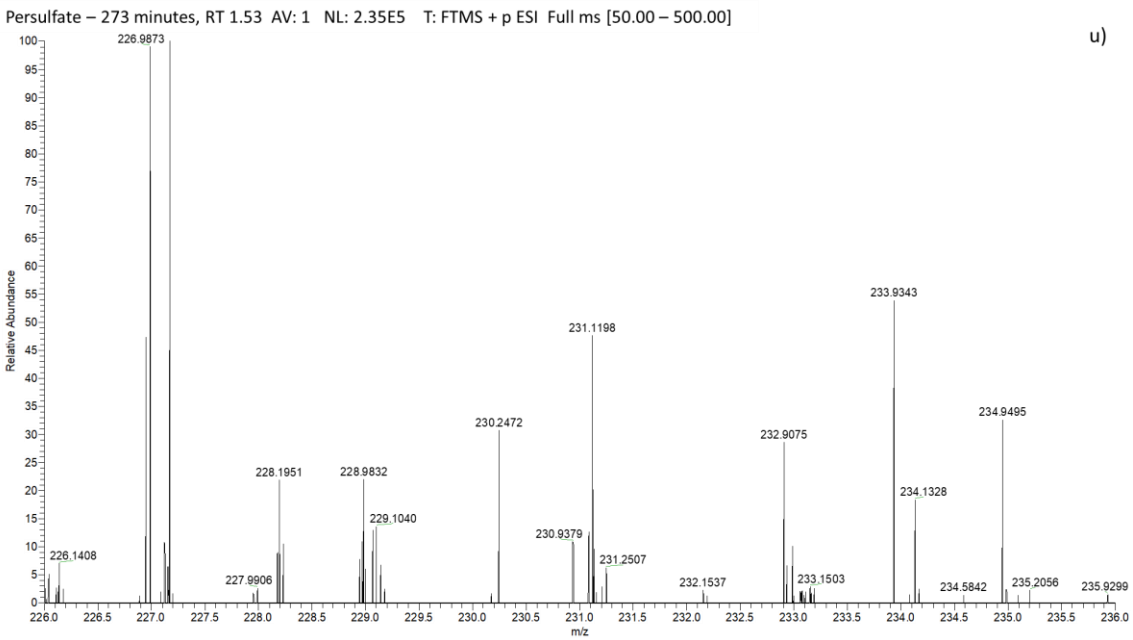

Figure A1. Continued

VITA

Laura Matzek was born in Knoxville, TN. She graduated from the University of Tennessee, Knoxville in 1998 with a Bachelor's of Science in Chemical Engineering. After graduation, she worked as an engineer for the DuPont Corporation in Chattanooga, TN for three years and for Intraspec, Inc in Oak Ridge, TN for five years. She was an instructor at Roane State Community College and Chattanooga State Community College before attending graduate school. Ms. Matzek will receive her doctorate in environmental engineering in May 2018. She currently lives in Lenoir City, TN with her husband and two children.